Vol. 50 ■ No. 1 ■ March 2022

JNMT

Journal of Nuclear Medicine Technology

FEATURED IMAGE

Renal Cortical Scarring: ^{68}Ga-PSMA-11 PET Versus ^{99}mTc-DMSA Scanning in a Case of Pyelonephritis. Ismet Sarikaya et al. See page 49.

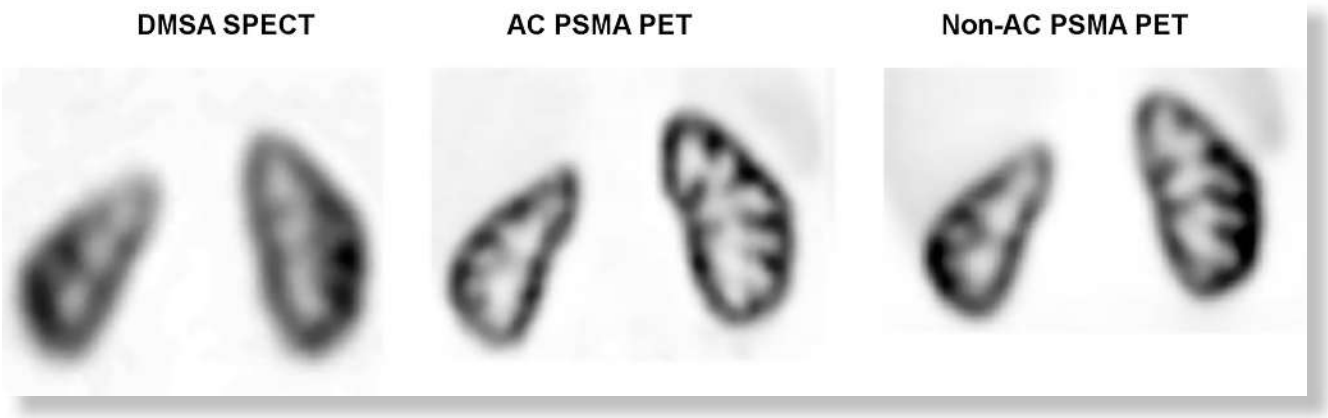

SNMMI Value Initiative
SOCIETY OF NUCLEAR MEDICINE & MOLECULAR IMAGING

A STREAMLINED CLINICAL CARE PATH ENABLED BY DIGITAL 360° SPECT/CT IMAGING

VERITON-CT®

DIGITAL SPECT/CT

Optimization of every step

For optimal patient outcomes, clinicians require access to imaging that ensures the most accurate diagnosis and appropriate treatment management decisions.

Spectrum Dynamics has integrated its ground-breaking Broadview Technology design into the VERITON-CT system, providing a digital platform that handles routine 3D workflow in one place. The result is optimization of every step, from image acquisition to interpretation.

VERITON-CT digital SPECT/CT combines the best-in-class CZT detectors, novel system design, high resolution CT, and advanced software technology to elevate the performance of CZT digital SPECT.

Digital Technology
360° design for high sensitivity and coverage

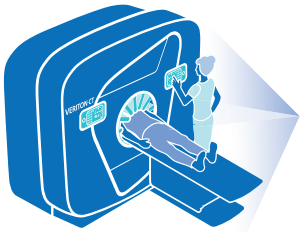

Workflow is reproducible and optimized for patient needs

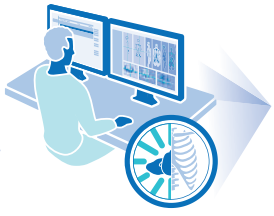

Image quality tools in TruView Console for advanced reconstruction and artifact reduction for both NM and CT data

Quantitative analysis
accessible in TruView Console integration with MIM-SD platform

Comprehensive results
from transformative technology that provides a greater volume of high quality data for informed decision-making

spectrum-dynamics.com

SPECTRUM
DYNAMICS MEDICAL

Pass the NMTCB CT Exam. We *GUARANTEE* It!

Because **MIC** is all about ***outcomes***.

Over 30 Years!

We guarantee you'll pass the NMTCB CT Exam or *your money back!*

- Technologists must complete 35 hours of didactic education related to CT during the 3 year period prior to applying for the CT Exam.
- NMTCB has approved MIC's **CT Registry Review Program** along with **Sectional Anatomy & Imaging Strategies** to ***completely satisfy that 35-hour CT didactic requirement!***
- Excellent companion for technologists in hybrid imaging.

There's no better time to participate in

MIC's Self-Study CE

- Prepare for **CT certification**
- Satisfy NMTCB's **prerequisite**
- Ensure the **highest standards**

Ask for the CNMT discount when you enroll in both courses!

Technologists and their managers agree:
"MIC's courses really work!"

Sectional Anatomy & Imaging Strategies™

Learn the essentials of sectional imaging in a convenient self-study format!

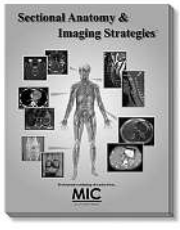

- Patient positioning, artifact reduction, image orientation, slice thickness, etc., for each clinical area.
- Explains sectional imaging with over 1,000 images and figures. The perfect companion to **The CT Registry Review Program**.
- 18 Credits
- 6 StudyModules

The CT Registry Review Program™

Pass the CT Exam after completing this course or we will refund your entire tuition!

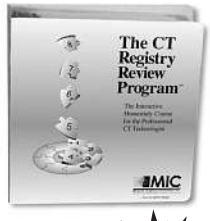

5th Ed!

- Learn **essential** and **advanced** topics on the NMTCB and ARRT CT Exam.
- Prior training in CT is recommended.
- Pass the NMTCB or ARRT Exam in CT or your money back!
- 22 Credits
- 8 StudyModules

A Proud Member of...
SNMMI

Call today for your
Free Info Kit
800-589-5685
or visit www.MIC*info*.com

MIC
Medical Imaging Consultants, Inc.
1037 US Highway 46, Suite G2 • Clifton, NJ 07013 • 800-589-5685
...for *your* perfect image.™

JNMT03/22

MIRION TECHNOLOGIES

STREAMLINED. SIMPLE. ACCURATE.

Meet the New Measure for Dose Calibration

CRC® DOSE CALIBRATOR FAMILY

Combine the speed and accuracy you need to measure and prepare doses with the performance and reliability that you've come to expect in one of the industry's finest packages.

CRC®-55tPET Dose Calibrator (Touch Screen)

CRC® - PC Smart Chamber

Network Ready with Remote Connectivity
The Most Advanced in Dose Calibration.

Visit capintec.com

Driving Innovation, Together: CAPINTEC, INC. Part of Mirion Technologies | BIODEX Part of Mirion Technologies

Visit capintec.com to learn how we can support your unique requirements.

OPS-3442 - 2/22

JNMT

Volume 50, Number 1 • March 2022

Essential Learning Tools for Nuclear Medicine Technologists

SNMMI's best-selling books and comprehensive online learning programs are designed to support you at all stages of your career as a nuclear medicine technologist.

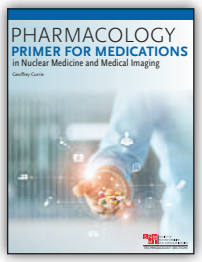

Pharmacology Primer for Medications in Nuclear Medicine and Medical Imaging

This practice-oriented text provides a concise overview of the basic principles of pharmacology that will help you thoroughly understand indications, contraindications, warnings, precautions, proper use, drug interactions, and adverse reactions for each medication used in medical imaging. Also available with CE Credit.

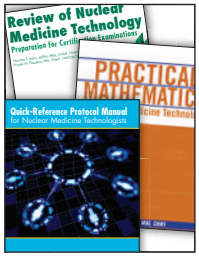

Technologist Study and Reference Combo

Save 10% when you purchase Review of Nuclear Medicine Technology, 5th Edition, Practical Mathematics in Nuclear Medicine Technology, 2nd Edition, and the Quick Reference Protocol Manual for Nuclear Medicine Technologists together as part of this new Technologist Study and Reference Combo.

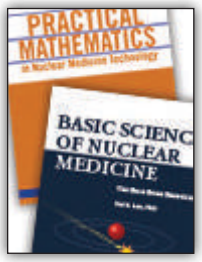

Technologist Math and Science Combo

Save 10% when you purchase *Practical Mathematics in Nuclear Medicine Technology, 2nd Edition* and *Basic Science of Nuclear Medicine: The Bare Bone Essentials* together as part of this new Technologist Math and Science combo.

Technologist Reference and Review Combo

Save 10% when you purchase *Quick Reference Protocol Manual for Nuclear Medicine Technologists* and *Review of Nuclear Medicine Technology, 5th Edition* together as part of this new Technologist Reference and Review combo.

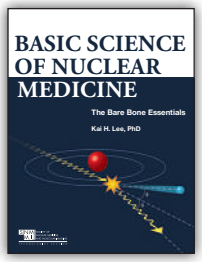

Basic Science of Nuclear Medicine: The Bare Bone Essentials

Basic Science of Nuclear Medicine: The Bare Bone Essentials is a great tool for nuclear medicine technologist students looking to better comprehend the fundamentals of the physics and technologies of modern-day nuclear medicine.

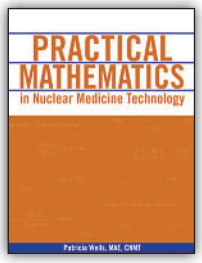

Practical Mathematics in Nuclear Medicine Technology, 2nd Edition

Informative word problems and explanations throughout *Practical Mathematics in Nuclear Medicine Technology* help you or your students prepare for the CNMT exam and real-life situations. *Purchase together with the Review of Nuclear Medicine Technology and save 10%.*

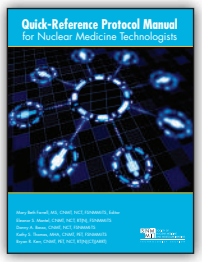

Quick Reference Protocol Manual for Nuclear Medicine Technologists

The *Quick Reference Protocol Manual for Nuclear Medicine Technologists* features protocols for 71 common nuclear medicine procedures. Each protocol lists the essential information for the procedure, including clinical indications and contraindications, patient preparation, and more.

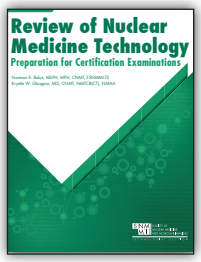

Review of Nuclear Medicine Technology, 5th Edition

The best-selling *Review of Nuclear Medicine Technology, 5th Edition*, gives you a detailed overview of nuclear medicine technology—covering patient care, instrumentation, radiopharmaceuticals, federal regulations, imaging of ten systems within the body, and radionuclide therapy—complemented by hundreds of self-evaluation questions and answers mirroring the structure of national certification examinations.

NEW FROM SNMMI-TS: PET/CT in Oncology, Parts 1 and 2

These books comes at a time where institutions are witnessing unprecedented numbers of PET referrals. Nuclear medicine professionals performing PET/CT in oncology must have the most up-to-date scientific and technical information possible in order to produce and interpret high-quality data to support optimal patient care.

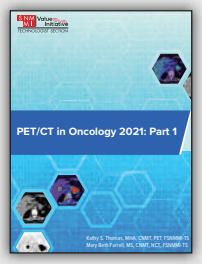

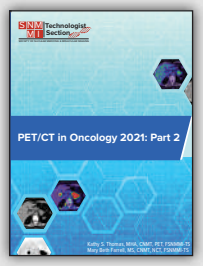

SNMMI Members, download a free digital copy.

Part 1 covers patient care, radiopharmaceuticals, brain tumors, head and neck tumors, neuroendocrine tumors, breast cancer, colorectal cancer, testicular and gynecologic cancers, musculoskeletal tumors, ^{18}F-NaF skeletal imaging, and bladder, renal and prostate cancers.

Part 2 covers PET/CT imaging in basic science, thyroid and adrenal cancer, lung cancer, gastric and esophageal cancers, pancreatic and liver cancer, malignant melanomas, lymphoma; radiotherapy; PET/MR in basic science; and future PET applications in PET oncology.

**Free shipping available on book orders within the continental United States.*

www.snmmi.org/TechTools

SNMMI Technologist Section
SOCIETY OF NUCLEAR MEDICINE & MOLECULAR IMAGING

JNMT Journal of NUCLEAR MEDICINE TECHNOLOGY

The Official Publication of **SNMMI-TS**

The *JOURNAL OF NUCLEAR MEDICINE TECHNOLOGY* (ISSN 0091-4916 [print]; ISSN 1535-5675 [online]) is published quarterly by the SNMMI, 1850 Samuel Morse Dr., Reston, VA 20190-5316; phone: (703) 708-9000; fax: (703) 708-9018. Periodicals postage paid at Reston, VA, and at additional mailing offi ces.

POSTMASTER: Send address changes to the *Journal of Nuclear Medicine Technology*, 1850 Samuel Morse Dr., Reston, VA 20190-5316.

EDITORIAL COMMUNICATIONS should be sent to the editor, Kathy S. Thomas, MHA, CNMT, PET, FSNMMI-TS, JNMT Office, SNMMI, 1850 Samuel Morse Dr., Reston, VA 20190-5316; phone: (703) 326-1185; fax: (703) 708-9018. To submit a manuscript, go to http://submit-tech.snmjournals.org.

BUSINESS COMMUNICATIONS concerning permission requests should be sent to the publisher, SNMMI, 1850 Samuel Morse Dr., Reston, VA 20190-5316; phone: (703) 708-9000; home page address: http://tech.snmjournals.org. Subscription requests, address changes, and missed issue claims should be sent to Membership Department, SNMMI, at the address above. Notify the Society of change of address and telephone number at least 30 days before date of issue by sending both the old and new addresses. Claims for copies lost in the mail are allowed within 90 days of the date of issue. Claims are not allowed for issues lost as a result of insufficient notice of change of address. For information on advertising, contact Team SNMMI (Kevin Dunn, Rich Devanna, and Charlie Meitner; (201) 767-4170; fax: (201) 767-8065; TeamSNMMI@cunnasso.com). Advertisements are subject to editorial approval and are restricted to products or services pertinent to nuclear medicine. Closing date is the 25th of the second month preceding the date of issue.

INDIVIDUAL SUBSCRIPTION RATES for the 2022 calendar year are $249 within the United States and Canada; $265 elsewhere. CPC IPM Sales Agreement No. 1415131. Sales of individual back copies are available for $58 at http://www.snmmi.org/subscribe (subscriptions@snmmi.org; fax: (703) 667-5134). Individual articles are available for sale online at http://tech.snmjournals.org.

MISSION: SNMMI-TS is dedicated to the advancement of molecular and nuclear medicine technologists by providing education, advocating for the profession, and supporting research to achieve clinical excellence and optimal patient outcomes. **VISION:** To be recognized as the leader in molecular imaging and therapy. To be dedicated to the advancement of the profession through adoption of emerging technologies.

JNMT Journal of NUCLEAR MEDICINE TECHNOLOGY

RADIATION SAFETY+ Review and Essentials

Let the SNMMI-TS Help You Prepare for the NMTCB's Radiation Safety Exam

Get the tools you need to successfully prepare for the exam with the **Radiation Safety + Review and Essentials** program. This 5 module/7.75 VOICE credit course provides a comprehensive review of all aspects of radiation safety including:

- Radiation physics and instrumentation
- Dosimetry
- Mathematics
- Security and control
- Shipping and receiving
- Disposal
- Emergency procedures
- Regulations
- Radiation protection and ALARA
- Radionuclide therapy best practices

2022 NMTCB Radiation Safety Exam Dates Announced!

Begin Your Preparation!

Order this popular program today!

You'll review content on CT. X-ray, fluoroscopy, and MRI, as well as optimizing radiation exposure, including appropriateness criteria, Image Wisely/Image Gently, and special populations. Plus, test what you've learned with a 150 question "Mock Exam," to ensure you're fully prepared for the exam.

Member: $99 | Non-Member: $249

Get started today!
www.snmmi.org/RadiationPlus

SNMMI Technologist Section
SOCIETY OF NUCLEAR MEDICINE & MOLECULAR IMAGING

An Update on Education Amidst the Pandemic

Dusty M. York, CNMT, PET, RT(N)(CT)

Two years ago, life as we know it changed—and it continues to evolve. What effect has the pandemic had on nuclear medicine technologist (NMT) educational programs and students?

In 2020, NMT programs were faced with the challenge to convert in-person programs to virtual almost overnight. Needless to say, programs have faced numerous challenges over the past two years. The pandemic left programs in a scramble to adopt an online delivery platform and learn how to engage an anxiety-ridden population virtually, and clinical rotations were suspended. Educators and students alike are still learning how to navigate this new world and its continuously evolving changes.

According to data provided by the American Registry of Radiologic Technologists, the total number of first-time examinees in nuclear medicine technology in 2020 was down 29% compared to 2019 (pre-pandemic). In 2021, it was up 150% compared to 2020 and up 9% compared to 2019. Similarly, the Nuclear Medicine Technologist Certification Board reported a total of 637 candidates for the entry-level Certified Nuclear Medicine Technologist exam during the 2021 year compared to 715 in 2019 and 601 in 2020. The 2021 exam data showed an 11% decrease in the total number of candidates from the pre-pandemic 2019 data.

Over the past two years, programs have cycled in and out of a seminormal routine with the occurrence of each new COVID-19 variant. Clinical requirements have undergone a constant succession of updates, and programs have battled to keep students informed. Fortunately, most programs are now reporting enhanced communication with their clinical affiliates. In addition, many programs are reporting that clinical affiliates are now typically providing the personal protective equipment necessary for clinical rotations.

Today, students are learning to live and learn in a new environment. Many programs have returned to fully on-site operations and are falling back into a more routine operation, while others have embraced a virtual world. Those that are in-person have expressed that their biggest concern at this time is attendance. Intermittent periods of absence of faculty and students through COVID-related illness, isolation, and quarantine have proved difficult to navigate.

COVID policies are most often driven by the academic institution rather than by individual academic programs; in addition, programs are required to follow COVID policies of their affiliated clinical sites if the policies are related to clinical education. What do vaccine requirements look like for nuclear medicine programs and their students? Colleges and universities vary greatly on their vaccine requirement status. At first glance, it seems that state-operated facilities are less likely to require vaccination than privately run universities; this is because of the laws associated with state-run facilities. Regardless of ownership status, however, students must abide by medical affiliate requirements in order to participate in clinical rotations. The vaccine mandate was recently upheld, and clinical facilities are requiring employees, students, and program faculty to be vaccinated.

Dusty M. York, CNMT, PET, RT(N)(CT)

The SNMMI-TS has been working to identify ways in which we can help. SNMMI-TS provides students free membership throughout their time in a nuclear medicine program; this provides them access to numerous FREE online courses and sessions. In 2021, the SNMMI-TS offered the first ever focused full-day *student* course, which provided the opportunity to connect with leaders in the field while learning about the next steps in their career path, how to stand out from their peers (resume building and networking), and the numerous career opportunities available to them as NMTs. A similar program is planned for 2022, again aiming to help students as they transition into the work world. In addition, the SNMMI-TS has a FREE online review course and mock exam available to SNMMI-TS students studying for their certification exam. Finally, the SNMMI-TS has a dedicated Student and Recent Graduate Task Force focused on creating programming and benefits to support early career professionals.

The field of nuclear medicine and molecular imaging continues to grow and expand with new therapeutic agents, and the demand for highly skilled NMTs has increased, despite the challenges created by the pandemic. According to the Bureau of Labor Statistics Occupational Outlook Handbook (www.bls.gov/ooh), "employment of nuclear medicine technologists is projected to grow 8 percent from 2020 to 2030 … About 1,500 openings for nuclear medicine technologists are projected each year, on average, over the decade." The SNMMI-TS is excited about this growth, but we know that educators and students need more support, more funding, and more time to teach the critical skills needed to be a highly qualified NMT. If students or program directors have ideas that they would like considered, we encourage them to email memberinfo@snmmi.org to share them with the Task Force.

2022—A "Ditto" of 2021?

Kathy S. Thomas, MHA, CNMT, PET, FSNMMI-TS

Editor, *JNMT*

It's mid-January, and for some, 2022 threatens to be a "ditto" of 2021. The Mid-Winter Meeting, a live event we were all looking forward to after missing the opportunity to gather in 2021, has now transitioned to a virtual event once again. Borders are closing—again—and the pandemic continues to impact every aspect of our lives. Yet, with the challenges the past two years have brought, the nuclear medicine community remains strong, continues to advance new imaging and therapeutic techniques, and, most important, supports our colleagues' professional growth.

The 4 continuing education (CE) articles in this issue present a diverse selection of topics. The SNMMI Clinical Trials Network Research Series continues, with a review of the regulatory process of radiopharmaceuticals (*1*). In the next CE article, the use of α-emitting radionuclides—a newer topic in nuclear medicine—is described. Brian Serencsits et al. present an in-depth discussion on radiation safety considerations for today's α-emitting therapeutic protocols (*2*). In the third CE article, Elad Nevo et al. continue the PET/MRI series, discussing PET/MRI protocols and procedures (*3*). Finally, Li and colleagues examine the ongoing question of the appropriate collimator for ^{123}I thyroid imaging, comparing low- and medium-energy collimators (*4*).

The scientific manuscripts offer an assortment of topics, including cardiac, renal, and instrumentation discussions. An examination of the noninvasive approach to diagnosing cardiac amyloidosis with ^{99m}Tc-PYP (*5*) and the results of a predictive model to elute a bolus from an ^{82}Rb generator as a function of generator age (*6*) are presented. In addition, 2 articles on the use of ^{68}Ga-PSMA-11 in renal PET imaging are included: a correlative assessment of ^{68}Ga-PSMA-11 renal PET parameters and renal function tests (*7*) and a comparison of ^{68}Ga-PSMA-11 with ^{99m}Tc-DSMA for evaluating pyelonephritis (*8*).

Cultural diversity and the need for professional development in cultural proficiency continue to challenge educators and the medical community worldwide. Geoff Currie offers an interesting discussion on the professional development activities in nuclear medicine that target proficiency and create culturally safe clinical environments for the Indigenous population (*9*).

Additional topics of interest include an exploration of the changing education methods in Japan during the pandemic and the results of establishing a national diagnostic reference level (DRL) in Kuwait when the ALARA principle of dose optimization is not fully implemented.

The teaching case studies provide helpful images demonstrating key facts or concepts in clinical nuclear medicine and molecular imaging.

Kathy S. Thomas, MHA, CNMT, PET, FSNMMI-TS

JNMT continues to look for new topics, clinical research, CE articles, protocols, tips, and pointers. If you have ideas or suggestions or are considering writing but maybe need some help getting started, please contact me at ksthomas0412@msn.com. Help is available!! If writing isn't your thing, but you're willing to share your expertise by becoming a reviewer for *JNMT,* please contact me!

Thank you all for your continued dedication and perseverance in these difficult times. Please stay safe and healthy.

REFERENCES

1. Jeffers CD, Frye SA, Hoffman JM. SNMMI Clinical Trials Network (CTN) Research Series for Technologists: clinical research primer—regulatory process part I: how and when radiopharmaceuticals can be used. *J Nucl Med Technol.* 2022;50:2–9.
2. Serencsits B, Chu BP, Pandit-Taskar N, McDevitt MR, Dauer LT. Radiation safety considerations and clinical advantages of α-emitting therapy radionuclides. *J Nucl Med Technol.* 2022;50:10–16.
3. Nevo E, Kamvosoulis P, Currie GM. PET/MRI, part 3: protocols and procedures. *J Nucl Med Technol.* 2022;50:17–24.
4. Li Y, Choi E, Hayrapetian A. Comparison of low-energy and medium-energy collimators for thyroid scintigraphy with ^{123}I. *J Nucl Med Technol.* 2022;50:25–29.
5. Lee C, Chao C-J, Agasthi P, et al. Global and regional variations in transthyretin cardiac amyloidosis: a comparison of longitudinal strain and ^{99m}Tc-pyrophosphate imaging. *J Nucl Med Technol.* 2022;50:30–37.
6. Scott AW, Hyun M, Kim J. Predictive model for ^{82}Rb generator bolus times as a function of generator lifetime. *J Nucl Med Technol.* 2022;50:38–42.
7. Schierz J-H, Sarikaya I, Albatineh AN, Sarikaya A. Assessing the correlation between ^{68}Ga-PSMA-11 renal PET parameters and renal function tests. *J Nucl Med Technol.* 2022;50:43–48.
8. Sarikaya I, Alqallaf A, Sarikaya A, Baqer A, Kazem N. Renal cortical scarring: ^{68}Ga-PSMA-11 PET versus ^{99m}Tc-DMSA scanning in a case of pyelonephritis. *J Nucl Med Technol.* 2022;50:49–53.
9. Currie GM. *Yindyamarra Winhanganha:* a conduit to Indigenous cultural proficiency. *J Nucl Med Technol.* 2022;50:66–72.

SNMMI Clinical Trials Network Research Series for Technologists: Clinical Research Primer—Regulatory Process, Part I: How and When Radiopharmaceuticals Can Be Used

Charlotte Denise Jeffers[1], Sarah A. Frye, CNMT, NMTCB(PET), NMTCB(NCT), CCRP[2], and John M. Hoffman[3]

[1]*Department of Radiology, University of Alabama at Birmingham, Birmingham, Alabama;* [2]*Department of Clinical Health Sciences, Saint Louis University, St. Louis, Missouri; and* [3]*Huntsman Cancer Institute, University of Utah School of Medicine, Salt Lake City, Utah*

CE credit: For CE credit, you can access the test for this article, as well as additional *JNMT* CE tests, online at https://www.snmmilearningcenter.org. Complete the test online no later than March 2025. Your online test will be scored immediately. You may make 3 attempts to pass the test and must answer 75% of the questions correctly to receive Continuing Education Hour (CEH) credit. Credit amounts can be found in the SNMMI Learning Center Activity. SNMMI members will have their CEH credit added to their VOICE transcript automatically; nonmembers will be able to print out a CE certificate upon successfully completing the test. The online test is free to SNMMI members; nonmembers must pay $15.00 by credit card when logging onto the website to take the test.

The radiopharmaceutical development and approval process in the United States has changed dramatically over the past decade with the emergence of several new and exciting diagnostic and therapeutic drugs. This impressive expansion is a direct result of the symbiotic relationship that exists between drug development, clinical research, and improved regulatory guidance. The correlative increase in clinical research has introduced diverse opportunities for newcomers in medical and scientific professions. Knowing how to successfully navigate the clinical research process can be challenging for a novice. The pathway is highly regulated and, with the addition of radiopharmaceuticals, may be confusing and daunting. Moreover, very little clinical research education and training is provided in the typical collegiate curricula for these new initiates. This article will familiarize the reader with the U.S. regulatory process by providing basic definitions and understanding of how and when radiopharmaceuticals can be used in clinical research, including those involving investigational new drug applications and radioactive drug research committees. A later article will expand the reader's clinical research knowledge by focusing on the identity and role of the institutional review board.

Key Words: radiopharmaceutical; clinical research; clinical trial; investigational new drug; investigational new drug application; radioactive drug research committee

J Nucl Med Technol 2022; 50:2–9
DOI: 10.2967/jnmt.121.263499

Clinical research using both approved drugs and investigational new drugs (INDs) continues to augment scientific knowledge, direct the next wave of approved radiopharmaceuticals, and expand indications for currently approved drugs. Knowing the regulations for how and when radiopharmaceuticals can be used in the clinical research setting is a crucial component for ensuring safe and effective outcomes. The sheer volume and granularity of material on the subject is vast and, to many, time-prohibitive. The intent of this article is to guide the reader through the expanse of radiopharmaceutical clinical research regulations to help build a solid base of knowledge.

BACKGROUND

Radiopharmaceuticals are a subset of traditional pharmaceuticals. In the United States, the primary requirements to establish safety and efficacy come from the U.S. Food and Drug Administration (FDA), an agency of the U.S. Department of Health and Human Services. The regulations are identified in the *Code of Federal Regulations* (CFR), which is a compilation of rules and regulations formulated by the federal government. The CFR has 50 titles, each being dedicated to a particular agency or branch of the federal government. Title 21 is dedicated to food and drugs and comprises 3 chapters, which are further divided into 1,499 parts. These regulations may be referenced in clinical research documents, support materials, and in this article. For example, 21 CFR §312 means title 21 of the *Code of Federal Regulations,* section 312.

Additionally, the FDA publishes guidance documents on certain subjects. Although guidance documents are not enforceable, they represent the FDA's current thinking on a subject and provide practical information.

As with most topics today, federal regulations and guidance documents are easily searched on the Internet. To ensure the veracity of the information, one should use an official government website. The FDA federal regulations can be found through a variety of official online sources, including the FDA website (https://www.fda.gov), the electronic CFR website (https://www.ecfr.gov), the regulations.gov website (www.regulations.gov), and the U.S

Received Nov. 10, 2021; revision accepted Dec. 16, 2021.
For correspondence or reprints, contact Charlotte Denise Jeffers (charlottejeffers@uabmc.edu).
Published online Dec. 21, 2021.

Department of Health and Human Services website (https://www.HHS.gov).

DEFINITIONS

Before we embark on a discussion of radiopharmaceutical clinical research, we need to review the following terms that are defined or referenced in 21 CFR or other research sources such as FDA guidance documents.

Adverse event means any untoward medical occurrence associated with a drug in humans, whether or not considered drug-related.

Case report form is a printed, optical, or electronic document containing all the protocol-required information recorded for the study or reported to the sponsor on each trial subject (*1*).

Clinical investigation means any experiment in which a drug is administered or dispensed to—or is used involving—one or more human subjects. The terms *clinical investigation, clinical study, clinical research,* and *clinical trial* are deemed to be synonymous for the purposes of this article.

Contract research organization means a person that assumes, as an independent contractor with the sponsor, one or more of the obligations of a sponsor, for example, design of a protocol, selection or monitoring of investigations, evaluation of reports, and preparation of materials to be submitted to the FDA.

Current good manufacturing practices are regulations containing minimum requirements for the methods, facilities, and controls used in manufacturing, processing, and packing of a drug product (*2*).

FDA approval of a drug means that data on the drug's effects have been reviewed and the drug is determined to provide benefits that outweigh its known and potential risks for the intended population (*3*).

Institutional review board (IRB) means any board, committee, or other group formally designated by an institution to review, approve the initiation of, and conduct periodic review of biomedical research involving human subjects. The primary purpose of such review is to ensure the protection of the rights and welfare of the human subjects.

IRB approval means the determination by the IRB that the clinical investigation has been reviewed and may be conducted at an institution within the constraints set forth by the IRB and by other institutional and federal requirements.

IND means a new drug or biologic drug that is used in a clinical investigation. The term also includes a biologic product that is used in vitro for diagnostic purposes. The terms *investigational drug* and *IND* are deemed to be synonymous for the purposes of this article.

IND application is a request from a clinical study sponsor to the FDA to authorize administration of an investigational drug or biologic product to humans.

Investigator means an individual who actually conducts a clinical investigation (i.e., under whose immediate direction the study is conducted or the drug is administered or dispensed to a subject). If an investigation is conducted by a team of individuals, the investigator is the responsible leader of the team. The lay terms *principal investigator* and *primary investigator* are often used for the investigator.

Investigator's brochure is a comprehensive document summarizing the information obtained about an investigational product during a drug trial.

Multisite (or multicenter) clinical trial involves the implementation of the same clinical protocol at 2 or more independent investigational sites where participants are seen for an intervention or outcomes assessment. In a multisite trial, investigational sites are typically administratively or corporately distinct from each other (*4*).

New drug application (NDA) is the vehicle through which a drug sponsor formally proposes that the FDA approve a new pharmaceutical for sale in the United States. To obtain this authorization, a drug manufacturer submits in an NDA nonclinical (animal) and clinical (human) test data and analyses, drug information, and descriptions of manufacturing procedures.

Single-site clinical trial uses one investigational site to conduct and coordinate the protocol. Although a single-site clinical trial may enroll participants from multiple locations, those participants will receive an intervention or undergo outcome assessments under the direction and oversight of one research team located at one investigational site (*4*).

Site initiation visit is part of a sponsor's monitoring plan to ensure that participating sites comply with protocol requirements and conduct the study appropriately. An initiation visit takes place after the sponsor has selected the site for participating in a clinical trial and typically before patient enrollment.

Sponsor means an entity that takes responsibility for and initiates a clinical investigation. The sponsor may be an individual, pharmaceutical company, governmental agency, academic institution, private organization, or other organization. The sponsor does not actually conduct the investigation unless the sponsor is a sponsor-investigator. The terms *sponsor* and *sponsor-investigator* are deemed to be synonymous for the purposes of this article.

Sponsor-investigator means an individual who both initiates and conducts an investigation and under whose immediate direction the investigational drug is administered or dispensed. The term does not include anything other than an individual. The requirements applicable to a sponsor-investigator under this part include both those applicable to an investigator and those applicable to a sponsor. The terms *sponsor* and *sponsor-investigator* are deemed to be synonymous for the purposes of this article.

Subject means a human who participates in an investigation, either as a recipient of the IND or as a control. A subject may be a healthy human or a patient with a disease.

OVERVIEW OF RADIOPHARMACEUTICAL CLINICAL RESEARCH PROCESSES

21 CFR allows pharmaceutical products to be administered to human patients or subjects under any of the following 5 conditions:

1. A U.S. lawfully marketed drug administered under clinical care. These are drugs that have been studied in an IND clinical trial process. All data gathered during the clinical trial are submitted by the sponsor to the FDA in an NDA application. If the FDA determines that the NDA application meets all requirements, including, but not limited to, proving safety and efficacy, the drug will be approved and may be marketed and sold in the United States.
2. Emergency-use authorization. An FDA emergency-use authorization is a temporary permit to allow a drug to be administered to human patients without the requirement that clinical trials be completed and before an NDA application is approved. Emergency-use authorizations are approved to respond to designated chemical, biologic, radiologic, and nuclear emergencies. For example, coronavirus 2019 vaccines were approved under an emergency-use authorization in the United States before their eventual approval by the FDA.
3. A U.S. lawfully marketed drug administered within a clinical trial or other research project. Generally, regulations in 21 CFR §312 require that sponsors who wish to study a drug or biologic product in humans submit an IND application to the agency. However, these regulations also provide for the exemption of some studies from the requirement to submit an IND application if they meet certain criteria (5).
4. An IND administered within a clinical trial, clinical study, or other research project under an authorized IND application.
5. A U.S. lawfully marketed (i.e., FDA-approved) or investigational drug administered for basic research within a research study or project under a radioactive drug research committee (RDRC) (21 CFR §361).

The remainder of this article will focus on details for conditions 3–5.

IND APPLICATION FOR MARKETED DRUGS

Determining whether an IND application is needed to conduct a clinical investigation of a marketed (i.e., FDA-approved) drug depends primarily on the intent of the investigation and the degree of risk associated with the drug in the investigation. A clinical investigation of a marketed drug is exempt from the IND application requirements if all of the following criteria are met: The drug product is lawfully marketed in the United States. The investigation is not intended to be reported to the FDA as a well-controlled study in support of a new indication and there is no intent to use it to support any other significant change in the labeling of the drug. In the case of a prescription drug, the investigation is not intended to support a significant change in the advertising for the drug. The investigation does not involve a route of administration, dose, patient population, or other factor that significantly increases the risk (or decreases the acceptability of the risk) associated with the drug product. The investigation is conducted in compliance with the requirements for review by an IRB and with the requirements for informed consent. The investigation is conducted in compliance with the requirements of 21 CFR §312.7 (i.e., the investigation is not intended to promote or commercialize the drug product).

The potential sponsor of a planned clinical investigation using an approved drug is responsible for determining whether the investigation meets the criteria for an exemption. If there is uncertainty about whether the exemption criteria are met, the potential sponsor can seek advice from the FDA on the applicability of the IND regulations (*5*).

IND APPLICATIONS

During a new drug's early preclinical development, the sponsor's primary goal is to determine whether the product is reasonably safe for initial use in humans and whether the compound exhibits pharmacologic activity that justifies commercial development. When a product is identified as a viable candidate for further development, the sponsor then focuses on collecting the data and information necessary to establish that the product will not expose humans to unreasonable risks when used in limited, early-stage clinical studies (*6*) .

Unless exempted, the sponsor for a clinical study must obtain authorization from the FDA for conducting the study by submitting an IND application. Such authorization must be secured before interstate shipment and administration of any new drug that is not the subject of an approved NDA (*6*).

IND Application Categories

The FDA recognizes 2 main IND application categories: commercial and research. A commercial IND application is one for which the sponsor (usually a corporate entity) intends to commercialize the product by eventually submitting a marketing application. A research (noncommercial) IND application is one for which the sponsor (generally an individual investigator, academic institution, or nonprofit entity) does not intend to later commercialize the product (*6*).

There are 3 main types of IND applications: investigator, emergency-use, and treatment or expanded-access applications. The emergency-use and expanded-access IND applications have some overlapping similarities. An investigator IND application (sometimes referred to as an investigator-initiated IND) is submitted by a physician who both initiates and conducts an investigation (i.e., the physician is the sponsor-investigator) and under whose immediate direction the investigational drug is administered or dispensed. A physician might submit a research IND application to propose studying an unapproved drug or an approved product for a new indication or in a new patient population. An emergency-use IND application allows the FDA to authorize use of an experimental drug in an emergency situation that does not allow time for submission of an IND application in accordance with 21 CFR §312.23 or 21 CFR §312.20. It is also used for patients who do not meet the criteria of an existing study protocol or if an approved study protocol does not exist. A treatment or expanded-access IND application, sometimes called compassionate use, is used for experimental drugs showing promise in the clinical testing for serious or immediately life-threatening conditions while the final clinical work is being conducted and the FDA review is taking place. This type of application

covers the use of IND products outside clinical trials to diagnose, monitor, or treat patients with serious or immediately life-threatening diseases or conditions when there are no comparable or satisfactory alternative treatment options. Under the FDA's current regulations, there are 3 categories of expanded access: expanded access for individual patients, including for emergency use (this differs from an emergency-use application because it is based on a single patient), expanded access for intermediate-sized patient populations (generally smaller than those typical of a treatment IND or treatment protocol—a treatment protocol is submitted as a protocol to an existing IND by the sponsor of the existing IND), and expanded access for widespread treatment use through a treatment IND or treatment protocol (designed for use in larger patient populations) (*7*).

The distinction between administering an investigational drug in the setting of a traditional clinical trial versus emergency use or an expanded-access IND lies in the intended use. In a traditional clinical trial, the intention is to understand the safety and effectiveness of the investigational drug; in expanded access and emergency use, the intention is treatment (*7*). Emergency-use and expanded-access IND applications are not part of the clinical research pathway and are therefore beyond the scope of this article.

IND Application Submission Pathway

INDs progress through FDA-regulated exploratory or traditional IND clinical research phases.

An exploratory IND (sometimes referred to as phase 0 studies or eIND) is a clinical trial that is conducted early in phase 1, involves very limited human exposure, and has no therapeutic or diagnostic intent (e.g., screening studies or microdose studies) (*8*). This is not a required phase but is a useful option in certain circumstances. Depending on the study, the informational requirements for exploratory IND studies are more flexible than for traditional IND studies. The IND is filed separately from a traditional IND application submission.

Traditional IND phases include phase 1, with a primary goal of assessing the safety of the drug; phase 2, with a primary goal of assessing efficacy and safety and determining the dose; phase 3, with a primary goal of assessing efficacy and monitoring adverse effects; and phase 4, which is postmarketing surveillance.

IND Application Process

The IND application requirements and processes for commercial versus noncommercial (i.e., research) INDs differ with respect to the route of filing. All commercial IND applications must be filed electronically, whereas noncommercial IND applications can be filed by electronic or paper options (*9*).

Sponsors of IND applications may obtain advice and guidance from the FDA at any stage of IND development. Before filing an IND application, the sponsor may have questions regarding key components such as protocol design, drug specifics or pharmacology, and toxicology information. In these cases, the FDA allows the IND sponsor to request a pre-IND meeting (*9*). If granted, questions are provided to the FDA in advance of the scheduled meeting. After the meeting, the FDA provides formal responses to help guide critical decisions for the IND application submission.

The IND application must contain information in 3 broad areas: animal pharmacology and toxicology studies, manufacturing information, and clinical protocols and investigator information. Animal pharmacology and toxicology studies provide preclinical data to permit an assessment as to whether the product is reasonably safe for initial testing in humans. Also included are any previous experience with the drug in humans (can include use in countries outside the United States). Manufacturing information is information pertaining to the composition, manufacturer, stability, and controls used for manufacturing the drug substance and the drug product. This information is assessed to ensure that the company can adequately produce and supply consistent batches of the drug. Clinical protocols and investigator information are detailed protocols for proposed clinical studies to assess whether the initial-phase trials will expose subjects to unnecessary risks. Also, information is provided on the qualifications of clinical investigators—professionals (generally physicians) who oversee the administration of the experimental compound—to assess whether they are qualified to fulfill their clinical trial duties. Finally, commitments are made to obtain informed consent from the research subjects, to obtain review of the study by an IRB, and to adhere to the IND regulations in 21 CFR §312 (*6*).

Once the IND is submitted, the sponsor must wait 30 calendar days before initiating any clinical trials. During this time, the FDA has an opportunity to review the IND for safety to ensure that research subjects will not be subjected to unreasonable risk (*6*). During or at the end of the 30-d review, the FDA may either accept the IND application, allowing the clinical research to go into effect, or it may place the IND on clinical hold. The FDA does not "approve" an IND application but will provide authorization through a study-may-proceed letter or communication.

Clinical Hold

A clinical hold is an order issued by the FDA to the sponsor of an IND application to delay a proposed clinical investigation or to suspend an ongoing investigation. All or some of the investigations conducted under an IND application may be placed on clinical hold. When a proposed study is placed on clinical hold, subjects may not be given the investigational drug. When an ongoing study is placed on clinical hold, no new subjects may be recruited to the study and given the investigational drug; patients already in the study are expected to be taken off therapy involving the investigational drug unless treatment continuation is specifically permitted by the FDA in the interest of patient safety. Within 30 d of the clinical hold, the FDA will provide the applicant with a written explanation of the basis for the hold (*10*).

The IND sponsor is expected to address the cited deficiencies in writing and submit a complete response to the issues identified in the clinical-hold letter in a separate submission. Once the complete response to all clinical hold deficiencies has been received, the FDA will review the submission within 30 calendar days and determine whether the applicant's response to the clinical hold satisfactorily addresses the issues. The investigation may resume after the FDA has notified the applicant that the investigation may proceed (*10*).

If an IND applicant disagrees with the reasons cited for the clinical hold, the applicant may request reconsideration of the decision through the ombudsman and in accordance with dispute resolution procedures (*10*). If all investigations covered by an IND application remain on clinical hold for 1 y or longer, the IND application may be considered by the FDA for inactive status (21 CFR §312.42).

Active INDs

Once an IND application is authorized (active), a drug manufacturer may legally ship or provide the investigational drug to the investigators named in the application. An investigator may not administer an investigational drug to human subjects until the IND application goes into effect and the protocol and informed consent form have been approved by the IRB of record.

IND Management

Sponsors of active INDs are required to provide oversight to ensure adequate protection of the rights, welfare, and safety of human subjects and the quality of the clinical trial data submitted to the FDA. To meet these requirements, sponsors are responsible for monitoring the trial and sending periodic updates, any necessary amendments, and reports related to their applications to the FDA (*6*).

A sponsor may transfer responsibility for any or all obligations to a contract research organization. Any such transfer must be described in writing. If not all obligations are transferred, each of the obligations being assumed by the contract research organization must be described. If all obligations are transferred, a general statement that all obligations have been transferred is acceptable. Any obligation not covered by the written description is deemed not to have been transferred.

Although the sponsor's responsibilities for a research IND versus a commercial IND do not differ, the monitoring plan may vary significantly because of the intent and complexity of the IND. The monitoring plan should focus on preventing or mitigating important and likely risks to critical data and processes. Regulations are not specific about how sponsors are to conduct such monitoring and are therefore compatible with the complexities of the IND and allow for a range of approaches to monitoring that will vary depending on multiple factors.

Monitoring. Although the methods of monitoring may differ, either an on-site or a centralized approach may be used.

On-site monitoring is an in-person evaluation performed by sponsor personnel or representatives at the sites at which the clinical investigation is being conducted. On-site monitoring can identify data entry errors (e.g., discrepancies between source records and case report forms) and missing data in source records or case report forms, provide assurance that study documentation exists, assess the familiarity of the site's study staff with the protocol and required procedures, and assess compliance with the protocol and investigational product accountability. On-site monitoring can also provide a sense of the quality of the overall conduct of the trial at a site (e.g., attention to detail, thoroughness of study documentation, appropriate delegation of study tasks, and appropriate clinical investigator supervision of site staff performing critical study functions). On-site monitoring can therefore be particularly helpful early in a study, especially if the protocol is complex and includes novel procedures with which clinical investigators may be unfamiliar. Findings at the site may lead to training efforts at both the site visited and elsewhere. The on-site monitoring approach is used typically for research INDs but can also be used for commercial INDs.

Centralized monitoring is a remote evaluation performed by sponsor personnel or representatives (e.g., clinical monitors, data management personnel, or statisticians) at a location other than the sites at which the clinical investigation is being conducted. Centralized monitoring processes can provide many of the capabilities of on-site monitoring as well as additional capabilities.

One notable type of monitoring is the site initiation or site initiation visit. The site initiation visit is a critical study activity occurring before study recruitment and often involves sponsor personnel from a range of disciplines, including monitors. Key components of site initiation include ensuring that the clinical investigator and site staff understand their responsibilities: applicable regulatory requirements, study processes and procedures, and the sponsor's processes for monitoring the investigation (*11*).

IND Amendments. For any given IND application, the FDA may receive either a protocol amendment or an information amendment.

Regarding protocol amendments, once an IND application is in effect, the sponsor may amend the application as needed to ensure that the clinical investigations are conducted according to protocols included in the IND application. Sponsors are expected to submit protocol amendments for new protocols or changes to existing protocols before implementation of the respective changes. However, protocol changes intended to eliminate an apparent immediate hazard to human subjects may be implemented immediately, provided that the FDA is subsequently notified by protocol amendment and that the reviewing IRB is also notified. New studies may begin when the sponsor has submitted the change to the FDA for its review and the new protocol or changes to the existing protocol have been approved by the IRB with the responsibility for review and approval of the studies. The general types of protocol amendments are a new protocol, a change in protocol, or a new investigator.

An information amendment is any amendment to an IND application with information essential to the investigational product that is not within the scope of protocol amendments, safety reports, or annual reports. For example, information amendments to IND applications may include new toxicology, chemistry, or other technical information or a report regarding discontinuance of a clinical or nonclinical investigation.

IND Reports. At a minimum, IND safety reports and IND annual reports are required.

Regarding IND safety reports, the IND application sponsors or applicants are required to notify the FDA in a written safety report of any adverse experience associated with the drug that is both serious and unexpected or any findings from tests in laboratory animals that suggest a significant risk for human subjects, including reports of mutagenicity, teratogenicity, and carcinogenicity (*12*).

Regarding IND annual reports, the IND sponsors or applicants are expected to submit brief reports of the progress of the investigations conducted under their respective IND application within 60 d of the anniversary of the date that the application went into effect. An IND annual report is expected to include individual study information (there may be several protocols or studies submitted under one IND; information must be provided for each study), summary information for each protocol or study, an update to the general investigational plan for each protocol or study, an update to the investigator's brochure if applicable, significant protocol updates for each protocol or study, an update on foreign marketing developments, and a log of outstanding business (*13*).

RDRC

Under 21 CFR §361.1, human research using a radioactive drug or biologic product may be conducted under an RDRC and without an IND when that research is basic science research and is not intended for immediate therapeutic, diagnostic, or similar purposes, or to determine the safety and effectiveness of the radioactive drug or biologic product for such purposes (i.e., the research cannot constitute a clinical trial for the product).

Each RDRC must obtain FDA approval before it may approve research studies. Approval of an RDRC will remain in effect unless and until the FDA withdraws such approval. Approval of an RDRC may be withdrawn at any time for failure of the RDRC to comply with the requirements.

The regulations list 3 additional requirements for human subject research that may be conducted under an RDRC.

The first requirement is that the research must be approved by an RDRC that is approved by FDA on the basis of qualified study investigators, a properly licensed medical facility to possess and handle radioactive materials, appropriate selection and consent of research subjects, appropriate quality assurance of the radioactive drug administered, a sound research protocol design, reporting of adverse events by the investigator to the RDRC, and approval by an appropriate IRB.

The second requirement is that the pharmacologic dose of the radioactive drug to be administered must be known not to cause any clinically detectable pharmacologic effect in humans. Investigators must provide pharmacologic dose calculations based on clinical data in the published literature or from other valid human studies to show that the radioactive drug has no clinically detectable pharmacologic effect. This requirement means that RDRC protocols cannot include the use of drugs that have no documented previous human experience.

The third requirement is that the total amount of radiation to be administered as part of the study must be the smallest radiation dose practical to perform the study without jeopardizing the benefits of the study and must be within specified limits. Investigators must provide absorbed radiation dose calculations based on biologic distribution data from published literature or from other valid studies; provide an acceptable method of radioassay of the radioactive drug before its use to ensure that the radioactivity calculations actually reflect the administered activity; provide information demonstrating that the radioactive drug chosen for the study has the half-life, types of radiation emitted, radiation energy, metabolism, and chemical properties that result in the lowest dose to the whole body or specific organs with which it is possible to obtain necessary information; and identify adequate and appropriate instruments for the detection and measurement of the specific radioactive drug (*14*).

Human research under an RDRC must be considered basic science research and be done for the purpose of advancing scientific knowledge. As described in 21 CFR §361.1(a), this type of research differs from a clinical trial to determine safety and efficacy under an IND in several ways. It is intended to obtain basic information on metabolism (including kinetics, distribution, dosimetry, and localization) of a radioactive drug or human physiology, pathophysiology, or biochemistry. It is not intended for immediate therapeutic, diagnostic, or similar purposes to the study subject. It is not intended to determine the safety and effectiveness of a radioactive drug in humans as a therapeutic, diagnostic, or similar type of medical product.

Types of Studies Appropriate for RDRC Approval

The following are examples of types of basic science research that would be appropriate to conduct under an RDRC without an IND.

Metabolism and Excretion Studies. Metabolism and excretion studies usually use nonimaging radionuclides. After administration of the radioactive drug, samples can be obtained at various times from blood, urine, feces, accessible fluid or tissues, and expired gas. Samples can be analyzed to determine the amount, structure, and persistence of the parent molecule and various metabolites formed. Separate studies of metabolism or excretion can be conducted. A combined study is commonly known as a mass balance study. ^{14}C and ^{3}H are most commonly used for these studies, but other radionuclides can also be used, including γ-emitting radionuclides that can be imaged.

Noninvasive Functional Imaging or Molecular Imaging Studies. For most other types of research studies, the radioactive drug is usually selected for its imaging properties (i.e., PET, SPECT, or γ-scintigraphy). The terms *noninvasive functional imaging* and *molecular imaging* are widely used to describe this category of studies, which include the types of studies described in the following paragraphs.

Biodistribution studies investigate the time course for delivery, uptake, and retention of a radioactive drug at various tissue sites in the body. The goal is to determine whether there are any sites in the body at which the radioactive drug is excluded or at which the radioactive drug preferentially accumulates. An understanding of the variation of these processes within the population is often the main objective.

Pathophysiology studies determine whether the presence or absence of pathophysiologic conditions (e.g., preferential uptake or exclusion by tumors compared with adjacent tissues) influences the distribution and persistence of the radioactive drug.

Receptor binding or occupancy studies characterize the kinetics between the radioactive drug and receptors or other binding sites throughout the body and characterize the radioactive drug binding affinity to these receptors. The primary objective is to determine whether localization is specific or nonspecific. In some cases, the observed variation within the population or among populations is a major endpoint. In other studies, the goal may be to develop hypotheses related to disease states, receptor polymorphisms, or therapeutic interventions.

Transport process studies evaluate transport proteins, many of which regulate the extracellular and intracellular distribution of ions and other endogenous compounds in the body, as well as exogenous molecules, such as drugs. Radioactive drugs can be used to determine the relative abundance and specificity of such transporters in various tissues.

Enzyme activity studies use radioactive drugs as molecular probes to determine rates of synthesis or degradation of signaling molecules through enzymes, which help to control the concentrations of critical signaling molecules.

Multistep biochemical process studies evaluate the many biochemical and molecular processes that represent the net effect of a complex array of serial and parallel pathways (*14*).

What Information Must Be Submitted to the RDRC for Review and Approval

Investigators should provide sufficient information to the RDRC so they can determine whether a study meets the conditions of 21 CFR §361.1(b) and does not need an IND. The RDRC should be provided with information on the following topics:

Radiation Dose to Subjects. Limits are provided under 21 CFR §361.1(b) (*3*)(i).

Pharmacologic Dose. Investigators must provide pharmacologic dose calculations based on clinical data in the published literature or from other valid human studies to show that the radioactive drug has no clinically detectable pharmacologic effect.

Consent. Each investigator must select appropriate human subjects and obtain the review and approval of an IRB that conforms to the requirements of 21 CFR §56.

Number of Subjects. The number of research subjects enrolled in a protocol under an RDRC can vary. Many studies under an RDRC start with 30 research subjects or fewer. At the time a research proposal is approved by an RDRC, to allow the exposure of more than 30 subjects the RDRC must submit a special summary of information immediately, but in no later than 7 calendar days, to the FDA.

Women of Childbearing Potential. In 21 CFR §361.1(d) (*5*), it is required that a woman of childbearing potential state in writing that she is not pregnant or that, on the basis of a pregnancy test, she be confirmed as not pregnant, before she may participate in a study under an RDRC.

Pediatric Subjects. Although studies involving pediatric subjects are permissible in special circumstances under §361.1, few pediatric studies have been conducted in recent years under the RDRC mechanism. Section 361.1(d) (*5*) requires that for studies under an RDRC, subjects be at least 18 y of age and legally competent. Exceptions to this rule are permitted only when it can be demonstrated to the RDRC that the study represents a unique opportunity to gain information not currently available or that the study requires the use of research subjects less than 18 y of age and is without significant risk to the subject. When reviewing proposed pediatric studies under an RDRC, the IRB must approve only those studies that meet the criteria in, and satisfy all other requirements of, 21 CFR 50, subpart D.

Quality of Radioactive Drug. All radioactive drugs (PET and non-PET drugs) produced under an RDRC are required to meet appropriate sterility, endotoxin, chemical, pharmaceutical, radiochemical, and radionuclidic standards of identity, strength, quality, and purity as needed for safety and be of such uniform and reproducible quality as to give significance to the research study conducted. To ensure product quality, non-PET radioactive drugs studied under an RDRC must comply with the current good-manufacturing-practice regulations in 21 CFR 210 and 211. PET radioactive drugs must be produced in accordance with the standards under USP Chapter <823>, "Radiopharmaceuticals for PET: Compounding."

Research Protocol. The investigator must provide sufficient information for the RDRC to conclude that scientific knowledge and benefit are likely to result from the study.

Adverse Reactions. The investigator must, within no more than 7 calendar days, report to the RDRC all adverse effects associated with the radioactive drug in the research study. The RDRC must, within no more than 7 calendar days, report to the FDA all adverse reactions probably attributable to the use of the radioactive drug in the research study.

Approval by an IRB. The investigator must obtain IRB approval of the study protocol. Once obtained, proof of IRB

approval must be provided to the RDRC. IRBs are required to conduct continuing review of research at intervals appropriate to the degree of risk, but not less than once a year.

Labeling. The packaging, label, and labeling of the radioactive drug must be compliant with federal, state, and local laws on radioactive materials (*14*).

CONCLUSION

Although clinical research using radiopharmaceuticals may seem daunting to newcomers, one need not be overwhelmed. As this article has shown, a basic knowledge of applicable clinical research regulations, terms, and processes can equip the reader with the necessary resources to ensure safe and effective outcomes.

DISCLOSURE

No potential conflict of interest relevant to this article was reported.

ACKNOWLEDGMENT

We thank SNMMI-TS Fellow LisaAnn Trembath, MSM, NMTCB, from Avid Radiopharmaceuticals for comments on the manuscript.

REFERENCES

1. E6(R2): good clinical practice. International Council for Harmonisation website. https://www.ich.org/page/efficacy-guidelines. Accessed January 27, 2022.
2. Current good manufacturing practice (CBMP) regulations. Food and Drug Administration website. https://www.fda.gov/drugs/pharmaceutical-quality-resources/current-good-manufacturing-practice-cgmp-regulations. Updated September 21, 2020. Accessed January 27, 2022.
3. Development and approval process: drugs. Food and Drug Administration website. https://www.fda.gov/drugs/development-approval-process-drugs. Updated October 18, 2019. Accessed January 27, 2022.
4. Investigator-initiated multi-site clinical trials: frequently asked questions. National Heart, Lung, and Blood Institute website. https://www.nhlbi.nih.gov/grants-and-training/funding-opportunities/foa-Investigator-Initiated-Multi-Site-Clinical-Trials-FAQ#. Accessed January 27, 2022.
5. Guidance for clinical investigators. sponsors, and IRBs: investigational new drug applications (INDs)—determining whether human research studies can be conducted without an IND. Food and Drug Administration website. https://www.fda.gov/media/79386/download. Published September 2013. Accessed January 27, 2022.
6. Investigational new drug (IND) application. Food and Drug Administration website. https://www.fda.gov/drugs/types-applications/investigational-new-drug-ind-application. Updated February 24, 2021. Accessed January 27, 2022
7. Expanded access to investigational drugs for treatment use: questions and answers—guidance for industry. Food and Drug Administration website. https://www.fda.gov/media/85675/download. Published June 2016. Updated October 2017. Accessed January 27, 2022.
8. Guidance for industry, investigators, and reviewers: exploratory IND studies. Food and Drug Administration website. https://www.fda.gov/media/72325/download. Published January 2006. Accessed January 27, 2022.
9. Guidance for industry: formal meetings between the FDA and sponsors or applicants. Food and Drug Administration website. https://www.fda.gov/media/72253/download. Published May 2009. Accessed January 27, 2022.
10. Guidance for industry: submitting and reviewing complete responses to clinical holds. Food and Drug Administration website. https://www.fda.gov/media/72548/download. Published October 2000. Accessed January 27, 2022.
11. Guidance for industry: oversight of clinical investigations—a risk-based approach to monitoring. Food and Drug Administration website. https://www.fda.gov/media/116754/download. Published August 2013. Accessed January 27, 2022.
12. IND application reporting: safety reports. Food and Drug Administration website. https://www.fda.gov/drugs/investigational-new-drug-ind-application/ind-application-reporting-safety-reports. Updated October 19, 2021. Accessed January 27, 2022.
13. IND application reporting: annual reports. Food and Drug Administration website. https://www.fda.gov/drugs/investigational-new-drug-ind-application/ind-application-reporting-annual-reports. Updated December 23, 2015. Accessed January 27, 2022.
14. Guidance for industry and researchers: the radioactive drug research committee—human research without an investigational new drug application. Food and Drug Administration website. https://www.fda.gov/media/80097/download. Published August 2010. Accessed January 27, 2022.

Radiation Safety Considerations and Clinical Advantages of α-Emitting Therapy Radionuclides

Brian Serencsits[1], Bae P. Chu[1], Neeta Pandit-Taskar[2], Michael R. McDevitt[2], and Lawrence T. Dauer[1]

[1]*Department of Medical Physics, Memorial Sloan Kettering Cancer Center, New York, New York; and* [2]*Department of Medical Physics, Memorial Sloan Kettering Cancer Center, New York, New York*

CE credit: For CE credit, you can access the test for this article, as well as additional *JNMT* CE tests, online at https://www.snmmilearningcenter.org. Complete the test online no later than March 2025. Your online test will be scored immediately. You may make 3 attempts to pass the test and must answer 75% of the questions correctly to receive Continuing Education Hour (CEH) credit. Credit amounts can be found in the SNMMI Learning Center Activity. SNMMI members will have their CEH credit added to their VOICE transcript automatically; nonmembers will be able to print out a CE certificate upon successfully completing the test. The online test is free to SNMMI members; nonmembers must pay $15.00 by credit card when logging onto the website to take the test.

α-emitting radionuclides provide an effective means of delivering large radiation doses to targeted treatment locations. $^{223}RaCl_2$ is Food and Drug Administration–approved for treatment of metastatic castration-resistant prostate cancer, and ^{225}Ac (^{225}Ac-lintuzumab) radiolabeled antibodies have been shown to be beneficial for patients with acute myeloid leukemia. In recent years, there has been increasing use of α-emitters in theranostic agents with both small- and large-molecule constructs. The proper precautionary means for their use and surveying documentation of these isotopes in a clinical setting are an essential accompaniment to these treatments. **Methods:** Patient treatment data collected over a 3-y period, as well as regulatory requirements and safety practices, are described. Commonly used radiation instruments were evaluated for their ability to identify potential radioactive material spills and contamination events during a clinical administration of ^{225}Ac. These instruments were placed at 0.32 cm from a 1.0-cm ^{225}Ac disk source for measurement purposes. Radiation background values, efficiencies, and minimal detectable activities were measured and calculated for each type of detector. **Results:** The median external measured dose rate from $^{223}RaCl_2$ patients ($n = 611$) was 2.5 μSv h^{-1} on contact and 0.2 μSv h^{-1} at 1 m immediately after administration. Similarly, ^{225}Ac-lintuzumab ($n = 19$) patients had median external dose rates of 2.0 μSv h^{-1} on contact and 0.3 μSv h^{-1} at 1 m. For the measurement of ^{225}Ac samples, a liquid scintillation counter was found to have the highest overall efficiency (97%), whereas a ZnS α-probe offered the lowest minimal detectable activity at 3 counts per minute. **Conclusion:** In this article, we report data from 630 patients who were undergoing treatment with the α-emitting isotopes ^{223}Ra and ^{225}Ac. Although α-emitters have the ability to deliver a higher internal radiation dose to the exposed tissues than can other unsealed radionuclides, they typically present minimal concerns about external dose rate. Additionally, α-radiation can be efficiently detected with appropriate radiation instrumentation, such as a liquid scintillation counter or ZnS probe, which should be prioritized when surveying for spills of α-emitters.

Key Words: α-emitters; actinium; radium; nuclear medicine; radiation efficiency

Received Apr. 19, 2021; revision accepted Sep. 26, 2021.

For correspondence or reprints, contact Brian Serencsits (serencsb@mskcc.org).

Published online Nov. 8, 2021.

J Nucl Med Technol 2022; 50:10–16
DOI: 10.2967/jnmt.121.262294

Radionuclides that are α-emitters offer a unique and effective way of treating various types of cancer by delivering a high–linear-energy-transfer focal radiation deposition to a treatment site. The physical characteristics of high particle energy, often 5–9 MeV, and a short (<100 μm) particle range in tissue make α-emitting radionuclides attractive sources to deliver large radiation doses to targeted tissues (*1*). α-particles create dense ionization tracks that can produce multiple damages to the DNA, resulting in less repairable double-strand break damage (*2,3*). This ability allows radiopharmaceutical carriers of α-emitting radionuclides to produce efficient cell death in targeted tumor cells while sparing untargeted normal healthy tissues beyond the range of the α-emissions (*4,5*).

Certain α-emitting radionuclides, such as ^{223}Ra, ^{225}Ac, and ^{227}Th, are part of a radioactive decay chain with multiple α-particle emissions that result in a total emission energy per decay that is typically 2 orders of magnitude higher than for conventional β-particle theranostics. This characteristic provides an advantage for clinical applications because the necessary administered activities for effective therapy are hundreds of times less than their β-particle or photon-emitting counterparts (*6*). Therefore, the radiation exposure rates due to particle and photon emissions from an α-emitting radionuclide's progeny pose little to no external concern and are not a safety-limiting factor at the submillicurie quantities used in clinical practice. This ability to deliver smaller activities, with minimal radiation exposure concern, allows α-emitting radionuclides to be advantageous for radiation safety considerations, encompassing both occupational staff exposure and adherence to patient release criteria at the federal and state levels.

Initially used in 1912 for the treatment of ankylosing spondylitis, ^{224}Ra was the first α-emitting radionuclide to

be used in a clinical application (*7*). However, it was not until much later, in 2013, that $^{223}RaCl_2$, now produced by Bayer Pharmaceuticals under the name Xofigo, became the first Food and Drug Administration–approved α-emitting radionuclide therapy for the treatment of prostate cancer with metastatic bone lesions (*8*). More recently, other α-emitters, such as ^{225}Ac and ^{227}Th, have begun to see expanded use in clinical trials. ^{227}Th is produced by the decay of the long-lived parent isotope ^{227}Ac through the same processes already used for its decay product, ^{223}Ra (*9*). Found naturally in the neptunium decay series seen in Figure 1, the current supply of ^{225}Ac comes from fissile ^{233}U and its decay product ^{229}Th, which were first produced during investigation into nuclear weapons and reactors (*10*). ^{225}Ac can be separated and purified from ^{229}Th through a combination of ion exchange and extraction chromatographic methods (*11*). Alternative methods to produce ^{225}Ac have been explored, the most promising being a $^{226}Ra(p,2n)^{225}Ac$ reaction, which has not been widely used but is being further explored (*12*).

Three α-emitting radionuclides currently in use at Memorial Sloan Kettering Cancer Center under specific institutional protocols will be addressed in this paper; these include $^{223}RaCl_2$ for metastatic castration-resistant prostate cancer, ^{225}Ac monoclonal antibody lintuzumab for acute myeloid leukemia, and the recently initiated ^{227}Th-labeled antibody–chelator conjugate BAY 2701439 (Bayer) for targeting tumors expressing human epidermal growth factor receptor 2. $^{223}RaCl_2$ has been used for treatment of symptomatic patients with metastatic castration-resistant prostate cancer, and its use has resulted in an overall improvement in quality of life and increased length of overall survival (*13,14*). Although the therapeutic efficacy of ^{225}Ac, with a half-life of 10 d, is still in the early research stages, ^{213}Bi, the final radioactive daughter product in the decay chain, has been used in clinical trials and shown to be safe and therapeutically efficacious in patients with acute myeloid leukemia (*15*).

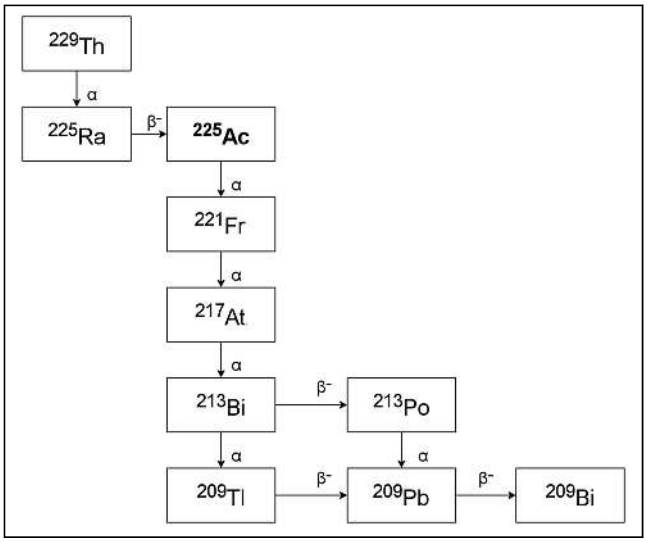

FIGURE 1. Decay of ^{225}Ac via neptunium series.

Here, we provide an overview of our experience using α-emitting radionuclides in current and recently completed clinical trials, with a focus on the preparation, administrative procedures, radiation safety precautions, and regulatory requirements that must be met to safely administer α-emitting radionuclides in a clinical setting. In addition, radiation detection equipment is evaluated to see the varying effectiveness for monitoring the α-emitter ^{225}Ac in the clinical setting, to help guide individuals on the proper selection of survey equipment.

MATERIALS AND METHODS

Regulatory Framework

When preparing to administer α-emitting radionuclides, an institution must first fulfil regulatory requirements. The U.S. Nuclear Regulatory Commission offers guidance documents on the types of precautions and instrumentation that must be present for proper administration of α-emitting radionuclides. These documents will be addressed alongside perspectives from groups such as the International Commission on Radiation Protection, the National Council on Radiation Protection and Measurements, and the National Research Council.

Many general broad-scope radioactive material licenses for medical use include only "any byproduct material with atomic numbers 1 through 83" as designated by regulation 1,556, volume 11, of the U.S. Nuclear Regulatory Commission (*16*). Most α-emitting radionuclides, including all those discussed in this paper, have an atomic number greater than 83 and must be specifically documented on a radioactive material license. The maximum possession amount should be estimated from the proposed patient load, estimated activity needed per patient, and waste storage capabilities.

Training required by the Nuclear Regulatory Commission for an authorized user to administer unsealed byproduct material can be found in title 10, part 35, subpart E, of the *Code of Federal Regulations*; included are items related to education, training and experience, and board certification (*17*). For individuals to become authorized users, they must also be approved by an institution's internal radiation safety committee. In addition to approving authorized users for the administration of radioactive materials, the most important part of the radiation safety committee's job is to instill a proper safety culture in staff members' daily routine and make safety the top priority (*18*). This task can be accomplished through a plethora of means, such as a robust radiation safety training program, proper workflow processes, and widespread monitoring and self-auditing practices.

Overview of α-Emitting Radionuclide Therapy

In a review of applicable α-emitting radionuclide protocols at Memorial Sloan Kettering Cancer Center, all radionuclides were administered according to vendor or internal protocol recommendations. $^{223}RaCl_2$ was administered as a slow bolus intravenous injection over 3–5 min, whereas ^{225}Ac- and ^{227}Th-labeled antibodies were administered over a 15- to 30-min infusion. All 3 protocols have completed, or plan to complete, a dose escalation or expansion study to determine dose-limiting patient toxicity levels. The results of the completed dose escalation studies are shown in Table 1. As shown, $^{223}RaCl_2$ and ^{225}Ac treatment activities were based on patient weight, whereas planned ^{227}Th doses were based strictly on fixed activity levels.

Treatment Preparation

The requirements for the administration of radioactive materials will vary widely depending on the type of radioactive material being administered. For staff directly handling these radionuclides, procedures such as the use of long-handled tools or shielded syringes may be applied to help minimize extremity radiation exposure but are often unnecessary for the lower activities being used. Before treatment, α-emitting radionuclides should be stored such that both the β-radiation and the photon radiation are reasonably shielded. The α-emitters are stored in either Plexiglas or lead, depending on the isotope. ^{223}Ra Xofigo is shipped (and stored) as unit dose syringes in a self-made container (Xofigo Plastic Pig [XPP]; Cardinal Health), remaining in the container until the syringe is removed by the nuclear medicine physician for treatment. ^{225}Ac and ^{227}Th are shipped (and stored) in a small lead container from the vendors. The isotopes are diluted in-house and are placed in a plastic syringe. Once in the syringe, they are placed under 1/8″ lead sheet until administered by the physician.

Because of minimal external dose-rate readings, patients may be treated in locations without lead shielding or other radiation-limiting interventions. Most treatments using α-emitting radionuclides involve either an injection or an infusion of radioactive material through a syringe, allowing for a closed system that delivers radioactive materials directly into the bloodstream to limit the risk of contamination events or radiation exposure to staff members. Since α-particles are of great concern for inhalation and ingestion, proper care should be taken to mitigate the risk of these intake pathways. Proper personal protective equipment, such as gloves (double preferred) and laboratory coats, should always be worn by staff administering α-emitting radionuclides. Absorbent pads should be placed around the injection or infusion site to mitigate the risk of spreading contamination in the event of a spill.

Special Considerations

Needle sticks and skin contamination during treatments are considered special events and must be treated promptly and properly because of possible intake of radioactive material. Rapid cleaning of the area and continual monitoring must be performed. Methods for evaluating radioactive material intake (i.e., bioassay) and the need for further investigation are described in Nuclear Regulatory Commission regulatory guide 8.9. In special monitoring situations, suspected intake of material must be evaluated with a scope commensurate with the potential risk (*19*).

If radioactive material intake is suspected, a bioassay test is the preferred method for estimating the amount of material ingested or inhaled. A single 24-h biospecimen sample may be sufficient, but regular daily measurements could be needed for higher intakes. For α-emitting radionuclides, including all 3 of those reviewed here, fecal bioassays are preferred since feces contain a larger percentage of the excreta than does urine (*20*). Intake retention functions can be used to estimate the total intake of radioactive material, which can then determine the cumulative total internal dose (committed effective dose equivalent) to a staff member. This is done using the values from title 10, part 20, appendix B, of the *Code of Federal Regulations* for the appropriate annual limits on intake value for each isotope, as well as any necessary tissue weighting factors from International Commission on Radiological Protection publication 103 (*21,22*). The committed effective dose equivalent, added to any external occupational exposure, is called the total effective dose equivalent for an individual and carries a limit of 5,000 mrem annually in the United States. Equation 1 calculates the occupational dose from internal exposures (committed effective dose equivalent). The annual limit on intake values is the amount of radioactive material that would need to be inhaled or ingested to reach the annual occupational

TABLE 1
Memorial Sloan Kettering Cancer Center α-Emitting Radionuclide Dose Escalation and Expansion Clinical Protocols

Radionuclide	Activity administered (kBq kg^{-1})	Total treatment cycles	Period between cycles (wk)
^{223}Ra			
Phase 1.1	50	1	NA
Phase 1.2	100	1	NA
Phase 1.3	200	1	NA
Phase 2	50	6	4
Phase 3	50	6	4
NIST-adjusted Xofigo	55	6	4
^{225}Ac			
Phase 1.1	18.5	1	NA
Phase 1.2	37	1	NA
Phase 1.3	74	1	NA
Phase 1.4	148*	1	NA
Phase 1.5	111	1	NA
^{227}Th (in progress)			
Phase 1.1	1,500 kBq†	4	6
Phase 1.2	2,500 kBq†	4	6
Phase 1.3	3,500 kBq†	4	6
Phase 1.4	4,500 kB†	4	6
Phase 1.5	6,000 kBq†	2	6
	Additional 25% increase	2	6

*Dose-limiting toxicity seen at phase 1.4.
†Patients receiving ^{227}Th receive fixed dose values instead of weight-based doses.
NA = not applicable; NIST = National Institute of Standards and Technology.

dose limit for a radiation worker without any other exposure, with examples shown in Table 2.

$$\text{Committed effective dose equivalent} = \text{intake} \times \frac{\text{occupational dose limit}}{\text{appropriate annual limits on intake}} \times \text{tissue weighting factor.} \quad \text{Eq. 1}$$

Contamination Survey Instrumentation

Regular surveying practices, proper radiation instrumentation, and methods for decontamination should always be present during radioactive material administration. An α-probe, such as a ZnS scintillation detector or a similar device, may be preferable to a standard Geiger–Müller (GM) detector for the detection of α-emitting radionuclides. α-probes can filter out the measurement of β-particles or photons, allowing them to have lower background levels of radiation and a subsequently lower minimal detectable activity (MDA). In addition, the mica film on the outside of a standard GM detector makes direct measurement of α-particles difficult and inefficient but still possible if the film is less than approximately 7 mg cm^{-2} (*23*). Such a film filters out most low-energy α-particles and leads to a lower efficiency for those that can be measured. Coupled with a higher background reading, such filtering increases the difficulty of detecting small amounts of α-emitting radionuclides with a standard GM detector. Instead, GM detectors focus on measuring the associated β-particle and photon emissions from daughter nuclei. Although GM detector efficiency can reach about 33% for high-energy β-particles, photon efficiencies are generally poor and often less than 1% for low-energy photons such as those produced by ^{99m}Tc or ^{125}I (*24*). A low MDA, and reasonable efficiency, are crucial for measuring the low levels of surface contamination needed to meet regulatory requirements such as the 1,000 disintegrations/(min * 100 cm^2) combined activity for most α-emitters (*25*).

Radiation Instrumentation Statistics

^{223}Ra efficiencies, MDA levels, dose rates, and decay pathways were previously examined, in detail, by Dauer et al. (*26*). The decay pathway for ^{223}Ra via the actinium decay series can be seen in Figure 2. ^{225}Ac has a decay pathway similar to that of ^{223}Ra, which contains a mixture of different decay modalities, including both α- and β-decay (*27*). A net value of 4 primary α-particle decays, 2 primary β-particles, and numerous γ-ray emissions is present in the decay process between radioactive ^{225}Ac and stable ^{209}Bi. The effectiveness of various radiation detection equipment for ^{225}Ac was measured experimentally by dissolving solid actinium nitrate in a 0.1 M HCl solution. The solution was then diluted and pipetted onto a 1.0-cm-diameter filter disk. Before application, the ^{225}Ac used in this process was decayed in storage to ensure secular equilibrium with daughter products, a process that takes approximately 24 h (*28*). Portable instrumentation was placed in a repeatable geometry in which the detector face was 0.32 cm from the filter disk. These radiation detectors were connected to an integrating scaler configured to accumulate counts for 1 min, and the measurement was repeated 10 times for both background and source counts. Stand-alone instrumentation, such as that used for wipe tests, was adjusted to count for 10 min for both sample and background counts. Efficiencies for each instrument were calculated by the measured count rates divided by the dose-calibrated activity. MDA was subsequently calculated using Equation 2 with the empirically determined conversion factor from dpm to other desired activity unit, if applicable (*C*), efficiencies (*E*), background count rates (R_b), source count times (t_s), background count times (t_b), and constant value, k_1, of 1.645 representing a 1-sided 95% CI (*29*).

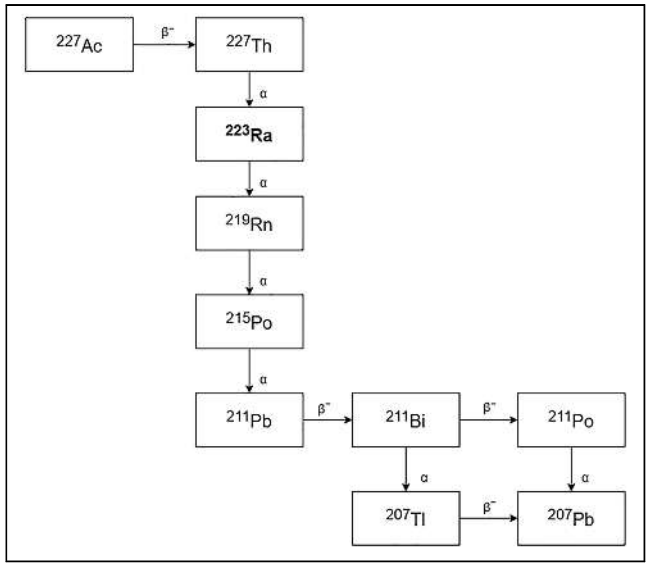

FIGURE 2. Decay of ^{223}Ra via actinium series.

$$\text{MDA} = \frac{k_1{}^2 + 2k_1\sqrt{R_b t_s\left(1+\frac{t_s}{t_b}\right)}}{t_s \text{ E C}}. \quad \text{Eq. 2}$$

The portable survey detectors used for efficiency and MDA testing were a ZnS α-probe (model 43-2; Ludlum), a thin windowed GM probe (model 44-9; Ludlum), and an NaI low-energy γ-probe (model 44-3; Ludlum). These portable detectors are used for real-time measurements and personnel surveys at the site of use. Stand-alone ionizing-radiation spectrometers such as a liquid scintillation counter (model TriCarb 2900TR; Perkin Elmer) and a γ-counter (Wizard2; Perkin Elmer) were also tested. These stand-alone detectors are often used for quantifying removable contamination survey results for documentation purposes. ^{225}Ac, used for efficiency measurements, was supplied by the U.S. Department of Energy, Oak Ridge National Laboratory. Values for the efficiencies of various radiation instrumentation, and their associated MDAs, for ^{225}Ac are examined in more detail in Table 3.

TABLE 2
Restrictive Annual Limit on Intake Values for Select α-Emitting Radionuclides and Radionuclides in Common Medical Use

Radionuclide	Decay mode	Restrictive annual limit on intake (MBq)
^{18}F	β	1,850
^{99m}Tc	IT	2,960
^{131}I	β	1.11
^{223}Ra	α	0.026
^{225}Ac	α	0.011
^{227}Th	α	0.011

TABLE 3
Removable Contamination Efficiencies and MDAs for Commonly Used Radiation Detection Equipment Integrated over 1-Minute Count Time for ^{225}Ac

Instrument	Background (cpm)	Efficiency (cpm/dpm)	MDA	
			dpm	Bq
Portable survey meters				
α-probe (ZnS)	0	0.07	3	0.05
Thin window β-/γ-probe (GM)	33	0.18	147	2.47
Low-energy γ-probe (NaI)	234	0.06	1,128	18.82
Radiometric detectors				
Liquid scintillation counter	36	0.97	13	0.22
γ-counter	288	0.13	547	9.13

cpm = counts per minute; dpm = disintegrations per minute.

RESULTS

Treatment Data and Precautions

Administrations of $^{223}RaCl_2$ ($n = 611$) and ^{225}Ac-lintuzumab ($n = 19$) to patients were reviewed for various safety considerations. The median age of $^{223}RaCl_2$ patients was 72.26 y ± 8.93 y (range, 46.53–92.94 y), with administered activities of 4.81 ± 0.95 MBq. The median age of ^{225}Ac-lintuzumab patients was 77.90 y ± 9.72 y (range, 56.35–87.60 y), with administered activities of 3.00 ± 1.68 Bq. Radiation doses to members of the staff and the public from patients receiving either $^{223}RaCl_2$ or ^{225}Ac-lintuzumab were considered minimal. $^{223}RaCl_2$ dose-rate readings were minimal, with a median of 2.5 ± 0.07 μSv h^{-1} on contact (i.e., on the external surface of the patient's body; external dose-rate readings for these patients were taken near the heart due to intravenous injections and infusions yielding the highest results there). Likewise, ^{225}Ac-lintuzumab had similar readings of 1.7 ± 1.2 μSv h^{-1} on contact. All activity and dose-rate readings were taken with ionization chambers immediately after the therapy.

Radiation Detector Measurements

Radiation detection equipment was evaluated to determine detector efficiency, MDAs, and the feasibility of use during administrations of ^{225}Ac. The data for an unshielded radioactive source of ^{225}Ac are summarized in Table 3. MDAs were calculated with a k_1 value of 1.645, representative of the 95% CI. Efficiency levels were calculated and rounded to the nearest whole percentage point.

DISCUSSION

External exposure rates for patients receiving α-emitting radionuclides were found to be low, as expected. With median dose rates of less than 0.5 μSv h^{-1} at a 1-m distance, patients may return to their regular lifestyle immediately after treatment, without radiation precautions. This advantage allows for effective treatment while avoiding some common precautions needed for other types of radiopharmaceutical treatments. Low external dose rates also allow for better patient care by staff members by removing the constraints and limitations of occupational radiation exposure. Specimens containing bodily fluids should continue to be handled with care by staff members to avoid accidental intake of the radioactive material.

Because of low external dose rates, no patient—under reasonable assumptions—will subject a member of the public to 1 mSv of radiation exposure, the necessary requirement for the release of patients administered radioactive materials as designated by Regulatory Guide 8.39 of the U.S. Nuclear Regulatory Commission (*30*). Instructions for the proper control of bodily fluids were given to minimize the risk—to the public or members of the household—of receiving a dose from accidental ingestion of material after patient release, as seen in Figure 3. The instructions include sitting while urinating or defecating, properly washing the hands after encountering any bodily fluids, promptly cleaning any vomitus or bodily fluid spills, and using a condom during sexual intercourse. The instructions are given for 1 wk after therapy, though data suggest that most excretion of radioactive material occurs within the first 72 h (*31*). Beyond this point, the amount of radioactive material remaining is inconsequential to the overall dose received by the public.

From a radiation detection standpoint, as shown in Table 3, there are advantages and disadvantages to different radiation detectors. α-probes offer the best mix of efficiency, low background, and low MDA for surveillance purposes—because of the sulfide's ability to filter out non–α-radiation—which allows for a near-zero background. The extremely low background allows even the smallest amount of radioactive material to be detected by the scintillator, as is helpful in slight-contamination events. Liquid scintillation counters also offer desirable results but not necessarily the rapid results needed during regular administrations and surveys; they also come with both a higher initial cost and higher upkeep expenses. The data show that a GM detector offers higher efficiency than a ZnS α-probe but also a higher MDA

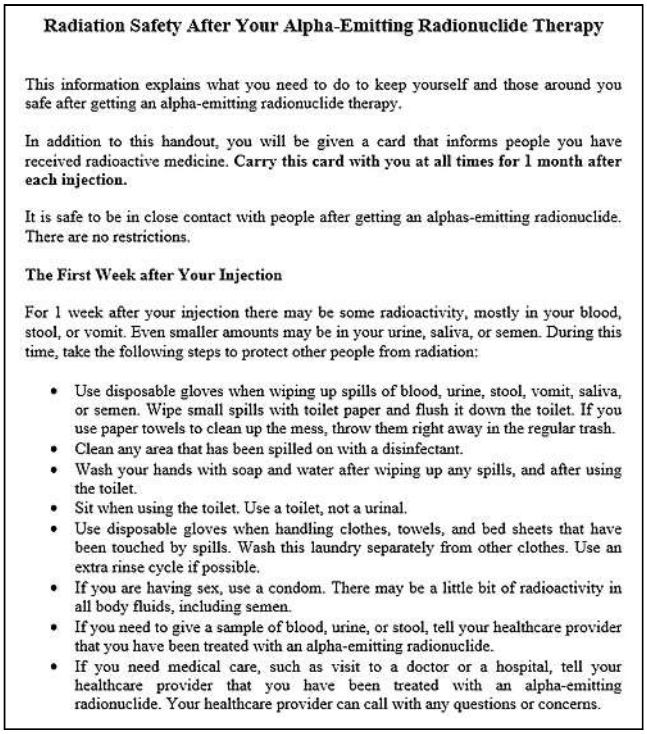

Radiation Safety After Your Alpha-Emitting Radionuclide Therapy

This information explains what you need to do to keep yourself and those around you safe after getting an alpha-emitting radionuclide therapy.

In addition to this handout, you will be given a card that informs people you have received radioactive medicine. **Carry this card with you at all times for 1 month after each injection.**

It is safe to be in close contact with people after getting an alphas-emitting radionuclide. There are no restrictions.

The First Week after Your Injection

For 1 week after your injection there may be some radioactivity, mostly in your blood, stool, or vomit. Even smaller amounts may be in your urine, saliva, or semen. During this time, take the following steps to protect other people from radiation:

- Use disposable gloves when wiping up spills of blood, urine, stool, vomit, saliva, or semen. Wipe small spills with toilet paper and flush it down the toilet. If you use paper towels to clean up the mess, throw them right away in the regular trash.
- Clean any area that has been spilled on with a disinfectant.
- Wash your hands with soap and water after wiping up any spills, and after using the toilet.
- Sit when using the toilet. Use a toilet, not a urinal.
- Use disposable gloves when handling clothes, towels, and bed sheets that have been touched by spills. Wash this laundry separately from other clothes. Use an extra rinse cycle if possible.
- If you are having sex, use a condom. There may be a little bit of radioactivity in all body fluids, including semen.
- If you need to give a sample of blood, urine, or stool, tell your healthcare provider that you have been treated with an alpha-emitting radionuclide.
- If you need medical care, such as visit to a doctor or a hospital, tell your healthcare provider that you have been treated with an alpha-emitting radionuclide. Your healthcare provider can call with any questions or concerns.

FIGURE 3. Example of radiation safety precautions for patients receiving α-emitting therapies.

because of higher background radiation levels. With MDAs below those used for regulatory purposes for most α-emitters, a GM detector may be a suitable alternative for a program because of cost and availability. Larger survey areas and longer count times can always be implemented to help lower a detector's MDA when needed. Low-energy scintillation probes and γ-counters should not be used to measure for α-emitting radionuclides since their MDA may be near or above the surface contamination levels that require remediation under normal circumstances.

CONCLUSION

There has been a growth of interest in, and use of, α-emitting radionuclides in the treatment of cancer because of their higher radiotoxicity per unit of administered activity relative to radionuclides emitting β-, γ-, or x-rays. With robust administrative and engineering controls, α-emitting radionuclides can be handled and administered safely for clinical use. Proper personal protective equipment, training techniques, and radiation detection instrumentation are crucial for reducing contamination events and protecting the clinical staff and the public. Patient release instructions for α-emitters can be limited to only hygiene precautions to prevent the accidental inhalation or ingestion of radioactive material by another individual. This policy allows patients to resume their everyday lives free of the external radiation restrictions that may accompany other radionuclide therapies. With all their advantages, α-emitting radionuclides continue to be a leading option in radionuclide therapy and can be safely administered.

DISCLOSURE

This research was funded in part through the NIH/NCI Cancer Center support grant P30 CA008748. No other potential conflict of interest relevant to this article was reported.

KEY POINTS

QUESTION: Are current patient precautions and radiation survey equipment sufficient for safe and compliant radionuclide therapies containing α-emitting radionuclides?

PERTINENT FINDINGS: External dose-rate readings from patients receiving radioactive materials continue to be low in clinical trials and Food and Drug Administration–approved treatments. Radiation detection equipment such as ZnS detectors and liquid scintillation detectors are preferable to the more commonly used GM counter.

IMPLICATIONS FOR PATIENT CARE: Radiation safety precautions for patients receiving α-emitting radionuclide therapy can continue to include only hygiene-related precautions for ^{225}Ac and ^{227}Th while maintaining compliance with federal guidance and regulations.

REFERENCES

1. Humm JL. Dosimetric aspects of radiolabeled antibodies for tumor therapy. *J Nucl Med.* 1986;27:1490–1497.
2. Graf F, Fahrer J, Maus S, et al. DNA double strand breaks as predictor of efficacy of the alpha-particle emitter Ac-225 and the electron emitter Lu-177 for somatostatin receptor targeted radiotherapy. *PLoS One.* 2014;9:e88239.
3. Nikula TK, McDevitt MR, Finn RD, et al. Alpha-emitting bismuth cyclohexylbenzyl DTPA constructs of recombinant humanized anti-CD33 antibodies: pharmacokinetics, bioactivity, toxicity and chemistry. *J Nucl Med.* 1999;40:166–176.
4. Jurcic JG, Rosenblat TL. Targeted alpha-particle immunotherapy for acute myeloid leukemia. *Am Soc Clin Oncol Educ Book.* 2014;e126–e131.
5. Humm JL, Sartor O, Parker C, Bruland OS, Macklis R. Radium-223 in the treatment of osteoblastic metastases: a critical clinical review. *Int J Radiat Oncol Biol Phys.* 2015;91:898–906.
6. Sgouros G. Dosimetry of internal emitters. *J Nucl Med.* 2005;46(suppl 1):18S–27S.
7. Fisher DR. Alpha particle emitters in medicine. Presented at: Conference on Dosimetry of Administered Radionuclides; September 21–22, 1989; Washington, DC.
8. Makvandi M, Dupis E, Engle JW, et al. Alpha-emitters and targeted alpha therapy in oncology: from basic science to clinical investigations. *Target Oncol.* 2018;13:189–203.
9. Abou DS, Pickett J, Mattson JE, Thorek DLJA. Radium-223 microgenerator from cyclotron-produced trace actinium-227. *Appl Radiat Isot.* 2017;119:36–42.
10. Alvarez R. Managing the uranium-233 stockpile of the United States. *Sci Glob Secur.* 2013;21:53–69.
11. Scheinberg DA, McDevitt MR. Actinium-225 in targeted alpha-particle therapeutic applications. *Curr Radiopharm.* 2011;4:306–320.
12. Apostolidis C, Molinet R, McGinley J, Abbas K, Mollenbeck J, Morgenstern A. Cyclotron production of Ac-225 for targeted alpha therapy. *Appl Radiat Isot.* 2005;62:383–387.
13. Terrisse S, Karamouza E, Parker CC, et al. Overall survival in men with bone metastases from castration-resistant prostate cancer treated with bone-targeting radioisotopes: a meta-analysis of individual patient data from randomized clinical trials. *JAMA Oncol.* 2020;6:206–216
14. Dizdarevic S, Jessop M, Begley P, Main S, Robinson A. ^{223}Ra-dichloride in castration-resistant metastatic prostate cancer: improving outcomes and identifying predictors of survival in clinical practice. *Eur J Nucl Med Mol Imaging.* 2018;45:2264–2273.
15. Rosenblat TL, McDevitt MR, Mulford DA, et al. Sequential cytarabine and alpha-particle immunotherapy with bismuth-213-lintuzumab (HuM195) for acute myeloid leukemia. *Clin Cancer Res.* 2010;16:5303–5311.
16. *Consolidated Guidance About Materials Licenses: Program-Specific Guidance About Licenses of Broad Scope—Final Report (NUREG-1556).* Vol 11, revision 1. Office of Nuclear Material Safety and Safeguards; 2017.

17. Medical uses of byproduct material. In: *Code of Federal Regulations.* Title 10, part 35. U.S. Nuclear Regulatory Commission; 2008.
18. Yonekura Y, Mattsson S, Flux G, et al. ICRP publication 140: radiological protection in therapy with radiopharmaceuticals. *Ann ICRP.* 2019;48:5–95.
19. *Regulatory Guide 8.9: Acceptable Concepts, Models, Equations, and Assumptions for a Bioassay Program*. U.S. Nuclear Regulatory Commission; 1993.
20. *Interpretation of Bioassay Measurements (NUREG/CR-4884)*. U.S. Nuclear Regulatory Commission; 1987.
21. Part 20: standards for protection against radiation. U.S. Nuclear Regulatory Commission website. http://www.nrc.gov/reading-rm/doc-collections/cfr/part020. Updated March 24, 2021. Accessed January 14, 2022.
22. ICRP. The 2007 recommendations of the International Commission on Radiological Protection: ICRP publication 103. *Ann ICRP.* 2007;37:1–332.
23. Steinmeyer P. G-M pancake detectors: everything you've wanted to know (but were afraid to ask). *RSO Magazine.* 2005; 10:7–17.
24. Knoll G. *Radiation Detection and Measurement.* Vol. 4. Wiley; 2010:218–219.
25. *Consolidated Guidance About Materials Licenses: Program-Specific Guidance About Medical Use Licenses (NUREG-1556)*. Vol 9, revision 2. U.S. Nuclear Regulatory Commission; 2008.
26. Dauer LT, Williamson MJ, Humm J, et al. Radiation safety considerations for the use of $^{223}RaCl_2$ DE in men with castration-resistant prostate cancer. *Health Phys.* 2014;106:494–504.
27. Robertson AKH, Ramogida CF, Schaffer P, Radchenko V. Development of ^{225}Ac radiopharmaceuticals: TRIUMF perspectives and experiences. *Curr Radiopharm.* 2018;11:156–172.
28. Pandya DN, Hantgan R, Budzevich MM, et al. Preliminary therapy evaluation of ^{225}Ac-DOTA-c(RGDyK) demonstrates that Cerenkov radiation derived from ^{225}Ac daughter decay can be detected by optical imaging for in vivo tumor visualization. *Theranostics.* 2016;6:698–709.
29. Attachment I: counting statistics for laboratory and portable instruments. U.S. Nuclear Regulatory Commission website. https://www.nrc.gov/docs/ML1101/ML110100788.pdf. Published January 2011. Accessed January 14, 2022.
30. Regulatory guide 8.39: release of patients administered radioactive materials. U.S. Nuclear Regulatory Commission website. https://www.nrc.gov/docs/ML0833/ML083300045.pdf. Published April 1997. Accessed January 14, 2022.
31. Yoshida K, Kaneta T, Takano S, et al. Pharmacokinetics of single dose radium-223 dichloride (BAY 88-8223) in Japanese patients with castration-resistant prostate cancer and bone metastases. *Ann Nucl Med.* 2016;30:453–460.

PET/MRI, Part 3: Protocols and Procedures

Elad Nevo[1], Peter Kamvosoulis[2], and Geoff Currie[3,4]

[1]Department of Radiology, Lucille Packard Children's Hospital, Stanford University, Palo Alto, California; [2]Magnetic Resonance Department, New York–Presbyterian/Weill Cornell Medical Center, New York, New York; [3]School of Dentistry and Health Science, Charles Sturt University, Wagga Wagga, New South Wales, Australia; and [4]Department of Radiology, Baylor College of Medicine, Houston, Texas

CE credit: For CE credit, you can access the test for this article, as well as additional *JNMT* CE tests, online at https://www.snmmilearningcenter.org. Complete the test online no later than March 2025. Your online test will be scored immediately. You may make 3 attempts to pass the test and must answer 75% of the questions correctly to receive Continuing Education Hour (CEH) credit. Credit amounts can be found in the SNMMI Learning Center Activity. SNMMI members will have their CEH credit added to their VOICE transcript automatically; nonmembers will be able to print out a CE certificate upon successfully completing the test. The online test is free to SNMMI members; nonmembers must pay $15.00 by credit card when logging onto the website to take the test.

The emergence of PET and MRI as a hybrid modality has demanded new approaches to protocols and procedures. Although protocols for MRI and PET individually lend themselves to synergistic and simultaneous approaches, there are a number of unique challenges and patient preparations that require consideration. This article provides insight into the protocols, procedures, and challenges associated with simultaneous PET/MRI in both adult and pediatric populations. Although protocols may be specific to applications or pathologies of interest, a richer discussion of the clinical applications of PET/MRI is beyond the scope of this article and will be detailed in part 4 of the series. The foundation of PET/MRI protocols is an understanding of the various MRI sequences, which are outlined succinctly. The principles outlined for protocols and procedures are general, and specific application will vary among departments. Given that the procedures for PET are well established among the readership of this journal, this article emphasizes MRI factors unless specific variations in standard PET protocols or procedures are driven by the simultaneous MRI. This article is the third in a 4-part integrated series sponsored by the PET/MR and Publication Committees of the Society of Nuclear Medicine and Molecular Imaging–Technologist Section.

Key Words: PET/MR; PET; MRI; sequences; protocols

J Nucl Med Technol 2022; 50:17–24
DOI: 10.2967/jnmt.121.262544

The emergence of PET fused with CT required variations in protocols to accommodate the sequential PET/CT procedure. The more complex and time-consuming protocols and procedures for MRI simultaneously obtained with PET require more careful consideration. Although most PET/MRI investigations use ^{18}F-FDG, several other ^{18}F tracers and those chelated to radiometals, such as ^{68}Ga and ^{64}Cu, are expected to emerge. There are 3 main aspects of PET/MRI protocols and procedures: patient preparation for both MRI and PET procedures, the imaging procedures themselves, and quality assurance procedures. Patient preparation and the imaging protocol need to be considered for both adult and pediatric populations.

PET/MRI combines the high sensitivity and quantification of molecular-level tracers of PET with the exquisite soft-tissue contrast and some functional imaging parameters of MRI (*1*). Despite these benefits, the major limitation is the complex array of MRI sequences that could be performed and the time cost per bed position. For PET/CT, 2–4 min per bed position is typical of a whole-body scan, but in clinical PET/MRI, as many as 5 MRI sequences could require 5–10 min per bed position (*1*). There are several benefits to optimizing the MRI sequence timing to the standardized PET bed position. First, it maintains the consistency associated with quantitation (e.g., SUV) between and within sites. Second, extending PET bed position timing has a marginally increased impact (particularly during the latter part of the acquisition) on both radionuclide decay and target-to-background ratio. Recent developments in ultrafast MRI sequences have shortened the MRI acquisition to 3–5 min per bed position (*1*), although 2–4 min might be considered optimal. It is possible to adjust protocols for MRI sequences beyond the PET bed position timing to accommodate the extended MRI sequences after the PET acquisition is completed or, alternatively, 15 min before commencing the PET acquisition.

MRI SEQUENCES

A typical MRI examination consists of imaging the body part of interest multiple times with varying parameters that produce images with different tissue weightings. Each tissue weighting serves to provide a different clinical insight. PET/MRI is generally a whole-body examination, which for most represents imaging from the base of the skull to the thighs, consistent with approaches to PET/CT. The absence of the CT radiation dose issues for the brain and eyes means that it has become more common in PET/MRI

Received May 6, 2021; revision accepted Aug. 20, 2021.
For correspondence or reprints, contact Geoff Currie (gcurrie@csu.edu.au).
Published online Sep. 28, 2021.

to image the vertex through the thighs. For some indications or in a pediatric setting, the vertex of the skull to the toes is the norm. PET/MRI acquires the PET and MRI data simultaneously, with each bed position having 2–4 different MR image sequences. Conversely, PET/CT is acquired sequentially with a rapid CT component. Thus, if the MRI sequences selected do not prolong the bed position, PET/MRI could be a faster acquisition by the margin of the CT acquisition (seconds). Nonetheless, PET/MRI also has sequential MRI acquisitions with the localizer before the PET acquisition and the potential for additional sequences without PET at the end that extend the protocol marginally (minutes) but are generally negligible in the overall protocol. Both the contrast protocols and the positioning of the patient confound these times. Nonetheless, optimizing the MRI sequences for PET/MRI is critical for patient comfort and compliance and for the diagnostic integrity of the examination. Perhaps the simplest way to consider sequences is to first consider T1- and T2-weighted images and then explore specific sequences. The following sequences are not exhaustive but represent the more common sequences in MRI (the more detailed discussion will be reserved for those sequences relevant specifically to PET/MRI protocols): spin echo (T1 short repetition time and echo time, T2 long repetition time and echo time, fast spin echo, dual echo, and proton density–weighted long repetition time and short echo time); gradient echo (GRE) (susceptibility-weighted imaging; T1-weighted volume-interpolated spoiled GRE, which could be referred to as volume-interpolated breath-hold examination [VIBE] or liver acquisition with volume acquisition, depending on the manufacturer; T2 and T2*; steady-state free precession; and dual GRE); inversion recovery (short-tau inversion recovery [STIR] fat suppression and fluid-attenuated [long tau] inversion recovery [FLAIR] fluid suppression); T1- or T2-weighted imaging; diffusion-weighted imaging (DWI) (apparent diffusion coefficient maps [postprocessed sequence]); diffusion tensor imaging and tractography of nerves; perfusion-weighted imaging (T1 gadolinium contrast-enhanced and arterial spin labeling [noncontrast technique]); functional MRI; MR angiography (MRA) (contrast-enhanced MRA, time-of-flight angiography [without or with contrast], and phase-contrast MRI [noncontrast technique]). More detailed treatment of less frequent, less relevant (to PET/MRI), or more novel sequences is beyond the scope of this article and can be explored in the broader literature.

In PET images, the shade of gray or color represents count density or counts per pixel or per voxel. In CT, the shade of gray represents the degree of attenuation or tissue density (*2*). For MRI, the shade of gray of tissues represents signal intensity, with white typically being a high signal intensity and black being a low signal intensity. In PET, relative quantitation is undertaken visually or with calculations that compare the count density on the structure of interest to a reference tissue. Examples include a tumor-to-liver comparison and a comparison of the regional cerebral cortex to the contralateral side or cerebellum. For MRI, intensity is also compared between the tissue of interest and reference tissues, with the term *hyperintense* indicating whiter, brighter, greater intensity than the reference tissue; *hypointense* indicating darker or lower intensity than the reference tissue; and *isointense* meaning the same brightness or intensity as the reference tissue (e.g., a brain tumor relative to surrounding brain tissue).

The image formation process and pulse sequences have been explained in a previous article in this series (*3*), but there is a need to briefly define several specific terms. After radiofrequency excitation, the time for the signal to return to equilibrium is called relaxation time and the signal produced is referred to as free induction decay (*4*,*5*). The time between each radiofrequency pulse is called the repetition time (*4*,*5*). The echo signal is termed spin echo, is stronger than the free induction decay signal, and is measured at the peak time of the echo (*4*,*5*). Free induction decay is formed by a single radiofrequency pulse (often thought of as 90° but technically not necessarily). GRE is formed by 1 radiofrequency pulse with a gradient reversal. Spin echo is formed with 2 radiofrequency pulses (e.g., 90° and 180°), and stimulated echo is formed with 3 or more radiofrequency pulses. *Hahn echo* is a term generally used to refer to echo produced by radiofrequency pulses other than 90° and 180° (but technically could include 90° and 180° pulses) (*4*,*5*).

T1 Images

T1-weighted images are a standard part of any MRI protocol. As the term suggests, the T1 pulse sequence highlights differences between tissues based on T1 relaxation times or longitudinal relaxation (sometimes referred to as spin lattice relaxation time) (*3–6*). As outlined in Figure 1, the proton dipoles align with the magnetic field after the radiofrequency pulse. The proton dipoles then revert back (relax) to nearly their original orientation. The time it takes an individual tissue to relax results in different signal intensities. For example, water content, air, and bone have a slow relaxation, which produces a lower signal and a darker representation on images. Conversely, fat, protein-rich fluid, and slow-flowing blood have a rapid relaxation time that produces a whiter or brighter signal on images. T1-weighted spin echo produces the truest T1 signal but generally takes longer to acquire, typically anywhere from 2 to 5 min. An alternative option is to use T1-weighted GRE, which uses the properties of the gradient coils inside the MR scanner to generate the T1-weighted images faster than conventional spin echo techniques. Clearly, this is advantageous for simultaneous PET/MRI, for which bed position time needs to be optimized, but as outlined in the previous article in this series (*3*), the coils themselves can produce artifacts in the PET images. GRE images are also more susceptible to artifacts caused by inhomogeneity in the magnetic field as a result of metal or blood products

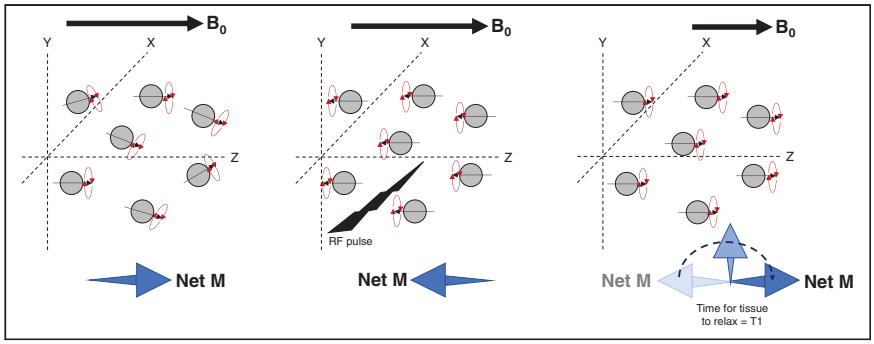

FIGURE 1. Schematic representation of T1 signal produced by longitudinal relaxation. Proton dipoles have net magnetism in magnetic field (left) but become aligned after radiofrequency pulse (middle) and produce T1 signal on relaxation (right). B_0 = magnetic field; M = magnetism; RF = radiofrequency.

(e.g., pixel swap). Pixel swap is an artifact associated with the Dixon technique, in which the algorithm confuses water and fat pixels; this artifact is most typical of the extremities or of areas with a low fat signal. These sequences are also more susceptible to motion artifacts and anatomic wrap-around artifacts. Regardless, T1-weighted GRE allows multiple sequences with imaging for less than 30 s. These phenomena can be further exploited using paramagnetic contrast agents (e.g., gadolinium) to produce several variations to the T1 pulse sequence.

Gadolinium Enhancement and Fat Suppression

T1 signal intensity is amplified by gadolinium-based contrast agents, which, compared with noncontrast T1 images, produce brighter (more intense) signals from tissues. In effect, this brightness appears to shorten the T1 relaxation times, given that the intensity of slow-relaxation-time tissues has now become brighter. Although this phenomenon helps us understand the process, the reality is that the relaxation time is not actually shortened; instead, the signal itself is increased from tissues. One application would be in diseased tissue in which increased perfusion or tissue permeability (e.g., injury, tumor, or inflammation) results in a higher concentration of contrast agent and a disproportionate increase in signal intensity compared with normal tissues.

Unfortunately, fat tissues are already very intense, and increases in intensity may not be easily distinguished from normally intense tissues. As a result, fat suppression sequences are typically imaged after contrast administration to reduce the fat signal (e.g., phase-contrast techniques and inversion recovery sequences). These sequences might also be referred to as fat-attenuated or fat saturation. Nonetheless, both fat-saturated and non–fat-saturated images provide useful insights, but in the context of multiple sequences and time cost, it is not convenient to run both pulse sequences. An alternative is the Dixon dual-echo sequence, which uses algorithms and the inherent properties of the signal (chemical shift) generated by fat and water in MRI to generate both fat-saturated and non–fat-saturated image sets from a single acquisition. In essence, water and fat precess at different rates, which means cyclically they will be in-phase and out-of-phase (a little like the seconds hand of a clock being out-of-phase with the minutes hand until each minute that they approximately become in-phase). By acquiring in-phase and out-of-phase images, the algorithm can produce 4 separate sequences: in-phase (water plus fat), out-of-phase (water minus fat), fat (in-phase minus out-of-phase), and water- or fat-suppressed/fat-saturated (in-phase plus out-of-phase). Acquisition of an ultra-fast GRE Dixon technique requires about 15–20 s per bed position. In addition, this acquisition is 3-dimensional and can be reformatted into multiple planes during postprocessing with minimal image resolution loss. This technique is essential for generating the MR attenuation correction sequence maps for the PET data (*3*).

T2 Images

As with T1-weighted images, T2 pulse sequences are a standard part of most MRI protocols and might also be referred to as T2-weighted images. As these terms suggest, the T2 pulse sequence highlights differences between tissues based on T2 relaxation times or transverse relaxation (sometimes referred to as spin–spin relaxation) (*4*,*5*). As outlined in Figure 2, the proton dipoles align with the

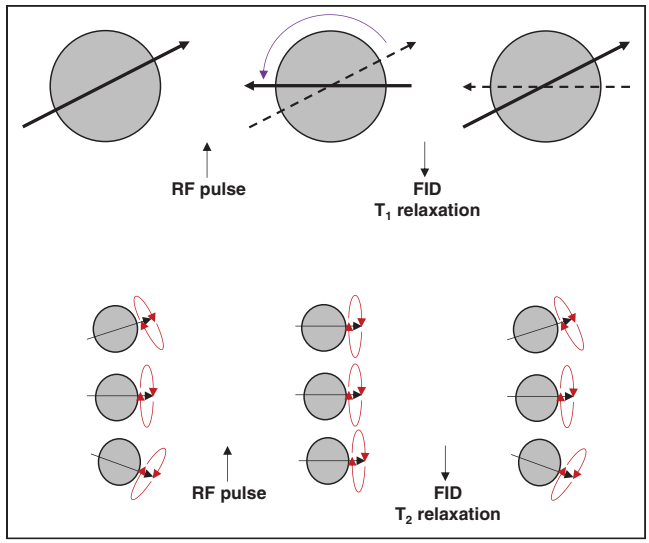

FIGURE 2. Schematic representation of difference between T1 (top) and T2 (bottom) signal production. For T1, proton dipoles become aligned after radiofrequency pulse and produce T1 signal on relaxation. T2 signals relate to precession of proton dipoles relaxing back to ground state. FID = free induction decay; RF = radiofrequency.

magnetic field after the radiofrequency pulse. The proton dipoles then revert back (relax) to nearly their original orientation for the T1 signal. Each proton dipole also has precession altered in alignment by the radiofrequency pulse. The time it takes an individual tissue to relax precession alignment results in different signal intensities. For example, water content and brain gray matter produce a high intensity signal whereas muscle, fat, and white brain matter produce intermediate intensities. A minor issue relating to T2 sequences is the influence of inhomogeneous magnetic fields on tissue T2 relaxation times, sometimes referred to as T2*. T2 then is the truest T2 signal using a spin-echo sequence. Gadolinium contrast medium is not used because it shortens T2 relaxation and thus suppresses rather than amplifies the signal; T2 sequences are therefore run before contrast enhancement. The exception is the T2 FLAIR steady-state GRE sequence, which shows contrast enhancement due to a mixed T1 and T2 signal.

Typically, T2-weighted images are used to visualize a pathologic process such as edema. Again, there are several ways to achieve this goal. Traditional spin echo techniques to obtain T2 images are time-prohibitive, and thus, several methodologies have been developed to decrease the time it takes to acquire them. The fastest of these is ultra-fast spin echo, which has image acquisition times under a minute typically. Another option is the fast relaxation fast spin echo technique; this technique is slower than the ultra-fast spin echo technique but substantially faster than spin echo. Since both fat and water produce a bright signal on T2 imaging, obtaining fat-saturated T2 images can help better define the nature of what is visualized. Like T1 sequences, fat suppression can be achieved with STIR sequences, which are useful from an imaging perspective but limited by the 5-min sequence time.

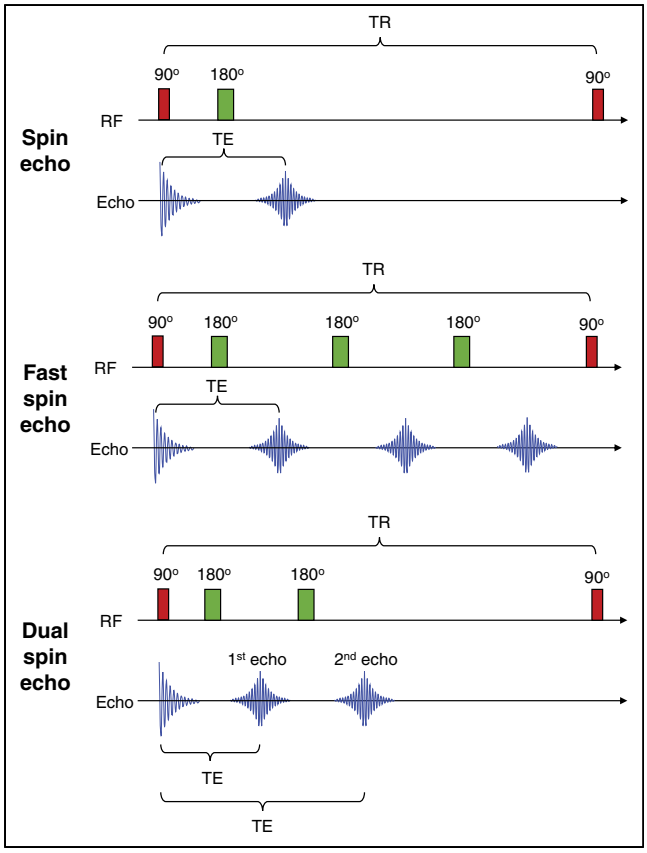

FIGURE 3. Schematic representation of MR sequences. Spin echo uses 90° followed by 180° radiofrequency pulse to produce echo. Fast spin echo uses 90° followed by multiple 180° radiofrequency pulse to produce multiple echoes. Dual spin echo, as name suggests, produces 2 echoes from 90° followed by repeated 180° radiofrequency pulse. TE = echo time; TR = repetition time.

Proton Density

Proton density sequences use the nature of MRI (proton or hydrogen ion imaging) to image the density of protons (*4*). Tissues with high density or proton intensity include fluid and fat, similar to T2. Since the technique was useful in differentiating high-intensity fluid from low-intensity fibrocartilage and intermediate-intensity hyaline cartilage, it is often used for joint imaging, with FLAIR displacing its use in brain imaging.

Spin Echo

Spin echo uses 90° radiofrequency excitation pulses (Fig. 3) to flip longitudinal magnetism (T1) and dephases transverse magnetism (T2). The subsequent 180° radiofrequency-refocusing pulse rephases the spins to produce coherence (*4*,*5*). Thus, recovery of transverse magnetism produces a spin echo. Fast spin echo is the same principle as spin echo (Fig. 3) except it uses a series of rapidly applied 180° radiofrequency-rephasing pulses to produce multiple echoes (echo train length) within the same repetition time (*4*,*5*), allowing more rapid data collection but having a limit on echo train length (typically less than 7 for T1). The echo time may vary from echo to echo in the train and may produce different characteristics (contrast vs. resolution, for example). T1 is generated from the initial echoes and T2 from the later echoes. Longer echo train lengths with short echo times degrade contrast and produce blur but may be useful for enhanced T2 images. Dual echo (Fig. 3) is the same principle as fast spin echo with an echo train length of 2, with the first echo usually being proton density and the second T2-weighted imaging.

GRE

GRE uses bipolar gradient pulses after the 90° excitation radiofrequency pulse (*4*,*5*). For standard GRE, there is no 180° refocusing radiofrequency pulse as depicted in Figure 4. The addition of one or more of the 180° refocusing pulses produces fast GRE sequences. Standard GRE uses a negatively pulsed gradient to dephase the spin, which is then rephased with a second positively pulsed gradient, generating the echo signal independently of the 180° refocusing radiofrequency pulse.

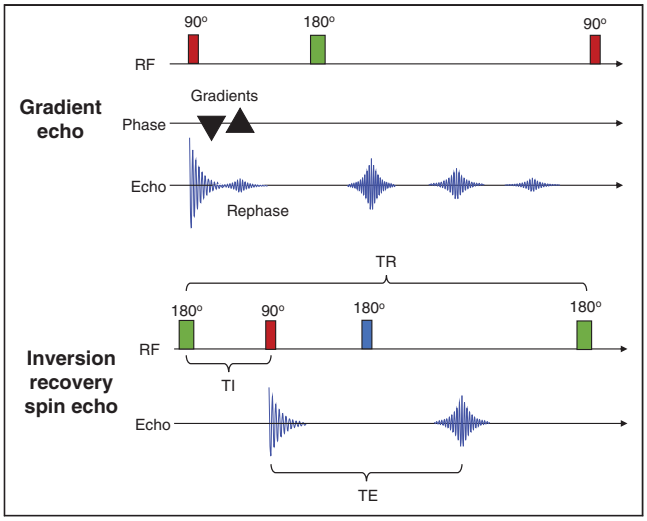

FIGURE 4. (Top) Schematic representation of GRE in which 90° radiofrequency pulse is followed by bipolar gradients first dephasing free induction decay and then rephasing free induction decay. (Bottom) Schematic representation of inversion recovery spin echo in which 180° radiofrequency pulse is followed by 90° radiofrequency pulse. RF = radiofrequency; TE = echo time; TR = repetition time.

Inversion Recovery

STIR is a fat suppression sequence (Fig. 4) that uses an inversion time for T1 in which the inversion time is ln2 (~0.693) multiplied by the T1 for fat. The sequence works because the T1s for fat and water are different (*4*,*5*). In the same way, water suppression can be accomplished using FLAIR sequences (FLAIR can resemble T2 images). Although these approaches produce fairly homogeneous suppression of water or fat, they are not specific for fat and water so can cause decreased demarcation of tissues. Furthermore, they are incompatible with gadolinium contrast administration because the apparent shortening of contrast-enhanced tissues will be impacted (suppressed) by a short inversion recovery time.

DWI

DWI is a type of MRI that shows how fluid is moving through tissues (extracellular space). Using a strong gradient, greater diffusion results in greater dephasing, and the signal is therefore reduced. As a result, DWI is effective in identifying restricted diffusion of water molecules as a higher signal intensity. DWI can be used to assess tissue edema, ischemia, and cellularity (e.g., proliferation of tumor cells). DWI represents an image set with different b-values. The b-value is a value that reflects gradient strength and timing, and so, the higher the b-value the stronger the diffusion. DWI is a combination of true diffusion values and the T2 signal, and therefore, the lower the b-value the more T2-weighted the image is (*4*). Different tissues and resultant pathologies exhibit diffusion behaviors different from random Brownian motion to constrained motion in 1 voxel direction. Injury that changes water diffusion will change the DWI signal. Diffusion tensor imaging is a variation on DWI that measures diffusion in multiple directions, which allows mapping of nerve fibers and tractography. An apparent diffusion coefficient map is literally a map or tensor of the actual diffusion values for tissues without the influence of T2.

Other Sequences

Functional MRI is a cluster of MRI approaches designed to reveal regional or time-dependent variations in MR signal and is associated primarily with brain imaging. Functional MRI targets a variety of physiologic parameters and uses numerous MRI sequences. Perfusion-weighted imaging is mostly gadolinium T1 images but also arterial spin labeling without gadolinium (*4*). Susceptibility-weighted imaging sequences exploit the T2* sequence susceptibility to small fluctuations in magnetic field and, consequently, can distinguish calcium from blood. This ability is useful in differentiating blood products in various pathologic processes.

MRA generates images with a high degree of contrast between tissues and blood. The images are associated with blood flow rather than vessel structures. Some aspects of flow are predictable and can be used to generate image contrast, whereas other aspects of flow can create procedure difficulties or artifacts (e.g., turbulence, velocity, or direction changes). There are several approaches to MRA. The first is contrast-enhanced MRA, which uses gadolinium contrast agents to shorten the T1 relaxation time and enhance the brightness of blood signals (*4*,*5*). Time-of-flight MRA does not use contrast agents but instead captures the unsaturated spins of flowing blood with GRE sequences to produce a bright vascular image (*4*,*5*). Phase-contrast MRA uses amplitude and phase information to image blood flow velocity (*4*,*5*).

PATIENT PREPARATION

Patients need to undergo the preparation associated with both the PET scan and the MRI scan. For PET, this preparation will include fasting and instructions regarding radiation safety. For MRI, the screening questionnaire for magnetic safety and gadolinium contrast needs to be completed. Additionally, PET imposes limitations on strenuous activity and requires management of any patients who are diabetic. Patients need to be screened for metals to ensure there are no unsafe implants or devices going into the MRI environment. A lot of the prescreening can be accomplished as the exam is being ordered or scheduled by asking just a few questions targeting implants that could contraindicate the exam (e.g., pacemakers, magnetic spinal rods, cochlear implants, or palate expanders) or that could impact image quality (e.g., dental spacers or braces). When patients arrive for their appointment, they are also required to fill out a more comprehensive MRI metal screening form, which is then reviewed verbally with trained MRI personnel to

ensure safety. Patients should also undergo a visual inspection before entering zone 4 (the PET/MRI scan room) as a final verification that nothing unsafe is going into the magnet.

Patient history can be especially useful in image interpretation, and taking a robust patient history is therefore an essential part of patient preparation. In oncology, for example, some patients receive bone marrow–stimulating medications at the end of a cycle of therapy that may alter biodistribution of the radiopharmaceutical in PET imaging. If a delay in scheduling after these peak effects is not ideal, this information will assist with the accurate interpretation of the PET/MRI data.

Protocols vary across clinical sites and across radiopharmaceuticals; however, an uptake phase of 45–90 min is typical. Patients are usually injected intravenously in an ambient environment to minimize stimulation. Recent investigations have demonstrated higher dose extravasation rates associated with manual injection using a syringe/needle or syringe/butterfly apparatus (*7*–*9*). Lower extravasation rates are achieved with canula use with autoinjector infusion. For patients undergoing gadolinium contrast sequences, a single canula might be used for both the PET tracer administration and the later gadolinium administration. Clearly, care with line security is crucial throughout the uptake phase and patient positioning.

Patient compliance is an important consideration given the extended time of the PET/MRI procedure. Compared with MRI, PET has the additional requirements of fasting and blood sugar level adjustment, in addition to the long uptake phase without stimulation. Compared with PET, MRI has the additional time and complexity associated with coil and patient setup, screening for magnetism-susceptible objects, and noise. Additionally, the PET/MRI gantry can create issues associated with claustrophobia, even in patients with no previous history of claustrophobia. For some patients, compliance requires the preadministration of anxiolytics such as diazepam. In some cases, sedation or general anesthesia may be required, adding complexity to both the protocol and patient care. Sedation and general anesthesia are generally not initiated until at least 30 min after administration of the PET radiopharmaceutical but in some circumstances may be administered immediately after radiopharmaceutical injection.

PET/MRI PROTOCOLS

PET acquisition parameters are generally the same for both PET/CT and PET/MRI. Each bed position is acquired at 2- to 4-min intervals. In PET/CT, the PET portion determines the bulk of the length of the procedure, with CT being performed very quickly in a sequential model. Contrast CT protocols clearly extend the overall imaging procedure. Conversely, in PET/MRI, the images are acquired simultaneously and PET cannot progress to the next bed position until all the MRI sequences are completed. PET/MRI procedures commence with a localizer, comparable to the topogram in a PET/CT scan, to be used for planning both the PET bed positions and the MRI sequences at each bed position. In PET/MRI, a specific MR attenuation correction sequence is obtained at each bed position to create the attenuation correction maps for PET reconstruction. In addition, depending on the region being imaged and the pathology of interest, several other sequences will be performed at each bed position. Although the Dixon method is referenced in this article for attenuation correction, there are several other approaches to attenuation correction in clinical practice, as well as others emerging from development as detailed in the second article in this series (*3*).

Reducing artifacts from respiratory motion is an important consideration. Breath-hold techniques can be effective if the sequence is short enough and the patient is compliant. Such techniques work particularly well for the short-duration T1-weighted images, but even ultrafast sequences are too long for T2 breath-hold approaches. Respiratory triggering can be used, or images can be gated, or synchronized, to the patient's respiratory cycle. Respiratory gating works best when patients are breathing at a steady regular rate. The third option performs respiratory motion correction based on liver motion during respiration by tracking an MRI voxel at the apex of the liver.

More recent interest in accelerated protocols with 4-, 3-, 2-, and even 1-min bed positions have spurred debate about the benefits of reduced time and the image quality for PET and MRI (*1*). The counter debate is that compromising a full MRI sequence to minimize the time per bed position undermines the value and insights of MRI. Nonetheless, a hybrid protocol might permit a longer application of a suite of MRI sequences and a longer PET acquisition (or potentially dynamic imaging during the uptake phase) for the single bed position of interest, followed by reduced sequences and standard PET bed positions for the remainder of the acquisition.

MRI-only acquisitions during the radiopharmaceutical uptake time may assist in reducing the acquisition time associated with each PET/MRI bed position. For example, MR images of the total spine that are acquired before the combined PET/MRI sequence can be coregistered with the latter if the patient has not moved, with gadolinium contrast spine sequences added after the PET/MRI sequence. This approach could save the patient considerable time and optimize the PET/MRI sequence, especially when considering that the duration of precontrast total-spine imaging can vary between 30 and 90 min depending on patient-related factors.

Whole-Body Oncology PET/MRI

Although protocols will vary substantially from site to site and depending on equipment and clinical indications, for the purpose of a general overview it is useful to consolidate whole-body PET/MRI protocols into several scenarios. In each scenario, the MRI sequence commences with a

localizer scan followed by attenuation correction and then by T1, T2, and then special sequences if appropriate. The first approach (*1*,*10*) is a fairly standard set of 5 MRI sequences per bed position with a total acquisition time of 5–8 min per bed position that includes T1-weighted Dixon for attenuation (<15 s), DWI with 3 b-values (almost 1.5 min), T1-weighted volume-interpolated spoiled GRE (VIBE) (<30 s), T2-weighted single-shot half spin echo (~30 s to 1 min), T2-weighted STIR (2 min), and T1-weighted volume-interpolated spoiled GRE, after contrast administration if appropriate (18 s).

In this first approach to PET/MRI, after the conclusion of the whole-body exam a more specific region may be added to the standard sequences, for example, the prostate bed. For this approach, it would be prudent to perform the whole-body PET/MRI first to capitalize on disease localization, enhance PET target-to-background contrast in the targeted region, and acquire critical data to avoid noncompliance issues.

To minimize MRI sequence timing to better match each PET bed position without compromising diagnostic quality, some axial MR images can be replaced with images in the coronal plane. Typically, 3 axial bed positions are equivalent to 1 bed position in the coronal plane. For example, high-quality T2 and STIR sequences can be run in the coronal plane. Additionally, a coronal VIBE can be imaged in addition to the axial plane VIBE.

A second approach uses a wider range of sequences per bed position for the whole-body acquisition, and these might vary depending on the nature of the investigation. The result is a more comprehensive suite of MRI sequences for the whole-body PET/MRI but a longer scanning time beyond 10 min for key bed positions corresponding to the region of interest (Fig. 5). In this scenario, a basic set of sequences (e.g., 3) might be applied to each bed position whereas the broader suite is applied to the key bed position (including long PET imaging time). The basic sequences might be Dixon attenuation correction, coronal T1 fast spin echo (or coronal VIBE to include fat saturation), and axial T2-weighted imaging, for example. Advanced sequences are applied to specific bed positions covering regions of specific interest and may include, without being limited to, T2 fast spin echo, STIR, DWI, dynamic contrast-enhanced, and pre- and postcontrast T1. Specifically, PET/MRI with a focus on liver neoplasia might insert the extended suite of sequences as bed position 3 of 5 and include a breath-hold technique. The thoracic region might insert the extended suite over 2 bed positions and include respiratory gating. Head and neck cancer would have the longer sequences at bed position 1, and pelvic pathology would also have the broader suite of sequences at bed position one, because for most whole-body applications imaging commences from the head and progresses to the thighs. For the pelvis, given bladder excretion of PET tracers, imaging starts at the pelvis and progresses to the head.

This second approach has the advantage of a single imaging session with all data included in a single whole-body protocol. Unfortunately, this approach can increase the time per bed position and, thus, impact the SUV for each bed position because the uptake time after injection for each bed position is progressively extended. Longer sequences could threaten later bed positions if compliance becomes an issue. Importantly, an increased MRI sequence time increases the potential for heating of patient tissues and implants, posing a safety issue. In both approaches, the use of dedicated imaging increases the quality of the procedure by combining the attributes of PET with the MRI sequences. Further, the PET/MRI combination enriches, deepens, and broadens anatomic, physiologic, and biochemical insights regarding tissues and organs.

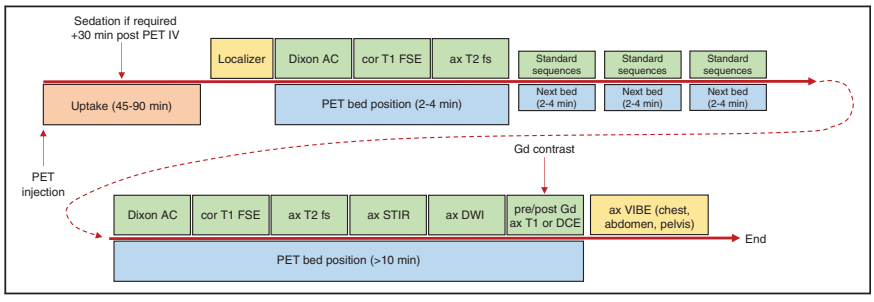

FIGURE 5. Flowchart of example of PET/MRI sequence used for whole-body oncology studies. 3D = 3-dimensional; AC = attenuation correction; ax = axial; cor = coronal; DCE = dynamic contrast-enhanced; DSC = dynamic susceptibility contrast; fs = fat saturation; FSE = fast spin echo; Gd = gadolinium; IV = intravenous injection; LGE = late gadolinium enhancement; SPAIR = spectral attenuated inversion recovery; T1WI = T1-weighted imaging.

Neurologic and Cardiac PET/MRI

The value of PET/MRI in the brain and heart arises from the simultaneous acquisition and coregistration of structural information provided by standard MRI sequences, physiologic insights provided by advanced MRI sequences, and molecular and metabolic status provided by PET (*11*). Although rapid PET protocols have emerged for brain and cardiac imaging in 5 min for a single bed position, 10–15 min for a single bed position are more typical. This longer window (compared with whole-body oncology bed positions) allows a broader range of MRI sequences without extending the length of the study. It is also possible that a standard PET/MRI study of the brain or heart with 10–15 min per bed position might be followed by a whole-body PET/MRI with 3–5 min per bed position. In this scenario, the sequences are different from the sequence for the whole body, reflecting both the change in time per bed position and the purpose of the MRI examination.

PET/MRI of the brain generally requires the following sequences

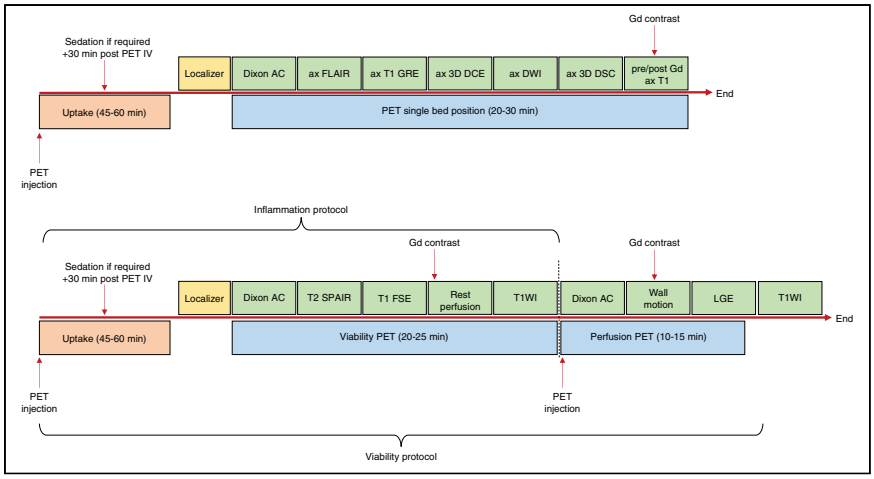

FIGURE 6. Flowchart of example of PET/MRI sequence used for brain studies (top) and cardiac studies (bottom). 3D = 3-dimensional; AC = attenuation correction; ax = axial; DCE = dynamic contrast-enhanced; DSC = dynamic susceptibility contrast; FSE = fast spin echo; Gd = gadolinium; IV = intravenous injection; LGE = late gadolinium enhancement; SPAIR = spectral attenuated inversion recovery; T1WI = T1-weighted imaging.

(Fig. 6): attenuation correction with T1-weighted Dixon GRE; conventional brain MRI with T1-weighted, T2-weighted, diffusion-weighted, susceptibility-weighted, and contrast-enhanced T1-weighted imaging; advanced sequences with perfusion-weighted imaging, functional MRI, diffusion tensor imaging, contrast-enhanced T1-weighted imaging, fast GRE, MR spectroscopy, and FLAIR, depending on the clinical indication; and simultaneous PET acquisition with any of several radiotracers, including ^{18}F-FDG, 3′-deoxy-3′-^{18}F-fluorothymidine, ^{18}F-fluoromisonidazole, ^{18}F-florbetapir, *O*-(2-^{18}F-fluoroethyl)-L-tyrosine, or 6-^{18}F-fluoro-L-dopa.

PET/MRI of the heart generally requires the following sequences (Fig. 6): attenuation correction with T1-weighted Dixon GRE; conventional cardiac MRI with T1 fast spin echo, T2 spectral attenuated inversion recovery, and contrast-enhanced T1-weighted imaging; advanced sequences with late gadolinium enhancement, rest perfusion (GRE, echoplanar imaging, and steady state free precession) and wall motion (electrocardiography gating, harmonic phase analysis, and spatial modulation of magnetization), depending on clinical indication; and simultaneous PET acquisition with any of several radiotracers, including ^{18}F-FDG for viability, perfusion tracers based on ^{82}Rb, ^{13}N, or ^{18}F, and novel inflammatory or amyloid markers.

CONCLUSION

PET/MRI is a relatively new imaging modality that, to establish a reliable niche in the imaging market, requires development of universal, practical, and reliable protocols. Protocol development should have a foundation of evidence-based standards for PET, for MRI, and for PET/MRI combined. Patient compliance and diagnostic integrity are central factors for protocol development. Although the complexity of PET/MRI protocols appears onerous, sequence rationalization has produced universally accepted streamlined protocols that fit within the time constraints of standard PET bed positions.

DISCLOSURE

No potential conflict of interest relevant to this article was reported.

REFERENCES

1. Lindemann ME, Stebner V, Tschischka A, Kirchner J, Umutlu L, Quick HH. Towards fast whole-body PET/MR: investigation of PET image quality versus reduced PET acquisition times. *PLoS One*. 2018;13:e0206573.
2. Currie G, Hewis J, Bushong S. Tomographic reconstruction; a non-mathematical overview. *J Med Imaging Radiat Sci*. 2015;46:403–412.
3. Currie G, Kamvosoulis P, Bushong S. PET/MRI part 2: technologic principles. *J Nucl Med Technol*. 2021;49:217–225.
4. Bushong SC, Clarke G. *Magnetic Resonance Imaging: Physical Principles and Biological Principles*. 4th ed. Elsevier; 2015:19–197.
5. Hashemi RH, Bradley WG, Lisanti CJ. *MRI: The Basics.* 2nd ed. Lippincott Williams and Wilkins; 2004.
6. Currie GM. Pharmacology, part 5: CT and MRI contrast media. *J Nucl Med Technol*. 2019;47:189–202.
7. Currie GM, Sanchez S. Topical sensor metrics for ^{18}F-FDG positron emission tomography dose extravasation. *Radiography*. 2021;27:178–186.
8. Sanchez S, Currie G. Topical sensor for the assessment of positron emission tomography dose extravasation: metric performance with an autoinjector. *J Nucl Med Technol*. 2020;48:363–371.
9. Sanchez S, Currie G. Topical sensor for the assessment of injection quality for ^{18}F-FDG, ^{68}Ga-PSMA and ^{68}Ga-DOTATATE positron emission tomography. *J Med Imaging Radiat Sci*. 2020;51:247–255.
10. Parikh N, Friedman KP, Shah SN, Chandarana H. Practical guide for implementing hybrid PET/MR clinical service: lessons learned from our experience. *Abdom Imaging*. 2015;40:1366–1373.
11. Miller-Thomas MM, Benzinger TLS. Neurological applications of PET/MR. *Magn Reson Imaging Clin N Am*. 2017;25:297–313.

Comparison of Low-Energy and Medium-Energy Collimators for Thyroid Scintigraphy with ^{123}I

Yuxin Li[1], Esther Choi[2], Artineh Hayrapetian[3], Emmanuel Appiah-Kubi[4], Jonathan Gershenson[1], Nazanin H. Asvadi[5], and Gholam R. Berenji[1]

[1]Department of Radiology, VA Greater Los Angeles Healthcare System, Los Angeles, California; [2]Department of Radiology, Penn State Health, Milton S. Hershey Medical Center, Hershey, Pennsylvania; [3]UCLA Ahmanson Translational Theranostics Division, Los Angeles, California; [4]Department of Radiology, Ohio State University Wexner Medical Center, Columbus, Ohio; and [5]Department of Radiology, Saint Vincent Hospital, Worcester, Massachusetts

CE credit: For CE credit, you can access the test for this article, as well as additional JNMT CE tests, online at https://www.snmmilearningcenter.org. Complete the test online no later than March 2025. Your online test will be scored immediately. You may make 3 attempts to pass the test and must answer 75% of the questions correctly to receive Continuing Education Hour (CEH) credit. Credit amounts can be found in the SNMMI Learning Center Activity. SNMMI members will have their CEH credit added to their VOICE transcript automatically; nonmembers will be able to print out a CE certificate upon successfully completing the test. The online test is free to SNMMI members; nonmembers must pay $15.00 by credit card when logging onto the website to take the test.

^{123}I thyroid scintigraphy can be performed with either a low-energy or a medium-energy (ME) collimator. The high-energy photon emissions from ^{123}I cause septal penetration with scattered photons, which deteriorate image quality. The aim of this study was to evaluate the impact of collimator choice on ^{123}I thyroid scintigraphy in clinical practice. **Methods:** Forty-seven patients who underwent thyroid planar scintigraphy with both a low-energy, high-resolution (LEHR) collimator and a ME collimator were prospectively recruited using the same imaging protocol. Image quality, collimator sensitivity, and estimation of thyroid size were assessed between LEHR and ME collimators and were compared with thyroid ultrasonography as the gold standard. **Results:** Images acquired with the ME collimator demonstrated reduced scattered background noise, improved thyroid-to-background contrast, and increased sensitivity in the thyroid gland compared with images acquired by the LEHR collimator. Manual measurement of the thyroid length is more accurate using the ME collimator. Automatic estimation of the thyroid area using the same thyroid threshold is larger in ME collimator images than in LEHR collimator images. **Conclusion:** Compared with the LEHR collimator, the ME collimator generates cleaner ^{123}I thyroid scintigraphy images with less background noise and has higher collimator sensitivity for thyroid imaging. Different thyroid thresholds should be used to estimate the thyroid area and volume between low and ME collimators.

Key Words: endocrine; image processing; collimator; iodine-123; medium energy; thyroid scintigraphy

J Nucl Med Technol 2022; 50:25–29
DOI: 10.2967/jnmt.121.262517

For thyroid imaging, ^{123}I is a more ideal radioisotope than ^{131}I because ^{123}I is comparable to ^{99m}Tc, has less septal penetration with better image quality, and exposes the patient to less radiation (*1,2*). It has the most abundant γ-rays, at 159 keV, which is comparable to the 140 keV from ^{99m}Tc, and can be imaged with pinhole, low-energy, or medium-energy (ME) collimators (*3*). A pinhole collimator provides more details for imaging small organs such as the thyroid glands. However, a pinhole collimator cannot be used to estimate the functional thyroid size and volume, which are used frequently for dose calculation in radioiodine therapy. A low-energy, parallel-hole collimator, especially the low-energy, high-resolution (LEHR) collimator, is the most widely used collimator in nuclear medicine imaging, mainly because of its advantage for imaging ^{99m}Tc-labeled radiopharmaceuticals. The LEHR collimator has been frequently used for ^{123}I thyroid scintigraphy, with the major advantage of avoiding collimator switching between studies using ^{99m}Tc-labeled compounds and shorter acquisition times.

^{123}I also emits a small percentage (<3%) of higher-energy photons exceeding 400 keV. These high-energy photons can penetrate the collimator septum and generate scattered photons, which are detected in the 159-keV window (*4*). Septal penetration leads to reduced imaging quality, especially for the LEHR collimator with a thinner septum, resulting in more septal penetration. A ME collimator with a thicker septum results in less septal penetration for ^{123}I imaging than does a low-energy collimator. The ME collimator has been recommended for several nuclear medicine studies using ^{123}I with semiquantitative evaluation (*5–8*). However, whether the ME collimator is superior to LEHR for thyroid scintigraphy with ^{123}I in clinical practice has not been well documented. This study was designed to evaluate the impact of choosing between LEHR and ME collimators on ^{123}I thyroid scintigraphy in clinical practice.

Received May 4, 2021; revision accepted Sep. 13, 2021.
For correspondence or reprints, contact Gholam R. Berenji (gholam.berenji@va.gov).
Published online Sep. 28, 2021.

MATERIALS AND METHODS

Patients

In total, 47 consecutive patients referred for thyroid scintigraphy with ^{123}I were prospectively recruited at the Veterans Affairs Greater Los Angeles Health Care System between October 2015 and November 2016. There were 35 men and 12 women, with an average age of 61 y. Thyroid scintigraphy was performed for evaluation of hyperthyroidism (37 patients) or thyroid nodules (10 patients).

Thyroid Scintigraphy

All patients underwent thyroid scintigraphy with both a large-rectangular-field-of-view Siemens BiCore LEHR collimator and ME collimators sequentially with the same camera. The specifications of the LEHR and ME collimators are listed in Table 1. To reduce the influence of different imaging times after ^{123}I administration, half our patients underwent LEHR collimator imaging first, immediately followed by ME collimator imaging, and the other half underwent ME collimator imaging first, immediately followed by LEHR collimator imaging. All patients received 7,400 kBq (200 μCi) of ^{123}I. Thyroid imaging started at approximately 4 h 30 min after the 4-h thyroid uptake measurement. Images were acquired using a Siemens Symbia T16 SPECT/CT γ-camera. The following acquisition parameters were used: anterior view, 128 × 128 matrix, zoom factor of 1, pixel size of 2.4 mm, acquisition time of 7 min for both LEHR and ME collimators, and an energy window of 15% centered at 159 keV. The distance between the collimator and the patient's face was kept to 2.54 cm (1 in) or as close as the patient could tolerate.

Thyroid Ultrasonography

There were 22 patients who also underwent thyroid ultrasonography within 3 mo of thyroid scintigraphy. Thyroid ultrasonography was performed using either the Philips EPIQ 7G or the GE Healthcare XDclear real-time ultrasound scanner with high-resolution 6- to 15-MHz linear array transducers. Each thyroid lobe was scanned in both transverse and longitudinal planes. The maximum length, width, and depth of each thyroid lobe were measured. The volume of each thyroid lobe was calculated with the standard formula for ellipsoid volumes: volume (mL) = $\pi/6 \times$ length (cm) × width (cm) × depth (cm).

Image Analysis

All scintigraphic images were viewed and analyzed using an Oasis general nuclear medicine package, which included a thyroid analyzing application (Segami Corp.). Using a lower threshold of 30% of the maximum pixel counts in the image frame, an isocontour of the thyroid gland was created automatically with the Oasis thyroid application. Total thyroid counts, background-corrected total thyroid counts, and counts per pixel were calculated within the thyroid isocontour. The length of each thyroid lobe was manually measured by 5 nuclear medicine physicians using the Oasis thyroid application. The thyroid area was automatically calculated with the Oasis thyroid application by applying different thresholds (20%, 25%, 30%, 35%, 40%, and 45%). The thyroid volume was calculated using the empiric method that is being used at the VA Greater Los Angeles Health Care System: thyroid volume (mL) = area of thyroid gland (cm^2) × length (cm) × 0.321. The differences between the LEHR and ME collimator for thyroid length measurement and volume estimation were compared using ultrasonography as the gold standard for thyroid measurement.

Statistical Analysis

GraphPad Prism 8 was used to perform statistical analyses. Data distributions were assessed using the D'Agostino–Pearson omnibus test. Normally distributed data are summarized as mean ± SD, and nonparametric data are summarized as median and interquartile range. Variables from different groups were compared using the Student *t* test (2-tailed paired samples assuming unequal variance) for parametric variables and the Mann–Whitney test (2-tailed paired samples) for nonparametric variables. Significance was defined as a *P* value of less than 0.05, and the 95% CIs are reported when appropriate. Comparison of thyroid size measurements among different methods was analyzed with linear regression and Bland–Altman plot analyses (*9*).

RESULTS

There was a clear difference in image quality between LEHR and ME collimators, as demonstrated in Figure 1. ME collimator planar images demonstrated significantly less background noise, better thyroid-to-background contrast, and an overall much cleaner image than did LEHR collimator images. The LEHR images demonstrated a slightly better spatial resolution than the ME images, although the difference was very subtle by visual inspection. Ten patients were referred for evaluation of known thyroid nodules. There was no difference between LEHR and ME collimator images in identifying these nodules.

TABLE 1
Siemens BiCore Collimator Specifications

Parameter	LEHR	ME
Hole shape	Hexagon	Hexagon
Number of holes (×1,000)	148	14
Hole length	24.05 mm	40.64 mm
Septal thickness	0.16 mm	1.14 mm
Hole diameter	1.11 mm	2.94 mm
Sensitivity at 10 cm	5.46 cpm/kBq (^{99m}Tc)	7.43 cpm/kBq (^{67}Ga)
Geometric resolution at 10 cm	6.4 mm (^{99m}Tc)	10.8 mm (^{67}Ga)
System resolution at 10 cm	7.5 mm (^{99m}Tc)	12.5 mm (^{67}Ga)
Septal penetration	1.5% (^{99m}Tc)	1.2% (^{67}Ga)
Weight	22.1 kg	63.5 kg

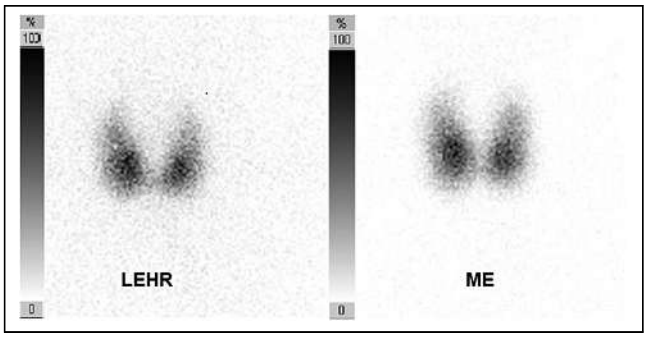

FIGURE 1. Planar anterior view of thyroid scintigraphy from LEHR collimator and ME collimator.

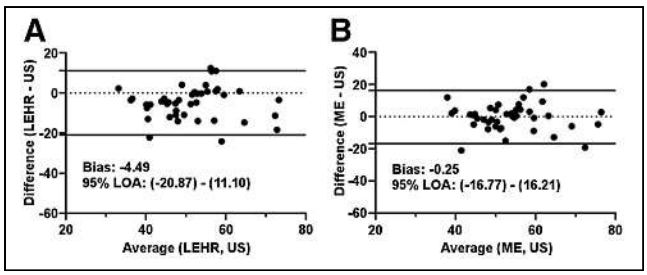

FIGURE 3. Bland–Altman plot analyses of thyroid length measurement between ultrasonography with LEHR collimators (A) and ultrasonography with ME collimators (B). LOA = limit of agreement; US = ultrasonography.

The total photon counts from the whole large-field-of-view camera were 36% higher in the LEHR collimator images than in the ME collimator images (Fig. 2A). In contrast, the total thyroid counts (thyroid area was defined by applying 30% of threshold), background-corrected total thyroid counts, and count density as determined by counts per pixel in thyroid tissue from the LEHR collimator images were significantly less than those from the ME collimator images (Figs. 2B–2D).

By visual inspection, the ME collimator images demonstrate a slightly larger thyroid size than the LEHR collimator images for most patients. When thyroid length was measured manually from the planer scintigraphy images, the LEHR collimator measurement and ME collimator measurement correlated similarly with the ultrasonography measurement, as determined by the Pearson correlation coefficient (r = 0.69 for LEHR and r = 0.66 for ME). The Bland–Altman plot analyses demonstrated less bias from the ME collimator measurement than from the LEHR collimator measurement, as compared with ultrasonography (Figs. 3A and 3B). Interobserver variations in thyroid length measurement were similar between LEHR and ME as determined by the intraclass correlation coefficient (LEHR, 0.92, with 95% CI of 0.88–0.96; ME, 0.91, with 95% CI of 0.87–0.95).

The automatically calculated area using the threshold of the maximum average pixel is inversely proportional to the threshold percentage being used. For the same image, the lower threshold resulted in a larger area, and a higher threshold resulted in a smaller area. For volume estimation using LEHR collimator images, 35% of the threshold yielded the closest volume estimation with the least bias, as compared with ultrasonography (Fig. 4A). For volume estimation using ME collimator images, the same threshold (35%) yielded an overestimation with increased bias, and 40% of the threshold yielded the closest volume estimation with the least bias, as compared with ultrasonography (Figs. 4B and 4C). As compared with ultrasonography, the LEHR and ME collimators demonstrated a similar spread of limits of agreement in both thyroid length and volume estimation.

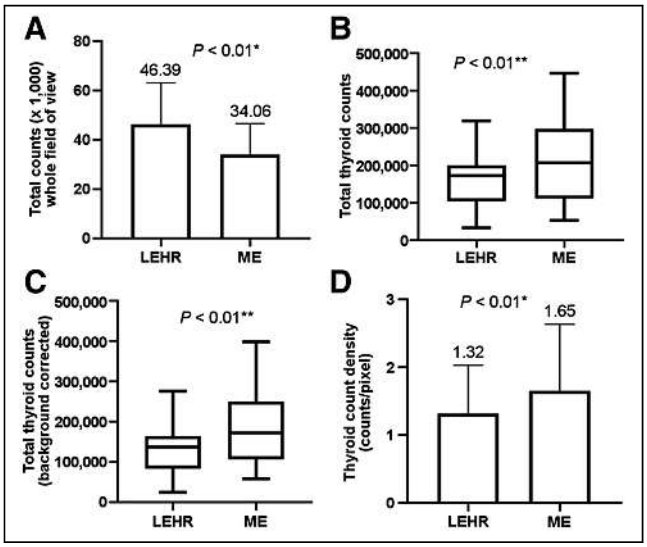

FIGURE 2. Comparison of photon counts between LEHR collimator and ME collimator. (A) Total counts from whole rectangular field of view of collimator. (B–D) Counts within thyroid isocontour measured by applying 30% of threshold. A and D represent mean with SD. B and C represent median with interquartile range. *Significance was determined by Student t test. **Significance was determined by Mann–Whitney test.

DISCUSSION

The most striking difference between the LEHR and ME collimator images is the background noise. The ME collimator images demonstrate a significantly less noisy background and are much cleaner than the LEHR collimator images. This effect is related to a reduction of septal penetration of high-energy photons from ^{123}I. Septal penetration is most prominent in the low-energy collimator, which has a thinner collimator septum (Table 1). Septal penetration produces scattered photons, which pass through collimator holes and reach the sodium iodine crystals from the detector. The noisy background counts are barely visible from the ME collimator images but are quite obvious from the LEHR collimator images.

It is interesting to notice that, as compared with the ME collimator, the LEHR collimator yielded more total counts for the large field of view covering the whole collimator surface (Fig. 2A) but significantly fewer total counts from thyroid tissue (Figs. 2B–2D). Other studies have demonstrated that the LEHR collimator has a higher sensitivity than the ME collimator for ^{123}I imaging using phantoms (*5,7*). The

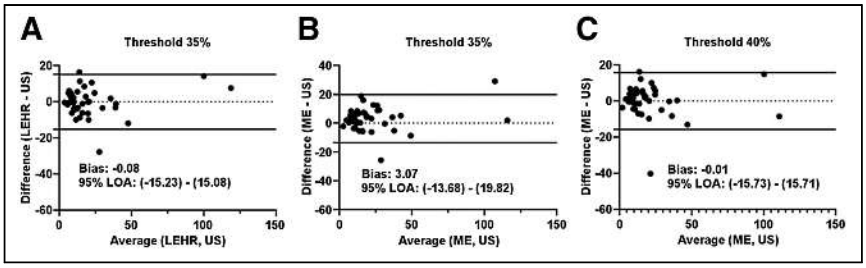

FIGURE 4. Bland–Altman plot analyses of thyroid volume estimation between ultrasonography with LEHR collimators (A) and ultrasonography with ME collimators (B and C) by applying different thresholds.

increased sensitivity of the LEHR collimator is probably due to more scattered photons from background. Scattered photons detected by the detector may be more obvious in patients than in the phantom study, as the higher-energy photons may undergo scattering in the human body before they reach the collimator. These scattered photons deteriorate image quality and increase background noise. For thyroid tissue evaluation, the ME collimator demonstrates significantly higher sensitivity than the LEHR collimator for thyroid ^{123}I scanning in clinical patients. The increased sensitivity for thyroid scans with the ME collimator is due mainly to the increased diameter of the collimator holes, allowing detection of more photons parallel to the collimator holes.

The ME collimator has lower spatial resolution than the LEHR collimator; however, the difference is not very obvious for thyroid ^{123}I imaging in patients (Fig. 1), probably because of an improved imaging quality with less septal penetration and scattering from the ME collimator. In addition, the increased total thyroid counts from the ME collimator also contribute to improved image quality, thus partially compensating for the disadvantage of lower spatial resolution. No difference was observed in identifying functional nodules between LEHR and ME collimators in this study. However, the patient sample size was fairly small, and only 10 patients were referred for evaluation of known thyroid nodules. The increased sensitivity of the ME collimator with improved thyroid-to-background contrast suggests that images can be acquired with less scanning time than for the LEHR collimator if a fixed-count imaging protocol is used. This advantage may potentially benefit SPECT imaging, which requires significantly longer scanning times using a ME collimator for SPECT imaging and may subsequently reduce the chance of patient motion.

The slightly larger thyroid gland visualized in ME collimator images is most likely due to increased thyroid photon counts in ME collimator images. Although thyroid scintigraphy is less precise than anatomic imaging modalities such as MRI or ultrasound in estimating thyroid size or volume, it is still convenient to have an estimation of functional thyroid volume using thyroid scintigraphy. This is especially helpful for ^{131}I treatment with a calculated dose protocol, which is frequently used clinically. The LEHR collimator imaging resulted in slight underestimation of the thyroid length compared with ultrasonography measurement as the standard. Manual measurement of thyroid length is more accurate in the ME collimator images than in the LEHR collimator images, probably because of increased collimator sensitivity and improved thyroid-to-background contrast with the ME collimator.

Various thyroid volume calculation methods using scintigraphy include either manual measurement of thyroid size or automatic calculation of thyroid area (*10*). No universal method has been widely accepted by the nuclear medicine community. The automatic calculation of thyroid area by applying different thresholds of the maximum average pixel using software is the most commonly applied method to estimate thyroid size. This method is more precise than a manually drawn thyroid contour or thyroid border, which usually generates significant variability. Because of the significant difference in thyroid photon counts and sensitivity between LEHR and ME collimators, applying the same threshold will result in an increased area estimation in ME collimator images when compared with LEHR collimator images. Therefore, different thresholds should be used to estimate the thyroid areas for LEHR and ME collimator images.

A 35% threshold in the LEHR collimator images yielded the closest volume estimation as compared with ultrasonography estimation, and a 40% threshold in the ME collimator images yielded similar results. These thresholds are higher than in other studies, which used thresholds of between 20% and 30% (*11,12*). This difference is probably due to different imaging protocols and different formulas to calculate thyroid volume. Our image acquisition time was 7 min. Other studies used 5 min, had a longer distance between the collimator and the patient, or used a fixed-count protocol (*11–14*). In addition, volume estimation from planar thyroid scintigraphy reported by others was larger than from ultrasonography and was also dependent on different formulas (*12,14*). Appropriate thresholds should be based on different volume calculation formulas, different imaging protocols, and different scanners. Measurement from the ME collimator images was consistently higher than measurement from the LEHR collimator images when both used the same imaging protocol and same threshold. Therefore, a higher threshold should be used for ME collimator images. Alternatively, the difference could be adjusted by applying a different formula or scaling factor.

Measurement of both thyroid length and thyroid volume between LEHR and ME collimator images demonstrated a similar spread of 95% limits of agreement, suggesting that the LEHR and ME collimators have similar precision and variation when compared with ultrasonography measurement. In terms of thyroid volume estimation using planar thyroid scintigraphy, either the LEHR or the ME collimator could generate relatively reliable results if an appropriate formula is being used. It has been reported that SPECT is more accurate

and precise than planar scintigraphy to estimate thyroid volume (*12,13*). Whether an ME collimator could improve the imaging quality and volume estimation for thyroid tissue in SPECT imaging still needs to be determined.

CONCLUSION

^{123}I thyroid imaging with ME collimators produces less scattered background noise, improved thyroid-to-background contrast, and higher collimator sensitivity than does imaging with LEHR collimators. Manual measurement of thyroid length is more accurate with the ME collimator; however, different thyroid thresholds should be used to estimate the thyroid area and volume for the LEHR and ME collimators.

DISCLOSURE

No potential conflict of interest relevant to this article was reported.

ACKNOWLEDGMENTS

We thank Josephine Ribe, David Sun, and Ralph Mendoza at the VA Greater Los Angeles Healthcare System for assistance with thyroid scintigraphy.

REFERENCES

1. Atkins HL, Klopper JF, Lambrecht RM, Wolf AP. A comparison of technetium 99M and iodine-123 for thyroid imaging. *AJR.* 1973;117:195–201.
2. Wellman HN, Anger RT Jr. Radioiodine dosimetry and the use of radioiodines other than ^{131}I in thyroid diagnosis. *Semin Nucl Med.* 1971;1:356–378.
3. McKeighen RE, Muehllehner G, Moyer RA. Gamma camera collimator considerations for imaging ^{123}I. *J Nucl Med.* 1974;15:328–331.
4. Dobbeleir AA, Hambye AS, Franken PR. Influence of high-energy photons on the spectrum of iodine-123 with low- and medium-energy collimators: consequences for imaging with ^{123}I- labelled compounds in clinical practice. *Eur J Nucl Med.* 1999;26:655–658.
5. Geeter FD, Franken PR, Defrise M, Andries H, Saelens E, Bossuyt A. Optimal collimator choice for sequential iodine-123 and technetium-99m imaging. *Eur J Nucl Med.* 1996;23:768–774.
6. Verberne HJ, Feenstra C, de Jong WM, Somsen GA, van Eck-Smit BL, Busemann Sokole E. Influence of collimator choice and simulated clinical conditions on ^{123}I-MIBG heart/mediastinum ratios: a phantom study. *Eur J Nucl Med Mol Imaging.* 2005;32:1100–1107.
7. Macey DJ, DeNardo GL, DeNardo SJ, Hines HH. Comparison of low- and medium-energy collimators for SPECT imaging with iodine-123-labeled antibodies. *J Nucl Med.* 1986;27:1467–1474.
8. Inoue Y, Suzuki A, Shirouzu I, et al. Effect of collimator choice on quantitative assessment of cardiac iodine-123 MIBG uptake. *J Nucl Cardiol.* 2003;10:623–632.
9. Bland JM, Altman DG. Statistical methods for assessing agreement between two methods of clinical measurement. *Lancet.* 1986;1:307–310.
10. Long DT, King MA, Sheehan J. Comparative evaluation of image segmentation methods for volume quantitation in SPECT. *Med Phys.* 1992;19:483–489.
11. Pant GS, Kumar R, Gupta AK, Sharma SK, Pandey AK. Estimation of thyroid mass in Graves' disease by a scintigraphic method. *Nucl Med Commun.* 2003;24:743–748.
12. van Isselt JW, de Klerk JM, van Rijk PP, et al. Comparison of methods for thyroid volume estimation in patients with Graves' disease. *Eur J Nucl Med Mol Imaging.* 2003;30:525–531.
13. Zaidi H. Comparative methods for quantifying thyroid volume using planar imaging and SPECT. *J Nucl Med.* 1996;37:1421–1426.
14. Wesche MF, Tiel-van Buul MM, Smits NJ, Wiersinga WM. Ultrasonographic versus scintigraphic measurement of thyroid volume in patients referred for ^{131}I therapy. *Nucl Med Commun.* 1998;19:341–346.

Global and Regional Variations in Transthyretin Cardiac Amyloidosis: A Comparison of Longitudinal Strain and ^{99m}Tc-Pyrophosphate Imaging

Christopher Lee*[1], Chieh-Ju Chao*[1], Pradyumna Agasthi[1], Amith R. Seri[1], Amar Shere[1], Lanyu Mi[2], Lisa Brown[1], Chance Marostica[1], Timothy Barry[1], Ming Yang[3], Julie Rosenthal[1], Samuel Unzek[4], Farouk Mookadam[1], and Reza Arsanjani[1]

[1]*Department of Cardiovascular Diseases, Mayo Clinic Arizona, Phoenix, Arizona;* [2]*Department of Research, Division of Biomedical Statistics and Informatics, Mayo Clinic Arizona, Phoenix, Arizona;* [3]*Department of Radiology, Mayo Clinic Arizona, Phoenix, Arizona; and* [4]*Banner–University Medical Center Phoenix, Phoenix, Arizona*

There are limited data on the head-to-head comparison of ^{99m}Tc-pyrophosphate (^{99m}Tc-PYP) and echocardiographic strain imaging in the assessment of transthyretin (TTR) cardiac amyloidosis. **Methods:** At Mayo Clinic Arizona, patients who had undergone both a ^{99m}Tc-PYP scan and a transthoracic echocardiogram within a 90-d period were retrospectively identified for chart review and strain imaging analysis. Patients were divided into 2 groups according to their ^{99m}Tc-PYP results (PYP-positive [PYP+] or PYP-negative [PYP−]) for the comparison. A standard 17-segment model was used for segmental, regional, and global longitudinal strain comparison. A P value of less than 0.05 was deemed significant. **Results:** In total, 64 patients were included, the mean age was 75.1 ± 13.0 y, and 57 (89.1%) were male. Comparing the PYP+ to the PYP− group, the left ventricular global longitudinal strain was significantly worse in the former (PYP+ vs. PYP−, −10.5 ± 2.6 vs. −13.1 ± 4.1; $P = 0.003$). PYP+ patients also had worse regional basal strain (−4.6 ± 2.6 vs. −8.8 ± 4.0, $P < 0.001$) and a trend toward worse midventricular strain (−9.6 ± 4.0 vs. −11.7 ± 4.4, $P = 0.07$), but there was no statistical difference in the apical region (−17.6 ± 4.73 vs. −19.0 ± 6.46, $P = 0.35$). This is consistent with an apex-sparing pattern shown by the relative apical longitudinal strain index (1.3 ± 0.5 vs. 1.0 ± 0.3, $P = 0.008$). Segment-to-segment analysis demonstrated a significant difference in strain between PYP+ and PYP− segments in 4 segments: basal inferior ($P = 0.006$), basal anterolateral ($P = 0.01$), apical septal ($P = 0.002$), and apical inferior ($P = 0.001$). Left ventricular diastolic dysfunction was significantly different, with 17 (77.3%) patients in the PYP+ group versus 15 (36.6%) in PYP− participants ($P = 0.002$). **Conclusion:** Our study suggested that ^{99m}Tc-PYP uptake is related to overall worse LV segmental, regional, and global longitudinal strain function, as well as diastolic function, compared with patients without ^{99m}Tc-PYP uptake. These data are important for helping clinicians learn about the echocardiographic function features related to ^{99m}Tc-PYP uptake and can help generate hypotheses for future studies.

Key Words: cardiology; correlative imaging; ^{99m}Tc-pyrophosphate imaging; longitudinal strain; transthyretin cardiac amyloidosis

Received Jan. 3, 2021; revision accepted Aug. 5, 2021.

For correspondence or reprints, contact Christopher Lee (christopherlee@penmedicine.edu).

*Contributed equally to this work.

Published online Dec. 21, 2021.

J Nucl Med Technol 2022; 50:30–37
DOI: 10.2967/jnmt.120.261893

Amyloidosis is a heterogeneous group of disorders involving the extracellular deposition of insoluble amyloid protein that can occur in different organs. Amyloidosis can be either inherited or acquired. The cardiac manifestation of amyloidosis includes heart failure, conduction disease, syncope, and sudden cardiac death (*1*). So far, whereas over 30 different amyloidogenic proteins have been described, cardiac amyloid deposition and the development of cardiomyopathy are associated with types of amyloid proteins, most commonly transthyretin (TTR) and amyloid light chain (AL) proteins (*2*).

Concerning the diagnosis of cardiac amyloidosis (CA), endomyocardial biopsy–demonstrated amyloid deposition remains the gold standard and is also important for protein typing (*3*). However, newer noninvasive approaches can potentially allow earlier detection of CA with a minimal side-effect profile. In patients with a noncardiac biopsy demonstrating amyloid deposition, cardiac involvement has been defined—by a consensus opinion from the 10th International Symposium on Amyloidosis—as either a positive heart biopsy and or increased left ventricular (LV) wall thickness (interventricular septal thickness > 12 mm) in the absence of hypertension or other potential causes of true LV hypertrophy (*4*). Making an early diagnosis of cardiac amyloid has significant clinical implications concerning the poor prognosis of late-stage CA (*1,5*). However, as of 2019, TTR remained underdiagnosed; there were still 10%–15% of older adults with heart failure who might have unrecognized wild-type TTR (*5*).

Historically, the diagnosis of CA had involved a high index of clinical suspicion and consideration of a constellation of symptoms. Increased wall thickness noted on the echocardiogram was initially seen as a clue to CA; however, the same finding can also be present in other clinical conditions, such

as hypertrophic cardiomyopathy and hypertensive heart disease (*6,7*). In clinical practice, a comprehensive evaluation of echocardiography parameters or involving other noninvasive studies is generally required to better differentiate these conditions. The characteristic apex-sparing pattern of myocardial strain distribution was suggestive of CA rather than other etiologies when the initial echocardiographic findings raised the concerns (*7–9*). The apex-sparing strain pattern has been observed in both AL- and TTR-type CA (*10,11*). A difference in myocardial strain dysfunction between different subtypes has also been reported (*10*).

The other widely used noninvasive modality is ^{99m}Tc-pyrophosphate (^{99m}Tc-PYP) imaging, which is highly sensitive and specific for the diagnosis of TTR-related amyloidosis without the need for endomyocardial biopsy (*12*). A recent European study using ^{99m}Tc-hydroxymethylene diphosphonate determined the regional distribution of nuclear tracer uptake in patients with TTR-related CM, a distribution that was similar to the apex-sparing pattern of strain echocardiographic imaging (*13*). The difference in uptake by human TTR and AL cardiac tissues is believed to be related to the microcalcifications in human TTR cardiac tissue, which are more common than in AL cardiac tissue (*14*).

Despite being commonly used for the assessment of CA, strain echocardiography and ^{99m}Tc-PYP imaging findings have yet to be compared directly with each other. Differences in echocardiographic parameters were also reported between the AL and TTR subtypes of CA.

We designed this study to compare the echocardiographic strain distribution patterns between patients with positive ^{99m}Tc-PYP results (PYP+ group) and negative ^{99m}Tc-PYP results (PYP− group). We hypothesized that ^{99m}Tc-PYP uptake correlates with worse echocardiographic LV strain function.

MATERIALS AND METHODS

The study protocol complied with the Declaration of Helsinki and was approved by the Mayo Clinic institutional review board. Informed consent was waived because the study was deemed to pose minimal risk (retrospective chart review and data analysis only).

Patient Population

All consecutive patients who had undergone both ^{99m}Tc-PYP scanning for suspected CA and, within 90 d, transthoracic echocardiography from October 2015 to March 2018 at a single center (Mayo Clinic, Arizona) were retrospectively selected. There was a high clinical suspicion of CA in these individuals, including increased LV wall thickness in the absence of significant hypertension, and findings were more suggestive of CA than of hypertrophic cardiomyopathy. These individuals subsequently underwent serum protein electrophoresis, urine protein electrophoresis, and a serum free light chain assay and were then referred for ^{99m}Tc-PYP scanning (*15*).

Each patient's transthoracic echocardiogram study was reviewed for image-quality selection criteria, which included acceptable-quality echocardiogram images of the standard apical 4-, 3-, and 2-chamber views, to allow for complete strain imaging analysis. Adequate quality was defined as no more than 2 segments of unreadable strain, which was the only metric that resulted in exclusion of otherwise eligible participants from final analysis.

Patient Demographics, Electrocardiograms, Biomarkers, and Ancillary Data

Detailed review of electronic health records yielded a broad dataset, including participant demographics (age, sex), body mass index (kg/m^2), creatinine, estimated glomerular filtration rates, troponin, N-terminal prohormone B-type natriuretic protein, and clinical parameters such as the presence or absence of low voltage on electrocardiography, pleural effusion, and pericardial effusion.

Echocardiography and Strain Imaging

Measurement of LV diastolic function, including descriptions and acquisition of specific parameters, has been outlined by Nagueh et al. (*16*). The original transthoracic echocardiogram reports were reviewed to obtain echocardiographic structural, systolic, and diastolic functional parameters, including LV ejection fraction (%), LV mass (g), LV mass index (g/m^2), LV stroke volume (mL), cardiac index (L/m^2/min), mitral E-wave velocity (m/s), mitral A-wave velocity (m/s), mitral E/A ratio, mitral E wave deceleration time (ms), tissue Doppler medial e′ velocity (m/s), E/e′ ratio medial, E/e′ ratio lateral, tricuspid annulus systolic excursion by M-mode (mm), right ventricular systolic pressure (mm Hg), and the presence of diastolic dysfunction. All echocardiographic parameters were measured according to the American Society of Echocardiography guidelines (*17,18*).

Strain imaging was retrospectively completed using commercial software, EchoInsight (Trust Bio-sonics). Strain imaging was initially generated using the 18-segment model. Global longitudinal strain (GLS) and regional longitudinal strain values for the apical, mid, and basal regions were abstracted as reported by EchoInsight. Both strain and ^{99m}Tc-PYP imaging were represented using the standard 17-segment American Heart Association model (*18*). Strain modeling was converted from the 18-segment model to the 17-segment model to allow direct comparability (Fig. 1). This conversion process involved averaging of strain segments 13–18 from the 18-segment model; this average was then taken to represent segments 13–17 in the 17-segment model.

^{99m}Tc-PYP Imaging

^{99m}Tc-PYP scanning was performed using a standard American Society of Nuclear Cardiology protocol containing both planar and SPECT/CT series (*18*). After intravenous administration of 370 MBq of ^{99m}T-PYP, 15-min and 3-h delayed anterior-view planar images of the chest (matrix, 256 × 256) were acquired, followed by a SPECT/CT scan of the chest.

On the 3-h anterior planar image, circular regions of interest were placed around the heart and contralateral right chest to measure the counts and calculate the heart–to–contralateral-lung ratio (heart-to-contralateral ratio). Heart-to-contralateral values higher than 1.4 are considered indicative of TTR CA with a high PPV. Heart-to-contralateral values in the range of 1.3–1.4 can be seen with TTR amyloidosis, especially when activity is seen in the myocardium on SPECT/CT.

On SPECT/CT images, semiquantitative grading (0–3 scale) is based on visual inspection of tracer uptake in the myocardium, compared with that in the rib (*19*).

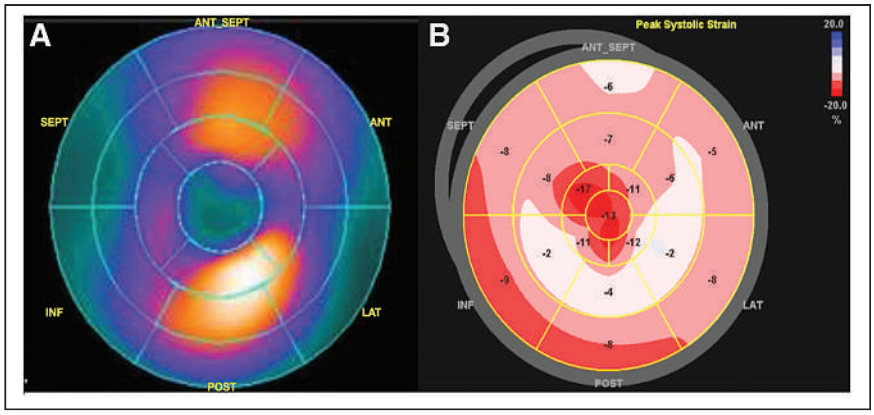

FIGURE 1. Side-by-side comparison of American Heart Association 17-segment model bull's-eye color-mapping plots of ^{99m}Tc-PYP scan (A) and speckle-tracking strain imaging (B) in representative case with positive ^{99m}Tc-PYP findings. Panel A demonstrates intense LV myocardium uptake in anterior and inferior segments and no uptake at apex. Panel B demonstrates characteristic apex-sparing distribution pattern of peak LV longitudinal systolic strain. In this case, segments with uptake are associated with worse strain function. Values in panel B stand for segmental peak longitudinal systolic strain of each segment. ANT = anterior; INF = inferior; LAT = lateral; POST = posterior; SEPT = septal.

Other variables include the heart-to-contralateral ratio of the counts on anterior view planar scintigraphy images and a SPECT/CT-based semiquantitative scale of the myocardial radiotracer uptake. A positive ^{99m}Tc-PYP scan is defined as one on which any of the 17 segments is deemed to be ^{99m}Tc-PYP–positive according to the American Society of Nuclear Cardiology guidelines (*20*). ^{99m}Tc-PYP scan results were reported using the bull's-eye 17-segment model.

Electrocardiograms, Biomarkers, and Ancillary Data

The electronic health records were reviewed for patient demographic and other clinical data, including participant demographics (age, sex), body mass index, serum creatinine, estimated glomerular filtration rates, troponin, N-terminal prohormone B-type natriuretic protein, and clinical parameters such as the presence or absence of low voltage on electrocardiography, pleural effusion, and pericardial effusion.

Statistical Analysis

Descriptive statistics are used to summarize demographic and clinical characteristics. Mean and SD, with 2-sample *t* testing for group comparison, are presented for normally distributed continuous variables, and median and interquartile range, with Wilcoxon rank-sum testing, are used to describe nonnormally distributed continuous data. Categoric variables are summarized as frequency (%), with Fisher exact testing for comparison. As for strain imaging parameters, a 2-sample *t* test was used for global, regional, and segmental analysis. The 17 segments were categorized into 3 regions (basal, mid, and apical) for regional analysis. Relative apical longitudinal strain index (RALSI) was calculated as average apical LS/average basal LS + average mid LS (*8*). Regional analysis was done to compare the mean longitudinal strain between participants with positive ^{99m}Tc-PYP findings in any segment and those with a completely negative ^{99m}Tc-PYP scan. Segment analysis was done to compare the mean strain in PYP+ versus PYP− participants in each corresponding segment. The analysis was conducted using SAS 9.4 (SAS Institute). All tests were 2-sided, and a P value of less than 0.05 was considered statistically significant.

Pearson correlation between ^{99m}Tc-PYP scan findings and strain parameters, with graphical illustration, is shown in Supplemental Tables 1–4 (supplemental materials are available at http://jnmt.snmjournals.org). For PYP− participants, GLS correlated strongly with the apical, mid, and basal regions, with a Pearson correlation coefficient of more than 0.6 ($P < 0.001$). The apical region was significantly strongly associated with the mid region, with a correlation coefficient of 0.7 ($P < 0.001$), but was not significantly associated with the basal region, with a small correlation coefficient of 0.28 ($P = 0.08$) (Supplemental Tables 1 and 2). For PYP+, GLS correlated strongly with the apical and mid regions but not with the basal region, with a strong Pearson correlation coefficient of more than 0.8 ($P < 0.001$) for the apex and mid region but 0.22 ($P = 0.32$) for the basal region. The apical region was significantly associated with the mid region, with a medium Pearson correlation coefficient of 0.55 ($P = 0.009$), but not with the basal region ($P = 0.44$). The mid region was not significantly associated with the basal region ($P = 0.92$). The basal region was not statistically associated with the global, apical, or mid regions ($P > 0.05$ for all) (Supplemental Tables 3 and 4).

RESULTS

Patient Demographics and Variables

In total, 77 consecutive patients were identified, and 64 were included in the final analysis. The mean age of the participants was 75.1 ± 2.9 y, ranging from 41 to 103 y. PYP+ patients were significantly older than PYP− patients (81.0 ± 8.4 vs. 72.0 ± 13.8, $P = 0.002$). Male participants represented 89.1% of all participants, and there were no female participants in the PYP+ group; however, differences in the sex distributions between the 2 groups were not statistically significant. LV septal thickness (18.3 ± 3.0 vs. 14.1 ± 3.4 mm, $P = 0.0001$) and posterior wall thickness (16.4 ± 2.6 vs. 13.1 ± 3.0 mm, $P = 0.0004$), LV mass (352.3 ± 108.5 vs. 272.4 ± 101.5 g, $P = 0.005$), and LV mass index (175.7 ± 51.8 vs. 137.2 ± 42.5 g/m^2, $P = 0.002$) were significantly higher in the PYP+ group. There was no difference in mortality rate between the 2 groups. Patient demographics and selected variables with a breakdown per PYP group are outlined in Table 1.

Global and Regional Longitudinal Strain Comparison

The global, apical, mid, and basal regions were compared between participants with any ^{99m}Tc-PYP positivity and those with a completely negative scan (Table 2). The average GLS (PYP+ vs. PYP−, −10.5 ± 2.6 vs. −13.1 ± 4.1; $P = 0.003$) and the average basal segment longitudinal strain (−4.6 ± 2.6 vs. −8.8 ± 4.0, $P < 0.001$) differed significantly between the PYP+ and PYP− groups, with the PYP+ group having

TABLE 1
Patient Demographics

Demographic	PYP+ (n = 22)	PYP− (n = 42)	Total (n = 64)	P
Age	81.0 (8.4)	72.0 (13.8)	75.1 (12.9)	0.002*
Sex, male	22 (100.0%)	35 (83.3%)	57 (89.1%)	0.09†
Body mass index	27.0 (3.5)	27.2 (5.3)	27.1 (4.8)	0.89*
Systolic blood pressure (mm Hg)	119.8 (16.4)	136.6 (27.5)	130.6 (25.3)	0.029†
Diastolic blood pressure (mm Hg)	73.7 (11.93)	80.5 (15.73)	78.1 (14.74)	0.070†
Hypertension	12 (63.2%)	25 (73.5%)	37 (69.8%)	0.536†
History of coronary artery disease	6 (31.6%)	10 (29.4%)	16 (30.2%)	1.000†
History of diabetes mellitus	2 (10.5%)	10 (29.4%)	12 (22.6%)	0.174†
β-blocker	10 (52.6%)	22 (64.7%)	32 (60.4%)	0.559†
Calcium channel blocker	1 (5.3%)	9 (26.5%)	10 (18.9%)	0.076†
Angiotensin-converting-enzyme inhibitor	3 (15.8%)	5 (14.7%)	8 (15.1%)	1.000†
Angiotensin receptor blocker	5 (26.3%)	5 (14.7%)	10 (18.9%)	0.465†
Spironolactone	4 (21.1%)	5 (14.7%)	9 (17.0%)	0.706†
Amiodarone	0 (0.0%)	1 (2.9%)	1 (1.9%)	1.000†
Creatine	1.3 (1.1–1.5)	1.3 (1.1–1.8)	1.3 (1.1–1.7)	0.44‡
N-terminal prohormone B-type natriuretic protein	3,095.0 (1,640.0–7,323.0)	3,097.0 (1,238.5–8,832.5)	3,097.0 (1,407.0–7,447.0)	0.99‡
Low voltage on electrocardiography	6 (28.6%)	5 (11.9%)	11 (17.5%)	0.1575†
LV septal wall thickness (mm)	18.3 (2.96)	14.1 (3.43)	15.7 (3.83)	0.0001*
LV posterior wall thickness (mm)	16.4 (2.63)	13.1 (2.99)	14.3 (3.28)	0.0004*
LV mass (g)	352.3 (108.5)	272.4 (101.5)	300.7 (110.1)	0.005*
LV mass index (g/m^2)	175.7 (51.8)	137.2 (42.5)	150.4 (49.1)	0.002*
LV End-diastolic diameter (mm)	44.5 (6.69)	47.2 (6.95)	46.2 (6.91)	0.143*
Ejection fraction (%)	47.9 (15.2)	51.8 (15.2)	50.5 (15.2)	0.34*
Stroke volume (mL)	65.6 (25.7)	76.4 (25.1)	72.5 (25.6)	0.1146‡
Cardiac index (L/m^2/min)	2.4 (0.83)	2.8 (0.88)	2.6 (0.88)	0.075†
Tricuspid annular plane systolic excursion by M-mode (mm)	12.3 (3.30)	17.2 (5.36)	15.8 (5.29)	0.0250‡
Pericardial effusion	8 (36.4%)	6 (14.3%)	14 (21.9%)	0.0584†
Heart-to-contralateral ratio	1.7 (0.4)	1.1 (0.2)	1.3 (0.4)	<0.001†
PYP scale¶	0 (0.0%)	30 (71.4%)	30 (46.9%)	<0.001†
0	2 (9.1%)	7 (16.7%)	9 (14.1%)	
1	6 (27.3%)	2 (4.8%)	8 (12.5%)	
2	14 (63.6%)	3 (7.1%)	17 (26.6%)	
3	0 (0.0%)	30 (71.4%)	30 (46.9%)	

*Unequal-variance 2-sample t test.
†Fisher exact test.
‡Wilcoxon rank-sum test.
¶Qualitative value for interpretation is determined by comparing uptake in myocardium. Grade 0 = no myocardial uptake, grade 1 = myocardial uptake less than bone uptake, grade 2 = myocardial uptake equal to bone uptake, grade 3 = myocardial uptake greater than bone uptake.
Qualitative data are number and percentage; continuous data are mean and SD or median and interquartile range.

worse myocardial function. A trend was observed in the average midsegment longitudinal strain (-9.6 ± 4.0 vs. -11.7 ± 4.4, $P = 0.07$). In contrast, there was no statistical difference in the average apical longitudinal strain between the 2 groups (-17.6 ± 4.7 vs. -19.0 ± 6.5, $P = 0.35$). RALSI was found to be 1.3 ± 0.5 in PYP+ patients and 1.0 ± 0.3 in PYP− patients ($P = 0.008$). The global and regional longitudinal strain analysis, along with RALSI, demonstrated overall worse myocardial function in PYP+ patients, with an apex-sparing pattern.

TABLE 2
Regional Comparison in PYP+ Vs. PYP− Participants Using 17-Segment Model

Region	PYP + (n = 22)	PYP− (n = 42)	Total (n = 64)	P*
Global (%)	−10.5 (2.6)	−13.1 (4.1)	−12.2 (3.9)	0.003
Apex (%)	−17.6 (4.7)	−19.0 (6.5)	−18.5 (5.9)	0.35
Mid (%)	−9.6 (4.0)	−11.7 (4.4)	−11.0 (4.6)	0.07
Basal (%)	−4.6 (2.6)	−8.8 (4.0)	−7.3 (4.1)	<0.001

*2-sample t test.

Segment-to-Segment Comparison

Segment-to-segment analysis (Table 3) demonstrated a statistically significant difference in strain between PYP+ and PYP− patients in 4 segments: basal inferior ($P = 0.006$), basal anterolateral ($P = 0.01$), apical septal ($P = 0.002$), and apical inferior ($P = 0.001$). No other segments demonstrated a statistically significant difference. The segments with a significant difference in strain were in either the basal or the apical segments.

Comparison of LV Diastolic Dysfunction

LV diastolic dysfunction significantly differed between the 2 groups, occurring in 17 (77.3%) patients in the PYP+ group versus 15 (36.6%) in the PYP− group ($P = 0.002$). When the PYP+ group was compared with the PYP− group, the medial E/e′ ratio was significantly higher in the PYP+ group, and the mean mitral A wave velocity and the medial and lateral e′ velocity measurements were significantly lower in the PYP− group. Also, we observed trends toward a higher mean E/A ratio and lateral E/e′ ratio in the PYP+ group. These data consistently demonstrated worse diastolic function in PYP+ patients. Detailed data are summarized in Table 4.

DISCUSSION

Our CA patient cohort had a similar age, sex, and race distribution to that in published data (*10,21–23*); the absence of female cases in the PYP+ group was likely due to the small sample size, as PYP+ is known to have a male-predominant population according to previous reports. LV mass and LV mass index were significantly higher in PYP+ patients. PYP+ patients were older than PYP− patients. To the best of our knowledge, this was the first study that demonstrated a difference in global and regional strain patterns among the TTR subtype CA, as determined by ^{99m}Tc-PYP imaging, and provided a segment-to-segment comparison between PYP+ and PYP− segments. Our study showed the correlations

TABLE 3
Segment-to-Segment Comparison in PYP+ Vs. PYP− Participants Using 17-Segment Model Individually

		PYP−		PYP+		
Segment	Region	n	Mean (%)	n	Mean (%)	P*
Basal	Anterior	49	−8.5 (6.82)	12	−5.7 (4.31)	0.17
	Anteroseptal	54	−13.3 (7.58)	8	−14.3 (6.86)	0.73
	Inferoseptal	50	−19.3 (8.09)	9	−20.3 (7.55)	0.71
	Inferior	44	−8.7 (6.44)	16	−3.3 (6.27)	0.006
	Inferolateral	46	−11.7 (8.40)	15	−10.9 (6.51)	0.74
	Anterolateral	51	−19.7 (8.63)	9	−11.8 (8.57)	0.01
Mid	Anterior	45	−8.3 (6.00)	18	−6.3 (4.69)	0.20
	Anteroseptal	40	−10 (5.92)	21	−8.4 (4.63)	0.31
	Inferoseptal	41	−18.9 (8.91)	22	−18.0 (5.69)	0.61
	Inferior	45	−9.4 (8.64)	18	−7.6 (6.12)	0.42
	Inferolateral	48	−9.1 (6.12)	14	−7.9 (4.07)	0.52
	Anterolateral	49	−16.4 (8.25)	14	−15.6 (6.44)	0.76
Apical	Anterior	51	−12.4 (4.80)	12	−10.2 (3.09)	0.15
	Septal	41	−13.1 (4.96)	22	−9.9 (2.85)	0.002
	Inferior	42	−13.1 (4.90)	21	−9.7 (2.80)	0.001
	Lateral	51	−12.4 (4.76)	12	−10.2 (3.31)	0.13
	Apex	55	−12.2 (4.67)	8	−10.5 (3.83)	0.33

*2-sample t test.
Data in parentheses are SDs.

TABLE 4
LV Diastolic Function Parameters

Parameter	PYP+ (n = 22)	PYP− (n = 42)	Total (n = 64)	P
Presence of diastolic dysfunction	17 (77.3%)	15 (36.6%)	32 (50.0%)	0.002*
Peak tricuspid regurgitation velocity (m/s)	2.7 (0.44)	2.9 (0.46)	2.8 (0.46)	0.176†
Right ventricular systolic pressure (mm Hg)	40.3 (12.7)	44.1 (15.1)	42.8 (14.3)	0.3370‡
E-wave velocity (m/s)	0.9 (0.8–1.0)	0.8 (0.7–1.0)	0.9 (0.7–1.0)	0.70†
A-wave velocity (m/s)	0.5 (0.3–0.7)	0.8 (0.6–0.9)	0.7 (0.5–0.9)	0.03†
E/A ratio	2.0 (1.1–3.0)	1.2 (0.9–1.8)	1.3 (1.0–2.0)	0.06†
E deceleration time (ms)	154.5 (140.0–189.0)	178.0 (139.0–205.0)	170.0 (140.0–205.0)	0.46†
Tissue doppler medial e′ > velocity (cm/s)	3.3 (1.9)	4.7 (1.7)	4.2 (1.9)	0.009†
Tissue doppler lateral e′ > velocity (cm/s)	4.4 (2.0)	6.3 (2.3)	5.6 (2.4)	0.009†
E/e′ ratio medial	32.4 (18.3)	22.0 (12.1)	25.8 (15.3)	0.02‡
E/e′ ratio lateral	21.8 (9.2)	17.0 (10.3)	18.8 (10.1)	0.07‡

*Fisher exact test.
†Wilcoxon rank-sum test.
‡2-sample t test.
Qualitative data are number and percentage; continuous data are mean and SD or median and interquartile range.

between ^{99m}Tc-PYP uptake and myocardial strain function impairment and provided insight on the underlying mechanism.

Correlations Between ^{99m}Tc-PYP Uptake and Myocardial Strain Function Impairment

Our results demonstrated an overall compromised myocardial strain function and the basal-to-apex gradient (apex sparing) in both PYP+ and PYP− groups, as is consistent with prior studies and again supports the concept of apex sparing regardless of the background pathogenesis of CA (*10,11, 24,25*). Our study further provided a head-to-head comparison between the 2 groups and revealed significantly worse LV GLS and basal regional strain in the PYP+ group, with a trend toward a worse mid ventricular regional strain and a relatively spared apical regional strain. This result is also reflected by the significantly higher RALSI in the PYP+ group, indicating a larger gradient of longitudinal strain. In the segment-to-segment comparison, the PYP+ segments generally had worse segmental strain function, despite not reaching statistical significance in every segment.

Our findings provided qualitative evidence for the correlations between ^{99m}Tc-PYP uptake and impaired myocardial strain function in patients with suspected CA. A previous European study found that quantified ^{99m}Tc-hydroxymethylene diphosphonate uptake in patients with TTR-related CA had an apex-sparing pattern similar to that of strain echo imaging (*13*) and suggested a higher amyloid burden in the basal region as the underlying mechanism. Our study supports the concept and further provided a head-to-head comparison of the nuclear tracer uptake and strain function, as echocardiography was not performed in the other study.

We also attempted to compare our results with prior studies that assessed myocardial strain function in different subtypes of CA. However, because of a lack of endomyocardial biopsy results to confirm the certain subtype, it is difficult to directly compare our results with these studies. Our PYP+ group contained TTR-related CA; however, this population can still include wild-type TTR and hereditary TTR, which may present with a different LV strain function (*10*). Quarta et al. reported better LV GLS in patients with hereditary TTR (−15% ± 4%) than in those with wild-type TTR (−11% ± 3%) or AL-type TTR (−12% ± 4%) in 172 endomyocardial biopsy–confirmed patients (*10*). Our PYP+ group had a mean LV GLS similar to that of the wild-type TTR group. Compared with Quarta's report, our PYP+ patients were 5–6 y older and had a higher LV mass index and mildly impaired LV ejection fraction (*10*), which can represent more severe phenotypes of the disease and therefore can be related to worse LV GLS. Another study reported no difference in LV GLS among 3 major subtypes (AL, wild-type TTR, and hereditary TTR) of CA, with an impaired LV GLS strain at about −10% (*11*). Surprisingly, despite the worse LV GLS across all 3 groups, all LV ejection fractions were within the reference range in their study. The above studies show that patients with hereditary TTR might have a heterogeneous presentation concerning their LV GLS, potentially explaining our observation of worse LV GLS in the PYP+ group.

Longitudinal strain impairment is known to correlate with amyloid burden as measured by histopathology staining and late gadolinium enhancement on cardiac MR images (*11*). Our observation suggests that longitudinal strain impairment is also related to ^{99m}Tc-PYP uptake from the segmental to the global level. Although the exact mechanism of PYP uptake remains unclear, a potential mechanism such as microcalcification of myocardial tissue may play a role in the development of strain function impairment (*14*). This possibility is also supported by Gucht et al., who observed an apex-sparing pattern of ^{99m}Tc-hydroxymethylene diphosphonate uptake (*13*).

The value of investigational amyloid PET agents in clinical trials and the literature for diagnosis and investigation of CA has been encouraging. However, there is still a lack of convincing clinical evidence in distinguishing TTR CA from AL CA (*25*).

In brief, despite having a similar compromised GLS and basal-to-apex regional strain gradient pattern, the overall worse global strain function and higher RALSI can potentially be used to characterize PYP+ patients. With the advantage of being readily available and free of radiation, speckle-tracking strain imaging can become a more valuable noninvasive diagnostic tool in the assessment of CA by providing additional subtyping and prognostic information before an advanced imaging study such as ^{99m}Tc-PYP.

Diastolic Dysfunction in PYP+ or PYP− Patients

Although the apex-sparing strain pattern is characteristic in CA patients, diastolic dysfunction also plays an important role in their clinical presentation and can independently predict mortality (*26*). Diastolic dysfunction in CA patients has been observed in early studies and can deteriorate with progression of the disease (*27,28*). We observed significantly worse diastolic function measured by E/A ratio, medial and lateral e′ velocity, and E/e′ ratio in the PYP+ group than in the PYP− group. To the best of our knowledge, this was the first report to compare PYP+ and PYP− patients, and our findings indicate that ^{99m}Tc-PYP uptake can be a surrogate marker for worse cardiac diastolic function patients with suspected CA. Again, because the significantly older age in our PYP+ group may reflect a later stage of the disease, this result should be interpreted carefully.

Limitations

The study was limited by its retrospective, single-center design. The relatively low number of participants was due to the strict enrollment criteria for participants undergoing ^{99m}Tc-PYP scanning and, within 90 d, strain imaging at a single center. To sufficiently power future similar studies, participants will likely need to be enrolled from multiple centers. The comparison of strain imaging using the 18-segment model and ^{99m}Tc-PYP imaging using the 17-segment model was troublesome and may significantly compromise the segment-to-segment comparison of the apical strain. Efforts were made to minimize this discrepancy as much as possible. Because the intervals between ^{99m}Tc-PYP injection and scintigraphy scanning can lead to different false-positive rates among different protocols, caution should be take when generalizing our results to different scanning protocols.

With limited endomyocardial biopsy results, we were not able to further identify the patients in the PYP+ group as hereditary or wild-type TTR, which may present with different levels of myocardial strain dysfunction.

CONCLUSION

With the advance of imaging technology, noninvasive approaches such as ^{99m}Tc-PYP imaging have become an essential part in the diagnosis of CA, without the need for endomyocardial biopsy. Our study suggested that ^{99m}Tc-PYP uptake is related to overall worse LV segmental, regional, and GLS function, as well as diastolic function, than is no ^{99m}Tc-PYP uptake. Our work provides important data allowing clinicians to appreciate the echocardiographic features related to ^{99m}Tc-PYP uptake and can serve as a hypothesis-generating tool for future investigators.

DISCLOSURE

No potential conflict of interest relevant to this article was reported.

KEY POINTS

QUESTION: How do ^{99m}Tc-PYP imaging and echocardiographic strain imaging compare in the assessment of TTR CA?

PERTINENT FINDINGS: Our study suggested that ^{99m}Tc-PYP uptake is related to overall worse LV segmental, regional, and GLS function, as well as diastolic function, compared with no ^{99m}Tc-PYP uptake.

IMPLICATIONS FOR PATIENT CARE: These data are important for helping clinicians learn about the echocardiographic function features related to ^{99m}Tc-PYP uptake and can help generate hypotheses for future studies.

REFERENCES

1. Dubrey SW, Hawkins PN, Falk RH. Amyloid diseases of the heart: assessment, diagnosis, and referral. *Heart.* 2011;97:75–84.
2. Larsen BT, Mereuta OM, Dasari S, et al. Correlation of histomorphological pattern of cardiac amyloid deposition with amyloid type: a histological and proteomic analysis of 108 cases. *Histopathology.* 2016;68:648–656.
3. Maleszewski JJ. Cardiac amyloidosis: pathology, nomenclature, and typing. *Cardiovasc Pathol.* 2015;24:343–350.
4. Gertz MA, Comenzo R, Falk RH, et al. Definition of organ involvement and treatment response in immunoglobulin light chain amyloidosis (AL): a consensus opinion from the 10th international symposium on amyloid and amyloidosis. *Am J Hematol.* 2005;79:319–328.
5. Ruberg FL, Grogan M, Hanna M, Kelly JW, Maurer MS. Transthyretin amyloid cardiomyopathy. *J Am Coll Cardiol.* 2019;73:2872–2891.
6. Williams LK, Frenneaux MP, Steeds RP. Echocardiography in hypertrophic cardiomyopathy diagnosis, prognosis, and role in management. *Eur J Echocardiogr.* 2009;10:iii9–iii14.
7. Pagourelias ED, Mirea O, Duchenne J, et al. Echo parameters for differential diagnosis in cardiac amyloidosis. *Circ Cardiovasc Imaging.* 2017;10:e005588.
8. Phelan D, Collier P, Thavendiranathan P, et al. Relative apical sparing of longitudinal strain using two-dimensional speckle-tracking echocardiography is both sensitive and specific for the diagnosis of cardiac amyloidosis. *Heart.* 2012;98:1442–1448.
9. Liu D, Hu K, Nordbeck P, Ertl G, Störk S, Weidemann F. Longitudinal strain bull's eye plot patterns in patients with cardiomyopathy and concentric left ventricular hypertrophy. *Eur J Med Res.* 2016;21:21.
10. Quarta CC, Solomon SD, Uraizee I, et al. Left ventricular structure and function in transthyretin-related versus light-chain cardiac amyloidosis. *Circulation.* 2014;129:1840–1849.
11. Ternacle J, Bodez D, Guellich A, et al. Causes and consequences of longitudinal LV dysfunction assessed by 2D strain echocardiography in cardiac amyloidosis. *JACC Cardiovasc Imaging.* 2016;9:126–138.
12. Perugini E, Guidalotti PL, Salvi F, et al. Noninvasive etiologic diagnosis of cardiac amyloidosis using ^{99m}Tc-3,3-diphosphono-1,2-propanodicarboxylic acid scintigraphy. *J Am Coll Cardiol.* 2005;46:1076–1084.
13. Gucht AVD, Cottereau A-S, Abulizi M, et al. Apical sparing pattern of left ventricular myocardial ^{99m}Tc-HMDP uptake in patients with transthyretin cardiac amyloidosis. *J Nucl Cardiol.* 2017;25:2072–2079.
14. Stats MA, Stone JR. Varying levels of small microcalcifications and macrophages in ATTR and AL cardiac amyloidosis: implications for utilizing nuclear medicine studies to subtype amyloidosis. *Cardiovasc Pathol.* 2016;25:413–417.

15. Witteles RM, Liedtke M. AL amyloidosis for the cardiologist and oncologist: epidemiology, diagnosis, and management. *JACC CardioOncol.* 2019;1:117–130.
16. Nagueh SF, Smiseth OA, Appleton CP, et al. Recommendations for the evaluation of left ventricular diastolic function by echocardiography: an update from the American Society of Echocardiography and the European Association of Cardiovascular Imaging. *J Am Soc Echocardiogr.* 2016;29:277–314.
17. Lang RM, Badano LP, Mor-Avi V, et al. Recommendations for cardiac chamber quantification by echocardiography in adults: an update from the American Society of Echocardiography and the European Association of Cardiovascular Imaging. *J Am Soc Echocardiogr.* 2015;28:1–39.e14.
18. Cerqueira MD, Weissman NJ, Dilsizian V, et al.; American Heart Association Writing Group on Myocardial Segmentation and Registration for Cardiac Imaging. Standardized myocardial segmentation and nomenclature for tomographic imaging of the heart: a statement for healthcare professionals from the Cardiac Imaging Committee of the Council on Clinical Cardiology of the American Heart Association. *Circulation.* 2002;105:539–542.
19. Bokhari S, Castaño A, Pozniakoff T, Deslisle S, Latif F, Maurer MS. ^{99m}Tc-pyrophosphate scintigraphy for differentiating light-chain cardiac amyloidosis from the transthyretin-related familial and senile cardiac amyloidoses. *Circ Cardiovasc Imaging.* 2013;6:195–201.
20. Dorbala S, Ando Y, Bokhari S, et al. ASNC/AHA/ASE/EANM/HFSA/ISA/SCMR/SNMMI expert consensus recommendations for multimodality imaging in cardiac amyloidosis: part 1 of 2—evidence base and standardized methods of imaging. *J Nucl Cardiol.* 2019;26:2065–2123.
21. Sperry BW, Vranian MN, Hachamovitch R, et al. Subtype-specific interactions and prognosis in cardiac amyloidosis. *J Am Heart Assoc.* 2016;5:e002877.
22. Pinney JH, Whelan CJ, Petrie A, et al. Senile systemic amyloidosis: clinical features at presentation and outcome. *J Am Heart Assoc.* 2013;2:e000098.
23. Connors LH, Sam F, Skinner M, et al. Heart failure resulting from age-related cardiac amyloid disease associated with wild-type transthyretin. *Circulation.* 2016;133:282–290.
24. Nardozza M, Chiodi E, Mele D. Left ventricle relative apical sparing in cardiac amyloidosis. *J Cardiovasc Echogr.* 2017;27:141–142.
25. Yang M, Arsanjani R, Roarke MC. Advanced nuclear medicine and molecular imaging in the diagnosis of cardiomyopathy. *AJR.* 2020;215:1208–1217.
26. Chacko L, Martone R, Bandera F, et al. Echocardiographic phenotype and prognosis in transthyretin cardiac amyloidosis. *Eur Heart J.* 2020;41:1439–1447.
27. Hartmann A, Frenkel J, Hopf R, et al. Is technetium-99m-pyrophosphate scintigraphy valuable in the diagnosis of cardiac amyloidosis? *Int J Card Imaging.* 1990;5:227–231.
28. Klein AL, Hatle LK, Burstow DJ, et al. Doppler characterization of left ventricular diastolic function in cardiac amyloidosis. *J Am Coll Cardiol.* 1989;13:1017–1026.

Predictive Model for ^{82}Rb Generator Bolus Times as a Function of Generator Lifetime

Alexander W. Scott[1], Mark Hyun[1], and Jennifer Kim[2]

[1]*Department of Imaging, Cedars-Sinai Medical Center, Los Angeles, California; and* [2]*Department of Clinical Research Operations, City of Hope, Duarte, California*

^{82}Rb cardiac PET is largely used to study myocardial perfusion with function and to calculate myocardial blood flow (MBF) and coronary flow reserve or myocardial flow reserve. Although the dosing activity of ^{82}Rb is determined by the patient weight, the infusion volume and activity concentration varies with the age of the ^{82}Rb generator. We sought to predict the needed bolus volume of ^{82}Rb to help evaluate the accuracy of MBF findings. **Methods:** Data were collected from deidentified tickets of an ^{82}Rb generator, including the instantaneous eluted activity flow rate. The times to reach 4 activity levels—740, 1,110, 1,480, and 1,665 MBq (20, 30, 40, and 45 mCi, respectively)—were also calculated. The activity flow rate for the largest bolus was fitted to determine the functional form. The time to reach each bolus level was fitted as a function of the generator age, and 95% CIs were created. **Results:** The activity flow rate was fitted with a growth-saturation model, allowing a calculation of bolus volume. The amplitude of the fit was observed to also be influenced by the time since the last elution and possibly other clinical factors. Elution times to reach the 4 activity levels were plotted versus generator age. The linearized data were fitted, and 95% CIs were created symmetrically around the fit. The 95% CI band allowed a prediction of elution time to achieve each bolus size for future generators, as a function only of generator age. **Conclusion:** A predictive model was created for elution times from this brand of ^{82}Rb generator as a function of generator age. The value of this model is in determining whether the necessary amount of activity can be extracted from a generator before reaching one of the backup infusion settings, such as volume limits per administration, given a generator age. Some sites may also control the bolus duration for better MBF calculations, since predicting the time for the injection to complete may determine whether MBF and coronary flow reserve calculations are meaningful.

Key Words: ^{82}Rb; modeling; physics

J Nucl Med Technol 2022; 50:38–42
DOI: 10.2967/jnmt.120.256917

Although both myocardial perfusion SPECT and PET imaging provide valuable information on the 3-dimensional distribution of radiotracers into myocardium, there are several physical differences by which PET has a clear advantage over SPECT (*1*). PET has a high spatial and temporal resolution, reliable attenuation and scatter correction, short imaging protocols using short-lived positron-emitting radiotracers to acquire 3-dimensional acquisitions simultaneously (which offers tracer kinetic models to obtain absolute myocardial blood flow [MBF] measurements for rest and stress, where *coronary flow reserve* or *myocardial flow reserve* are terms interchangeable with *rest MBF* and *stress MBF,* respectively), and relative perfusion and function analysis as well. These important properties of myocardial perfusion PET imaging translate into high diagnostic accuracy, consistent high-quality images, low radiation exposure, short acquisition protocols, routine quantification of MBF, and strong prognostic power.

According to a position statement by the American Society of Nuclear Cardiology and the Society of Nuclear Medicine and Molecular Imaging (*2*), rest–stress PET myocardial perfusion imaging is a preferred test for patients with known or suspected coronary artery disease who meet appropriate criteria and are unable to exercise adequately. Rest–stress PET myocardial perfusion imaging is recommended for patients with suspected coronary artery disease who also meet one or more of the following criteria: patients with poor-quality, equivocal, or inconclusive results on prior stress imaging or results that are discordant with clinical or other diagnostic test results, including findings at coronary angiography; high-risk patients with advanced kidney disease, diabetes, or known disease in the left main coronary artery, multiple coronary arteries, or the proximal left anterior descending coronary artery; patients who have undergone heart transplantation; young patients with coronary artery disease; and patients who need MBF to assess microvascular function.

According to a joint position paper of the Society of Nuclear Medicine and Molecular Imaging Cardiovascular Council and the American Society of Nuclear Cardiology (*3*), under resting conditions, autoregulation of myocardial tissue perfusion occurs in response to local metabolic demands. Rest MBF has been shown to vary linearly according to the product of heart rate and systolic blood pressure (*3,4*). Interpretation of the stress MBF results together with coronary flow reserve (myocardial flow reserve) accounts for the confounding effects of resting hemodynamics (heart rate and systolic blood pressure). To ensure accurate estimates of

Received Dec. 29, 2020; revision accepted Aug. 11, 2021.
For correspondence or reprints, contact Alexander Scott (alexander.scott@cshs.org).
Published online Sep. 28, 2021.

MBF and coronary flow reserve (myocardial flow reserve), it is critical to verify that each dynamic series is acquired and analyzed correctly. Therefore, it is important to note that consistent tracer injection profiles improve the reproducibility of MBF measurements and to ensure adequate sampling of the compete arterial blood input function (*3*).

Assessment and correction of patient motion between the first-pass transit phase and the late-phase myocardial retention images are essential, as motion can otherwise introduce a large bias in the MBF estimates compared with the relative perfusion image findings. The peak height of blood pool time–activity curves at rest and stress should be comparable if similar radiotracer activities are injected. If there are substantial differences, extravasation or incomplete delivery of tracer may have occurred and may result in inaccurate MBF estimates. Because variations in the tracer injection profile can adversely affect MBF accuracy, blood pool time–activity curve should be visually examined for multiple peaks or broad peaks, which may suggest poor-quality injections due to poor-quality intravenous catheters, arm positioning, or other confounding factors from the patient's physiology (*3*).

Another potential source of variability in radiotracer delivery is the ^{82}Rb generator itself. The current recommendation is to inject a weight-based activity level to minimize population radiation dose (or collective dose, due to the ^{82}Rb procedures) (*5*). The ability to deliver a large dose for a large body habitus may be compromised as the generator reaches the end of its lifetime, since the activity curve for the daughter isotope delivered from a generator must vary as the parent isotope decays. The peak height of the activity curve will vary depending on whether the activity is injected as a bolus (activity concentrated in time and location) or is injected continuously as the generator struggles to produce. A recent guide from the American Society of Nuclear Cardiology and the Society of Nuclear Medicine and Molecular Imaging on PET measurements of MBF (*6*) recommends the following to control the duration of a bolus for accurate MBF measurement: ensure a good, free-flowing forearm intravenous line (20-gauge or larger) for tracer administration; flush with saline immediately after the tracer administration to help clear the blood pool activity; review and compare the rest–stress time–activity curves on dynamic images as a quality control; apply motion correction on dynamic images as needed; follow the weight- or body mass index–based dosing consistently; and schedule obese patients for an earlier generator cycle to minimize administering the suboptimum tracer activity because of the volume limit. The last 2 points, regarding bolus duration and weight-based dosing, are dependent on generator performance.

For these reasons, it may be of interest to develop a method for calculating the bolus length for a patient given that patient's weight and the age of the generator (defined as days after calibration). If the time to achieve a complete bolus injection exceeds a level set by the nuclear cardiologist, or would exceed the infusion cart's infusion volume limit setting, then the patient will not receive the diagnostic quality as ordered. The examination may need to be rescheduled for a time when the generator is fresher or when the next generator has been installed, or the clinical approach may need to be changed. This article provides a formula for this calculation, which is based on deidentified injection printouts for a CardioGen-82 (Bracco) ^{82}Rb generator covering its full clinical life.

MATERIALS AND METHODS

The data sample came from deidentified tickets (data output) produced by 3 CardioGen-82 generators. All 3 were calibrated for 3,700 MBq (100 mCi) and were in use for 1 mo each, for a total of 491 elutions. Each generator was retired from clinical use after 1 mo, following institutional policy. One generator was studied independently, and then all generator data were combined for an overall analysis. The following information was extracted from each ticket: date, time, total injected volume, total injected activity, and injected activity rate at each second during the injection. For each elution, the peak injected activity rate was recorded and a calculation was made of the injection duration in seconds to inject up to 4 different activity levels (740, 1,110, 1,480, and 1,665 MBq [20, 30, 40, and 45 mCi, respectively]).

Two separate datasets were created for the purpose of predicting generator behavior. The first dataset was the complete injected activity curve for each injection, for the purpose of predicting the required time to administer a certain amount of activity. The injected activity rate curve of one large bolus injection was fitted using Microsoft Excel to determine the functional form of the bolus over time, and this functional form was applied to the other elutions. Once the functional form was verified, the peak injected activity rate was used as a proxy for the amplitude of the fit when comparing the individual elutions.

The second dataset consisted of the time to reach 4 different injected activity level as a function of the age of the generator, in days since calibration. For each of the chosen activity levels, 95% CI bands were created by fitting the data in OriginPro (OriginLab Corp.) using an exponential growth function of the form $y(t)=y_0+A\cdot\exp\left(\frac{t}{t_1}\right)$, where $y(t)$ is the time to achieve a certain bolus of activity given a generator age t,y_0 is the threshold time (the generator is being eluted but activity is not injected until a threshold of 37 MBq [1.0 mCi]/s), A is the amplitude (s), and t_1 is the growth constant. A 95% CI band was created symmetrically around the fit by shifting y_0 (the y intercept) by $\pm\Delta y$ to encompass 95% of the data between the shifted curves. The fit and 95% CI band allowed prediction of the time to achieve that bolus size for future generators as a function of generator age.

RESULTS

The plot of injected activity per second over time for a single large bolus was well fitted by a growth-saturation model of the form $y(t)=y_0+A\cdot(t-t_0)\cdot\exp(-C\cdot(t-t_0))$, shown in Figure 1. The reduced χ^2 of the fit was 0.61 using an uncertainty of 5% on the activity from the injection cart's dose calibrator. This model allowed calculation of the total injected activity at any time during the elution. However, the peak injected activity rate did not follow an exponential decay with the age of the generator but peaked

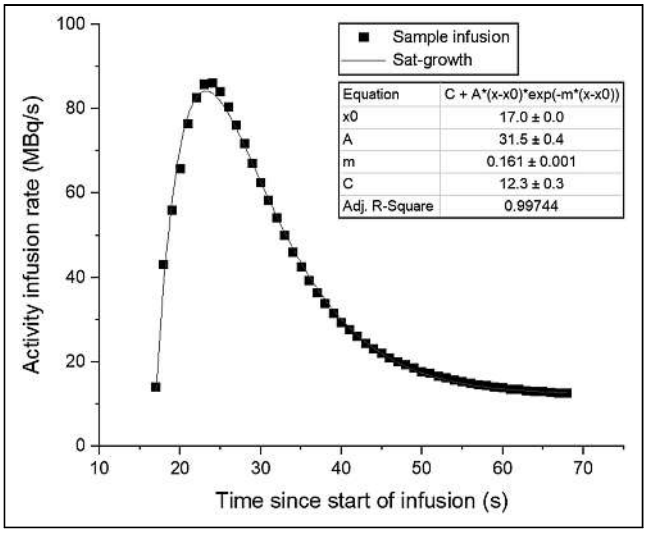

FIGURE 1. Activity infusion rate data and fit for sample bolus from February 9, 2017, with fit parameters for growth-saturation curve of form $y(t)=y_0+A\cdot(t-t_0)\cdot\exp(-C\cdot(t-t_0))$.

within a week of the calibration date of the generator. Also, the peak injected activity rate fluctuated throughout the day, as shown by the spread of peak injection activity rates in Figure 2.

The time to administer 4 different injected activity levels separated into distinct regions, although the bands that contained 95% of the data did overlap at low generator ages, as shown in Figure 3. The 740-MBq (20 mCi) activity level band contained results from 459 elutions, the 1,110-MBq (30 mCi) band contained results from 454 elutions, the 1,480-MBq (40 mCi) band contained results from 169 elutions, and the 1,665-MBq (45 mCi) band contained results from 60 elutions. The parameters of the best fit to the data,

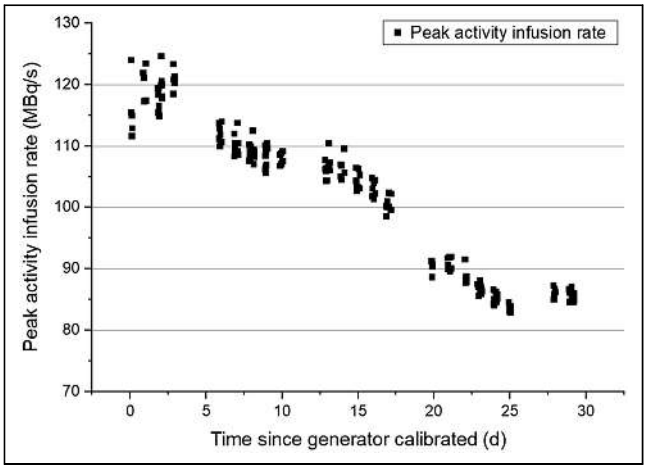

FIGURE 2. Peak activity infusion rate for each study from one representative generator as function of generator age. Amplitude of activity rate curve did not decrease exponentially with generator age as expected. There is also up to 10% variation in peak activity rates within a single day.

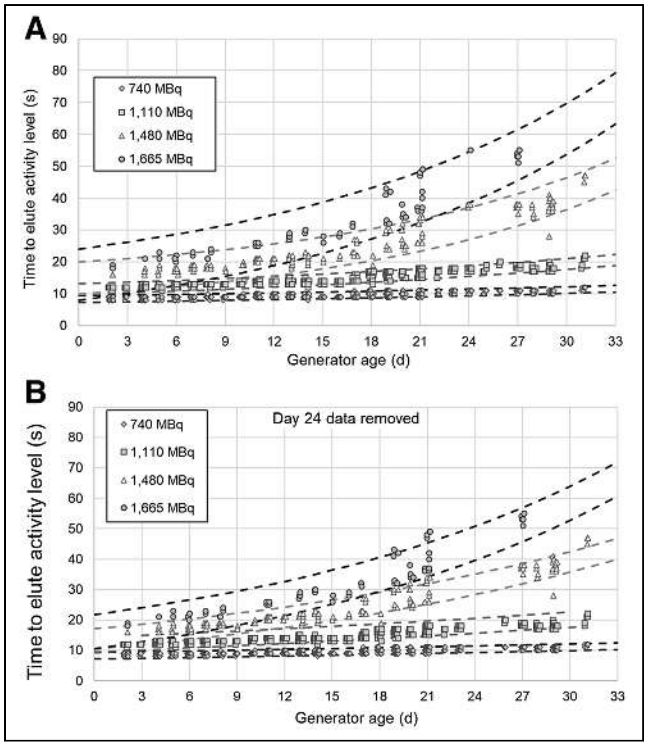

FIGURE 3. Best fit bands for 4 activity levels and time to elute each, as function of generator age. Each band contains 95% of data points for each injected activity level. Data are combined from 3 separate ^{82}Rb generators. Top image is with anomalous results from day 24; bottom image is without.

along with the Δy of the 95% CI bands, are listed in Table 1. These are the parameters of 4 exponential growth models (for the 4 target activity levels studied) of the form $y(t)=y_0+A\cdot\exp(t/t_1)$. Given the age of the generator, the user can calculate the duration of the bolus (s) that will produce one of the 4 activity levels described. Alternatively, the user can take an upper limit for the bolus duration and use the formula $t=t_1\cdot\ln\left(\frac{y-y_0}{A}\right)$ to calculate the last day of generator life on which that bolus can (on average) be achieved.

Some data were excluded from this fit; data from the first 3 d of each generator, when the peak activity rate was increasing, were removed. Also, a single generator had data from 2 d that did not conform to the distribution of the other points, as evidenced by a large residual to the fit, and these data were removed.

DISCUSSION

Although the injected activity rate was well fitted, the amplitude did not depend solely on the physics of radioactive decay. The peak output activity rate (used as a proxy for the amplitude in the growth-saturation fit) increased for the first few days of use and then decreased throughout the week, except the rate did not decrease consistently over the weekend. The generator was not used over the weekend, but the data in Figure 2 for Fridays and Mondays do not

TABLE 1
Fit Parameters for Time to Elute Certain Activity Levels as Function of Generator Age, Following Functional Form $y(t)=y_0+A\cdot\exp\left(\frac{t}{t_1}\right)$

Fit (mCi)	*y* intercept (y_0) (s)	Amplitude (A) (s)	Growth constant (t_1) (d^{-1})	Band range (s)
20	6.05	2.31	37.54	±1.05
30	6.25	5.21	32.60	±1.70
40	9.25	5.70	17.33	±5
45	2.93	13.12	20	±8
Modified 45	16.22	3.15	10.96	±2.5

Additional fit was performed for largest eluted activity (1,665 MBq) to demonstrate that data could be more precisely fitted without 2 days' worth of generator results.

show a consistent pattern. Following a similar pattern, a correlation between peak injection activity rate and length of time since the last elution was observed.

^{82}Sr and ^{82}Rb are in secular equilibrium, and a generator that is eluted every 10 min will have a daughter-to-parent ratio of 99.7%; because clinical practice dictates no less than 10 min between elutions, a correlation was unexpected. The correlation was determined using the Pearson method to produce a coefficient and correlation likelihood; for 1 generator, 100% of days with clinical use showed a 95% likelihood or greater correlation between the eluted peak activity rate and generator rest times. This positive correlation held true even to 350 min since the last elution, which is more than 2 orders of magnitude greater than the half-life of the ^{82}Rb daughter isotope. The variation in peak output due to time since the last elution (a maximum difference of 10%) is greater than the variation between days as the generator ages, as shown in Figure 4. Although longer rest times will have some marginal benefit to bolus lengths as the generator ages, the variability of peak output with generator rest times is one of the confounding factors in presenting a completely deterministic model.

These 2 complications are consistent with findings from the initial development of the ^{82}Sr/^{82}Rb generator by TRIUMF (*7*). As the generator was eluted over time, the distribution of ^{82}Sr within the generator column changed from a narrow band at the top of the column to a much broader peak toward the bottom. Therefore, one would expect the diffusion rate to be higher later in the generator's life because of the greater surface area covered with ^{82}Sr. In a private communication with a Bracco scientist (Dr. Adrian Nunn, oral communication, February 20, 2018), it was confirmed that rest periods of longer than 10 min should result in greater activity in solution because chemical equilibrium has not yet been reached.

Regarding the fit to the second dataset, the prediction band for 1,665 MBq (45 mCi) had much less precision than the bands for other activity levels, having a bandwidth of 8 s compared with 1–2 s for 740- and 1,110-MBq (20 and 30 mCi) activity levels. Subtracting 1 d of data from each of 2 different generators reduced the bandwidth to 2.5 s while keeping 52 of the 60 data points. Although there is not a priori justification for this change to the dataset, it does suggest that the true distribution of bolus times is more narrow and that there is an uncontrolled variable causing longer elution times on certain days. One possibility is that the intravenous gauge used clinically was different for those 2 d, since the elution times were significantly longer given the eluted activity.

The clinical significance of the model was varied across different dose limits. The effect of the bolus lengthening can be best seen at 42 d, which is the generator expiry limit. For an elution of 740 MBq (20 mCi), the model

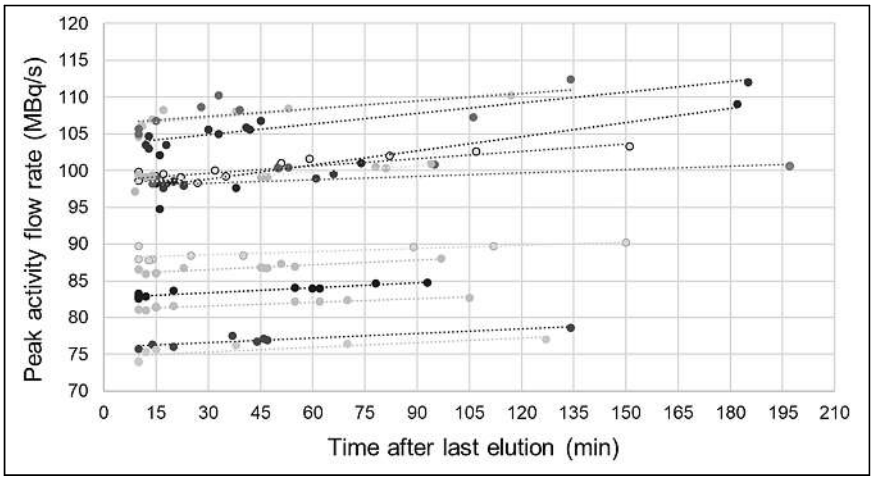

FIGURE 4. Peak activity injection rate for each elution, compared with time since last elution. Lines connect data from same day, such that points come from same generator age. Ten minutes is minimum spacing for clinical use, and no studies had time of less than this value since last elution. On the basis of secular equilibrium assumptions, ^{82}Rb/^{82}Sr ratio should be 99.7% of its maximum at 10 min. Elution continues to produce higher peak activity rates with resting times up to 3 h, the longest time measured.

predicts an elution time of 13 s at day 42, which is not much more than the 8.5 s predicted for day 2. Meanwhile, the 1,665-MBq (45 mCi) model predicts an elution time of 110 s at day 42, in contrast to the 17 s required on day 2.

Our institution limits the infusion to 50 mL to a patient, which although more restrictive than the prescribing information limit of 100 mL, may be more relevant to clinical practice. With a flow rate setting of 50 mL/min, and a start-up time of approximate 14 s, the maximum elution time is 74 s before triggering the elution to stop. For a cutoff time of 74 s, the model predicts that the last day to achieve 1,665 MBq (45 mCi) is day 34; the last day to achieve 1,480 MBq (40 mCi) is day 42. The other 2 activity levels, 740 and 1,110 MBq (20 and 30 mCi), will not be limited before the expiry of the generator.

CONCLUSION

We were able to develop predictions for the time to elute a bolus of certain durations from an ^{82}Rb generator as a function of generator age. Given the flow rate (mL/min) setting selected by the user, the volume of the bolus can be determined from the duration of the elution. Although the eluted activity rate over time was well fitted by a growth-saturation curve, the amplitude of this curve was not dependent just on generator age but also on factors such as generator rest times and likely clinical factors such as patient circulatory resistance and gauge of an intravenous line as well.

There were real instances of truncated elutions; within the datasets collected, there were a few elutions in which the full prescribed activity was not delivered because of triggering of the limit on patient volume (50 mL). For a 1,665-MBq (45 mCi) prescribed activity on day 31 of the generator, the elution was cut off at 72 s because the patient volume limit was hit, and the observed elution time is within the prediction range. The prediction bands for different activity levels allow for a range of bolus injection times that run up to 66 $\pm$ 8 s for 1,665 MBq (45 mCi) on day 31.

The consequences of performing a coronary flow reserve examination using a bolus duration of 61 s (1,665 MBq, or 45 mCi, on day 30) could include erroneous myocardial flow reserve calculations. The authors of this article reviewed our institution's records for patients with myocardial flow reserve calculations and whose examinations resulted from different ^{82}Rb generators, but the data were sparse because this information was not included until somewhat recently. We plan to test our predictions on future generators to determine the broader applicability and to evaluate the clinical impact once more multiyear records are available.

DISCLOSURE

Mark Hyun served as a technical consultant to Astellas regarding the Lexiscan product. No other potential conflict of interest relevant to this article was reported.

ACKNOWLEDGMENTS

We acknowledge Jeffrey Metcalf, CNMT, for his assistance in collecting the data, Dr. Adrian Nunn of Bracco Imaging for information on ^{82}Rb generators, and Dr. Dan Berman, FACC, for contributing to the original research concept.

KEY POINTS

QUESTION: Can an ^{82}Rb generator bolus duration be predicted as a function of activity eluted and the generator age?

PERTINENT FINDINGS: For a particular generator model, the activity output rate was fitted with a growth-saturation curve and the times to achieve certain eluted activities were fitted as a function of generator age using an exponential curve and symmetric bands to capture 95% of the data points.

IMPLICATIONS FOR PATIENT CARE: Utilizing these calculations allows patients to be rescheduled if their predicted injection time given the prescribed ^{82}Rb activity and generator age would exceed the preset bolus duration limit.

REFERENCES

1. Dilsizian V. Transition from SPECT to PET myocardial perfusion imaging: a desirable change in nuclear cardiology to approach perfection. *J Nucl Cardiol.* 2016;23:337–338.
2. Bateman TM, Dilsizian V, Beanlands R, DePuey E, Heller G, Wolinsky D. American Society of Nuclear Cardiology and Society of Nuclear Medicine and Molecular Imaging joint position statement on the clinical indications for myocardial perfusion PET. *J Nucl Med.* 2016;57:1654–1656.
3. Murthy VL, Bateman TM, Beanlands RS, et al. Clinical quantification of myocardial blood flow using PET: joint position paper of the SNMMI Cardiovascular Council and the ASNC. *J Nucl Med.* 2018;59:273–293.
4. Nagamachi S, Czernin J, Kim AS, et al. Reproducibility of measurements of regional resting and hyperemic myocardial blood flow assessed with PET. *J Nucl Med.* 1996;37:1626–1631.
5. Case JA, deKemp RA, Slomka PJ, Smith MF, Heller GV, Cerqueira MD. Status of cardiovascular PET radiation exposure and strategies for reduction: an information statement from the Cardiovascular PET Task Force. *J Nucl Cardiol.* 2017;24:1427–1439.
6. Bateman TM, Heller GV, Beanlands R, et al. Practical guide for interpreting and reporting cardiac PET measurements of myocardial blood flow: an information statement from the American Society of Nuclear Cardiology, and the Society of Nuclear Medicine and Molecular Imaging. *J Nucl Med.* 2021;62:1599–1615.
7. Crackette RV. 82-Sr production from metallic Rb targets and development of an 82-Rb generator. *Appl Radiat Isot.* 1993;44:917–922.

Assessing the Correlation Between ^{68}Ga-PSMA-11 Renal PET Parameters and Renal Function Tests

Jan-Henning Schierz[1], Ismet Sarikaya[2], Ahmed N. Albatineh[3], and Ali Sarikaya[4]

[1]Department of Radiology, Municipal Hospital Dresden, Dresden, Germany; [2]Department of Nuclear Medicine, Faculty of Medicine, Kuwait University, Kuwait City, Kuwait; [3]Department of Community Medicine and Behavioral Sciences, Faculty of Medicine, Kuwait University, Kuwait City, Kuwait; and [4]Department of Nuclear Medicine, Faculty of Medicine, Trakya University, Edirne, Turkey

^{68}Ga-prostate-specific membrane antigen (PSMA) ligands are used for prostate cancer but also show high renal cortical uptake. In this study, we aimed to assess whether there is any correlation between renal PSMA PET parameters and renal function tests using the images of prostate cancer patients. **Methods:** ^{68}Ga-PSMA-11 PET/CT images of the patients with prostate cancer were retrospectively evaluated. The following PET parameters were obtained: SUV_{max}, SUV_{mean}, SUV_{max} corrected for lean body weight, SUV_{mean} corrected for lean body weight, volume, lean body weight–corrected total lesion glycolysis (TLG_{SUL}), and counts of both kidneys, as well as SUV_{mean} of the liver, blood pool, and spleen. Total TLG_{SUL}, total volume, kidney-to-liver ratio, and kidney–to–blood pool ratio were calculated. Creatinine values were obtained, and glomerular filtration rate (GFR) was calculated using the "Modification of Diet in Renal Disease" formula. Statistical analysis was performed to understand whether there is a correlation between the above parameters and renal function tests. **Results:** Twenty-five patients were included in this study. GFR was significantly and positively correlated and creatinine was significantly and negatively correlated with the ratios of renal SUV to liver SUV and renal SUV to blood pool SUV. GFR was marginally positively correlated with renal SUV_{mean} corrected for lean body weight, and creatinine was marginally negatively correlated with total TLG_{SUL}. Total renal parenchymal volume was significantly and directly (positively) associated with GFR and significantly and inversely (negatively) associated with creatinine. **Conclusion:** Renal ^{68}Ga-PSMA uptake appears to be correlated with renal function tests. Our method of measuring approximate renal parenchymal volume on PET images appears to be reliable.

Key Words: PET/CT; ^{68}Ga PSMA-11; kidney; renal function

J Nucl Med Technol 2022; 50:43–48
DOI: 10.2967/jnmt.121.262462

Prostate-specific membrane antigen (PSMA), also known as glutamate carboxypeptidase II or folate hydrolase, is a type II transmembrane protein that is found mainly in prostate tissue. PSMA is overexpressed in prostate cancer and various other malignancies and in extraprostatic normal tissues, with the highest expression being in the kidneys and salivary glands (*1–3*). In immunohistochemical analysis, detectable PSMA levels were identified in the brush borders and apical cytoplasm of a subset of proximal renal tubules, where PSMA is responsible for the reuptake of folates via epithelial brush cells (*1,4*). Renal folate reabsorption seems to be mediated primarily by the glycosylphosphatidylinositol-anchored protein folate receptor α, which is highly expressed at the brush-border membrane of proximal tubule cells (*1,4–6*).

^{68}Ga-PSMA ligands or inhibitors are novel PET radiotracers to image prostate cancer and its metastases (*7,8*). Recently, ^{68}Ga-PSMA-11 was approved by the Food and Drug Administration for prostate cancer imaging, and other PSMA ligands (^{68}Ga and ^{18}F) are currently being evaluated in Europe for approval by the European Medicines Agency (*9*). PSMA ligands radiolabeled with ^{177}Lu and ^{225}Ac are also used to treat prostate cancer metastases, with increasing success (*10,11*). Studies have reported no significant effect on renal function, although therapeutic radiolabeled PSMA ligands show high renal uptake and excretion (*12,13*).

In various articles, Sarikaya et al. have reported that ^{68}Ga-PSMA-11 shows excellent uptake and distribution in the renal parenchyma and demonstrates defects caused by various sizes of simple cortical cysts (*14–16*). In a patient with chronic pyelonephritis, the image resolution of renal PSMA PET as part of a prospective study in adults was superior to that of dimercaptosuccinic acid (DMSA) scanning (*17*).

DMSA is the current gold standard for renal cortical imaging, but there is a shortage of this tracer in various countries, including the United States, and there is a need for alternative radiotracers to image the renal cortex (*18*).

Renal uptake of ^{99m}Tc-DMSA has been shown to correlate well with the effective renal plasma flow, glomerular filtration rate (GFR), and creatinine clearance (*19–23*).

In this study, we wanted to determine whether there is a correlation between renal PSMA PET parameters and renal function tests. Our aim was to understand whether PSMA PET is suitable for renal cortical imaging and whether PSMA uptake parameters can be used to assess or estimate renal function in patients treated with radiolabeled PSMA ligands.

Received Apr. 19, 2021; revision accepted Jul. 7, 2021.
For correspondence or reprints, contact Ismet Sarikaya (isarikaya99@yahoo.com).
Published online Jul. 30, 2021.

MATERIALS AND METHODS

We retrospectively analyzed the ^{68}Ga-PSMA-11 PET/CT images of prostate cancer patients who had undergone renal function testing (creatinine) within 14 d of imaging. All images were obtained in the Nuclear Medicine Department at Dresden Municipal Hospital.

Tracer Production and Image Acquisition

^{68}Ga-PSMA-11 was radiolabeled with an automated module (Scintomics GRP) as described previously (*24*).

Whole-body PSMA PET/CT images were obtained using a Biograph 16 PET/CT camera (Siemens Healthineers) approximately 60 min after intravenous injection of 100–150 MBq (2.7–4.0 mCi) of ^{68}Ga-PSMA-11.

Before PET image acquisition, a low-dose, unenhanced CT scan from vertex to mid thigh was obtained for attenuation correction, anatomic localization, and gross anatomic correlation. The CT parameters included 16 mAs, 120 kV, a 0.8 pitch, 0.5s, 20 × 0.6 mm collimation, and a 5-mm reconstructed slice thickness.

The PET acquisition time was 3 min per bed position. The images were corrected for attenuation on the basis of the CT data, reconstructed using an iterative algorithm (Siemens TrueX), and reformatted, as well as fused online into transaxial, coronal, and sagittal views with Syngo Via MM Oncology VB40 (Siemens Healthineers).

PET Image Analysis

Because of intense activity in the kidneys, PET images were analyzed in low-intensity settings to better see the renal cortical uptake and distribution and accurately place a volume of interest (VOI) without including pelvicalyceal activity. For each kidney, the 3 orthogonal planes on CT and PET were adjusted to optimally draw an ovoid VOI around the respective kidney and exclude possible extrarenal or calyceal activity (Fig. 1). After the plane alignment, the VOI was drawn around the kidney and fitted around the external border of the cortex. To exclude the renal pelvis, we used a lower limit of at least 10 for SUV_{max} for an automatically created isocontour VOI (Fig. 1). Another attempt using a lower limit of 10% of SUV_{max} yielded suboptimal results, as a larger part of the renal pelvis was often included in the isocontour VOI when the kidney SUV_{max} was too low.

Measured Values

PET parameters (SUV_{max}, SUV_{mean}, volume, and total counts) for each kidney were determined on attenuation-corrected PET images. The SUV_{mean} of the liver, spleen, and blood pool was also obtained with standard VOIs provided by the software (Fig. 2).

Calculated Values

From the measured values, SUV_{max} corrected for lean body weight (SUL_{max}), SUV_{mean} corrected for lean body weight (SUL_{mean}), and lean body weight–corrected total lesion glycolysis (TLG_{SUL}) were calculated for each kidney using the lean body mass that was determined using the Janmahasatian formula to take into account the highly variant patient body mass index (ranging from 22.7 to 37.6) (*25*).

Finally, we calculated the mean renal SUV_{max}, SUL_{max}, SUV_{mean}, and SUL_{mean} (arithmetic mean of right and left kidneys), as well as kidney-to-liver and kidney–to–blood pool ratios, using mean renal SUV_{max} and SUV_{mean}.

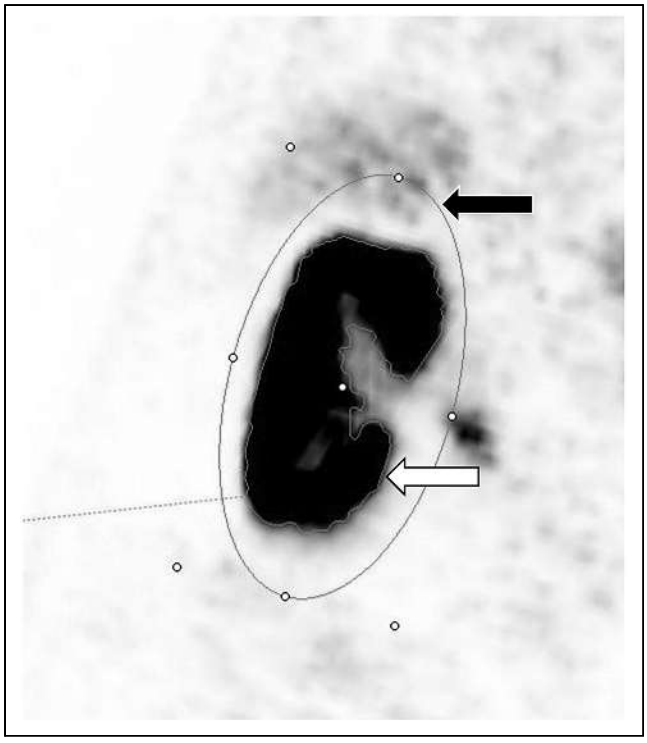

FIGURE 1. Example of VOI placement. Ovoid VOI is placed around kidney (black arrow). Software automatically traces edge with previously defined lower boundary of SUV_{max} of 10, thus establishing isocontour VOI with whole cortical kidney volume (white arrow).

We also calculated the total counts, total TLG, and total volumes of both kidneys (sum of values of both kidneys).

GFR was calculated using the "Modification of Diet in Renal Disease" formula (*26*).

Statistical Analysis

Statistics were analyzed using SPSS statistical software (version 27.0; IBM Corp.). Data were checked and cleaned for any abnormalities and coded accordingly. Simple descriptive statistics including mean, SD, minimum, and maximum were calculated.

The most common procedure to get a point estimate for strength of linear relationship between 2 continuous variables is to use the Pearson correlation coefficient—provided that the variables follow normal distributions. In the presence of outliers or when the data are not normally distributed but can be ranked, the Spearman rank correlation is the best option.

To get a CI estimate of the correlation coefficient in the case of nonnormal data or with a small sample size, and to diminish the effects of outliers, the bootstrap procedure (a computer-intensive resampling technique) can be implemented to produce a CI estimate for the correlation coefficient.

In this analysis, since some of the covariates were not normally distributed and there were some outliers, we used the Spearman rank correlation coefficient to estimate the strength of the linear relationship, and we used the bias-corrected and accelerated bootstrap method based on 2,000 resamplings to produce 95% CIs for the correlation coefficient.

To find the most parsimonious multiple-linear-regression model with covariates that are significantly associated with GFR and

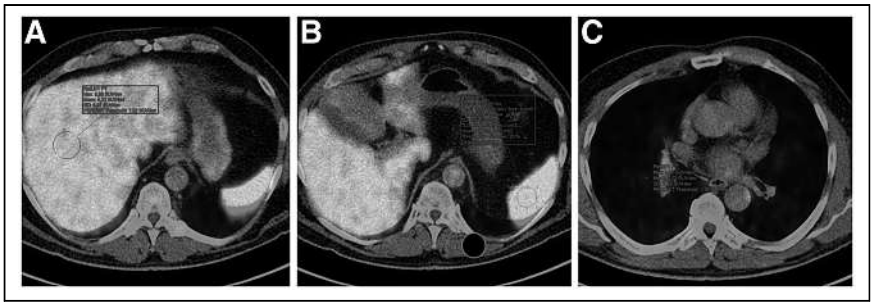

FIGURE 2. Example of VOI placement for liver (A), spleen (B), and blood pool (C). VOIs for liver and blood pool are drawn by software, whereas splenic VOI had to be drawn manually. Color version of this figure is available as supplemental file at http://tech.snmjournals.org.

creatinine, a stepwise regression method with backward substitution was implemented.

In the final multiple-linear-regression model, which resulted from the stepwise procedure, only significant covariates, their *P* values, and 95% CIs for their effect sizes were estimated. Outcomes were tested for normality. The linearity assumption between the outcome and the covariates was checked by Spearman rank correlation.

The final models were tested for significance, residuals were tested for normality, and multicollinearity was checked for all covariates to ensure that no 2 covariates that were highly correlated were included in the final model. All tests were 2-tailed, and a *P* value of less than 0.05 was considered statistically significant.

RESULTS

From 2018 to 2020, we included 25 men in this study, with a mean age of 71.6 y (SD, 9.84 y) and a mean body mass index of 28.7 (SD, 4.0). Patient characteristics, GFRs, and creatinine values are shown in Table 1. Two patients were excluded because of high calyceal activity. All patients received a diuretic (furosemide) injection. None of the patients had pyelonephritis or hydronephrosis. The mean interval between injection and imaging was 64 min, and the range was 60–70 min.

Isocontour VOIs using a lower threshold of more than 10 for SUV_{max} made it possible to quickly estimate the approximate renal parenchymal volume (Fig. 1), provided the renal pelvis contained no residual tracer, which would overestimate the renal counts, SUVs, and renal volumes (Fig. 3). In most patients, the kidneys had a symmetric appearance and uptake. Seven patients, however, showed either large cysts or defects, and 2 of those showed remarkable asymmetry in measured volume and TLG but not in uptake (SUV_{max} and SUV_{mean}) (Fig. 4).

Table 2 shows the mean SUV_{max}, SUV_{mean}, SUL_{max}, SUL_{mean} (arithmetic mean of right and left kidneys), total volume, and total TLG of the kidneys and the SUV_{mean} of the liver, blood pool, and spleen.

The estimated Spearman rank correlation coefficient between GFR and creatinine with several covariates, along with their *P* value and 95% CI estimate, are presented in Table 3. GFR was significantly and positively correlated with renal-to-liver and renal–to–blood pool ratios (mean renal SUV_{max}–to–liver ratio, mean renal SUV_{max}–to–blood pool ratio, mean renal SUV_{mean}–to–liver ratio, mean renal SUV_{mean}–to–blood pool ratio) and age, whereas it was marginally significantly and positively correlated with mean SUL_{mean}. GFR was significantly and negatively correlated with the SUV_{mean} of the blood pool.

On the other hand, creatinine was significantly and negatively correlated with renal SUV–to–liver and renal SUV–to–blood pool ratios (mean renal SUV_{max}–to–liver ratio, mean renal SUV_{max}–to–blood pool ratio, mean renal SUV_{mean}–to–liver ratio, mean renal SUV_{mean}–to–blood pool ratio) and age, whereas it was marginally significantly and negatively correlated with total TLG_{SUL}. It was marginally positively correlated with age and marginally negatively correlated with the SUV_{mean} of the blood pool.

TABLE 1
Descriptive Statistics for Patient Characteristics (n = 25)

Covariate	*n*	Mean	SD	Minimum	Maximum
Age	25	71.6	9.84	34	82
Weight	25	88.4	13.72	68	116
Height	25	175.4	5.07	163	182
Body mass index	25	28.70	4.0	22.7	37.6
GFR	25	78.64	17.71	53	134
Creatinine	25	85.32	17.02	50	114

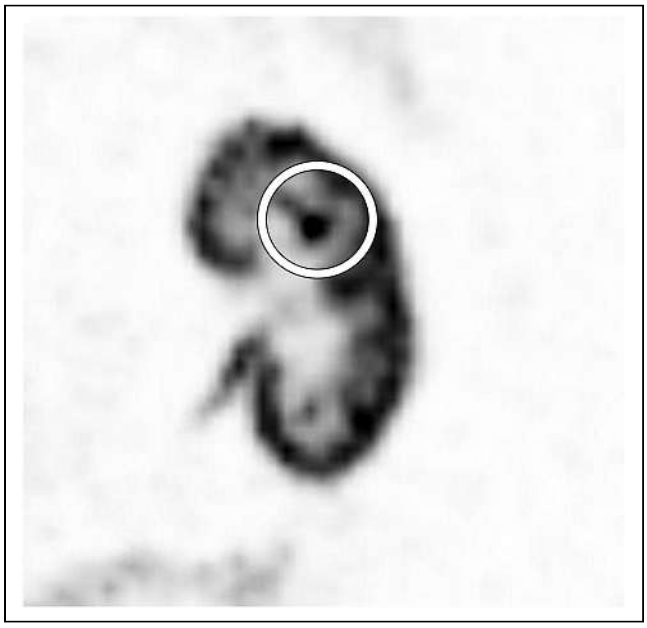

FIGURE 3. Example of excluded patient. Because of the large portion of calyceal tracer (circled), patient was omitted from measurement as software would add this area, falsifying measured values.

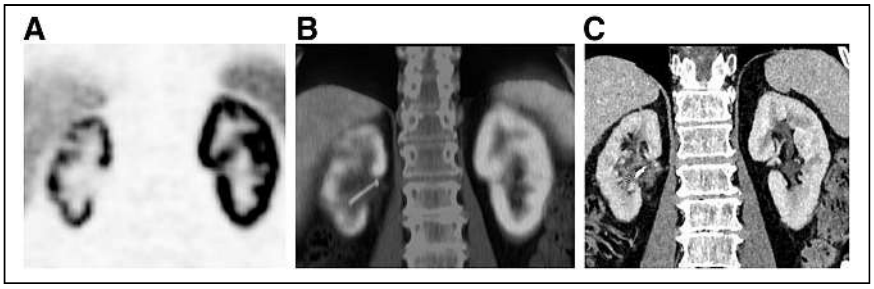

FIGURE 4. Example of strong asymmetry between kidneys. Because of mechanic outflow obstruction, right kidney atrophied and, later, nephrostomy was placed. Shown are PET (A), PET/CT (B), and contrast-enhanced CT (C). Color version of this figure is available as supplemental file at http://tech.snmjournals.org.

In 2 stepwise regression models for GFR and creatinine as outcomes, total renal parenchymal volume was significantly and directly (positively) associated with GFR ($\beta = 0.12$; $P = 0.008$; 95% CI, 0.035–0.205) and significantly and inversely (negatively) associated with creatinine ($\beta = -0.113$; $P = 0.009$; 95% CI, −0.195 to −0.032).

DISCUSSION

^{99m}Tc-DMSA is a radiotracer widely used to image the renal cortex. The scan is used mainly to detect renal parenchymal defects caused by acute pyelonephritis or renal sequelae (scarring) 6 mo after acute infection (*27–29*). It also helps detect renal abnormalities. The uptake quantification (percentage contribution to total renal function or parenchyma) is used to decide whether surgery is necessary and to assess the split renal function before surgery.

Currently, there is a shortage of DMSA cold kits in various countries, including the United States (*18*). ^{99m}Tc-glucoheptonate is another radiotracer used to image the renal cortex when ^{99m}Tc-DMSA is not available, but ^{99m}Tc-glucoheptonate is only partially concentrated in the kidneys and then excreted in the urine (*30*). ^{68}Ga-alizarin red S was studied in animals and humans as a renal cortical PET radiotracer in the 1980s (*30*). Recently, MRI has been gaining popularity in the diagnosis of pyelonephritis; however, because of complex planning and scan times, it is used only occasionally—that is, in cases of pregnancy, where it has its own drawbacks (*31*). In a recent metaanalysis study, Sarikaya et al. found overall equivalent sensitivity between MRI and DMSA scanning in detecting parenchymal changes in pyelonephritis, particularly in scar detection (*32*). There is a need for PET radiotracers to image the renal cortex with a higher resolution. Overall, PET scanners have higher spatial resolution than conventional γ-cameras and can detect smaller defects. On the other hand, new SPECT systems with cadmium-zinc-telluride detectors have better resolution than conventional scanners with sodium iodide detectors (*33*). Recently, Sarikaya et al. reported that ^{68}Ga-PSMA PET provides excellent images of the renal cortex, shows defects caused by various sizes of cysts, and provides higher-resolution images than DMSA scanning can (*14–17*).

Renal uptake of ^{99m}Tc-DMSA through planar and SPECT imaging in humans and animals has been shown to correlate well with renal function tests, such as effective renal plasma flow, GFR, and creatinine clearance (*19–23*).

TABLE 2
Measured Values for Renal PSMA PET Parameters ($n = 25$)

Covariate	*n*	Mean	SD	Minimum	Maximum
Mean SUV_{max}	25	57.75	20.68	21.90	100.95
Mean SUV_{mean}	25	27.68	10.68	12.97	57.75
Mean SUL_{max}	25	41.86	13.9	15.4	66.97
Mean SUL_{mean}	25	18.19	4.59	9.12	25.8
SUV_{mean} liver	25	4.46	1.38	2.1	6.8
SUV_{mean} bp	25	1.16	0.32	0.5	1.70
SUV_{mean} spleen	25	6.13	2.42	2.8	11.4
Renal SUV_{max}/liver ratio	25	14.33	6.95	3.22	32.65
Renal SUV_{max}/bp ratio	25	53.61	22.94	19.91	100.95
Renal SUV_{max}/spleen ratio	25	10.99	6.21	2.55	28.84
Renal SUV_{mean}/liver ratio	25	6.94	3.89	1.91	19.48
Renal SUV_{mean}/bp ratio	25	26.17	13.03	9.43	57.75
Renal SUV_{mean}/spleen ratio	25	5.23	4.86	1.51	16.50
Sum volume	25	354	93.61	194	567
Sum TLG	25	9,968.8	5,042.7	2,520	26,999
Sum TLG (SUL)	25	7,758.4	4,093.8	1,772.3	19,112.9
Sum counts	25	8,077.5	3,985.8	2,176	17,473

bp = blood pool.

TABLE 3
Spearman Rank Correlation Coefficient Estimate Between GFR and Creatinine, with Several Covariates Along with Their CI Using Bootstrapping with Bias-Corrected and Accelerated Method Based on 2,000 Resamples

	GFR			Creatinine ρ		
Covariate	ρ	*P*	95% CI	ρ	*P*	95% CI
SUV_{mean} liver	−0.310	0.132	−0.634, 0.118	0.218	0.295	−0.246, 0.606
SUV_{mean} bp	−0.415	0.039	−0.753, 0.064	0.346	0.090	−0.105, 0.723
SUV_{mean} spleen	−0.130	0.535	−0.519, 0.285	0.057	0.786	−0.423, 0.514
Mean SUV_{max}	0.199	0.340	−0.224, 0.596	−0.226	0.278	−0.583, 0.161
Mean SUV_{mean}	0.317	0.123	−0.090, 0.645	−0.329	0.108	−0.653, 0.063
Renal SUV_{max}/liver ratio	0.402	0.046	0.028, 0.706	−0.364	0.074	−0.731, 0.124
Renal SUV_{max}/bp ratio	0.471	0.018	0.115, 0.736	−0.422	0.036	−0.738, 0.017
Renal SUV_{max}/spleen ratio	0.245	0.237	−0.160, 0.614	−0.210	0.314	−0.631, 0.287
Renal SUV_{mean}/liver ratio	0.505	0.010	0.102, 0.786	−0.451	0.024	−0.800, 0.041
Renal SUV_{mean}/bp ratio	0.574	0.003	0.220, 0.832	−0.515	0.008	−0.820, −0.075
Renal SUV_{mean}/spleen ratio	0.353	0.083	−0.075, 0.689	−0.304	0.140	−0.708, 0.209
Sum counts	0.124	0.554	−0.245, 0.467	−0.159	0.446	−0.537, 0.269
Sum volume	−0.005	0.982	−0.391, 0.397	−0.038	0.856	−0.398, 0.324
Sum TLG	0.225	0.280	−0.166, 0.570	−0.268	0.195	−0.617, 0.164
Age	−0.683	0.001	−0.907, −0.344	0.565	0.003	0.175, 0.839
Weight	0.133	0.528	−0.224, 0.473	−0.175	0.402	−0.530, 0.220
Height	0.158	0.452	−0.279, 0.513	−0.194	0.354	−0.546, 0.217
Body mass index	0.061	0.773	−0.392, 0.466	−0.100	0.635	−0.481, 0.341
Mean SUL_{mean}	0.343	0.093	−0.031, 0.622	−0.329	0.108	−0.640, 0.075
Mean SUL_{max}	0.171	0.413	−0.229, 0.532	−0.190	0.362	−0.555, 0.230
Sum TLG (SUL)	0.334	0.103	−0.080, 0.644	−0.361	0.076	−0.653, 0.031

bp = blood pool; ρ = estimated Spearman rank correlation coefficient.
P values are based on 2-sided test.

Because of high renal cortical parenchymal uptake and an excellent distribution with ^{68}Ga-PSMA-11, in the current study we wanted to determine whether PSMA uptake correlates with renal function tests. We found a significant positive correlation between GFR and renal SUV–to–reference region ratios (liver and blood pool), as well as a marginal positive correlation with renal SUL_{mean}. Our statistical analysis also found a significant negative correlation between creatinine and renal SUV–to–reference region ratios, as well as a marginal correlation with renal sum TLG_{SUL}. Because the SUVs are affected by body weight and various other factors, we used renal SUV–to–reference region ratios and lean body mass–corrected SUVs. Blood pool SUV correlated negatively with GFR and positively with creatinine, as expected. Age also correlated negatively with GFR and positively with creatinine, as expected. In 2 stepwise regression models, total renal parenchymal volume was significantly and directly (positively) associated with GFR and significantly and inversely (negatively) associated with creatinine, as expected. With aging, kidney volumes reduce (*34*). Our method of measuring the approximate renal parenchymal volume on PET images appears to be reliable. Other studies tried to correlate CT kidney volume with renal function but found only weak or moderate correlations in selected patient populations (*35*).

Because radiolabeled PSMA ligands show high renal parenchymal uptake and renal excretion, studies have assessed renal function after ^{177}Lu-PSMA ligand treatments in metastatic prostate cancer patients. Studies have reported low renal toxicity in castration-resistant metastatic prostate cancer treated with ^{177}Lu-PSMA-617 (*12,13*). However, it would be interesting to study larger numbers of patients who underwent ^{177}Lu-PSMA therapy and correlate the renal function with the renal PSMA uptake parameters as we did in the current study. In animal models, DMSA uptake correlated with renal function loss in patients receiving chemotherapy (*36*). In a recent study, PSMA PET quantification of split renal function was compared with mercaptoacetyltriglycine scintigraphy, which showed a significant correlation between the 2 methods (*37*).

The limitations of our study include the relatively small number of patients and having no patients with a GFR below 50 mL/min, thus measuring GFR only in or just below the reference range for the ages. Further work on the mechanism and physiologic meaning of ^{68}Ga-PSMA-11 renal cortical uptake is also required.

CONCLUSION

^{68}Ga-PSMA-11 renal cortical uptake correlates with renal function tests, such as GFR and creatinine. Our method of measuring the approximate renal parenchymal volume on PET images appears to be reliable.

DISCLOSURE

No potential conflict of interest relevant to this article was reported.

REFERENCES

1. Silver DA, Pellicer I, Fair WR, Heston WD, Cordon-Cardo C. Prostate-specific membrane antigen expression in normal and malignant human tissues. *Clin Cancer Res.* 1997;3:81–85.
2. Mhawech-Fauceglia P, Zhang S, Terracciano L, et al. Prostate-specific membrane antigen (PSMA) protein expression in normal and neoplastic tissues and its sensitivity and specificity in prostate adenocarcinoma: an immunohistochemical study using multiple tumour tissue microarray technique. *Histopathology.* 2007;50:472–483.
3. Cunha AC, Weigle B, Kiessling A, Bachmann M, Rieber EP. Tissue-specificity of prostate specific antigens: comparative analysis of transcript levels in prostate and non-prostatic tissues. *Cancer Lett.* 2006;236:229–238.
4. Baccala A, Sercia L, Li J, Heston W, Zhou M. Expression of prostate-specific membrane antigen in tumor-associated neovasculature of renal neoplasms. *Urology.* 2007;70:385–390.
5. Samodelov SL, Gai Z, Kullak-Ublick GA, Visentin M. Renal reabsorption of folates: pharmacological and toxicological snapshots. *Nutrients.* 2019;11:2353.
6. Glutamate Carboxypeptidase II. In: Rawlings ND, Salvesen G, eds. *Handbook of Proteolytic Enzymes*. Academic Press; 2013:1620–1624.
7. Afshar-Oromieh A, Avtzi E, Giesel FL, et al. The diagnostic value of PET/CT imaging with the ^{68}Ga-labelled PSMA ligand HBED-CC in the diagnosis of recurrent prostate cancer. *Eur J Nucl Med Mol Imaging.* 2015;42:197–209.
8. Sonni I, Eiber M, Fendler WP, et al. Impact of ^{68}Ga-PSMA-11 PET/CT on staging and management of prostate cancer patients in various clinical settings: a prospective single-center study. *J Nucl Med.* 2020;61:1153–1160.
9. Zippel C, Ronski SC, Bohnet-Joschko S, Giesel FL, Kopka K. Current status of PSMA-radiotracers for prostate cancer: data analysis of prospective trials listed on ClinicalTrials.gov. *Pharmaceuticals.* 2020;13:12.
10. Violet J, Jackson P, Ferdinandus J, et al. Dosimetry of ^{177}Lu-PSMA-617 in metastatic castration-resistant prostate cancer: correlations between pretherapeutic imaging and whole-body tumor dosimetry with treatment outcomes. *J Nucl Med.* 2019;60:517–523.
11. Hofman MS, Emmett L, Sandhu S, et al. TheraP Trial Investigators and the Australian and New Zealand Urogenital and Prostate Cancer Trials Group. [^{177}Lu]Lu-PSMA-617 versus cabazitaxel in patients with metastatic castration-resistant prostate cancer (TheraP): a randomised, open-label, phase 2 trial. *Lancet.* 2021;397:797–804.
12. Yordanova A, Becker A, Eppard E, et al. The impact of repeated cycles of radioligand therapy using [^{177}Lu]Lu-PSMA-617 on renal function in patients with hormone refractory metastatic prostate cancer. *Eur J Nucl Med Mol Imaging.* 2017;44:1473–1479.
13. Gallyamov M, Meyrick D, Barley J, Lenzo N. Renal outcomes of radioligand therapy: experience of ^{177}lutetium-prostate-specific membrane antigen ligand therapy in metastatic castrate-resistant prostate cancer. *Clin Kidney J.* 2019;13:1049–1055.
14. Sarikaya I, Elgazzar AH, Alfeeli MA, Sarikaya A. Can gallium-68 prostate-specific membrane antigen ligand be a potential radiotracer for renal cortical positron emission tomography imaging? *World J Nucl Med.* 2018;17:126–129.
15. Sarikaya I, Sarikaya A. Current status of radionuclide renal cortical imaging in pyelonephritis. *J Nucl Med Technol.* 2019;47:309–312.
16. Sarikaya I. ^{68}Ga-PSMA ligand as potential ^{99m}Tc-DMSA alternative. *J Nucl Med.* 2019;60(11):12N.
17. Sarikaya I, Alqallaf A, Sarikaya A. Renal cortical ^{68}Ga-PSMA-11 PET and ^{99m}Tc-DMSA images. *J Nucl Med Technol.* 2021;49:30–33.
18. Lim R, Bar-Sever Z, Treves ST. Is availability of ^{99m}Tc-DMSA insufficient to meet clinical needs in the United States? A survey. *J Nucl Med.* 2019;60(8):14N–16N.
19. Taylor A Jr, Kipper M, Witztum K. Calculation of relative glomerular filtration rate and correlation with delayed technetium-99m DMSA imaging. *Clin Nucl Med.* 1986;11:28–31.
20. Taylor A. Quantitation of renal function with static imaging agents. *Semin Nucl Med.* 1982;12:330–344.
21. Kawamura J, Hosokawa S, Yoshida O, Fujita T, Ishii Y, Torizuka K. Validity of ^{99m}Tc dimercaptosuccinic acid renal uptake for an assessment for individual kidney function. *J Urol.* 1978;119:305–309.
22. Daly MJ, Jones W, Rudd TG, Tremann J. Differential renal function using technetium-99m dimercaptosuccinic acid (DMSA): in vitro correlation. *J Nucl Med.* 1979;20:63–66.
23. Groshar D, Embon OM, Frenkel A, Front D. Renal function and technetium-99m-dimercaptosuccinic acid uptake in single kidneys: the value of in vivo SPECT quantitation. *J Nucl Med.* 1991;32:766–768.
24. Kleynhans J, Rubow S, le Roux J, Marjanovic-Painter B, Zeevaart JR, Ebenhan T. Production of [^{68}Ga]Ga-PSMA: comparing a manual kit-based method with a module-based automated synthesis approach. *J Labelled Comp Radiopharm.* 2020;63:553–563.
25. Tahari AK, Chien D, Azadi JR, Wahl RL. Optimum lean body formulation for correction of standardized uptake value in PET imaging. *J Nucl Med.* 2014;55:1481–1484.
26. Levey AS, Bosch JP, Lewis JB, Greene T, Rogers N, Roth D. A more accurate method to estimate glomerular filtration rate from serum creatinine: a new prediction equation. Modification of Diet in Renal Disease Study Group. *Ann Intern Med.* 1999;130:461–470.
27. Piepsz A, Colarinha P, Gordon I, et al.; Paediatric Committee of the European Association of Nuclear Medicine. Guidelines for ^{99m}Tc-DMSA scintigraphy in children. *Eur J Nucl Med.* 2001;28:BP37–BP41.
28. Karmazyn BK, Alazraki AL, Anupindi SA, et al.; Expert panel on pediatric imaging. ACR appropriateness criteria® urinary tract infection: child. *J Am Coll Radiol.* 2017;14(suppl):S362–S371.
29. Mandell GA, Eggli DF, Gilday DL, et al. Procedure guideline for renal cortical scintigraphy in children. *J Nucl Med.* 1997;38:1644–1646.
30. Schuhmacher J, Maier-Borst W, Wellman HN. Liver and kidney imaging with Ga-68-labeled dihydroxyanthraquinones. *J Nucl Med.* 1980;21:983–987.
31. Mervak BM, Altun E, McGinty KA, Hyslop WB, Semelka RC, Burke LM. MRI in pregnancy: indications and practical considerations. *J Magn Reson Imaging.* 2019;49:621–631.
32. Sarikaya I, Albatineh AN, Sarikaya A. ^{99m}Tc-dimercaptosuccinic acid scan versus MRI in pyelonephritis: a meta-analysis. *Nucl Med Commun.* 2020;41:1143–1152.
33. Daghighian F, Sumida R, Phelps ME. PET imaging: an overview and instrumentation. *J Nucl Med Technol.* 1990;18:5–13.
34. Gong IH, Hwang J, Choi DK, et al. Relationship Among Total Kidney Volume, Renal Function and Age. *J Urol.* 2012;187:344–349.
35. Matsuo M, Yamagishi F, Higuchi A. A pilot study of prediction of creatinine clearance by ellipsoid volumetry of kidney using noncontrast computed tomography. *JMA J.* 2019;2:60–66.
36. Demir F, Demir M, Aygun H. Evaluation of the protective effect of edaravone on doxorubicin nephrotoxicity by [^{99m}Tc]DMSA renal scintigraphy and biochemical methods. *Naunyn Schmiedebergs Arch Pharmacol.* 2020;393:1383–1390.
37. Rosar F, Pauly P, Ries M, et al. Determination of split renal function by PSMA imaging: comparison of ^{68}Ga-PSMA-11 PET with ^{99m}Tc-MAG3 scintigraphy. *Am J Nucl Med Mol Imaging.* 2020;10:249–256.

Renal Cortical Scarring: ^{68}Ga-PSMA-11 PET Versus ^{99m}Tc-DMSA Scanning in a Case of Pyelonephritis

Ismet Sarikaya[1], Ahmed Alqallaf[2], Ali Sarikaya[3], Ali Baqer[4], and Nafisa Kazem[5]

[1]Department of Nuclear Medicine, Mubarak Al-Kabeer Hospital, Kuwait University, Kuwait City, Kuwait; [2]Department of Nephrology, Mubarak Al-Kabeer Hospital, Kuwait University, Kuwait City, Kuwait; [3]Department of Nuclear Medicine, Trakya University, Edirne, Turkey; [4]Department of Nuclear Medicine, Mubarak Al-Kabeer Hospital, Kuwait University, Kuwait City, Kuwait; and [5]Department of Nuclear Medicine, Mubarak Al-Kabeer Hospital, Kuwait University, Kuwait City, Kuwait

We previously reported the ^{68}Ga-labeled prostate-specific membrane antigen (PSMA)-11 and ^{99m}Tc-dimercaptosuccinic acid (DMSA) images of the first patient in our prospective research comparing renal ^{68}Ga-PSMA-11 PET with ^{99m}Tc-DMSA scanning in adults with pyelonephritis. Here, we present the renal cortical ^{68}Ga-PSMA-11 PET and ^{99m}Tc-DMSA images of our second patient, who had chronic recurring pyelonephritis and demonstrated renal parenchymal defects secondary to scarring in the kidney.

Key Words: DMSA scan; ^{68}Ga-PSMA-11; PET; pyelonephritis; renal scar

J Nucl Med Technol 2022; 50:49–53
DOI: 10.2967/jnmt.121.262415

Renal cortical imaging with ^{99m}Tc-dimercaptosuccinic acid (DMSA) is widely used to detect renal parenchymal changes due to acute pyelonephritis (reduced uptake) and renal sequelae (scars) (absence of uptake) 6 mo after acute infection (*1*). ^{99m}Tc-DMSA scanning is also used to quantify differential renal function, detect various renal abnormalities, and assess the functional status of multicystic kidneys (*1*). The ability to depict renal scarring via a ^{99m}Tc-DMSA scanning is important because scarring is a common cause of hypertension and because extensive scarring can lead to progressive renal impairment and end-stage renal disease (*2*). The presence of scarring can lead to a change in the treatment plan, such as starting different antibiotics, starting corticosteroids, treating bladder or bowel dysfunction, or performing surgical interventions to prevent further scar formation (*3*). Potential new treatments such as cyclooxygenase-2 inhibitors, superoxide dismutases, and matrix metalloproteinase-9 inhibitors may also prevent scar formation (*3*). A nonfunctioning or poorly functioning kidney due to chronic recurrent pyelonephritis may be surgically removed, as it may cause systemic complications such as sepsis, septic shock, and hypertension (*2*).

^{68}Ga-labeled prostate-specific membrane antigen (^{68}Ga-PSMA) ligands or inhibitors are currently used for initial staging of high-risk prostate cancer and, in cases of biochemical recurrence, for identifying the site of recurrence (*4–6*). These radiotracers also exhibit high physiologic uptake in the renal cortex. PSMA is a type II transmembrane protein, also known as glutamate carboxypeptidase II or folate hydrolase, which is found mainly in prostate tissue and is overexpressed in prostate cancer, in some extraprostatic normal tissues such as the kidneys and salivary glands, and in various other malignancies (*7–9*). Immunohistochemical analyses demonstrated detectable PSMA levels in the brush borders and apical cytoplasm of a subset of proximal renal tubules (*7*,*10*). The reason for the presence of PSMA in the renal proximal tubules is unknown but may be due to folate metabolism—that is, potential reuptake of folate in the kidneys (*11*).

We previously published ^{68}Ga-PSMA-11 PET images of the renal cortex of prostate cancer patients with and without cortical defects caused by various sizes of cysts (*2*,*12*,*13*). Given the high renal cortical uptake and excellent renal parenchymal distribution of ^{68}Ga-PSMA-11, we started a prospective research study comparing renal ^{68}Ga-PSMA-11 PET with ^{99m}Tc-DMSA scanning in adults with pyelonephritis. Our study was interrupted by the coronavirus disease 2020 Pandemic, but renal ^{68}Ga-PSMA-11 PET and ^{99m}Tc-DMSA images of our first patient have been published (*14*). In our first patient, neither ^{68}Ga-PSMA-11 PET nor ^{99m}Tc-DMSA scanning showed cortical defects, but ^{68}Ga-PSMA-11 PET demonstrated image quality superior to that of ^{99m}Tc-DMSA scanning. In the current report, we present renal ^{68}Ga-PSMA-11 PET and ^{99m}Tc-DMSA images of our second patient, who demonstrated cortical defects caused by scars.

MATERIALS AND METHODS

Our prospective study was approved by the Ethical Committee of the Health Sciences Center at Kuwait University and the Kuwait Ministry of Health. The study was conducted at Mubarak Al-Kabeer Hospital in Kuwait.

Received Apr. 8, 2021; revision accepted May 20, 2021.
For correspondence or reprints, contact Ismet Sarikaya (isarikaya99@yahoo.com).
Published online Jul. 30, 2021.

The patient provided written informed consent before the study. We obtained ^{68}Ga-PSMA-11 PET/CT and DMSA images of the kidneys.

^{68}Ga-PSMA ligand (PSMA-11) was radiolabeled at another institute (Radiopharmacy Unit at Kuwait Cancer Control Center) using a ^{68}Ge/^{68}Ga generator and a manual synthesis module (Isotope Technologies Garching).

Renal PET/CT images were obtained on a time-of-flight PET/CT camera (Philips Gemini) 60 min after intravenous injection of 48.1 MBq (1.3 mCi) of ^{68}Ga-PSMA-11. We intentionally used a low activity to reduce the radiation dose to the patient. A low-dose, unenhanced CT scan of the region of the kidneys was obtained for attenuation correction, anatomic localization, and gross anatomic correlation before the PET acquisition (30 mAs, 120 kV, pitch of 0.829, 0.5-s rotation time, 64 × 0.625 collimation, and 5-mm slice thickness). The PET acquisition time was 10 min per bed position for 2 bed positions. Because a low dose of activity was administered, the image acquisition time was longer than usual. The PET images were corrected for attenuation on the basis of the CT data, reconstructed using a standard iterative algorithm, and reformatted into transaxial, coronal, and sagittal slices. Maximum-intensity-projection images were also generated. Because of intense activity in the kidneys, the PET images were reviewed in a low-intensity setting to better assess the renal cortical uptake and distribution. Attenuation-corrected (AC) PET images, uncorrected (non-AC) PET images, PET/CT images, and low-dose CT images were reviewed to assess the anatomic location, size, and morphology of the kidneys; the uptake and distribution of radiotracer in the renal parenchyma; and any parenchymal defects or other abnormalities. Quantification of renal ^{68}Ga-PSMA-11 uptake was also performed. Because of unexpected high splenic uptake in this patient, we could not use automated volume-of-interest analysis with the software we had. We manually drew regions of interest around the kidneys in multiple transaxial slices to calculate the total activity in each kidney. In addition, we measured SUV_{max} and SUV_{mean} in both kidneys in both normal areas and areas with a parenchymal defect by placing a spheric region of interest over the renal cortex without exceeding the renal border.

Four days after PET imaging, ^{99m}Tc-DMSA images were obtained 3 h after intravenous injection of 111 MBq (3 mCi) of ^{99m}Tc-DMSA using a Symbia S SPECT scanner (Siemens) equipped with a high-resolution parallel-hole collimator. Multiple planar images were obtained in anterior, posterior, right posterior oblique, and left posterior oblique projections (10 min each, with a 20% window centered at 140 keV, a 256 × 256 matrix, and a zoom of 1.3). SPECT images of the kidneys were also obtained (a 20-s acquisition per view, 60 views, a 360° rotation, a 128 × 128 matrix, no zoom, and a 20% window centered at 140 keV). A standard iterative algorithm was used for image reconstruction. Images were reformatted into transaxial, coronal, and sagittal views. Uptake for each kidney was quantified using anterior and posterior planar images and the geometric mean.

RESULTS

The patient was a 49-y-old woman with a history of recurring pyelonephritis over the previous 14 mo. The last episode was a severe emphysematous pyelonephritis that occurred 2 mo before the current study (positive urine culture for *Candida albicans*) and was treated with antibiotics for 1 mo as an inpatient treatment. At the time of the study, the patient did not have any symptoms and urine cultures were negative. Renal ultrasound performed a month before the study demonstrated a dilated left renal pelvis and calyces with stones, preserved cortical thickness, and corticomedullary differentiation.

Planar and SPECT ^{99m}Tc-DMSA images demonstrated cortical defects, reduced uptake, and cortical irregularity in the upper and lower poles of the left kidney (Fig. 1). In the right kidney, no cortical defects were identified, with only slightly reduced uptake in the upper and lower poles, which could be a normal finding.

In the upper pole of the right kidney, the AC PET images had an artifact that seemed secondary to some possible unilateral patient motion that occurred as the patient passed urine during imaging. AC PET also showed reduced uptake and cortical defects in the upper and lower poles of the left kidney (Fig. 2). Splenic uptake was higher than usual in this patient, likely because of ^{68}Ga-colloid formation. In the normal physiologic distribution of ^{68}Ga-PSMA-11, splenic uptake is much lower than renal uptake and does not interfere with image interpretation (Fig. 3).

Non-AC PET images demonstrated similar findings to ^{99m}Tc-DMSA images, with cortical defects, reduced uptake, and irregularity in the upper and lower poles of the left kidney (Fig. 1). In the upper and lower poles of the right kidney, there was mildly reduced uptake similar to that on ^{99m}Tc-DMSA images. Bowel activity in the left upper quadrant did not affect the assessment of the left kidney but caused some overlap on the left kidney on maximum-intensity-projection images. Low-dose CT demonstrated small calculi in the lower pole of the left kidney. There were no cysts in the kidneys on low-dose CT.

Renal uptake was 35.5% on the left and 64.5% on the right with ^{99m}Tc-DMSA and 34.5% on the left and 65.5% on the right with ^{68}Ga-PSMA-11.

SUV_{max} and SUV_{mean} were 53 and 43, respectively, in the normal right-kidney parenchyma. In the left kidney, SUV_{max} and SUV_{mean} were 6.4 and 4, respectively, for the upper pole; 21.6 and 17.6, respectively, for the lower pole; and 52 and 41, respectively, for the mid cortical region.

DISCUSSION

^{99m}Tc-DMSA scanning is the current gold standard to assess the renal parenchyma and detect renal scarring, as has been described in detail in our recently published articles (*2*,*12*–*14*). Identification of renal scarring in patents with pyelonephritis is important because scarring is a common cause of hypertension and extensive scarring can cause progressive loss of renal function (*2*). In the management of patients with scarring due to pyelonephritis, further scarring might be prevented by a change in treatment plan, such as starting different antibiotics, supporting with other medications, treating bladder and bowel dysfunction, or performing surgical intervention (correcting vesicoureteral reflux) (*3*).

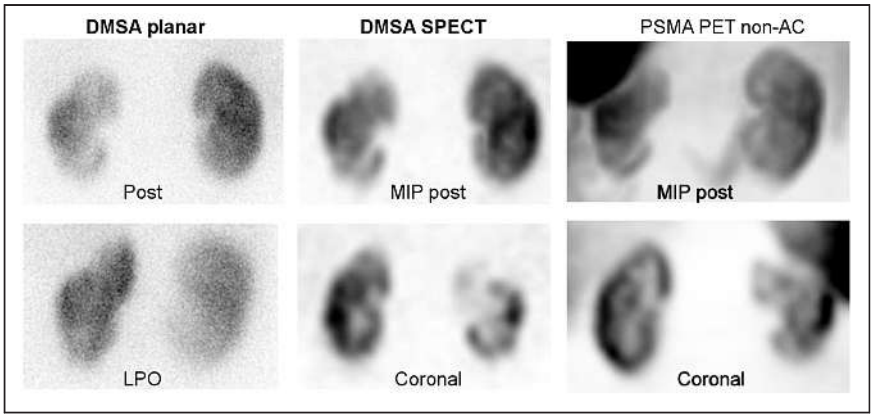

FIGURE 1. ^{99m}Tc-DMSA planar (posterior and left posterior oblique), ^{99m}Tc-DMSA SPECT (maximum-intensity projection in posterior view and selected coronal slice), and ^{68}Ga-PSMA-11 (non-AC maximum-intensity projection in posterior view and non-AC selected coronal slice) images demonstrating cortical defects or scars and reduced uptake in upper and lower poles of left kidney. Non-AC PET can be seen to have higher resolution than non-AC SPECT. LPO = left posterior oblique; MIP = maximum-intensity projection.

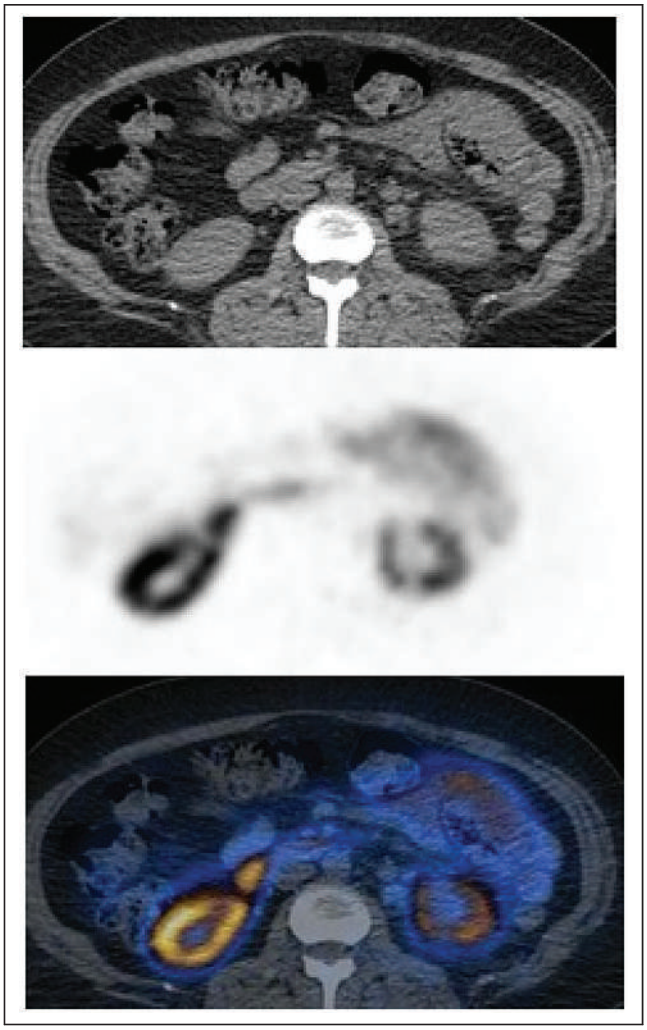

FIGURE 2. ^{68}Ga-PSMA-11 PET/CT (selected transaxial CT [top], PET [middle], and AC PET/CT [bottom]) images demonstrating reduced uptake in lower pole of left kidney and small cortical defect.

Potential new treatments may also prevent further scar development (*3*).

There is a shortage of DMSA cold kits in various countries, including the United States, and ^{99m}Tc-DMSA was therefore added to the drug-shortages list of the U.S. Food and Drug Administration in 2014 and has been commercially unavailable since then (*15*). Currently, there is not a good alternative to ^{99m}Tc-DMSA scanning. ^{99m}Tc-glucoheptonate is only partially concentrated in the kidneys and then is excreted in the urine (*1*). ^{68}Ga-alizarin red S was studied in animals and humans as a renal cortical PET radiotracer in the 1980s but was not used after that time (*16*). In a recent metaanalysis study, we compared ^{99m}Tc-DMSA scanning with MRI and found MRI and ^{99m}Tc-DMSA scanning to have overall equivalent sensitivity in detecting parenchymal changes in pyelonephritis, particularly in scar detection (*17*). MRI also has certain limitations and is not commonly in routine use to assess patients with pyelonephritis (*18*). We need new radiotracers, particularly PET tracers, that can selectively accumulate in the renal parenchyma and, compared with ^{99m}Tc-DMSA scanning, provide higher-resolution images of the kidneys, detect smaller cortical defects, and better quantify split renal function.

In our current patient, both ^{68}Ga-PSMA-11 PET (AC and non-AC) and ^{99m}Tc-DMSA scanning demonstrated cortical defects or scars in the left kidney with comparable image quality. Because of high splenic uptake from ^{68}Ga-colloid formation and some motion-related artifacts in the right kidney, image quality in our current patient was lower than in our previously reported patient (Fig. 3) (*14*). During the labeling procedure, formation of ^{68}Ga-colloid may occur and ^{68}Ga-colloid will accumulate in the spleen, liver, and bone marrow (*19*). Thin-layer chromatography is used to measure colloid content. We did not repeat the ^{68}Ga-PSMA-11 PET study in this patient because we did not want our patient to receive additional radiation exposure. Despite splenic uptake and some motion on the right side, AC and non-AC images successfully demonstrated scars in the left kidney.

Previously reported studies have demonstrated a good correlation between renal ^{99m}Tc-DMSA uptake and renal function tests such as effective renal plasma flow, glomerular filtration rate, and creatinine clearance (*20–24*). In our recently submitted retrospective study on 25 prostate cancer patients (Jan Henning Schierz et al., unpublished data, 2021), renal ^{68}Ga-PSMA-11 uptake appeared to correlate well with the results of renal function tests (creatinine and glomerular filtration rate).

There are certain advantages of ^{68}Ga-PSMA-11 PET over ^{99m}Tc-DMSA scanning, such as a shorter waiting time after injection (1 h vs. 3 h), a shorter half-life (68 min vs. 6 h),

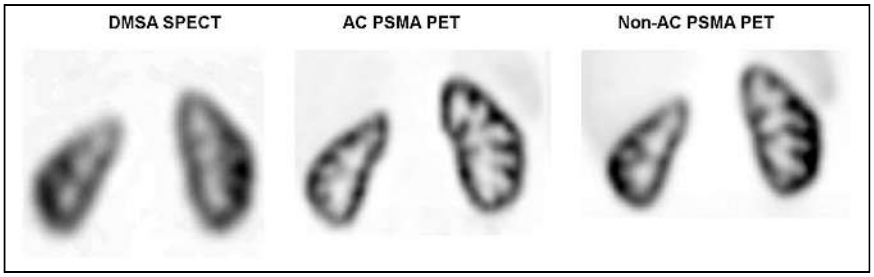

FIGURE 3. ^{99m}Tc-DMSA SPECT (selected coronal slice) and ^{68}Ga-PSMA-11 PET (AC and non-AC selected coronal slices) images of another patient with history of chronic recurrent pyelonephritis demonstrating mildly reduced uptake and cortical thinning in upper pole of right kidney with no parenchymal defects. Normal distribution of ^{68}Ga-PSMA-11 is seen, with only mild activity in liver and spleen.

and superior image quality, particularly with AC PET. The image acquisition time for our current patient was 20 min with ^{68}Ga-PSMA-11 PET because we used a low dose of activity to reduce the radiation dose to the patient (2 bed positions, 10 min per bed position, 48.1 MBq [1.3 mCi]). The image acquisition time for DMSA scanning was 55 min (30-min planar, 25-min SPECT). A longer acquisition time can cause patient discomfort and patient motion and result in image artifacts, requiring additional images and sedation in pediatric patients. The image acquisition time with ^{68}Ga-PSMA-11 PET can be further reduced to 6–7 min per bed position for 74 MBq (2 mCi), 4–5 min per bed position for 111 MBq (3 mCi), and 2–3 min per bed position for 148 MBq (4 mCi), but the kidney and effective doses will increase with higher activities. As we reported in our previous articles, absorbed adult kidney doses of ^{68}Ga-PSMA-11 and ^{99m}Tc-DMSA are 0.24 and 0.18 mGy/MBq, respectively, and effective adult doses are 0.022 and 0.0088 mSv/MBq, respectively (*25*,*26*). In our previously reported patient, estimated effective doses of 111 MBq (3 mCi) of ^{99m}Tc-DMSA and 74 MBq (2 mCi) of ^{68}Ga-PSMA-11 were 0.98 and 1.63 mSv, respectively. In our current patient, 48.1 MBq (1.3 mCi) of ^{68}Ga-PSMA-11 yielded an effective dose of 1.05 mSv, which is similar to the effective dose of ^{99m}Tc-DMSA. The additional radiation dose from CT in PET/CT is low because it is a low-dose CT scan and covers only the region of the kidneys. Non-AC PET also provides high-quality images of the renal parenchyma as seen in our current patient and in previous reports, and low-dose CT can therefore be omitted.

PET/CT cameras provide higher-resolution images than standard γ-cameras. In our patient, even low-dose non-AC PET provided images higher in quality than—or comparable in quality to—^{99m}Tc-DMSA SPECT. SPECT/CT provides higher-resolution images than SPECT, but we intentionally did not perform SPECT/CT on our patient to reduce the radiation dose in this research patient. Overall, PET/CT is known to provide higher-resolution images than SPECT/CT. On the other hand, SPECT systems with cadmium-zinc-telluride detectors have better resolution than conventional scanners with sodium iodide detectors (*27*).

The use and availability of ^{68}Ga-PSMA ligands for prostate cancer have been increasing. Recently, ^{68}Ga-PSMA-11 has been approved by the Food and Drug Administration for prostate cancer imaging. One limitation of ^{68}Ga-PSMA-11 PET is that it costs more than ^{99m}Tc-DMSA scanning: approximately $450 and $300, respectively, in our institute.

Quantification of uptake for each kidney showed results similar to those of ^{99m}Tc-DMSA scanning and ^{68}Ga-PSMA-11 PET. Because of high splenic uptake and limitations in our software, we could not perform automated volume-of-interest analysis on PSMA images, but in our recently submitted study, automated volume-of-interest analysis successfully provided total counts, volume, and SUVs for each kidney.

In our current patient, and in our previous patient with chronic pyelonephritis, ^{68}Ga-PSMA-11 PET appears to be a potential alternative to ^{99m}Tc-DMSA scanning. As discussed for our previous patient, its biodistribution and radiation dose in the pediatric population are not known, and further work is required to understand its mechanism of uptake, to determine the optimal injected activity, and to determine its dosimetry before its use as a renal cortical tracer can be supported.

CONCLUSION

The renal cortical scars caused by pyelonephritis were demonstrated well by ^{68}Ga-PSMA-11 PET.

DISCLOSURE

No potential conflict of interest relevant to this article was reported.

ACKNOWLEDGMENT

^{68}Ga-PSMA ligands are investigational PET radiotracers and as of now have not been approved by the U.S. Food and Drug Administration or European Medicines Agency. This article is about off-label use of ^{68}Ga-PSMA-11 for renal PET/CT imaging in adults.

REFERENCES

1. Mandell GA, Eggli DF, Gilday DL, et al. Procedure guideline for renal cortical scintigraphy in children. Society of Nuclear Medicine. *J Nucl Med.* 1997;38:1644–1646.
2. Sarikaya I, Sarikaya A. Current status of radionuclide renal cortical imaging in pyelonephritis. *J Nucl Med Technol.* 2019;47:309–312.
3. Murugapoopathy V, McCusker C, Gupta IR. The pathogenesis and management of renal scarring in children with vesicoureteric reflux and pyelonephritis. *Pediatr Nephrol.* 2020;35:349–357.
4. Afshar-Oromieh A, Avtzi E, Giesel FL, et al. The diagnostic value of PET/CT imaging with the ^{68}Ga-labelled PSMA ligand HBED-CC in the diagnosis of recurrent prostate cancer. *Eur J Nucl Med Mol Imaging.* 2015;42:197–209.

5. Sonni I, Eiber M, Fendler WP, et al. Impact of ^{68}Ga-PSMA-11 PET/CT on staging and management of prostate cancer patients in various clinical settings: a prospective single-center study. *J Nucl Med.* 2020;61:1153–1160.
6. Fendler WP, Eiber M, Beheshti M, et al. ^{68}Ga-PSMA PET/CT: joint EANM and SNMMI procedure guideline for prostate cancer imaging—version 1.0. *Eur J Nucl Med Mol Imaging.* 2017;44:1014–1024.
7. Silver DA, Pellicer I, Fair WR, Heston WD, Cordon-Cardo C. Prostate-specific membrane antigen expression in normal and malignant human tissues. *Clin Cancer Res.* 1997;3:81–85.
8. Mhawech-Fauceglia P, Zhang S, Terracciano L, et al. Prostate-specific membrane antigen (PSMA) protein expression in normal and neoplastic tissues and its sensitivity and specificity in prostate adenocarcinoma: an immunohistochemical study using multiple tumour tissue microarray technique. *Histopathology.* 2007;50:472–483.
9. Cunha AC, Weigle B, Kiessling A, Bachmann M, Rieber EP. Tissue-specificity of prostate specific antigens: comparative analysis of transcript levels in prostate and non-prostatic tissues. *Cancer Lett.* 2006;236:229–238.
10. Baccala A, Sercia L, Li J, Heston W, Zhou M. Expression of prostate-specific membrane antigen in tumor-associated neovasculature of renal neoplasms. *Urology.* 2007;70:385–390.
11. Ristau BT, O'Keefe DS, Bacich DJ. The prostate-specific membrane antigen: lessons and current clinical implications from 20 years of research. *Urol Oncol.* 2014; 32:272–279.
12. Sarikaya I, Elgazzar AH, Alfeeli MA, Sarikaya A. Can gallium-68 prostate-specific membrane antigen ligand be a potential radiotracer for renal cortical positron emission tomography imaging? *World J Nucl Med.* 2018;17:126–129.
13. Sarikaya I. ^{68}Ga-PSMA ligand as potential ^{99m}Tc-DMSA alternative. *J Nucl Med.* 2019;60(11):12N.
14. Sarikaya I, Alqallaf A, Sarikaya A. Renal cortical ^{68}Ga-PSMA-11 PET and ^{99m}Tc-DMSA images. *J Nucl Med Technol.* 2021;49:30–33.
15. Lim R, Bar-Sever Z, Treves ST. Is availability of ^{99m}Tc-DMSA insufficient to meet clinical needs in the United States? A survey. *J Nucl Med.* 2019;60(8):14N–16N.
16. Schuhmacher J, Maier-Borst W, Wellman HN. Liver and kidney imaging with Ga-68 labeled dihydroxyanthraquinones. *J Nucl Med.* 1980;21:983–987.
17. Sarikaya I, Albatineh AN, Sarikaya A. ^{99m}Tc-dimercaptosuccinic acid scan versus MRI in pyelonephritis: a meta-analysis. *Nucl Med Commun.* 2020; 41:1143–1152.
18. Mervak BM, Altun E, McGinty KA, et al. MRI in pregnancy: indications and practical considerations. *J Magn Reson Imaging.* 2019;49:621–631.
19. Brom M, Franssen GM, Joosten L, Gotthardt M, Boerman OC. The effect of purification of Ga-68-labeled exendin on in vivo distribution. *EJNMMI Res.* 2016; 6:65.
20. Taylor A Jr, Kipper M, Witztum K. Calculation of relative glomerular filtration rate and correlation with delayed technetium-99m DMSA imaging. *Clin Nucl Med.* 1986;11:28–31.
21. Taylor A. Quantitation of renal function with static imaging agents. *Semin Nucl Med.* 1982;12:330–344.
22. Kawamura J, Hosokawa S, Yoshida O, et al. Validity of ^{99m}Tc dimercaptosuccinic acid renal uptake for an assessment for individual kidney function. *J Urol.* 1978; 119:305–309.
23. Daly MJ, Jones W, Rudd TG, Tremann J. Differential renal function using technetium-99m dimercaptosuccinic acid (DMSA): in vitro correlation. *J Nucl Med.* 1979;20:63–66.
24. Groshar D, Embon OM, Frenkel A, Front D. Renal function and technetium-99m-dimercaptosuccinic acid uptake in single kidneys: the value of in vivo SPECT quantitation. *J Nucl Med.* 1991;32:766–768.
25. Mattsson S, Johansson L, Leide Svegborn S, et al. Radiation dose to patients from radiopharmaceuticals: a compendium of current information related to frequently used substances. *Ann ICRP.* 2015;44:7–321.
26. Sandgren K, Johansson L, Axelsson J, et al. Radiation dosimetry of [^{68}Ga]PSMA-11 in low-risk prostate cancer patients. *EJNMMI Phys.* 2019;6:2.
27. Daghighian F, Sumida R, Phelps ME. PET imaging: an overview and instrumentation. *J Nucl Med Technol.* 1990;18:5–13.

National Diagnostic Reference Levels for Nuclear Medicine in Kuwait

Meshari A. Alnaaimi[1,2], Mousa A. Alduaij[1], Faisal A. Shenawy[1], Musab M. Algaily[1], Talal S. Mohammedzein[1], Farida A. Alkandri[1], Mohammed O. Shaban[3], and Saud A. Alenezi[4,5]

[1]Nuclear Medicine Unit, Kuwait Cancer Control Centre, Shuwaikh, Kuwait; [2]Radiation Physics Department, Kuwait Cancer Control Centre, Shuwaikh, Kuwait; [3]Radiation Protection Department, Sharq, Kuwait; [4]Department of Nuclear Medicine, Faculty of Medicine, Kuwait University, Safat, Kuwait; and [5]Division of Nuclear Medicine, Department of Radiology, Saint Louis University, St. Louis, Missouri

The diagnostic reference level (DRL) is a patient-exposure optimization tool used to evaluate and provide guidance for radiation doses in medical imaging. In the past few decades, there has been a global increase in the number of diagnostic imaging procedures, including nuclear medicine procedures, and consequently in patient radiation exposure. This increase has encouraged international and national health-care organizations to take action and keep up with such changes to meet the expectation of increasing use of ionizing radiation in medicine. **Methods:** DRLs in Kuwait were established by investigating the administered activity of radiopharmaceuticals and CT radiation doses in hybrid imaging systems. The DRLs were determined on the basis of the 75th percentile of radiopharmaceutical administered activity distribution as recommended by the International Commission on Radiological Protection. **Results:** The DRLs determined in Kuwait agree well with other published DRLs in Europe, Japan, Korea, Australia, and the United States. **Conclusion:** This study presents the establishment process and the results of the first national DRLs for nuclear medicine procedures in Kuwait as a way to optimize radiation exposure.

Key Words: DRL; hybrid imaging; radiation exposure; ALARA dose optimization; radiation safety

J Nucl Med Technol 2022; 50:54–59
DOI: 10.2967/jnmt.121.262175

Over the past few decades, clinical use of diagnostic imaging procedures has been growing in an attempt to improve the accuracy of diagnosis and to resolve clinical dilemmas. This growth has included both the use of anatomic and radiologic modalities and the use of functional nuclear medicine modalities, including conventional and hybrid procedures such as SPECT/CT and PET/CT. Nearly 13.5 million nuclear medicine procedures were performed in the United States in 2016 (*1*). In Kuwait, more than 5,000 nuclear medicine procedures are performed every year. Unfortunately, the radiation dose to patients determined from the amount of administered radiopharmaceutical activity might vary by as much as 20-fold among different nuclear medicine departments (*2*). At the moment, no information is available on dose reference levels for nuclear medicine in Kuwait, and there is a similar lack of information from neighboring countries in the region. Therefore, the International Atomic Energy Agency has encouraged national and international initiatives to standardize and optimize activities administered to patients.

More than 20 years ago, the International Commission on Radiological Protection (ICRP) established the concept of reference dose guidelines for different imaging modalities to reduce and manage patient radiation exposure (*3,4*). The diagnostic reference level (DRL) is an effective tool for protection optimization in patient radiation exposure, particularly as dose limits are not applicable in medical exposure. DRL quantities should evaluate the amount of ionizing radiation used to perform a diagnostic, interventional, or nuclear medicine procedure and to assess the effective dose to patients. The radiation metric used as a DRL quantity should be easily measured or available, such as volume CT dose index and dose–length product for CT and administered activity in nuclear medicine (*4*). In this context, when a hybrid imaging procedure is performed—that is, 2 imaging modalities are used together—it is appropriate to set and present DRLs for both modalities independently. Two major guidelines for the recommended administered activities for nuclear medicine have been developed in Europe (*5*) and North America (*6*). Recent studies published in reputed medical journals have demonstrated multiple national initiatives to establish DRLs for nuclear medicine as a tool to control and reduce patient radiation exposure (*7–10*).

In 2012, a nuclear medicine global initiative was established that aims to promote human health by advancing the fields of nuclear medicine and molecular imaging, to encourage global collaboration in education, and to harmonize procedure guidelines and other policies that ultimately lead to improvements in quality and safety in the fields throughout the world (*11*). One of the recommendations of this initiative was that countries with no current guidelines on administered nuclear medicine activities in children should either develop their own or officially adopt currently existing ones.

Received Mar. 4, 2021; revision accepted Aug. 20, 2021.
For correspondence or reprints, contact Meshari Alnaaimi (m.alnaaimi@gmail.com).
Published online Sep. 28, 2021.

Nuclear medicine and hybrid imaging procedures may also increase radiation exposure to the general public because of the characteristics of the administered radiopharmaceuticals compared with diagnostic radiology procedures. This potential increased exposure has raised many concerns about potential radiation risks (*12*). Subsequently, various methods to reduce patient radiation exposure and optimize doses were developed, such as reference levels. In addition, there is a need to assess, monitor, and regularly review patient radiation doses during medical exposure. This study presents the establishment process and the results of the first DRLs for nuclear medicine procedures in Kuwait.

MATERIALS AND METHODS

The study was performed with Kuwait's Ministry of Health initiative to collect information about radiation doses from nuclear medicine studies and to set up national DRLs. A committee was formed by the Ministry of Health in 2016 to conduct a nationwide survey on the type of examinations commonly performed, administered activities of radiopharmaceuticals, types of imaging equipment available, quality control records, and standard procedures used to determine patient doses for nuclear medicine imaging studies as explained by ICRP publication 135 (*4*).

The amount of equipment and status of nuclear medicine in Kuwait were previously described and published by our academic group (*13*). The data were collected from 11 nuclear medicine departments as recommended by ICRP 135 to collect data from at least 10 facilities for the establishment of local DRLs. Each department was asked to enter the average administered activities used for nuclear medicine examinations. The number of reported protocols was 51 for general nuclear medicine and 4 for PET. Some protocols were conducted by only a few departments or were rarely used; hence, the DRL was calculated only if the protocol was used by more than 4 departments. Only 31 protocols met this condition. The Ministry of Health Ethics Committee approved this retrospective study, and the requirement to obtain informed consent was waived.

For each protocol, the dose distributions derived from current practice were generated in terms of 25th percentile, 50th percentile, 75th percentile, minimum, maximum, SD, and effective dose. The third quartile (75th percentile) of the average dose distribution reported by survey participants was used to establish national DRLs. The effective radiation dose received by patients from nuclear medicine procedures was estimated on the basis of the dose coefficients extracted from ICRP 106 and the Society of Nuclear Medicine and Molecular Imaging radiation dose tool (*14,15*). The results were compared with other countries' DRLs as indicated in international references. The conversion factors for administered activities for the most common nuclear medicine procedures in Kuwait were determined on the basis of patient weight. The recommended pediatric DRLs based on the European Association of Nuclear Medicine dosage card for administered activities with reference to weight or age (<15 y) were also presented.

The CT component of hybrid systems was used for attenuation correction or localization purposes only. The CT data were collected for the most commonly used protocols for PET/CT and SPECT/CT procedures. The 75th percentiles of the average volume CT dose index and dose–length product for the scanner were used to establish DRLs for the CT component in hybrid examinations as described by the CT working group in the United Kingdom (*16*). To estimate the effective radiation dose from the CT component of hybrid imaging, the dose–length products from the scanner-generated dose reports were multiplied by a conversion factor (*17*). All data analyses were undertaken using Excel (Office Pro Plus 2019; Microsoft).

RESULTS

Completed surveys of current practice were received from nuclear medicine departments in Kuwait for the protocols that met the conditions. For each procedure, the statistical distributions of the administered activities, proposed DRLs, and estimated effective doses for adult patients derived from current practice were generated (Table 1).

The DRLs in Kuwait were compared with DRLs recently internationally reported (Table 2). Pediatric reference DRLs are generally based on adult DRLs multiplied by a correction factor that was adopted from the European Association of Nuclear Medicine dosage card (Table 3). The recommended conversion factors adopted from the European Association of Nuclear Medicine dosage card and the North American consensus guidelines for administered activities based on patient weight are presented in Table 4.

Regarding hybrid imaging examinations, the DRLs of the CT component of SPECT/CT are listed in Table 5 for most commonly used protocols. The DRLs for the CT irradiation dose from PET/CT protocols for head and brain, vertex to thighs, and vertex to toes are listed in Table 6.

DISCUSSION

The ICRP introduced 3 principles that became a cornerstone in radiation protection. These principles evolved into 3 key words: justification, optimization, and limitation. Optimization aims to ensure that every exposure is performed with the lowest ionizing radiation needed to execute the procedure, following the "as low as reasonably achievable" principle. DRLs are considered an effective optimization tool for improving radiation protection in diagnostic medical imaging (*4*) and are not in any way dose limits or constraints, nor do they serve regulatory purposes. However, they aim to identify whether some common procedures present unusually high values, alerting the department to act accordingly by, for instance, reviewing procedures, protocols, or equipment.

The first national DRLs for commonly performed nuclear medicine imaging procedures in Kuwait, including hybrid imaging procedures such as PET/CT and SPECT/CT, were established in this study. Table 1 shows that there is a large variation in the reported administered activities. For instance, there is a dispersion (as variance) between the activities used for ^{99m}Tc-methyl diphosphonate bone scanning, as indicated by the large SD and the 3-fold difference between the maximum and minimum values. Thus, there is a need for reference levels and standardization of activities. The effective radiation doses for average-weight adults can be categorized according to Towson and Smart (*18*) into the following: high-dose (>10 mSv) procedures (^{67}Ga for infection and ^{131}I

TABLE 1
DRLs for Most Common Procedures in Kuwait

Scan	Radiopharmaceutical	25th percentile	50th percentile	75th percentile	Maximum	Minimum	SD	DRL (MBq)	Effective dose (mSv)
PET tumor	^{18}F-FDG	222	228	230	231	185	18	230	4.4
PET brain	^{18}F-FDG	223	228	231	231	222	3.9	231	4.4
PET	^{18}F-NaF	185	220	230	231	185	22	230	6.2
PET	^{68}Ga (DOTATATE/PSMA)	150	150	217	231	150	38	217	0.9
Gated blood pool	^{99m}Tc-RBC	740	740	850	1,100	740	115	850	5.6
MPI rest	^{99m}Tc-tetrofosmin, MIBI	914	958	976	1,039	884	49	976	7.4
MPI stress	^{99m}Tc-tetrofosmin, MIBI	914	958	976	1,039	884	49	976	7.4
Renal	^{99m}Tc-DMSA	185	200	200	250	180	20	200	1.5
Renal	^{99m}Tc-DTPA (GFR)	73	85	90	100	60	14	90	0.7
Renal	^{99m}Tc-MAG3	204	260	370	407	185	90	370	2.8
Bone	^{99m}Tc-methyl diphosphonate	897	927	944	1,110	459	171	944	7.2
Brain	^{99m}Tc-HMPAO	828	850	893	900	800	39	893	6.8
Gastrointestinal	^{67}Ga-citrate	13	15	20	25	10	5	20	2.0
Esophageal reflux	^{99m}Tc-DTPA	36	40	40	40	30	3	40	0.3
Hepatobiliary	^{99m}Tc-HIDA	200	200	210	220	190	10	210	1.6
Lung perfusion	^{99m}Tc-MAA	200	204	218	220	190	11	218	1.7
Parathyroid	^{99m}Tc-MIBI, tetrofosmin	850	875	900	900	800	35	900	6.8
Salivary gland	^{99m}Tc-pertechnetate	186	190	200	200	180	8	200	1.5
Testicular	^{99m}Tc-pertechnetate	500	550	600	600	400	82	600	4.6
Thyroid	^{131}I-iodide	200	200	200	250	180	25	200	10.4
Thyroid	^{99m}Tc-pertechnetate	185	185	185	250	185	21	185	1.4
Gastric emptying	^{99m}Tc-DTPA	13	15	37	37	10	5	37	0.3
Meckel diverticulum	^{99m}Tc-pertechnetate	250	264	278	278	220	24	278	2.1
Salivary gland	^{99m}Tc-pertechnetate	194	197	200	200	10	59	200	1.5
Renal cystogram	^{99m}Tc-pertechnetate	91	94	94	100	90	4	94	0.7
Testicular	^{99m}Tc-pertechnetate	500	520	520	555	500	17	520	4.0
Infection	^{67}Ga-citrate	200	200	220	220	200	10	220	22.0
Infection	^{99m}Tc-WBC (colloid/HMPAO)	663	725	750	800	500	94	750	5.7
Lymphoscintigraphy	^{99m}Tc-nanocolloid	36	40	40	40	30	3	40	0.3
CSF leak	^{99m}Tc-DTPA	386	370	370	407	370	14.7	370	2.8
CSF shunt patency	^{99m}Tc-pertechnetate, DTPA	80	80	80	100	80	8	80	0.6

PSMA = prostate-specific membrane antigen; RBC = red blood cell; MPI = myocardial perfusion imaging; MIBI = methoxyisobutylisonitrile; DMSA = dimercaptosuccinic acid; DTPA = diethylenetriamine pentaacetic acid; GFR = glomerular filtration rate; MAG3 = mercaptoacetyltriglycine; HMPAO = hexamethylpropyleneamine oxime; HIDA = hepatobiliary iminodiacetic acid; WBC = white blood cell; MAA = macroaggregated albumin; CSF = cerebrospinal fluid.

Dose distributions are presented in terms of 25th percentile, 50th percentile, 75th percentile, maximum, minimum, SD and effective dose associated with DRL of administered activity.

for thyroid cancer), moderate-dose (<10 mSv) procedures (^{18}F-NaF for bone imaging; ^{18}F-FDG for tumor and brain imaging; and ^{99m}Tc for bone, cardiac, brain, renal, lung, hepatobiliary, salivary, thyroid, and parathyroid scans), and low-dose (<1 mSv) procedures (the rest of the procedures).

It is noteworthy that the average reduction in effective doses when using DRLs in routine work is up to 25%. The impact of dose reduction is estimated by comparing the maximum to the DRL-recommended activities and is stronger when applied to high-dose procedures involving ^{67}Ga and ^{131}I radioisotopes. Additionally, the DRLs can also have a lower value, that is, the 25th percentile, as shown in Table 1, indicating that below a certain dose, the resulting image quality could be diagnostically insufficient. Thus, the 25th percentile is an indicator of the minimum dose that can be used to achieve acceptable image quality. As described by Korpela et al. (*19*) the first step in optimizing medical exposure is the establishment of national DRLs, which allow identification of unusually high or low activities compared with the national distribution.

Table 2 shows that the DRLs in Kuwait are comparable to, and agree well with, those reported from other countries. The DRL in Kuwait for ^{18}F-FDG tumor imaging is generally lower than those in the United States, the United Kingdom, Australia. The large differences between the ^{18}F-FDG DRL in Kuwait and those reported for other countries could reflect the fact that the data in this study were gathered recently (many years later than other reported data), at a time when scanners with more advanced imaging technology and sophisticated dose-saving technologies have been used; since that time, a greater awareness of the need for optimization may have come about.

For myocardial perfusion scans, especially rest studies, the DRLs tend to be higher than other values presented in Table 2. The higher DRLs could be due to the fact that the stress and rest parts of the study are performed on 2 different days and that the 1-d protocol is not routinely performed in Kuwait. Optimization of radiopharmaceutical activities for myocardial perfusion scans has been widely promoted by the establishment of the national DRLs.

TABLE 2
DRLs (MBq) in Kuwait Compared with Other Countries as Reported in the Literature

Scan	Radiopharmaceutical	Kuwait	Korea	Japan	Australia	U.K.	Brazil	United States (*27*)	European Union (*28*)
Tumor	^{18}F-FDG	230	370	240	310	400	370	461–710	200–400
Brain	^{18}F-FDG	231	370	240	250	250	350	—	—
Bone	^{99m}Tc-diphosphonate	944	925	950	920	600	1,110	848–1,185	500–1,110
Leukocyte	^{99m}Tc-HMPAO-WBC	892.5	888	—	800	200	—	—	300–600
Thyroid	^{99m}Tc-pertechnetate	185	217	300	215	80	444	—	75–222
Thyroid carcinoma	^{131}I-NaI	200	185	—	185	400	185	—	90–400
Parathyroid	^{99m}Tc-MIBI	900	740	800	900	900	740	—	400–900
Brain	^{99m}Tc-HMPAO	892.5	925	800	750	750	1,203	887–1,294	500–1,110
Cardiac	^{99m}Tc-MIBI or TF (MPI, rest)	976	555	900	620	800	444	519–1,153	560
Cardiac	^{99m}Tc-MIBI or TF (MPI, stress)	976	1,110	1,200	1,520	800	1,110	945–1,402	1,100
Cardiac	^{99m}Tc-RBC	740	740	—	1,030	800	—	916–1,301	600–1,000
Lung perfusion	^{99m}Tc-MAA	217.5	222	260	240	100	333	147–226	100–296
Lymphangioscintigraphy	^{99m}Tc-phytate	40	148		52	40	74	—	74–150
Hepatobiliary	^{99m}Tc-phytate	210	185	200	200	80	370	110–259	—
Salivary	^{99m}Tc-pertechnetate	370	370	370	200	80	555	—	—
Gastric emptying	^{99m}Tc-DTPA	37	111	—	44	12	—	31–50	150–540
Renal dynamic	^{99m}Tc-DTPA	90	555	400	500	300	449	407–587	—
Renal dynamic	^{99m}Tc-MAG3	370	500	400	305	100	—	283–379	100–370
Renal static	^{99m}Tc-DMSA	200	185	210	200	80	185	189–289	70–183
Radionuclide cystography	^{99m}Tc-pertechnetate	94	74	—	94	25	—	—	—

Recently, there have been several reviews of child and adolescent administered activities that led to development of pediatric guidelines in nuclear medicine (*20,21*). Table 3 shows the minimum recommended pediatric administered activities that can be used to minimize variations in the practice of pediatric nuclear medicine in Kuwait. These calculated activities are weight- and age-based. Table 4 shows the recommended conversion factors for administered activities based on patient weight. These factors can be used for children, adolescents, and adults who weigh more than average.

CT scanning in hybrid imaging procedures is performed for different purposes, ranging from obtaining diagnostic-quality high-dose images to ultra-low-dose images for attenuation-correction protocols (*22*). The variations between CT radiation doses delivered to the patient in hybrid imaging examinations is due mainly to the varied types of equipment settings and acquisition protocols. A detailed analysis of current practice in Kuwait for CT in hybrid imaging studies was demonstrated in a reported national dose audit (*23*). The DRLs of the CT portion associated with hybrid imaging procedures performed for attenuation correction and localization purposes in Kuwait are presented in Tables 5 and 6. CT dose can be optimized for PET/CT examinations by further investigating the CT protocol parameters that contribute to the dose received by patients.

The DRLs in Kuwait are consistent with those presented in the literature for nuclear medicine centers around the world. It is recommended that DRLs be reviewed periodically—for example, every 5 years. Periodic review of DRLs is required because imaging technologies and radiopharmaceuticals are rapidly advancing, and these advances can result in reducing the radiation doses to patients. Comparison with reference values such as DRLs is an effective tool to alert professionals in some departments that have not fully implemented the "as low as reasonably achievable" principle of dose optimization (*24*).

Because a DRL is supposed to be the activity needed for good, diagnosable image quality, it is not enough to evaluate

TABLE 3
Pediatric Minimum Recommended Administered Activities (5)

Scan	Radiopharmaceutical	1 y old (10 kg)	5 y old (19 kg)	10 y old (32 kg)	15 y old (≥55 kg)
Tumor	^{18}F-FDG	70	120	189	200
Brain	^{18}F-FDG	70	70	102	180
Bone	^{99m}Tc-diphosphonate	80	162	255	408
Bone	^{18}F-NaF	70	70	102	163
Lung perfusion	^{99m}Tc-MAA	15	26	41	65
Hepatobiliary	^{99m}Tc-phytate	28	49	77	122
Renal dynamic	^{99m}Tc-MAG3	23	33	45	61
Renal static	^{99m}Tc-DMSA	33	48	64	87
Radionuclide cystography	^{99m}Tc-pertechnetate	20	20	20	20
Meckel scan	^{99m}Tc-pertechnetate	20	26	41	65
Gastric emptying	^{99m}Tc-sulfur colloid	10	13	20	33

Data are in megabecquerels.

TABLE 4
Recommended Weight-Based Dosing Guidance on Administered Activities Based on Patient Weight

Scan	Radiopharmaceutical	MBq/kg
PET (tumor)	^{18}F-FDG	5.18
PET (brain)	^{18}F-FDG	3.7
PET	^{18}F-NaF	2.22
PET	^{68}Ga (DOTATATE/PSMA)	1.85
Gated blood pool	^{99m}Tc-RBC	8.14
MPI rest	^{99m}Tc-tetrofosmin, MIBI	10.73
MPI stress	^{99m}Tc-tetrofosmin, MIBI	10.73
Renal	^{99m}Tc-DMSA	1.85
Renal	^{99m}Tc-DTPA (GFR)	2.59
Renal	^{99m}Tc-MAG3	3.7
Bone	^{99m}Tc-methyl diphosphonate	9.25
Brain	^{99m}Tc-HMPAO	2.775
Gastrointestinal	^{67}Ga-citrate	1.85
Esophageal reflux	^{99m}Tc-DTPA	0.37
Hepatobiliary	^{99m}Tc-HIDA	1.85
Lung perfusion	^{99m}Tc-MAA	2.59
Parathyroid	^{99m}Tc-MIBI, tetrofosmin	5.55
Salivary gland	^{99m}Tc-pertechnetate	1.11
Testicular	^{99m}Tc-pertechnetate	7.4
Thyroid	^{131}I-iodide	0.555
Thyroid	^{99m}Tc-pertechnetate	1.11
Gastric emptying	^{99m}Tc-DTPA	0.37
Meckel diverticulum	^{99m}Tc-pertechnetate	1.85
Renal cystogram	^{99m}Tc-pertechnetate	0.37
Infection	^{67}Ga-citrate	1.11
Infection	^{99m}Tc-WBC (colloid/HMPAO)	27.75
Lymphoscintigraphy	^{99m}Tc-nanocolloid	0.259
CSF leak	^{99m}Tc-DTPA	2.59
CSF shunt patency	^{99m}Tc-pertechnetate + ^{99m}Tc, DTPA	0.259

PSMA = prostate-specific membrane antigen; RBC = red blood cell; MPI = myocardial perfusion imaging; MIBI = methoxyisobutylisonitrile; DMSA = dimercaptosuccinic acid; DTPA = diethylenetriamine pentaacetic acid; GFR = glomerular filtration rate; MAG3 = mercaptoacetyltriglycine; HMPAO = hexamethylpropyleneamine oxime; HIDA = hepatobiliary iminodiacetic acid; WBC = white blood cell; MAA = macroaggregated albumin; CSF = cerebrospinal fluid.

TABLE 5
DRLs for CT Used for Attenuation Correction and Localization in SPECT Scans in Terms of Volume CT Dose Index and Dose–Length Product and Effective Dose Associated with Hybrid CT of SPECT/CT

SPECT/CT protocol	Volume CT dose index (mGy)	Dose–length product (mGy·cm)	Effective dose (mSv)
Brain	5.6	163	2.44
Head and neck	4.5	181	2.74
Lung	2.1	69	1.03
Cardiac	1.2	32	0.48
Abdomen	1.7	65	0.98
Bone, general	2.7	166	2.49
Bone, extremities	2	169	2.53

TABLE 6
DRLs for CT Used for Attenuation Correction and Localization in PET Scans in Terms of Volume CT Dose Index and Dose–Length Product and Effective Dose Associated with Hybrid CT of PET/CT

PET/CT protocol	Volume CT dose index (mGy)	Dose–length product (mGy·cm)	Effective dose (mSv)
Brain	5.7	211	3.16
Oncology, vertex to mid thigh	4.2	677	5.66
Oncology, whole body (head to toe)	4.4	616	6.10

patient doses and set DRLs on the basis of only administrated activity regardless of image quality. Introduction of reference doses, including image quality criteria and the acceptable-quality dose (AQD principle), has been proposed (*25*). Thus, efforts are needed to develop reliable patient-specific methods to objectively analyze image quality in relation to dose. There are some large variations in the subjective analysis of image quality due to differences in physician preferences on what constitutes an image of diagnosable quality. Some of the approaches used to evaluate image quality need further evaluation, as demonstrated by the Japanese Society of Nuclear Medicine Technology (*26*).

CONCLUSION

This study established the first DRLs for adult and pediatric nuclear medicine imaging studies in Kuwait. The values should be periodically reviewed and updated as recommended by the ICRP. DRLs are an effective tool that can be used to reduce unnecessary patient exposure and to optimize radiation protection in the field of nuclear medicine imaging.

DISCLOSURE

No potential conflict of interest relevant to this article was reported.

ACKNOWLEDGMENTS

We thank the Medical Imaging Council and the nuclear medicine units who participated in this study for their contributions.

KEY POINTS

QUESTION: Can national DRLs be established for nuclear medicine in Kuwait, to be used as a tool to alert professionals when the "as low as reasonably achievable" principle of dose optimization is not fully implemented?

PERTINENT FINDINGS: National DRLs were established and used to identify variations in administered activities for nuclear medicine imaging procedures and to reduce unnecessary patient radiation exposure. The findings showed that the average reduction in radiation dose for nuclear medicine examinations based on national DRLs is up to 25%, compared with the range of doses observed previously in clinical practice.

IMPLICATIONS FOR PATIENT CARE: The DRL concept is a key component of radiation protection and optimization of patient imaging in the field of nuclear medicine.

REFERENCES

1. Mettler FA Jr, Mahesh M, Bhargavan-Chatfield M, et al. Patient exposure from radiologic and nuclear medicine procedures in the United States: procedure volume and effective dose for the period 2006-2016. *Radiology.* 2020;295:418–427.
2. Rehani MM, Vano E, Ciraj-Bjelac O, Kleiman NJ. Radiation and cataract. *Radiat Prot Dosimetry.* 2011;147:300–304.
3. Harding K, Thomson WH. Radiological protection and safety in medicine: ICRP 73. *Eur J Nucl Med.* 1997;24:1207–1209.
4. Vañó E, Miller DL, Martin CJ, et al. ICRP publication 135: diagnostic reference levels in medical imaging. *Ann ICRP.* 2017;46:1–144.
5. Lassmann M, Biassoni L, Monsieurs M, Franzius C, Jacobs F, for the EANM Dosimetry and Paediatrics Committees. The new EANM paediatric dosage card. *Eur J Nucl Med Mol Imaging.* 2008;35:1748.
6. Treves ST, Davis RT, Fahey FH. Administered radiopharmaceutical doses in children: a survey of 13 pediatric hospitals in North America. *J Nucl Med.* 2008;49:1024–1027.
7. Willegaignon J, Braga LF, Sapienza MT, et al. Diagnostic reference level: an important tool for reducing radiation doses in adult and pediatric nuclear medicine procedures in Brazil. *Nucl Med Commun.* 2016;37:525–533.
8. Alessio AM, Farrell MB, Fahey FH. Role of reference levels in nuclear medicine: a report of the SNMMI dose optimization task force. *J Nucl Med.* 2015;56:1960–1964.
9. Song HC, Na MH, Kim J, et al. Diagnostic reference levels for adult nuclear medicine imaging established from the national survey in Korea. *Nucl Med Mol Imaging.* 2019;53:64–70.
10. Abe K, Hosono M, Igarashi T, et al. The 2020 national diagnostic reference levels for nuclear medicine in Japan. *Ann Nucl Med.* 2020;34:799–806.
11. Fahey FH, Bom HH, Chiti A, et al. Standardization of administered activities in pediatric nuclear medicine: a report of the first nuclear medicine global initiative project, part 1—statement of the issue and a review of available resources. *J Nucl Med.* 2015;56:646–651.
12. Muzaffar R, Koester E, Frye S, Alenezi S, Sterkel BB, Osman MM. Development of simple methods to reduce the exposure of the public to radiation from patients who have undergone ^{18}F-FDG PET/CT. *J Nucl Med Technol.* 2020;48:63–67.
13. Elgazzar AH, Owunwanne A, Alenezi S. Structure and activities of nuclear medicine in Kuwait. *Semin Nucl Med.* 2016;46:359–367.
14. Nuclear medicine radiation dose tool. SNMMI website. http://www.snmmi.org/clinicalpractice/dosetool.aspx?itemnumber=1. Updated April 23, 2018. Accessed January 19, 2022.
15. Mattsson S, Johansson L, Leide Svegborn S, et al. Radiation dose to patients from radiopharmaceuticals: a compendium of current information related to frequently used substances. *Ann ICRP.* 2015;44(suppl):7–321.
16. Iball GR, Bebbington NA, Burniston M, et al. A national survey of computed tomography doses in hybrid PET-CT and SPECT-CT examinations in the UK. *Nucl Med Commun.* 2017;38:459–470.
17. Jurik AG, Bongartz G, Golding SJ, Leonardi M. The quality criteria for computed tomography. *Radiat Prot Dosimetry.* 1998;80:49–53.
18. Towson JE, Smart RC. Diagnostic reference activities for nuclear medicine in Australia and New Zealand. IAEA website. http://inis.iaea.org/Search/search.aspx?orig_q=RN:32039913. Published 2001. Accessed January 19, 2022.
19. Korpela H, Bly R, Vassileva J, et al. Recently revised diagnostic reference levels in nuclear medicine in Bulgaria and in Finland. *Radiat Prot Dosimetry.* 2010;139:317–320.
20. Poli GL, Torres L, Coca M, et al. Pediatric nuclear medicine practice: an international survey by the IAEA. *Eur J Nucl Med Mol Imaging.* 2020;47:1552–1563.
21. Koizumi K, Masaki H, Matsuda H, et al. Japanese consensus guidelines for pediatric nuclear medicine. Part 1: pediatric radiopharmaceutical administered doses (JSNM pediatric dosage card). Part 2: technical considerations for pediatric nuclear medicine imaging procedures. *Ann Nucl Med.* 2014;28:498–503.
22. Lima TVM, Gnesin S, Ryckx N, Strobel K, Stritt N, Linder R. Swiss survey on hybrid imaging CTs doses in nuclear medicine and proposed national dose reference levels. *Z Med Phys.* 2018;28:265–275.
23. Masoomi M, Al-Shammeri I, et al. Establishment of national DRL for CT in hybrid imaging studies (the second phase of the national NM CT (PET) dose audit for Kuwait population -2019). medRxiv website. https://www.medrxiv.org/content/10.1101/2020.09.20.20198176v1.full. Published September 23, 2020. Accessed January 19, 2022.
24. Roch P, Célier D, Dessaud C, Etard C, Rehani MM. Long-term experience and analysis of data on diagnostic reference levels: the good, the bad, and the ugly. *Eur Radiol.* 2020;30:1127–1136.
25. Rehani MM. Limitations of diagnostic reference level (DRL) and introduction of acceptable quality dose (AQD). *Br J Radiol.* 2015;88:20140344.
26. Fujiwara T, Hidaka K, Sugibayashi K, Matsumoto M, Kida T, Shiina K. Investigation of the relation between administered dose and image quality for pediatric ^{99m}Tc-DMSA renal scintigraphy: clinical study applying the JSNM pediatric dosage card. *Ann Nucl Med.* 2019;33:153–159.
27. *NCRP Report 172, Reference Levels and Achievable Doses in Medical and Dental Imaging: Recommendations for United States*. National Council on Radiation Protection and Measurement; 2012:75–81.
28. Radiation protection no. 180: diagnostic reference levels in thirty-six European countries. European Commission website. https://ec.europa.eu/energy/sites/ener/files/documents/RP180%20part2.pdf. Published 2014. Accessed January 20, 2022.

Changing Methods of Education During a Pandemic: Questionnaire Survey about Examinations for Nuclear Medicine Technology at Educational Institutions in Japan

Koji Nakaya[1], Masahisa Onoguchi[2], Hiroe Muto[1], Yasuyuki Takahashi[3], Hiroyuki Tsushima[4], Akihiro Kikuchi[5], Takayuki Shibutani[2], Kanae Matsuura[1], and Eisuke Yasuda[1]

[1]Department of Radiological Technology, Faculty of Health Science, Suzuka University of Medical Science, Suzuka, Japan; [2]Department of Quantum Medical Technology, Institute of Medical, Pharmaceutical, and Health Sciences, Kanazawa University, Kanazawa, Japan; [3]Department of Nuclear Medicine Technology, Hirosaki University Graduate School of Health Sciences, Hirosaki, Japan; [4]Department of Radiological Technology, Faculty of Health Sciences, Kobe Tokiwa University, Kobe, Japan; and [5]Department of Radiological Technology, Faculty of Health Science, Hokkaido University of Science, Sapporo, Japan

Coronavirus disease 2019 (COVID-19) has spread around the world. Its effects go far beyond health care: education has to be conducted so as to prevent infection among students and faculty. Accordingly, changes have occurred in Japan's educational institutions, including methods of preparing students for examinations for nuclear medicine. To assess the quality of training for radiologic technologists, we investigated the related changes undertaken at educational institutions. We investigated the lecture format for teaching nuclear medicine technology at Japanese institutions during COVID-19 and efforts to ensure the quality of conventional education. **Methods:** We sent a questionnaire to 19 Japanese institutions. It addressed the lecture format and initiatives in examinations for nuclear medicine technology in the first and second semesters of 2020. **Results:** We obtained responses from 17 institutions. In the first semester of 2020, the lecture format for nuclear medicine technology included remote, hybrid (combination of remote and face-to-face), and video-on-demand lectures. To reinforce the effect of the new teaching formats, institutions adopted various methods, such as enhancing the possibility of allowing students to ask questions, increasing the number of quizzes during lectures, delivering lectures to YouTube, and introducing an e-learning system. In the second semester of 2020, the lecture format included face-to-face, remote, hybrid, and video-on-demand lectures. In that second semester, the number of institutions providing face-to-face lectures while taking thorough measures against infection showed a marked increase. **Conclusion:** The institutions introduced various educational techniques and initiatives. They prioritized students' understanding of lecture content and applied what they considered the best teaching methods. Sharing information about the changes adopted at different institutions should help promote good radiologic technologists—even during a pandemic.

Key Words: lecture format; infection control; initiatives; new approaches; student education, COVID-19

J Nucl Med Technol 2022; 50:60–65
DOI: 10.2967/jnmt.121.262759

Received Jun. 15, 2021; revision accepted Sep. 14, 2021.
For correspondence or reprints, contact Koji Nakaya (nakaya@suzuka-u.ac.jp).
Published online Sep. 28, 2021.

Coronavirus disease 2019 (COVID-19) has had an impact on medicine and education. In many educational institutions, lectures have changed from a traditional face-to-face format to a remote or hybrid format (a hybrid format is a combination of face-to-face and remote lectures to hinder COVID-19 infection) (*1–5*). Teaching has to be undertaken in such a way as to prevent infection among students and faculty. Accordingly, changes have taken place in teaching at Japan's educational institutions, including teaching related to examinations for nuclear medicine technology. The examinations for nuclear medicine technology at universities in Japan have traditionally been based on a face-to-face lecture. Face-to-face lectures are adopted because teachers can proceed with the lecture while visually observing the level of understanding and satisfaction of students. However, because of the spread of COVID-19, Suzuka University of Medical Science shifted from face-to-face lectures to remote and hybrid formats in 2020. The usefulness of remote lectures has been cited (*2,5–7*). It has also been reported that remote lectures are becoming the standard for lectures in the future (*8*).

In a previous study, we obtained information from students using a questionnaire survey about their degree of understanding and satisfaction with remote lectures related to examinations for nuclear medicine technology. In that study, we reported very high levels of understanding and satisfaction with that remote format (*1*). To ensure the ongoing quality of training for radiologic technologists, we determined in the present study the changes that had taken place in educational methods at different institutions. We wanted to share information about the educational methods adopted by the institutions and investigate efforts toward infection control (during the lecture as a useful tool for training) for promoting high-quality medical personnel. We investigated the lecture format for teaching nuclear medicine technology at Japanese institutions during COVID-19, and we investigated efforts to ensure the quality of conventional education.

MATERIALS AND METHODS

Questionnaire Requests

We asked the lecturers responsible for proctoring examinations for nuclear medicine technology at 19 educational institutions in Japan to complete the questionnaire. We randomly selected 19 institutions from among all educational institutions teaching nuclear medicine technology in Japan. We asked that the questionnaire be completed between December 2020 and February 2021.

Questionnaire Content

For the first and second semesters of 2020, we asked lecturers about the lecture format they use before examinations for nuclear medicine technology and their assessment method for assigning grades. We asked the participants to provide free descriptions of initiatives and methods for preventing infection. We inquired about the lecture formats participants found most appropriate during COVID-19 and their reasons for choosing them. In Japan, the first semester is from April to September and the second from October to March.

RESULTS

Questionnaire Response Rate

In all, 17 institutions completed the questionnaire; 2 did not.

Lecture Format in First Semester of 2020

Figure 1 shows the results regarding lecture format for the first semester of 2020. Figure 1A indicates the lecture format for that first semester, and Figure 1B presents the results according to the number of students in each class. One participant was not responsible for teaching nuclear medicine in that first semester; thus, Figure 1 displays the data for the other 16 institutions. For the same reason with later results, Figures 2–4 show data from 16 institutions. Figure 1A indicates that the numbers of institutions that provided the lectures in remote, hybrid, video-on-demand, and other formats were 8, 5, 1, and 2, respectively. The other formats were a mixture of face-to-face, remote, and video-on-demand lectures (1 institution) or a mixture of face-to-face and video-on-demand lectures (1 institution). No institutions held only face-to-face lectures. Figure 1B indicates that many remote lectures were held at institutions where the number of students in each class was either small or large. Most of the institutions with classes of 51–100 students offered hybrid lectures.

Regular Examinations in First Semester of 2020

Figure 2 shows the results regarding the methods for regular examinations (assessment methods that evaluate the comprehension of a lecture and for assigning grades) in the first semester of 2020. Figure 2A presents details of the regular examination methods for that semester, and Figure 2B indicates the regular examination methods classified by lecture format. Figure 2A shows that the numbers of institutions that held regular examination in face-to-face, remote, reports, face-to-face-plus-computer-based, face-to-face-plus-reports, remote-plus-reports, and reports-plus-a-little-testing formats were 9, 1, 2, 1, 1, 1, and 1, respectively. Figure 2B indicates that when the lectures were held remotely, various examination methods were adopted to prevent infection.

Lecture Format in Second Semester of 2020

Figure 3 shows the results regarding the lecture format in the second semester of 2020. Figure 3A presents details of the format in that semester, and Figure 3B shows the results according to number of students per class. Figure 3A indicates that the numbers of institutions that held face-to-face, remote, hybrid, and other lecture formats were 7, 3, 5, and 1, respectively. The other lecture format, adopted by 1 institution, was a mixture of face-to-face and video-on-demand. Figure 3B shows that there was no difference in the lecture format according to the number of students. Some institutions held face-to-face lectures regardless of the number of students.

Regular Examination in Second Semester of 2020

Figure 4 shows the results for regular examinations (assessment method for assigning grades) for the second semester of 2020. Figure 4A presents the findings for regular examination methods in that semester, and Figure 4B show the results for regular examination methods according to lecture format. Figure 4A shows that the numbers of institutions adopting face-to-face, remote, remote-plus-reports, and reports-plus-a-little-testing formats were 13, 1, 1, and 1, respectively. There was a clear increase in the number of face-to-face examinations.

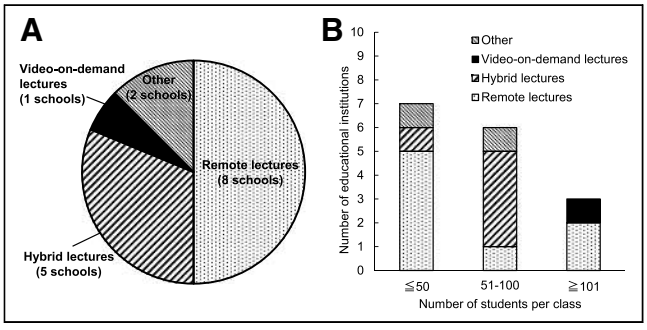

FIGURE 1. Lecture format in first semester of 2020: aggregation (A) and number of students per class (B). Other = combination of face-to-face, remote, and video-on-demand lectures (1 institution) and face-to-face and video-on-demand lectures (1 institution).

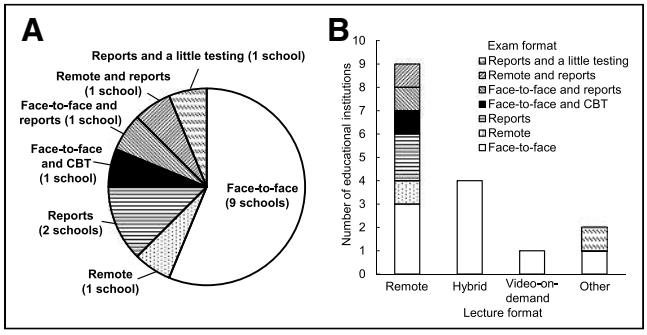

FIGURE 2. Regular examinations in first semester of 2020 (assessment method for assigning grades): aggregation (A) and categorization by lecture format (B). CBT = computer-based testing.

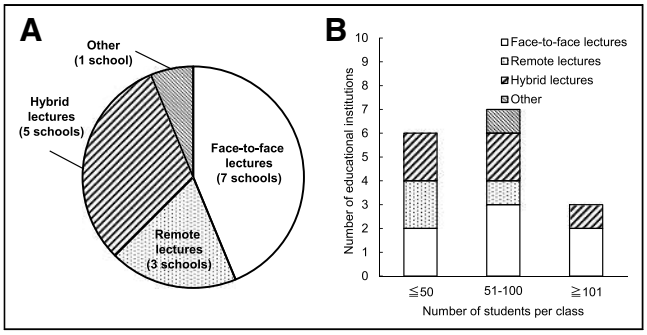

FIGURE 3. Lecture format in second semester of 2020: aggregation (A) and categorization by number of students per class (B). Other = combination of face-to-face and video-on-demand lectures (1 institution).

Free Descriptions of Initiatives and Approaches

Table 1 presents the results related to initiatives and new approaches at the institutions. The comments relate to free descriptions obtained in the questionnaire responses. We obtained many comments about new approaches to infection control. Regarding remote and video-on-demand lectures, there were many comments about improving student understanding. With respect to hybrid lectures, many comments related to reducing the number of class days.

Most Suitable Lecture Format During COVID-19

Figure 5 shows the results related to the optimal lecture format during the pandemic. The numbers of institutions that chose face-to-face, remote, and hybrid lectures were 7, 4, and 6, respectively. Some of the reasons for selecting face-to-face lectures were as follows: they facilitate confirmation of students' understanding; the risk of infection is higher off than on campus; and by attending lectures while taking measures against infection, students become more aware of such measures. Some of the reasons for choosing remote lectures were as follows: they prevent infection among faculty and students, and the quality of conventional education can be guaranteed when designing the content of remote lectures. One of the reasons for selecting hybrid lectures was that face-to-face lectures are also necessary because remote lectures may not monitor student achievement in real time.

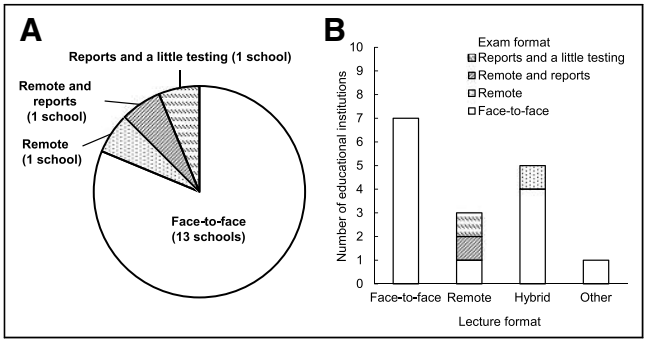

FIGURE 4. Regular examination in second semester of 2020 (assessment method for assigning grades): aggregation (A) and categorization by lecture format (B). Other = combination of face-to-face and video-on-demand lectures.

DISCUSSION

In this study, we investigated the lecture format with respect to teaching nuclear medicine technology before examinations at Japanese educational institutions during COVID-19. We also examined novel efforts to ensure the quality of conventional educational approaches and measures to achieve infection control.

We found that the methods adopted by the surveyed institutions changed significantly as a result of the pandemic. In the first semester of 2020, none of the institutions undertook face-to-face lectures: they switched to such formats as remote or hybrid lectures. The spread of COVID-19 caused the Japanese government to declare a state of emergency during April and May 2020. As a result, Japan's residents were asked to avoid unnecessary outings and maintain social distance (*9*).

In the first semester of 2020, remote and hybrid lecture formats were introduced toward controlling the infection. We observed that educational institutions with few students in classes tended to opt for remote lectures. Accordingly, the small class sizes meant that students could communicate and interact with lecturers remotely. In that way, lecturers were able to assess the learning levels of each student, which supported the remote lecture strategy.

Institutions with many students in each class provided remote and video-on-demand lectures, which meant that students did not have attend in person. To prevent clustering in the case of large classes, the studied institutions adopted a lecture format such that students did not come into close contact with one another.

By contrast, most of the educational institutions with classes of 51–100 students offered hybrid lectures. With the hybrid format, students who wished to take lectures remotely were able to do so, reducing the number attending face-to-face lectures. That format allowed lecturers to monitor students' understanding and satisfaction and teach accordingly. The hybrid format allowed adequate measures against infection.

In the first semester of 2020, the face-to-face format was the most frequently applied method for conducting regular examinations. However, some institutions that used remote lectures in the first semester adopted various test formats to prevent infection. Some institutions conducted testing remotely. Among the comments received from institutions that conducted remote testing were comments indicating that such tests did not allow confirmation that students were relying solely on their academic ability. When taking such tests, students showed their own face on the computer monitor. However, it would have been possible to browse study materials and cheat in such a way that it could not be seen on the monitor. Remote testing can prevent students from being infected, but the biggest disadvantage is that it cannot exclude such fraudulent activities. We received many comments stating that face-to-face testing was the best approach.

In the second semester of 2020, the number of institutions offering face-to-face lectures increased significantly. The reason for the increase was that COVID-19 infection control had

TABLE 1
Free Description of Suggested Initiatives and Approaches During Pandemic

Face-to-face lectures	Remote lectures	Hybrid lectures	Video-on-demand lectures
Distribute COVID-19–related information all at once so that students, faculty, and staff can keep up with latest information on COVID-19. Strengthen infection control. Distribute health observation cards, and require students to measure their temperature and check their symptoms every morning. Stagger start time of lectures in each major so that student traffic will not be dense. Give lectures in classrooms that can accommodate more than twice actual number of participants. Maintain distance between students, and secure social distance. Always open window. Install acrylic dividers, students always wear masks, disinfect microphones, disinfect hands before entering room, disinfect desks after lectures, and always ventilate.	Always administer quizzes online (e-learning system). Remote lectures provided more assignments than face-to-face lectures assignments, giving more time to review. Post videos and lesson materials online, and distribute all slides in PDF format. Provide increased explanations and figures in handouts. Take questions in real time using chat. Communicate with students via chat or email to eliminate points of confusion. Remote lectures eliminate time it takes to travel to school, allowing more time for studying.	Video distribution of board-style lectures with Keynote presentation software. Record lecture for day, and distribute it on YouTube. For small classrooms, capacity of classroom is set to 50%, and lectures are given in 2 classrooms (teachers move between 2 classrooms). For large classrooms, capacity will be 50%, and lectures are given in classroom. Limit school days by study year. Reduce school days. Divide class in half and alternate between face-to-face and remote lectures every other week. For students who do not have remote study environment, we have established a style that allows students to attend school by setting up listening area on campus.	Two videos of 40-min recorded lectures are screened in 90-min lecture. At end of each video, 10 review questions are prepared, and answers are submitted. Recorded video can be reviewed many times later.

begun to be established. Around March of 2020, the Prime Minister's Office of Japan announced that the "Three Cs" should be avoided: closed spaces, crowd places, and close-contact settings. The notification was introduced because of the increased risk of COVID-19 infection (*1,10*). Educational institutions that considered face-to-face lectures more effective could conduct teaching in that manner while avoiding the Three Cs. With face-to-face lectures, it is necessary to implement adequate infection control measures throughout the university. In the first half of 2020, there was no way of providing lectures while avoiding the Three Cs. Therefore, no educational institutions gave face-to-face lectures in the first semester.

In the second semester of 2020, the face-to-face format for regular examinations had also increased markedly. In that semester, the institutions had become accustomed to face-to-face infection control. Accordingly, regular examinations were often held in face-to-face format. But some institutions continued with remote or other examination formats because of the infection risk.

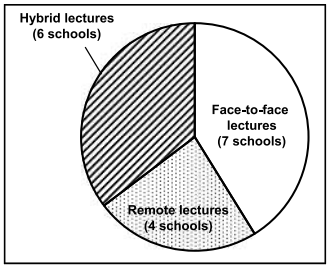

FIGURE 5. Optimal lecture format during COVID-19.

Regular examinations are essential for assessing student comprehension. In the regular examination for the lecture held in the second semester, infection control measures were taken, and face-to-face methods were adopted by many educational institutions. However, it cannot be denied that there is a risk of infection. Therefore, we would like to examine the methods used by some educational institutions in the regular examinations in the first semester of 2020. Some educational institutions have adopted the face-to-face-plus-reports format for regular examinations. By adopting this method, it is possible to reduce the risk of infection and evaluate the level of understanding of students in a short time. In the future, we would like to incorporate this type of regular examination into our lectures.

In the free description portion of the questionnaire, we received many comments related to methods of infection control. All institutions that held face-to-face lectures took thorough infection control measures. Many comments related to remote lectures addressed methods of improving student understanding. Unlike face-to-face lectures, the

remote format does not permit real-time evaluation of students' comprehension and satisfaction. Further, with the remote format, the lecturer is not physically present; the comments therefore indicated concern about the decline in concentration level with such teaching. This finding has been reported in previous studies (*1*). Accordingly, lecturers at institutions that conducted remote lectures devised methods that could obtain the same level of student understanding and satisfaction as did the face-to-face format.

The free descriptions of hybrid lectures included methods of reducing the number of class days. Lecturers wished to have direct contact with students to determine whether they understood the lecture content. Thus, institutions provided hybrid lectures and devised ways to reduce the number of attendance days.

Regarding video-on-demand lectures, the free descriptions mentioned ways of improving student understanding. Few institutions offered video-on-demand. However, there were comments about its merits because it allows multiple reviews of a lecture. It was evident from the free description that educational methods have changed completely to prevent COVID-19 infection. Each institution offered ways to prevent infection and improve understanding.

In the questionnaire, we asked about the optimal lecture format for COVID-19. Evidently, there were no clear differences in a comparison of face-to-face, remote, and hybrid lectures in terms of educational suitability; each institution held different views in this regard. All the institutions made efforts to prevent infection and improve understanding: they believed it was possible to teach in a way that ensured the quality of conventional education in any lecture format.

We investigated various lecture formats and initiatives undertaken by educational institutions under COVID-19. COVID-19 has completely changed all institutions, and they have moved away from conventional education. All the institutions we examined had addressed new educational challenges as a result of COVID-19. We wish to share these initiatives and methods adopted, thereby contributing to the promotion of medical education in society—even during a pandemic. In 2021 and 2022, we will continue to give the same lectures as in 2020. Now, mutant strains of COVID-19 are also prevalent, and lectures are given with strict infection control measures. If education policy in Japan changes in the future as a result of COVID-19, it will be necessary to prepare for such changes using the findings of this study.

Finally, we would like to talk about future prospects. It is unclear whether the new initiatives and lecture formats in COVID-19 investigated here will be used permanently. We would like to continue this survey to see what kinds of changes will be brought about in the future. In addition, we would like to investigate changes in student attitude ratings and satisfaction levels and student board examination scores in lectures at each educational institution. Each educational institution may make a difference by instituting these changes. In previous research, remote lectures were found to give students the same level of satisfaction and understanding as the conventional face-to-face lectures (*1*). Therefore, we believe that by designing lectures that satisfy students in any lecture format, we can provide lectures with a high degree of understanding and satisfaction in any lecture format. Moreover, regarding employment, the chances of getting hands-on training with radiation equipment are decreasing at all educational institutions to prevent infection, and many students are worried about whether they will be able to do their jobs well after finding employment. We would also like to investigate changes in methods of hands-on training that have resulted from COVID-19.

CONCLUSION

We investigated the lecture formats in nuclear medicine technology at educational institutions in Japan during COVID-19; we also examined new efforts to maintain the quality of education and ideas for infection control. We wish to share the related initiatives and ideas among teaching staff and to promote education of medical personnel who can contribute to society.

DISCLOSURE

No potential conflict of interest relevant to this article was reported.

ACKNOWLEDGMENTS

We thank the lecturers for completing the questionnaire, and we thank Edanz (https://jp.edanz.com/ac) for editing a draft of the manuscript.

KEY POINTS

QUESTION: During the time of COVID-19, what changes have been made to lecture formats for teaching nuclear medicine technology at Japanese educational institutions, and what efforts are being made to ensure the quality of conventional education?

PERTINENT FINDINGS: In case-control studies of 17 educational institutions in Japan, the lecture format during COVID-19 was not the conventional one; various school-specific methods were adopted to prevent infection. Associations between lecture styles were not observed in 17 institutional case-control studies.

IMPLICATIONS FOR PATIENT CARE: By sharing the results of this survey with each educational institution, it is possible to strengthen infection control measures and provide a high-quality conventional education.

REFERENCES

1. Nakaya K, Yasuda E, Muto H, et al. Educational effect of remote lectures for students aiming to become radiologic technologists: questionnaire on nuclear medicine examinations. *J Nucl Med Technol.* 2021;49:164–169.

2. Al-Balas M, Al-Balas HI, Jaber KM, et al. Distance learning in clinical medical education amid COVID-19 pandemic in Jordan: current situation, challenges, and perspectives. *BMC Med Educ.* 2020;20:341.
3. Shah M, Hameed BZ, Naik N, et al. The history and evolution of 'webinars' and their role in urology: the modern way of training, education and communication. *Cent European J Urol.* 2021;74:128–130.
4. Potra S, Pugna A, Pop MD, et al. Facing COVID-19 challenges: 1st-year students' experience with the Romanian hybrid higher educational system. *Int J Environ Res Public Health.* 2021;18:3058.
5. Patchoros G, Wenzler G. Satisfying program-level outcomes by integrating primary literature into the online classroom. *J Nucl Med Technol.* 2021;49: 170–174.
6. Letterie GS. Medical education as a science: the quality of evidence for computer-assisted instruction. *Am J Obstet Gynecol.* 2003;188:849–853.
7. Rotimi O, Orah N, Shaaban A, et al. Remote teaching of histopathology using scanned slides via Skype between the United Kingdom and Nigeria. *Arch Pathol Lab Med.* 2017;141:298–300.
8. Wijesooriya NR, Mishra V, Brand PLP, et al. COVID-19 and telehealth, education, and research adaptations. *Paediatr Respir Rev.* 2020;35:38–42.
9. Isumi A, Doi S, Yamaoka Y, et al. Do suicide rates in children and adolescents change during school closure in Japan? The acute effect of the first wave of COVID-19 pandemic on child and adolescent mental health. *Child Abuse Negl.* 2020;110:104680.
10. Information related to COVID-19. Prime Minister of Japan and His Cabinet website. https://japan.kantei.go.jp/. Accessed January 24, 2022.

Yindyamarra Winhanganha: A Conduit to Indigenous Cultural Proficiency

Geoffrey M. Currie

School of Dentistry and Medical Sciences, Charles Sturt University, Wagga Wagga, Australia

The First Nations peoples in the United States, Canada, Australia, and around the world are substantially disadvantaged by colonialization, including health inequity. For nuclear medicine, the cultural competence of the staff and cultural proficiency of the institution are important minimum expectations. This minimum can be achieved through a scaffold of Indigenous cultural training and immersion programs that allow the nuclear medicine department to be a culturally safe environment for Indigenous patients. Development of such programs requires careful planning and inclusivity of Indigenous people as the key stakeholders but, done appropriately, can positively drive the Indigenous equity pipeline. Central to this undertaking is an understanding of Indigenous ways of learning and the nexus of these ways of learning and learning taxonomies. There remain substantial gaps between the most culturally insightful and the least culturally insightful (individuals and institutions)—gaps that can be addressed, in part, by rich immersive professional development activities in nuclear medicine targeting cultural proficiency and creating culturally safe clinical environments. The opportunity lies before us to provide leadership in nation building and in *yindyamarra winhanganha*: living respectfully while creating a world worth living in.

Key Words: nuclear medicine; social asymmetry; Indigenous peoples; diversity; equity; equality

J Nucl Med Technol 2022; 50:66–72
DOI: 10.2967/jnmt.121.262436

The First Nations peoples around the world are substantially disadvantaged by colonialization (*1–4*). The histories of colonialization are similar in Australia, New Zealand, Canada, and the United States (*5*); however, there are more than 370 million Indigenous people in 70 countries globally (*1*). Inequity manifests in almost all aspects of the Western perceived quality of life, including health and education. Specifically, the average life expectancy across the world is 10 y lower for Indigenous people than for non-Indigenous people (*2*) whereas higher suicide rates and poorer general health are characteristic of Indigenous people (*1*). Key social determinants of health for Indigenous people relate to overcrowded housing, homelessness, lower levels of education (westernized), poorer numeracy and literacy, and lower incomes. Central to health-care inequity is that the Indigenous people's paradigm (square peg) does not fit the Westernized paradigm (round hole) of health or education. There are disparities between Indigenous and non-Indigenous Australians in chronic disease, communicable disease, infant health and mortality, mental health, and life expectancy (*6*). This situation reflects social and socioeconomic factors, including inequitable access to health services, lack of Indigenous people in the health-care workforce, leading to delayed attendance and underuse of services even when available, and sociocultural factors that combine with geographic and economic factors to decrease accessibility to health-care (*6*). A significant cultural issue is that institutionalized medicine provides a western strategy to closing the gap, thus failing to deliver pathways to services that embrace Indigenous beliefs and knowledge (*1*).

Health-care inequities are sustained, in part, by implicit and explicit racial bias but are also driven by extrinsic and intrinsic barriers to accessing health-care services among Indigenous peoples (*2–4*). Cultural competence and Indigenous cultural competence more specifically are critical parts of the curriculum for health-care professions—including professions in nuclear medicine—yet health asymmetry continues to be problematic. This difficulty reflects several complex processes associated with difficulties in changing engrained culture using a bottom-up approach (i.e., student education) and a lack of confidence among non-Indigenous health-care professionals in meeting the cultural needs of Indigenous patients (*7–9*). It is crucial, therefore, to develop—in parallel to the curriculum—initiatives to implement cultural competence in professional activities, continuing professional development activities, and postgraduate activities. The manner in which education providers and professional bodies develop and apply cultural competence to enhance understanding of social, historical, and cultural determinants and then apply this understanding to adapt and implement culturally appropriate health-care is important in the move toward cultural proficiency and equity.

Understanding of Indigenous needs and barriers can create culturally safe and more productive clinical environments for Indigenous patients, Indigenous colleagues, and the broader culturally diverse patient and staff populations. Although this discussion focuses on the Indigenous people of Australia, the knowledge is readily transferable to other Indigenous peoples across the globe and, more generally, to those confronting ethnicity-based social or health-care inequity. Indeed, the

Received Apr. 13, 2021; revision accepted Jun. 12, 2021.
For correspondence and reprints, contact Geoffrey M. Currie (gcurrie@csu.edu.au).
Published online Jul. 30, 2021.

Indigenous people of one land may be displaced geographically to another land (i.e., become a refugee), carrying social asymmetry associated with both their Indigenous status and their refugee status. The chasm of social and health inequity is deepened and widened by implicit, explicit, and historical racial bias. These biases reinforce social injustice weaved through the culture and policies of the institution (i.e., the established westernized culture in which implicit and explicit attitudes and behaviors are engrained in the policy and practice of an organization, government, or community collective) to drive systematic disadvantage to those in most need. *Yindyamarra winhanganha* is Wiradjuri language indigenous to the lands on which many of the Charles Sturt University (CSU) campuses occupy and translates to "living respectfully in a world worth living in." The phrase promotes "nation" building through respect, equity and unity. *Yindyamarra winhanganha* provides a sentinel to direct the path toward and a conduit to realize, *Indigenous cultural proficiency*.

Institution refers to the established westernized culture where implicit and explicit attitudes and behaviors are ingrained in the policy and practice of an organization, Government or community collective. *Nation* is a community of people who share language, culture and history. This people-focused and planet-focused (with the planet being defined as the land for which Indigenous people are proud stewards) Indigenous context of nation and nation building contrasts with the industrial and economic focus of colonized nation building.

CULTURAL SAFETY

Recent research identified 3 key characteristics valued by Indigenous Australians that are important in the nuclear medicine department and in health-care more generally (*10*). The first relates to accessibility of services. Nuclear medicine departments are not always open, easy-to-locate, or welcoming spaces. Furthermore, the nature of the services provided in nuclear medicine makes it difficult to colocate with other health services (excepting radiology). Second, consistent with the principle of personalized medicine and even precision medicine, Indigenous people value health-care that is appropriate and responsive to their holistic needs and beliefs. Some cultural norms are not easily accommodated within the nuclear medicine department, driven in part by issues of safety and in part by a lack of insight into cultural beliefs. Third, Indigenous people value culturally safe places where ethnicity and beliefs are respected. To provide a culturally safe environment requires more than cultural knowledge and awareness; it demands engagement through cultural values and attitudes (Fig. 1).

Part of cultural safety in nuclear medicine is related to patient education. The unequal power relationships between health practitioners and Indigenous patients contribute to health inequalities and health asymmetry at the individual and community levels (*5*). Cultural safety must recognize the historical and contemporary impacts of colonization on Indigenous people's capacity to trust social, institutional, and political structures (*5*).

CULTURAL COMPETENCE

Broadly, cultural competence is the capacity to respond to cultural diversity inside health-care systems (*11*), including understanding and respecting variations in patient health beliefs, values, preferences, behaviors, symptom recognition, thresholds for seeking care, expectations of health-care, compliance, and attitudes about diagnostic procedures (*12*). Cultural competence is an important strategy for addressing inequities, such as those in health and education, for Indigenous people but requires more than cultural awareness (*6*). Cultural competence is the attitudes and behaviors, reinforced through policy and practice, that enable effective cross-cultural collegiality and collaboration at the individual and system levels (*6*).

Endeavors to instill cultural competence in health-care delivery have confronted barriers because of a lack of strategy coherence and because evidence and insight are largely descriptive (*6*). Success in building a culturally competent health workforce is constrained by a lack of a consistent definition for—and language around—cultural competence, a lack of evidence of the impact of interventions, and a lack of identification of appropriate performance indicators. Cultural competence requires being capable of cultural self-assessment, valuing diversity, managing cultural dynamics, having cultural knowledge, adapting one's actions through cultural understanding, recognizing cultural differences, and understanding the impact that such differences make.

Recognizing cultural differences and understanding the value that those cultural differences bring to a community or team are an important part of cultural competence (Fig. 1). This quality allows easy demarcation from lower levels of cultural development—levels at which cultural differences might be seen as an opportunity for exploitation and discrimination or are recognized but either ignored or inappropriately responded to.

CULTURAL PROFICIENCY

Cultural proficiency requires, at the individual and institutional levels, the following: knowledge and skills to work effectively in cross-cultural environments; esteem for all forms of cultural difference; cultural reflection and self-assessment around values, beliefs, and bias; cultural humility; commitment to and valuing of diversity and justice; management of cultural dynamics; learning of cultural practices; adaptation of beliefs, systems, policy, and actions through cultural understanding; recognition and facilitation of bidirectional cultural conduits; and knowledge of how to learn about cultural differences.

Beyond the capabilities of cultural competence, cultural proficiency recognizes cultural differences and is equipped to respond effectively and affirmingly both individually and institutionally (Fig. 1). Cultural proficiency is a journey, not an endpoint.

TRAINING IN CULTURAL COMPETENCE AND PROFICIENCY

There have been initiatives and research outlining the value of stand-alone cultural competence workshops for health-care

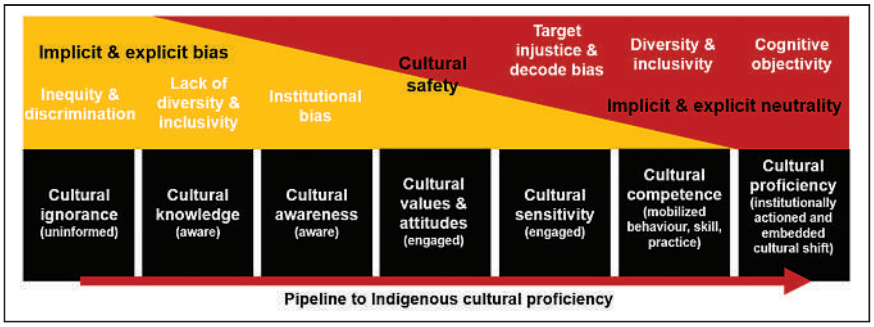

FIGURE 1. Indigenous cultural proficiency pipeline.

workers. Such workshops are often seen as a tick-the-box mentality that satisfies some tokenistic metric to build awareness. Research in Australia found that most industry-based Indigenous cultural training was at the cultural awareness level—well below the expected level of health-care practitioners (*13*). Conversely, university-sector Indigenous cultural training tended to provide a foundation of knowledge and awareness that scaffolded to values, attitudes, sensitivity, empathy, and entry-level cultural competence (*14*). Even when research indicates participants are now more confident working with Indigenous patients, confidence in this aspect of medicine, as in medicine generally, should not be mistaken for competence. Indeed, confidence in the absence of competence can produce deleterious and paradoxic effects. More effective programs include cultural immersions because they develop stronger insights into the connection between culture, history, tradition, beliefs, values, and the interplay with health and health behaviors. Through these rich and deep cultural experiences, a better understanding can be gained of barriers to health and health engagement and of language and communication styles, and potential strategies can be developed to better meet the health-promotion, health-education, and health-safety needs of Indigenous patients.

The journey through cultural awareness to enlightenment and cultural competence or proficiency is tortuous at best and demands commitment, patience, respect, empathy, and perseverance. The task for non-Indigenous health professionals is to challenge the ways of knowing, with the goal of decolonizing their attitudes, beliefs, and actions—a task that is tortuous and challenging yet rich and revelatory (*1*). There are challenges to confront as a result of historical injury to Indigenous people or cultural incompatibilities. Short-term strategies or changes in policy do not instill trust and confidence among Indigenous people. Strategies driven by well-intended white policy makers confront resistance and overlook the insights of the Indigenous people. Indeed, the idea that policy makers know what is best to improve the health and well-being of Indigenous peoples leaves a sense of tokenism and inevitable failure. Worse is the political point scoring of policy makers that parachute in and disrupt any real progress being made.

HEALTH-CARE INEQUITY

Inequity and bias associated with Indigenous health-care might manifest as a lack of diversity in the teams of health-care professionals. Diversity in the health-care team enables creative problem solving and implementation of solutions better suited to Indigenous patients. Inequity may also manifest from policy developed with homogeneous patient data (lacks Indigenous inclusivity). It is critical that data reflect diversity and be inclusive of Indigenous people; otherwise, there is a significant risk of widening health-care inequities for Indigenous populations.

There are numerous examples of bias that drives the Indigenous health-care inequity gap. Implicit bias or intrinsic bias relates to the attitudes and stereotypes that can unintentionally prejudice or bias. Explicit bias or extrinsic bias is our conscious attitudes and stereotypes that intentionally cause prejudice and bias, of which racial bias is prominent. Both implicit bias and explicit bias cause harm in society and health-care, and both can be deeply engrained in health-care culture and policy. Institutional bias refers to that which is weaved into the culture of the "institution" (a western paradigm) and creates a systematic advantage typically to those already enjoying advantages via social asymmetries. Historical biases are a type of institutional bias in which implicit or explicit bias has shaped historical records. As a result, when those records are used, the biases not only are learned by health-care workers and policy makers but are reinforced. Cognitive bias, a systematic bias common in human health interactions, is that in which observations from the environment around a patient are used in judgment and decision making. These observations can be discriminatory and rely heavily on intuition, which, in turn, is shaped by the personal experiences of the observer. Health-care is neither neutral nor objective; rather, it is embedded in and driven by social, political, and economic agendas. Indeed, health-care policy is frequently designed with parameters for discrimination and amplification of social inequalities. An essential element of the professional development and undergraduate training of nuclear medicine professionals is to develop the capability for critical reflection that reveals intrinsic bias to ensure not only that Indigenous people find nuclear medicine a culturally safe place but also that they encounter health-care professionals who exhibit the attitudes and behaviors of cultural competence. In turn, learning from structured and hidden curricula, and through cultural mentoring, will reengineer the cultural framework of the institution and produce cultural proficiency, thus debugging policy and practice from historical bias.

Indigenous health-care, including in nuclear medicine, confronts issues associated with accessibility to, and opportunity for, access when services are available. Many of the barriers are intrinsic to Indigenous people (e.g., lower uptake of available services), but it remains an expectation that health-care professionals will bridge any divides and work with Indigenous communities to develop culturally safe and appropriate

spaces. In turn, this work will increase Indigenous access to and use of expertise and assets. Inclusive in this effort is the obligation to make careers in health, including nuclear medicine, attractive and achievable for Indigenous people. In rural and remote Western Australia, the nuclear medicine needs of Indigenous Australians (oncology, cardiology, and renal services) are provided using a fly-in, fly-out service to provide access to remote communities. Indigenous people in these communities have a 30 times higher myocardial infarction rate than non-Indigenous people and a 50% lower 5-y cancer survival rate. But the success comes from culturally proficient nuclear medicine teams who are committed to closing the inequity divide and who work with the Indigenous community to meet its needs. Accessibility creates equality, but equity also demands opportunity. Well-thought-out strategy by culturally proficient teams is essential to ensure opportunity. Taking the services to the patient in communities that would otherwise not sustain a nuclear medicine service, and using telemedicine, overcome the cultural and socioeconomic barriers to services. A study in Western Australia showed comparative hospital services between metropolitan and regional communities (900 beds with 5,700 staff in the metropolitan hospital and 800 beds with 6,000 staff in the regional hospital) and revealed disparities (*15*). In metropolitan services, only 0.9% of the staff and 0.8% of the patient population were Indigenous. For regional services, 3.7% of the staff and 8% of the patient population were Indigenous. Although the study indicated that Indigenous people are underrepresented in the workforce of regional services, it also signaled that metropolitan services are lacking in cultural preparedness for local Indigenous patients and for those referred from lower-tier regional sites for specialist services. Also of note, health policy, including funding and rebates, is driven by metropolitan teaching hospitals whose data not only overlook the unique features of regional and rural communities but, expressly and grossly, underrepresent Indigenous people.

THE INDIGENOUS EQUITY PIPELINE

Traditionally, health and education institutions have lacked vertical and horizontal diversity, and it is only in recent decades that a shift has been seen to more inclusivity to overcome barriers to diversity. In health-care generally and nuclear medicine specifically, the philosophy is to "first do no harm" (nonmaleficence) and then improve outcomes (beneficence). To that end, development and implementation of a strategy to close the gap in health-care equity should not create or potentiate inequities but rather should actively mitigate inequities. The equity pipeline can be broken into 6 steps (Fig. 2):

1. Identifying the problem
2. Gathering supporting evidence
3. Defining outcomes
4. Developing a strategy
5. Implementing the strategy
6. Evaluating, reflecting, and refining

Problem identification can be driven by political, commercial, or economic forces. Institutional bias can be engrained in identifying the problem, gathering the evidence, and defining the outcomes. In health-care, the first 3 of these steps are frequently focused on issues associated with the health needs of those already advantaged or privileged. Policy-driving data generally reflect a metropolitan major teaching hospital cohort and seldom include socially or geographically isolated communities. There can also be censoring of data in a way that drives minority underrepresentation and lack of diversity in the data and demands more considered data curation. Outcomes associated with health-care costs discriminate against patients with, for example, higher degrees of morbidity, which in turn create inequity and bias associated with Indigenous groups with higher levels of morbidity. In essence, this discrimination redirects resources away from those in most need, perpetuating the inverse-care law. Strategy and policy development will reflect the diversity, or lack thereof, of the development team and any associated biases. Particular care is needed to ensure that policies do not embed and reinforce the lack of neutrality of the institution and data. There is a potential for bias and inequity when lack of objectivity influences performance metrics. Strategy implementation needs careful consideration and ongoing evaluation to ensure appropriateness for Indigenous populations. In the absence of evaluation of postimplementation performance and appropriate identification of those performance indicators, significant inequity and social injustice may emerge. Among the 6 steps in the pipeline, a spectrum for both diversity and inequity provides clues to cause and solution (Fig. 2). Central to the entire Indigenous equity pipeline is the mantra "nothing about us without us." Indigenous equity in health-care requires key-stakeholder engagement and inclusivity; too often, the institution rather than the nation is identified as the key stakeholder.

INDIGENOUS LEARNING

In nuclear medicine and health more generally, communication with Indigenous people is a key cultural competence skill but is also a valuable tool in creating a culturally safe environment for all patients. Understanding Indigenous ways of learning will drive improved promotion of health and improved dissemination of patient information, which in turn will drive trust, compliance, and increased health-care engagement. Understanding Indigenous ways of learning or knowing will also provide valuable insight to help the non-Indigenous health practitioner more deeply understand Indigenous barriers to health and health equity. Reflecting meaningfully on Indigenous ways of learning is a conduit to cultural proficiency. The first principle to consider, perhaps more broadly in health promotion than specifically in nuclear medicine, is the barriers to Indigenous learning. If Indigenous patients do not find that hospitals or clinical departments are a culturally safe place for learning, then health professionals need to venture into culturally safe places to better deliver key messages. At a macro

FIGURE 2. Focus of bias associated with the equity pipeline, beginning with underlying problem of diversity in data and development teams and transforming into outcomes of inequity.

level, this venture means engaging with Indigenous people in their communities—an effort that would be helped by including Indigenous members on the health-care team. At a micro level, this venture might be reflected by an individual health-care practitioner who exercises cultural proficiency skills in negating a culturally inappropriate physical space and providing the Indigenous patient with a culturally safe emotional and cognitive environment. In principle, such skills should be no different from the emotional intelligence and cultural competence skills that health-care practitioners use to create safe places for all patients, each with a unique suite of cultural needs. If patients do not learn where we teach, let us teach where they learn.

Likewise, when examining the ways by which Indigenous people learn or acquire knowledge, it is easy to focus on the unique media for the learning, and perhaps the challenges associated with them, rather than appreciating that the core philosophies are largely universal for all learning. Consider the following list of 8 ways of learning for Indigenous people (https://www.8ways.online/); perhaps with the exception of number 8, these are all important tools for learning regardless of ethnicity.

1. Story telling: use of a narrative to make a better connection with the patient and the information being communicated
2. Learning maps: mind maps that draw on the visual nature of learning to create visual pathways and connections among bits of information
3. Nonverbal communication: a vital tool in engagement and in conveying the importance of information
4. Symbols: metaphors or images that are used to reinforce understanding of concepts
5. Nonlinear learning: a way to accommodate lateral thinking and synthesis of new knowledge
6. Deconstruction-and-reconstruction models (learning in whole: watch one, do one, teach one) or scaffold learning (learning in parts)
7. Community links: use of the community to contextualize the value of learning and to provide a repository for sharing of learning within the community
8. Land links: connection of learning to local land, nature, and places, as captured perhaps in part by an emphasis on sustainability in general learning

Valuable insight comes from community engagement and cultural immersion. Australian Indigenous people tell dreamtime stories that survive intact over thousands of years. Like Indigenous people across the globe, Australian Indigenous people tell stories through a cultural bubble of song, dance, ceremony, art, and family that preserves the integrity of the message. If learning is weaved into cultural significance, we create not only a richer understanding and appreciation of the learning but also a map to guide us back to unremembered learning. Cultural acuity, competence, and proficiency are capabilities that health-care practitioners and educators alike should develop so that learning can be crafted into a cultural bubble for enhanced understanding by Indigenous and non-Indigenous patients and students.

TAXONOMIES OF INDIGENOUS CULTURAL PROFICIENCY

The journey to Indigenous cultural proficiency requires deep insight into Indigenous culture, Indigenous ways of learning, and one's own ways of learning. The journey is less tortuous through a cultural immersion style of learning and through appreciating the impact of learning taxonomies. Bloom's cognitive taxonomy can provide a valuable framework for learning that is widely cited in the educational literature. As learning outcomes are developed in university courses, Bloom's cognitive taxonomies are used to scaffold the learning from lower-order capabilities such as knowing and understanding through to higher-order capabilities such as evaluation and synthesis. Indeed, the knowledge domain that the cognitive taxonomies apply is also scaled from factual information through to metacognitive. This 2-dimensional taxonomy of learning is the very foundation of formal education yet simply affords early capabilities in the Indigenous equity pipeline (Fig. 3). In some regards, it is easy to understand why a focus on cognitive and knowledge domains, even collectively, reinforces bias and inequity. Progression to cultural safety and sensitivity (acuity) along the pipeline requires attention to the less-often-discussed affective domain of Bloom's taxonomy, in which feelings, attitudes, and values are scaffolded from receiving and responding through to internalized values. The step to cultural competence and proficiency requires command of the capabilities of Bloom's taxonomies in the psychomotor domain. Here, the emphasis is on behaviors, skills, and what individuals actually do and has a scaffold from perception through to adaption and organization (Fig. 3). The key point here is that overcoming barriers might be viewed as an insurmountable task but that the decolonized mind easily identifies the synergies between ways of learning and the application of westernized education taxonomies. It is not a case of abandoning or reengineering western approaches to learning but rather of adopting a more objective view of similarities to refine and integrate into an approach that is better for all.

THE CSU EXPERIENCE

CSU is a culturally proficient organization built on genuine respect for and engagement with our Indigenous communities. At an institutional level, Indigenous culture is authentically and visibly weaved through strategy, philosophy, and branding. Indigenous culture is respected during the course of any event, meeting, or class. At major university events, Indigenous elders perform a welcome-to-country address, which acknowledges the land and cultural significance of the meeting place. All meetings, whether in person or virtual, include an acknowledgment of country and a paying of respect to Indigenous elders and people—past, present, and future. At its inception, this comprised the meeting chair's reading an institutionally approved script. Today, meeting chairs deliver their own version of the original acknowledgment that reflects their own values and experiences. This is an authentic insight into the growing of cultural competence and proficiency through personal engagement with Indigenous cultural competence initiatives. The start of each class begins the same: for some, with the formally crafted statement, and for many others, with a personalized acknowledgment that embraces the cultural identity of Indigenous people.

The growth in the Indigenous cultural competence of the CSU staff is driven intrinsically by the strategy and branding of the university and extrinsically by programs designed to enrich Indigenous cultural proficiency. At an entry level, CSU offers an online Indigenous cultural competency program for all staff and students focused on the lower-order taxonomies of enhancing awareness and sensitivity. The significant impact of this program is the development of CSU as a culturally safe place for Indigenous staff and students. The program decolonizes thinking and helps individuals feel more confident about their contribution to closing the inequity gap. Beyond this foundation program, several staff members undergo enrichment through Indigenous cultural immersions. This might be, for example, participation in a traditional smoking ceremony that, for some, provides a cultural epiphany. For others, an overnight or 2- to 3-d immersion in an Indigenous community provides insight not only into how to develop cultural proficiency but also into barriers Indigenous communities confront that drive social asymmetry. In turn, this exercise arms participants with the rich insight they need to become effective policy makers in health, education, and other areas of governance. Students too, in some programs, are afforded the opportunity to undertake enrichment programs as primary health workers or educationalists in Indigenous communities. Such programs impart insights, values, and capabilities that can drive change in communities where Indigenous people are minorities.

CSU staff, students, and members of local, national, and professional communities can undertake postgraduate studies in the Wiradjuri language, culture, and heritage. The program creates awareness and motivation to reverse the colonization, dislocation, and dispossession of Indigenous people with immersion in and celebration of the Wiradjuri nation. All coursework programs at CSU—undergraduate and postgraduate—are mandated to include at least 1 subject (12.5% of an annual full-time study-load equivalent) approved as an Indigenous subject by the Indigenous Board of Studies. This requirement drives awareness in some students who are at a foundational level (cognitive domain) whereas other students, who have already mastered the cognitive foundation, may be driven to engage more deeply. One key performance indicator that speaks to the success of these programs is that CSU is the Australian university with the highest proportion of Indigenous students and, more importantly, with the highest retention and completion rates. One observation is that the increase in the proportion of students who are Indigenous reflects both an absolute increase in Indigenous enrollment and an increase in students identifying as Indigenous who might otherwise not share that identity. In either case, it speaks to the strategies that create culturally safe environments and reflect institutional cultural proficiency.

CSU has also invested in physical resources that support cultural safety and mirror Indigenous ways of learning—resources that are excellent for all students and staff. At the Wagga Wagga campus, open native spaces, including a large amphitheater, are often used for outdoor classes. Wagga Wagga campus also hosts an Indigenous food garden that not only provides an education resource but also supports biodiversity in a rich habitat. Each campus has a First Nations student center to bring Indigenous students together and provide culturally safe places. The Bathurst campus has a vibrant space dedicated as a meeting place for Wiradjuri elders. On the Port Macquarie campus, outdoor spaces include a lecture space (Fig. 4 background) and a fire pit that allows meeting and teaching in a yarning circle

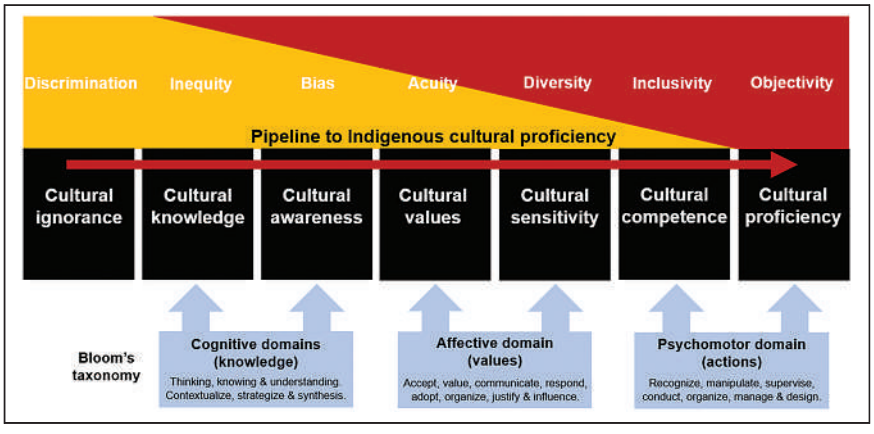

FIGURE 3. Bloom's taxonomy mapped against Indigenous cultural proficiency pipeline.

FIGURE 4. Outdoor learning space in Port Macquarie campus of CSU, with tiered lecture theater seating in background and covered yarning circle around fire pit for open discussion and meeting in foreground.

around the fire (Fig. 4). The significance of the yarning circle is equity (all facing the center), engagement, and open communication.

CONCLUSION

The divide associated with Indigenous inequities, despite the efforts of individuals, corporations, and policy makers, continues to be problematic. This divide reflects 2 maxims: that the health-care system is only as strong as its weakest link and that, unfortunately, there is a substantial gap between the most culturally insightful and the least culturally insightful. In turn, this gap perpetuates the inverse-care law, by which those in most need of health-care have disproportionately decreased access to it. Indigenous health-care without diversity and inclusivity in the workforce, and without rich immersive professional development activities targeting cultural proficiency using cognitive, affective, and psychomotor taxonomies, is counterintuitive to the first-do-no-harm mantra of western medicine and nonmaleficence. More importantly, such immersive strategies toward Indigenous cultural training and toward diversity and inclusivity help create culturally safe clinical environments for patients, helping reduce social and cultural barriers to Indigenous people accessing medical services. The commitment of non-Indigenous health-care professionals to developing cultural competence and proficiency is the essence of nation building and of living respectfully in a world worth living in: *yindya-marra winhanganha*.

DISCLOSURE

No potential conflict of interest relevant to this article was reported.

REFERENCES

1. Currie G, Wheat J, Wess T. Building foundations for Indigenous cultural competence: an institution's journey toward "closing the gap." *J Med Imaging Radiat Sci.* 2018;49:6–10.
2. Stephens C, Nettleton C, Porter J, Willis R, Clark S. Indigenous peoples' health: why are they behind everyone, everywhere? *Lancet.* 2005;366:10–13.
3. Anderson I, Robson B, Connolly M, et al. Indigenous and tribal peoples' health (the Lancet–Lowitja Institute Global Collaboration): a population study. *Lancet.* 2016;388:131–157.
4. Shapiro J, Lie D, Gutierrez D, Zhuang G. "That never would have occurred to me": a qualitative study of medical students' views of a cultural competence curriculum. *BMC Med Educ.* 2006;6:31.
5. Kurtz DL, Janke R, Vinek J, Wells T, Hutchinson P, Froste A. Health sciences cultural safety education in Australia, Canada, New Zealand, and the United States: a literature review. *Int J Med Educ.* 2018;9:271–285.
6. Bainbridge R, McCalman J, Clifford A, Tsey K. *Cultural Competency in the Delivery of Health Services for Indigenous People.* Australian Institute of Health and Welfare; 2015:1–42.
7. Brach C, Fraserirector I. Can cultural competency reduce racial and ethnic health disparities? A review and conceptual model. *Med Care Res Rev.* 2000;57(suppl 1):181–217.
8. Kumaş-Tan Z, Beagan B, Loppie C, MacLeod A, Frank B. Measures of cultural competence: examining hidden assumptions. *Acad Med.* 2007;82:548–557.
9. Butler M, McCreedy E, Schwer N, et al. *Improving Cultural Competence to Reduce Health Disparities.* Agency for Healthcare Research and Quality; 2016:1–7. Report 16-EHC006-EF.
10. Gomersall JS, Gibson O, Dwyer J, et al. What Indigenous Australian clients value about primary health care: a systematic review of qualitative evidence. *Aust N Z J Public Health.* 2017;41:417–423.
11. Leininger MM, McFarland MR. *Culture Care Diversity and Universality: A Worldwide Nursing Theory.* Jones and Bartlett Learning; 2006:1–41.
12. Betancourt J, Green A, Carrillo J. Defining cultural competence: a practical framework for addressing racial/ethnic disparities in health and health care. *Public Health Rep.* 2003;118:293–302.
13. Downing R, Kowal E, Paradies Y. Indigenous cultural training for health workers in Australia. *Int J Qual Health Care.* 2011;23:247–257.
14. Ewen SC, Paul DJ, Bloom GL. Do Indigenous health curricula in health science education reduce disparities in health care outcomes? *Med J Aust.* 2012;197:50–52.
15. Taylor EV, Lyford M, Parsons L, Mason T, Sabesan S, Thompson SC. "We're very much part of the team here": a culture of respect for Indigenous health workforce transforms Indigenous health care. *PLoS One.* 2020;15:e0239207.

^{18}F-Fluciclovine–Avid Axillary Lymph Nodes After COVID-19 Vaccination on PET/CT for Suspected Recurrence of Prostate Cancer

Justin G. Peacock[1,2], Elisabeth A. Banks[3], and Nathan McWhorter[1,2]

[1]Department of Radiology, Uniformed Services University, Bethesda, Maryland; [2]Department of Radiology, San Antonio Military Medical Center, San Antonio, Texas; and [3]College of Natural Sciences, University of Texas at Austin, Austin, Texas

Abnormally increased ^{18}F-FDG avidity of axillary lymph nodes has become a frequent diagnostic dilemma on PET/CT in the current climate of global vaccinations directed against severe acute respiratory syndrome coronavirus 2. This avidity is due to the inflammatory response evoked by vaccines and the nonspecific nature of ^{18}F-FDG uptake, which is increased in both malignant and inflammatory processes. Similarly, ^{18}F-fluciclovine, an amino acid analog indicated for the assessment of biochemical recurrence of prostate cancer, may also demonstrate nonspecific inflammatory uptake. We report a case of ^{18}F-fluciclovine PET/CT obtained for concern about prostate cancer. In this case, isolated avid lymph nodes were seen in the left axilla. A screening questionnaire revealed that the patient had recently received the second dose of the Pfizer-BioNTech coronavirus disease 2019 vaccine in his left shoulder, and hence, the uptake was determined to be reactive.

Key Words: PET/CT; COVID-19 vaccine; ^{18}F-fluciclovine; axillary lymph nodes; inflammation; prostate cancer

J Nucl Med Technol 2022; 50:73–74
DOI: 10.2967/jnmt.121.263001

Abnormal axillary lymph node avidity associated with vaccination was first reported in 2003 on ^{18}F-FDG PET/CT images of healthy individuals who had received the killed influenza vaccine in a study assessing lymphocyte activation (*1*). Since then, similar findings have been reported from numerous other vaccinations (*2*). Such findings are due to the inflammatory response elicited by vaccines and the resulting upregulation of glucose transporters by activated immune cells (*3*). With the widespread implementation of vaccinations in response to the coronavirus disease 2019 (COVID-19) pandemic, there has been a marked increase in this phenomenon, resulting in significant diagnostic challenges with ^{18}F-FDG PET/CT (*2*).

CASE REPORT

A 65-y-old man underwent surgery for prostate cancer. Subsequent pathologic evaluation revealed a Gleason score of 7 (3 + 4) with evidence of perineural invasion and 1 of 5 local lymph nodes positive for spread. There was no seminal vesicle invasion or extracapsular extension, and the surgical margins were negative. The overall stage was IVA (pT2, N1, M0). At 4 mo after surgery, there was a persistent detectable prostate-specific antigen level of 1.0 ng/mL, and ^{18}F-fluciclovine (Axumin; Blue Earth Diagnostics) PET/CT was performed for further assessment. The examination revealed 4 foci of avidity (SUV_{max}, 3.2) in the left axilla localizing to mildly enlarged but morphologically normal lymph nodes (Fig. 1). The remainder of the uptake was physiologic, with no other sites of pathologic radiotracer avidity. A review of the intake questionnaire showed that the patient had received the Pfizer-BioNTech COVID-19 vaccine in his left shoulder 17 d previously, and hence, the uptake was determined to be reactive. Subsequent clinical follow-up revealed an undetectable prostate-specific antigen level at 6 mo and again at 9 mo, confirming the benign nature of the uptake and the absence of residual malignancy.

DISCUSSION

Although ^{18}F-FDG is by far the most frequently used radiotracer in PET/CT, several additional radiotracers are in clinical use, including ^{18}F-fluciclovine for imaging in men with suspected prostate cancer recurrence. ^{18}F-fluciclovine is an amino acid analog and is taken up by prostate cancer (*4*). However, like ^{18}F-FDG, ^{18}F-fluciclovine can show increased uptake in inflammatory processes due to uptake by white blood cells. Given this fact, false-positive uptake has been reported in nonmalignant entities such as pneumonia, lymphadenitis, and ring worm infection (*4,5*). As with ^{18}F-FDG, ^{18}F-fluciclovine uptake by inflammatory processes tends to be mild compared with that by malignancy and most commonly has an intensity less than that in normal bone marrow (as in this case, with the L3 vertebra

Received Aug. 6, 2021; revision accepted Oct. 22, 2021.
For correspondence or reprints, contact Elisabeth Banks (libbybanks@utexas.edu).
Published online Dec. 6, 2021.

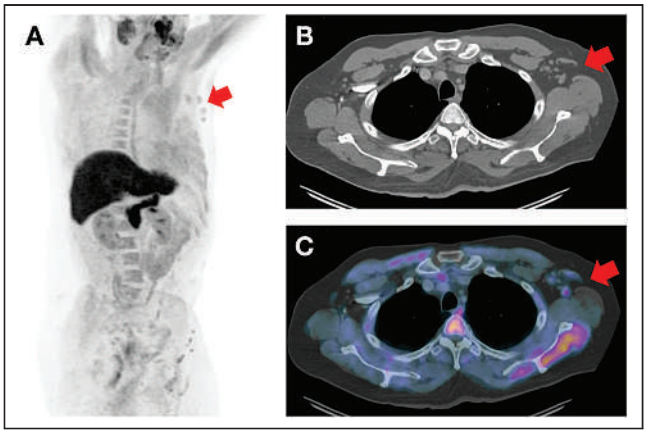

FIGURE 1. (A) ^{18}F-fluciclovine PET maximum-intensity projection revealed 4 foci of unexpected avidity in left axilla (arrow). Remainder of uptake was physiologic. (B and C) Axial CT (B) and axial ^{18}F-fluciclovine PET/CT (C) images show avidity localizing 4 mildly enlarged but morphologically normal lymph nodes (arrows). Remaining images (not shown) confirmed no other sites of potentially pathologic radiotracer avidity.

having an SUV_{mean} of 3.5). Hence, it is to be expected that, as with ^{18}F-FDG, low-grade avidity by axillary nodes will be a potential finding on ^{18}F-fluciclovine PET/CT after COVID-19 vaccination.

Recently, several prostate-specific membrane antigen PET tracers have received approval for use in the United States as an additional means for detecting prostate cancer. Despite their excellent performance, these, too, can demonstrate nonspecific uptake by inflammatory diseases such as pneumonia, and hence, it is likely only a matter of time before a case of COVID-19 vaccination–related uptake in the axillary lymph nodes is reported with these agents (*6*).

CONCLUSION

The case underlines the importance of correlating examination findings with disease pathophysiology, radiotracer mechanism of action, and clinical history to optimize the accuracy of PET/CT interpretation.

DISCLOSURE

No potential conflict of interest relevant to this article was reported.

REFERENCES

1. Iyengar S, Chin B, Margolick JB, et al. Anatomical loci of HIV-associated immune activation and association with viraemia. *Lancet.* 2003;362:945–950.
2. McIntosh LJ, Bankier AA, Vijayaraghavan GR, et al. COVID-19 vaccination-related uptake on FDG PET/CT: an emerging dilemma and suggestions for management. *AJR.* 2021;217:975–983.
3. Love C, Tomas MB, Tonco GG, et al. FDG PET of infection and inflammation. *Radiographics.* 2005;25:1357–1368.
4. Gusman M, Aminsharifi JA, Peacock JG, et al. Review of ^{18}F-fluciclovine PET for detection of recurrent prostate cancer. *Radiographics.* 2019;39:822–841.
5. Schuster DM, Nanni C, Fanti S, et al. Anti-1-amino-3-^{18}F-fluorocyclobutane-1-carboxylic acid: physiologic uptake patterns, incidental findings, and variants that may simulate disease. *J Nucl Med.* 2014;55:1986–1992.
6. Barbosa FG, Queiroz MA, Nunes RF, et al. Revisiting prostate cancer recurrence with PSMA PET: atlas of typical and atypical patterns of spread. *Radiographics.* 2019;39:186–212.

^{99m}Tc-Sulfur Colloid SPECT/CT in Diagnosis of Splenogonadal Fusion

Fatimah Ahmed Daghas, Jaber Abdulwahab Asiri, Habib Hassine, and Ali Ibrahim Aamry

Nuclear Medicine Unit/Radiology, King Saud Medical City, Riyadh, Saudi Arabia

A congenital abnormal connection between an accessory spleen and a gonad is called splenogonadal fusion. The parent of a 3-y-old boy brought him to King Saud Medical City because he had left scrotal swelling that had begun 1 y previously. ^{99m}Tc-sulfur colloid (SC) imaging has superior sensitivity and specificity in targeting the liver, spleen, and bone marrow, in that these are the only organs that ^{99m}Tc-SC can visualize. Furthermore, if these tissues appear anywhere other than their usual locations, such as in the case of an accessory spleen, ^{99m}Tc-SC imaging can identify them even without biopsy or—in the case of splenogonadal fusion—orchiectomy. In the current case, the patient underwent laparoscopy, the masses were removed, and orchiectomy was avoided. Histopathologic examination confirmed normal splenic tissue, matching the imaging results.

Key Words: gastrointestinal; pediatrics; SPECT/CT; accessory spleens; splenogonadal fusion; sulfur colloid

J Nucl Med Technol 2022; 50:75–77
DOI: 10.2967/jnmt.121.262233

Accessory spleens, which appear when there are deficient mesenchymal buds during development, can arise from the spleen when the gonads descend. The type of accessory spleen that is associated with the gonad is called splenogonadal fusion (SGF) (*1*).

SGF is also called ectopic scrotal spleen and usually presents before the age of 20 y; appearance in the left testis only is possible in boys younger than 10 y. The male-to-female ratio of SGF is 16:1 (*2*). Another published case (*3*) used nuclear medicine to rule out SGF. In the current case, SGF was diagnosed successfully using ^{99m}Tc-sulfur colloid (SC) imaging.

CASE REPORT

A 3-y-old boy was brought to King Saud Medical City by his parent because of left scrotal swelling that had first been noticed 1 y previously. Physical examination revealed unusual scrotal swelling that was painless and did not change in size on palpation. There was no history of trauma.

Ultrasound showed both testicles in the scrotum. The right measured 1.8 × 0.7 cm and had normal echogenicity and vascularity (Fig. 1A). The left measured 1.2 × 0.8 cm and also had normal echogenicity and vascularity. However, inseparable from the left testis was a well-defined, oval abnormal area of soft tissue that was of homogeneous echogenicity, measured 3 cm in length by 1.2 cm in diameter, and was adjacent to a feeding vessel (Fig. 1B). No obvious calcification was seen, and there was no evidence of a hydrocele or enlarged lymph nodes. The imaging differential diagnosis included an underlying testicular neoplasm, and ^{99m}Tc-SC imaging was performed to diagnose SGF.

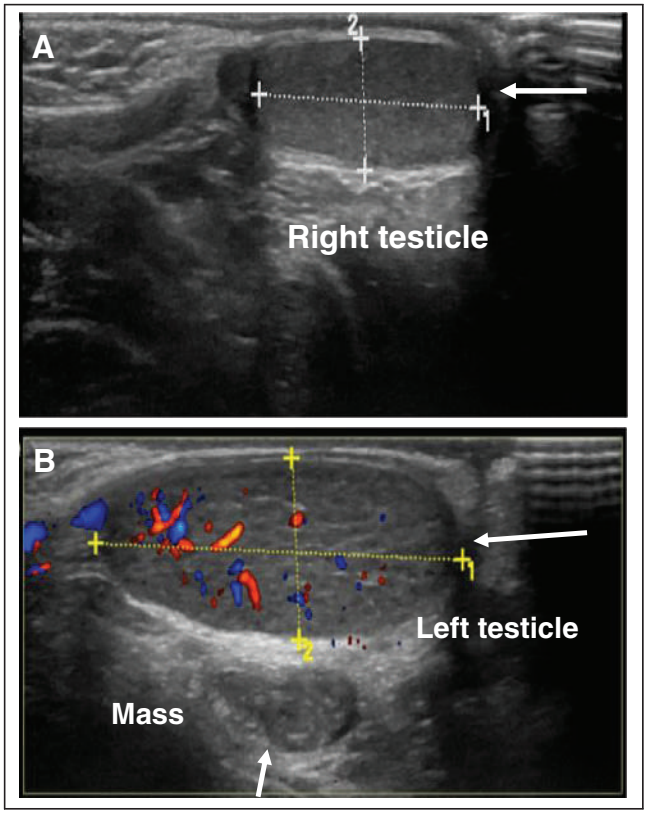

FIGURE 1. Ultrasound of scrotum. (A) Right testicle (arrow) measures 1.8 × 0.7 cm and shows normal echogenicity and vascularity. (B) Left testicle (horizontal arrow) measures 1.2 × 0.8 cm and shows normal echogenicity and vascularity. Well-defined, oval abnormal soft-tissue mass (vertical arrow) inseparable from left testis shows homogeneous echogenicity, measures 3 × 1.2 cm, and is adjacent to feeding vessel.

Received Mar. 6, 2021; revision accepted Jul. 20, 2021.
For correspondence or reprints, contact Fatimah Ahmed Daghas (f.daghas@ksmc.med.sa).
Published online Nov. 8, 2021.

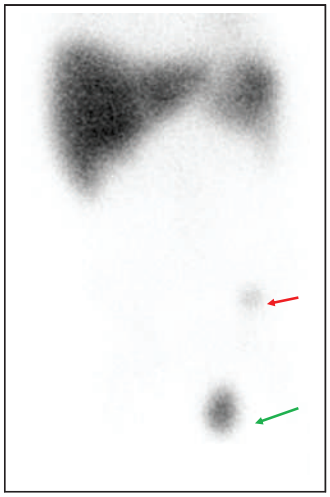

FIGURE 2. ^{99m}Tc-SC image. Anterior planar view of abdomen and pelvis shows normal biodistribution of tracer, with 2 abnormal focal areas of uptake. One (green arrow) is more intense than the other, is in scrotum, measures about 2 × 2 cm, and matches mass noted on previous ultrasound. The other (red arrow) is in anterior part of left iliac fossa.

The patient was injected with 92.5 MBq (2.5 mCi) of ^{99m}Tc-SC. First, a static image over the anterior and posterior abdomen was obtained for 10 min. Afterward, SPECT/CT was performed over the same region, using a 360° rotation, a 128 × 128 matrix, and a rate of 30 s per frame.

The liver was found to be in its normal anatomic location and to measure 11 × 10.5 cm, with adequate, homogeneously distributed tracer uptake throughout. The spleen, in its normal anatomic location, was visualized as well. It measured about 7 × 5 cm. The images also showed 2 abnormal focal areas of uptake (Fig. 2). The more intense of these was in the scrotum (anterior to the left testicle), measured about 2 × 2 cm, and matched the mass noted on the previous ultrasound (Fig. 1). The mass was hyperdense, compared with the normal density of the testis. The second focus of abnormal uptake was smaller (~1 cm of diameter) and less active, was in the anterior part of the left iliac fossa between the abdominal wall and the urinary bladder, and was highly suggestive of accessory spleen tissue. The imaging report concluded that the study gave a strong impression of SGF, with a small accessory spleen in the left iliac fossa and left testicle.

After these diagnostic tests, the patient underwent left laparoscopy with excision of the splenules in both the testis and the abdomen. The area was approached through an inguinal incision. Both specimens were sent for histopathologic examination, which found that they represented splenic tissue with no significant pathologic change.

DISCUSSION

SGF is an unusual medical disorder that presents from birth. This congenital malformation appears as splenic tissue in the gonad (*4*). Historically, SGF was first mentioned in 1913, by Sneath, a demonstrator of anatomy at the University of Manchester (*5*). There are 2 types of SGF, depending on whether the spleen and gonad are connected or unconnected (*4*). SGF is reported mostly in children and presents as an abnormal mass in the testicle. The first step to diagnosing SGF is the physical examination: the patient presents with pain in the left testis and swelling in the left scrotum. Ultrasound, CT, and MRI will show an abnormal mass in such cases.

In the current case, ultrasound, MRI, and CT revealed a discrete hemiscrotal soft-tissue mass inseparable from the left testis but failed to characterize the mass. ^{99m}Tc-SC imaging is a noninvasive modality capable of detecting ectopic functioning splenic tissue and, in this case, helped to characterize the scrotal mass and diagnose SGF noninvasively (Fig. 3).

Although our literature review indicated that few cases of SGF have been diagnosed with ^{99m}Tc-SC (*3*), we decided to send our patient to the nuclear medicine department for ^{99m}Tc-SC imaging to rule out SGF because this modality has a superior ability to differentiate between the distinctive tissues in such cases, on the basis of the percentage of the radiotracer distributed in the body. About 92% of ^{99m}Tc-SC bonds with the cells of the reticuloendothelial system. In other words, if the ^{99m}Tc-SC is prepared in the proper way in the hot lab and is imaged using the proper protocol, it will concentrate in only 3 organs: the liver, the spleen, and the bone marrow. In the current case, we saw high tracer

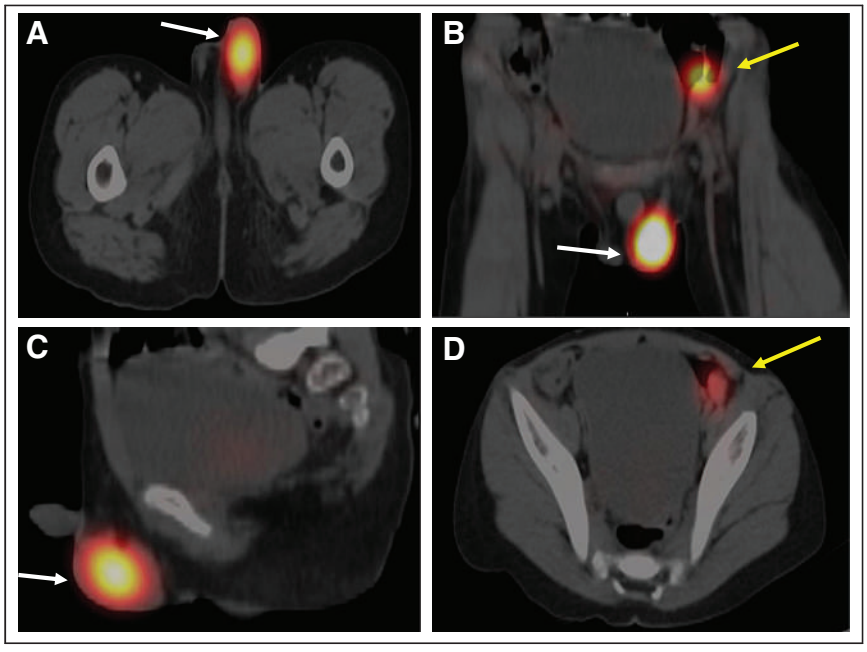

FIGURE 3. (A–C) ^{99m}Tc-SC SPECT/CT images showing 2 abnormal focal areas of uptake (white arrows) in axial (A), coronal (B), and sagittal (C) views and a second, less active focus (yellow arrow). (D) Axial SPECT/CT image showing that the less active focus (yellow arrow) is smaller (~1 cm in diameter) than the other focus and is in anterior part of left iliac fossa between abdominal wall and urinary bladder; as such, it is highly suggestive of accessory spleen tissue.

uptake in the liver and spleen (Fig. 2), but the rest of the body had no tracer uptake except for the 2 foci of abnormally high uptake that turned out to be accessory spleens.

CONCLUSION

^{99m}Tc-SC imaging helps to diagnose SGF noninvasively and has a potential role in the evaluation of testicular masses.

DISCLOSURE

No potential conflict of interest relevant to this article was reported.

REFERENCES

1. Bajwa SA, Kasi A. Anatomy, abdomen and pelvis, accessory spleen. National Center for Biotechnology Information website. https://www.ncbi.nlm.nih.gov/books/NBK519040/. Updated July 26, 2021. Accessed December 28, 2021.
2. Kadouri Y, Carnicelli D, Sayegh HE, Benslimane L, Nouini Y. Pathogenesis, diagnosis, and management of splenogonadal fusion: a literature review. *Case Rep Urol.* 2020;2020:8876219.
3. Guarin U, Dimitrieva Z, Ashley SJ. Splenogonadal fusion: a rare congenital anomaly demonstrated by ^{99}Tc-sulfur colloid imaging—case report. *J Nucl Med.* 1975; 16:922–924.
4. Bal K, Ermete M, Balci U, Dincel C. Splenogonadal fusion: a very rare congenital anomaly in the differential diagnosis of a testicular mass. *Turk J Urol.* 2014; 40:62–64.
5. Bhutani N, Kajal P, Sangwan V. Splenogonadal fusion. *J Pediatr Surg Case Rep.* 2020;59:101514.

Editorial Board Gender Balance

TO THE EDITOR: I read with interest a recent commentary in the *European Journal of Nuclear Medicine and Molecular Imaging* detailing the gender inequity associated with the composition of the journal editorial board (*1*). This was followed by further analysis (*2*) of 25 nuclear medicine journals across the United States, Europe, and Asia that reported the universality of the gross disparity between male and female members of the editorial boards for journals. Clearly, gender diversity on an editorial board provides valuable perspective and builds a culture of equality in the profession and research. Nonetheless, the analysis was at a loss to explain the gender differential (on the order of 4:1 favoring men).

Although the specific journals were not identified by name, the *Journal of Nuclear Medicine Technology* (*JNMT*) may have been overlooked because this analysis is far from representative. Indeed, the *JNMT* is a model for gender equality, with 11 female and 9 male editorial board members comprising a female editor, 8 female associate editors, 7 male and 1 female consulting editors, 2 male international consulting editors, and a female managing editor. The historically inclusive culture of the Society of Nuclear Medicine and Molecular Imaging Technologist Section and *JNMT,* combined with more equitable gender distribution among professional colleagues, provides a benchmark and formula for others to follow. Yet it also provides an insight that reflects the traditional male predominance of physician, physicist, and radiochemist numbers in the editorial board composition of medical and physics journals. The emergence of a greater gender balance across science, technology, engineering, and medicine (STEM) provides encouragement that the expertise of the profession, and thus journal editorship, will also find a balanced gender equilibrium.

It should be noted that this discussion, and the original works (*1,2*), do not accommodate nonbinary gender classifications or, indeed, other important aspects of diversity that enrich an editorial team (e.g., ethnicity, age/experience, and sexual orientation)—something to consider moving forward. But for now, this is an opportunity to celebrate the *JNMT* as an international leader and benchmark for gender equity.

REFERENCES

1. Gelardi F, Gozzi N. Women on board: mind the (gender) gap. *Eur J Nucl Med Mol Imaging.* 2021;48:3029–3032.
2. Evangelista L, Ekmekcioglu O, Kunikowska J. Gender balance in the editorial board of nuclear medicine journals. *Eur J Nucl Med Mol Imaging.* 2021;48:3749–3750.

Geoffrey M. Currie
Charles Sturt University
Wagga Wagga, Australia
E-mail: gcurrie@csu.edu.au

Published online Sep. 28, 2021.
DOI: 10.2967/jnmt.121.263047

Accreditation Standards for Nuclear Medicine Technologist Education: Revisions to Accredit Diagnostic CT Education in NMT Programs

Andrew T. Trout, MD, and Rodney C. Fisher, PhD, RT(R)(N)(CT)(BD), CNMT, JRCNMT Directors

The Joint Review Committee on Educational Programs in Nuclear Medicine Technology (JRCNMT) is recognized by the Council for Higher Education Accreditation to accredit postsecondary nuclear medicine technology (NMT) programs in the United States. The mission and vision of the JRCNMT are to ensure quality NMT education through programmatic accreditation and to advance NMT education, respectively. Toward these ends, the board continually evaluates the NMT educational landscape with a goal of maintaining and advancing education standards.

In 2020, in response to an assessment of the state of the field, the board revised the accreditation standards to provide accreditation for education in diagnostic computed tomography (CT) occurring in NMT programs sufficient to allow students to sit for CT certification. These new standards will go into effect in August 2022. The purpose of this article is to convey the perspective, intent, and expectations of the JRCNMT related to diagnostic CT education in NMT programs.

Hybrid and correlative imaging have long been an important part of the practice of nuclear medicine, and both clinical and didactic education in hybrid imaging have been required by the standards since 2011. CT is the dominant form of hybrid imaging performed in nuclear medicine departments, and many modern SPECT and PET cameras include CT scanners to allow sequential hybrid imaging. These CT scanners are not only capable of imaging for attenuation correction and localization but also able to produce diagnostic-quality CT images. Where permitted by state licensure, NMTs may be asked to perform diagnostic CT imaging as part of nuclear medicine examinations or as stand-alone examinations. Further, the board understands that in some markets, NMTs with additional certification in CT may be more sought after for employment as they can cover multiple needs for an imaging department.

Educational programs have responded to these market demands with some NMT programs already providing education in diagnostic CT sufficient for students to sit for CT certification. This combination of education has the chief benefit for students of preparing them to sit for dual certification upon graduation. Inclusion of CT content, however, has the potential to impact the broader NMT education and student experience within a program.

In providing accreditation for diagnostic CT education occurring in NMT programs, it is the intent of the board to recognize the importance and relevance of diagnostic CT to NMT, to recognize those programs that provide education in both modalities sufficient to allow students to sit for certification, and to ensure the quality of education in both NMT and diagnostic CT when combined in a program. Importantly, accreditation for diagnostic CT education applies only to programs providing complete education in diagnostic CT, sufficient to allow students to sit for certification upon graduation. Diagnostic CT content taught as part of an NMT program that is insufficient to allow students to sit for certification will not be separately accredited. Further, it is not the intent of the board to accredit diagnostic CT programs independent of NMT programs.

Revising the standards to provide accreditation for diagnostic CT education followed the formalized process for revision of the accreditation standards outlined in JRCNMT policies. In this case, a JRCNMT taskforce with physician, NMT program director, and technologist representation, including a technologist certified in CT who teaches in a CT program embedded in a radiography program, proposed initial revisions to the standards. Revisions were crafted to avoid bias toward a particular CT certification examination/board and it was the intent of the board to ensure that accredited programs provide sufficient didactic and clinical education to prepare students for either the ARRT or NMTCB CT examinations after the students pass their NMT examination(s). After board approval and modification, the proposed revisions were made available for public comment and for comment by the JRCNMT's collaborating organizations (The American College of Radiology [ACR], American Society of Radiologic Technologists [ASRT], The Society of Nuclear Medicine and Molecular Imaging [SNMMI], and the SNMMI Technologist Section [SNMMI-TS]) prior to adoption.

In revising the standards to include education in diagnostic CT, the board sought to structure the CT standards to parallel the NMT standards as much as possible. CT standards are additional requirements that must be met by programs offering diagnostic CT content sufficient for any number of students (does not have to be all students) to sit for certification. Programs seeking accreditation for diagnostic CT must also meet the accreditation standards for NMT education.

The revised standards, including the diagnostic CT standards, are available on the JRCNMT webpage (www.jrcnmt.org), and full description of the standards is beyond the scope of this article. The standards incorporate specific requirements for didactic and clinical education in diagnostic CT. Beyond standards specific to education requirements, there are standards that may require program attention to personnel credentials and experience. Specifically (paraphrased):

> B2.3 – At least one faculty member must be credentialed in diagnostic CT
>
> B3 – It is preferred, but not required, that affiliate education supervisors (AES) at affiliates offering diagnostic CT competencies hold current certification and registration in diagnostic CT. In the absence of this, the AES must have at least 2 years post-certification experience performing diagnostic CT
>
> D3.3 – One member of the Advisory Committee must represent the diagnostic CT component of the program

The intent of these standards is to ensure that personnel with diagnostic CT certification or specific diagnostic CT experience (AES) contribute to student education in diagnostic CT. The JRCNMT recognizes that it is not feasible at this time to require that the program director or clinical coordinator have CT certification. Further, the JRCNMT has not stipulated the employment status of the CT-certified faculty—they may be full-time, part-time, or adjunct. Programs should expect and be prepared to provide documentation of CT certification and/or experience as part of the accreditation process.

In addition to standards requiring personnel with certification and experience in CT, there are standards specifically aimed at ensuring that programs providing diagnostic CT education sufficient to allow students to sit for certification are programmatically structured to do so. Specifically (paraphrased):

> D2.1 – Programs must have program and course level student learning outcomes specific to diagnostic CT

The intent of these standards is to ensure that education in diagnostic CT receives the same program-level attention and assessment as NMT education. As part of the process of accreditation, the JRCNMT will be looking for one or more CT-specific program-level outcome and associated assessment methods and results.

The standards related to clinical education in diagnostic CT parallel the NMT standards, defining a competency list to which programs are expected to teach. Like for NMT, this is a list of tasks, skills, and knowledge that an entry-level CT technologist should be capable of upon program completion. This is not a list of examination types or procedures (e.g. CT of the head). It is the responsibility of the program to ensure that in the process of documenting diagnostic CT competencies that students receive sufficient breadth of exposure to meet clinical experience requirements necessary to qualify for certification. The standards are specifically written to allow diagnostic CT competencies to be obtained on either stand-alone CT machines or hybrid CT machines (SPECT/CT and PET/CT). Just like for NMT certification, programs will need to be aware of the specific didactic and clinical experience requirements of certifying organizations to which their students will be applying.

Finally, the revised standards include a requirement that programs must publish and disclose to students that certification in CT is a post-primary certification. Specifically (paraphrased):

> E1.4i – Eligibility to take either national certification examination in CT requires certification in nuclear medicine technology, radiography or radiation therapy first.

The JRCNMT recognizes that the revised standards will increase the reporting and documentation burden for programs. However, accrediting diagnostic CT education within NMT education programs serves the important purposes described above and provides an opportunity for programs to be recognized for the expanded education they may be providing to students.

Explore SNMMI's Online Career Center!

Explore the benefits of the SNMMI Career Center by logging in or creating a new account today.

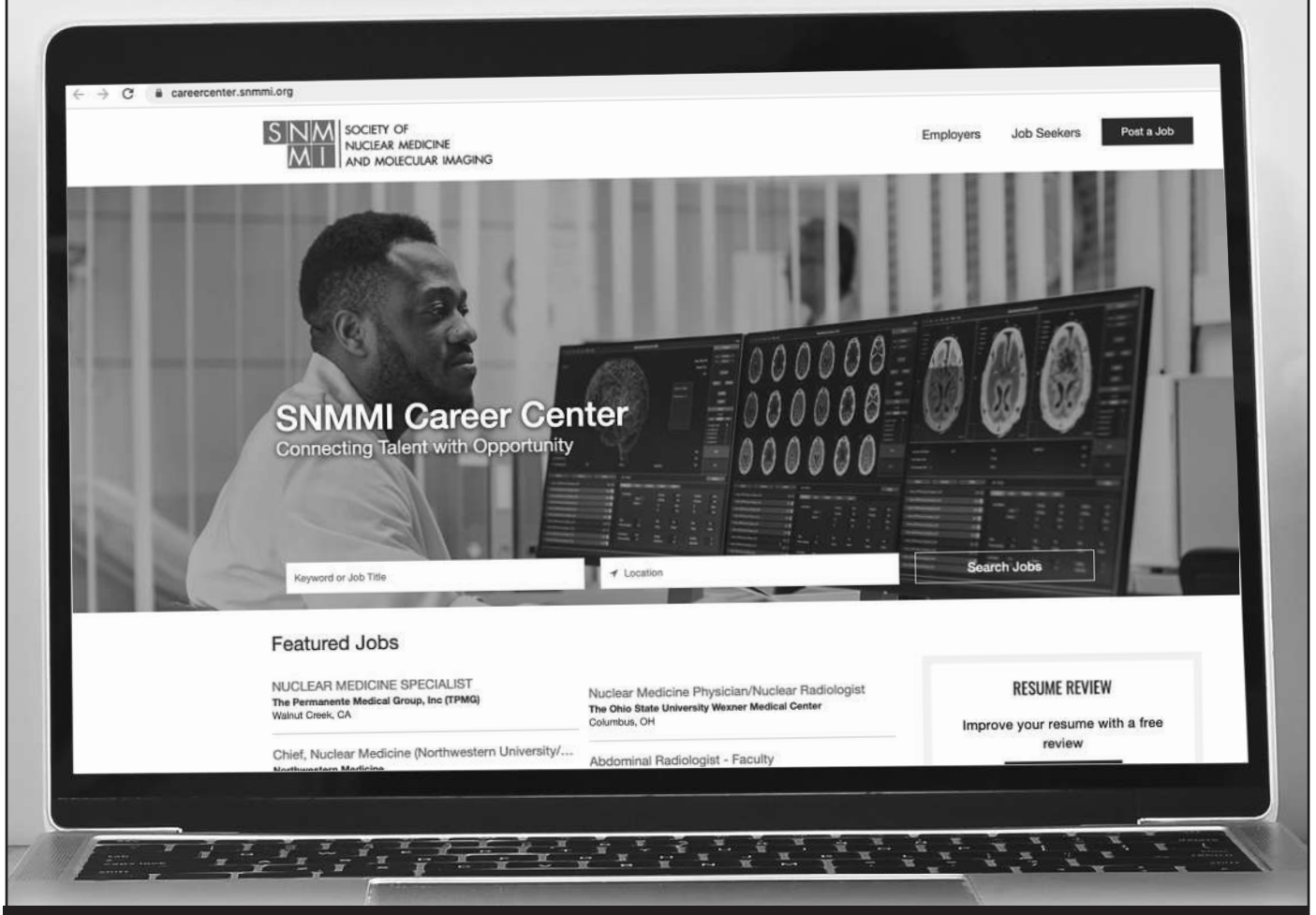

careercenter.snmmi.org

**Note: Single sign-on has been enabled for this platform and you can use your member login credentials to access the Career Center. If you are unsure of your password, to go to the SNMMI password reset link to create a new password.*

SNMMI Value Initiative

SOCIETY OF NUCLEAR MEDICINE & MOLECULAR IMAGING

REGISTRATION IS NOW AVAILABLE!

This year, the Annual Meeting will be offered as a hybrid event with in-person and remote registration options available—allowing you to customize your meeting attendance. Make your plans now to attend SNMMI's flagship meeting, in-person June 11-14 in Vancouver, BC, Canada, or virtually from your home or office.

Register Today

WWW.SNMMI.ORG/AM2022

SNMMI 2022 Annual Meeting